2012

Effluent Water Quality Improvement Using Silt Fences And Stormwater Harvesting

Ikiensinma Gogo-Abite
University of Central Florida

EFFLUENT WATER QUALITY IMPROVEMENT USING SILT FENCES AND STORMWATER HARVESTING

by

IKIENSINMA GOGO-ABITE
B.Tech. Rivers State University of Science and Technology, 1991
MSCE. University of Central Florida, 2005

A dissertation submitted in partial fulfillment of the requirements
for the degree of Doctor of Philosophy
in the Department of Civil, Environmental, and Construction Engineering
in the College of Engineering and Computer Science
at the University of Central Florida
Orlando, Florida

Summer Term
2012

Major Advisor: Manoj B. Chopra

ABSTRACT

Construction sites are among the most common areas to experience soil erosion and sediment transport due to the mandatory foundation tasks such as excavation and land grubbing. Thus, temporary sediment barriers are installed along the perimeter to prevent sediment transport from the site. Erosion and sediment transport control measures may include, but not limited to, physical and chemical processes such as the use of a silt fence and polyacrylamide product. Runoff from construction sites and other impervious surfaces are routinely discharged into ponds for treatment before being released into a receiving water body. Stormwater harvesting from a pond for irrigation of adjacent lands is promoted as one approach to reducing pond discharge while supplementing valuable potable water used for irrigation. The reduction of pond discharge reduces the mass of pollutants in the discharge. In the dissertation, presented is the investigation of the effectiveness of temporary sediment barriers and then, development of a modeling approach to a stormwater harvesting pond to provide a comprehensive stormwater management pollution reduction assessment tool.

The first part of the research presents the investigation of the performance efficiencies of silt fence fabrics in turbidity and sediment concentration removal, and the determination of flow-through-rate on simulated construction sites in real time. Two silt fence fabrics, (1) woven and the other (2) nonwoven were subjected to material index property tests and a series of field-scale tests with different rainfall intensities and events for different embankment slopes on a tilting test-bed. Collected influent and effluent samples were analyzed for sediment concentration and turbidity, and the flow-through-rate for each fabric was evaluated. Test results revealed that the woven and nonwoven silt fence achieved 11 and 56 percent average turbidity reduction

efficiency, respectively. Each fabric also achieved 20 and 56 percent average sediment concentration removal efficiency, respectively. Fabric flow-through-rates were functions of the rainfall intensity and embankment slope. The nonwoven fabric exhibited higher flow-through-rates than the woven fabric in both field-scale and laboratory tests.

In the second part of the study, a Stormwater Harvesting and Assessment for Reduction of Pollution (SHARP) model was developed to predict operation of wet pond used for stormwater harvesting. The model integrates the interaction of surface water and groundwater in a catchment area. The SHARP model was calibrated and validated with actual pond water elevation data from a stormwater pond at Miramar Lakes, Miramar, Florida. Model evaluation showed adequate prediction of pond water elevation with root mean square error between 0.07 and 0.12 m; mean absolute error was between 0.018 and 0.07 m; and relative index of agreement was between 0.74 and 0.98 for both calibration and validation periods. The SHARP model is capable of assessing harvesting safe-yield and discharge from a pond, including the prediction of the percentage of runoff into a harvesting pond that is not discharged.

The combination of silt fence and/or polyacrylamide PAM before stormwater harvesting pond in a treatment train for the reduction of pollutants from construction sites has the potential of significantly exceeding a performance standard of 85 percent reduction typically required by local authorities. In fact, the stringent requirement of equaling pre- and post-development pollutant loading is highly achievable by the treatment train approach. The significant contribution from the integration of the SHARP model to the treatment train is that real-time assessment of pollutant loading reduction by volume can be planned and controlled to achieve target performance standards.

To my mother, Charity and in memory of my father, Amakefonyama

ACKNOWLEDGMENTS

First and foremost, the author expresses his gratefulness to his major advisor Dr. Manoj B. Chopra for encouragement, guidance, and valuable contribution on the research and financial aid through his doctoral education at the University of Central Florida. He wishes to express his indebtedness to Dr. Marty Wanielista for the numerous helpful discussions, supports, and advice on the research and for accepting to serve on his graduate committee. The author further extends gratitude to Dr. John Weishampel and Dr. BooHyun Nam for serving on his graduate committee and their invaluable advice.

The author would like to express thanks to the Florida Department of Transportation for monetary support. Without their support, research such as this would not have been possible. He appreciates the invaluable staff and students of the Stormwater Management Academy, for their support and assistance in the collection of laboratory and field data. In particular, one would like to thank the following UCF research associate and students: Mike Hardin, Clayton Bender, Nicole Runnebaum, Jesus Ozuna, Jamie Capri, Rafiqul Chowdhury, Curtis Schneider and host of other research interns who gave extensive and timely efforts throughout the research.

Finally, the author appreciates his wife, Bolou without whose support, encouragement and tolerance could not have completed the program. Thanks to family and friends for their encouragement through the course of the program, and special thanks to Akins, Kesibo, Asikeotonwa, Arusaba, Happiness, Paul Ekwere and Mike Ngodigha.

TABLE OF CONTENTS

LIST OF TABLES

LIST OF FIGURES

LIST OF ABBREVIATIONS AND SYMBOLS

ΔS_{GW} = change in groundwater storage
ΔS_M = change in soil moisture storage
ΔS_P = change in pond storage
Δt = change in time [T]
ΔV = change in volume
A = cross sectional area of test specimen [L^2]
a = intercept of a linear regression line
AET = actual evapotranspiration volume [L T^{-1}]
b = gradient of a linear regression line
B = percentage of beads passing through specimen [%]
b_{TB} = width of the test-bed [L]
C = Celsius [Θ]
D = discharge [L T^{-1}]
d = index of agreement
d = soil layer depth [L]
$D(\theta)$ = soil water diffusivity [L T^{-1}]
DP = deep percolation [L T^{-1}]
d_{rel} = relative index of agreement
E = free surface water evaporation [L T^{-1}]
E = Nash-Sutcliffe coefficient
E = rainfall event
e_a = actual vapor pressure [M L^{-2}]
eff = effluent
$e^o(T_{hr})$ = saturation vapor pressure curve at T_{hr} [M L^{-2}]
E_{rel} = relative Nash-Sutcliffe coefficient
e_s = saturation vapor pressure [M L^{-2}]
ET = evapotranspiration [L T^{-1}]
E_T = performance efficiency for turbidity reduction [%]
ET_c = crop evapotranspiration (L T^{-1})
E_{TS} = performance efficiency for total solid removal [%]
F = cumulative infiltration [L]
F = Fahrenheit [Θ]
f = infiltration rate [L T^{-1}]
F_p = cumulative infiltration at surface ponding [L]
f_p = infiltration rate at ponding [L T^{-1}]
G = soil heat flux density [M L^{-2} T^{-1}]
h = head of water on specimen [L]

H = hydraulic potential head difference [L]
H = initial drainage depth [L]
H = maximum grass height [L]
$h(\theta_i)$ = negative pressure head [L]
H_{AR} = harvested volume [L]
h_{BW} = depth of backwater upstream [L]
h_{cb} = bubbling pressure head [L]
h_s = water depth [L]
I, i = rainfall intensity [L T^{-1}]
I_a = initial abstraction [L]
I_{IRR} = irrigation volume [L]
in./hr. = inches per hour
inf. = influent
$K(\theta)$ = unsaturated hydraulic conductivity of soil layer [L T^{-1}]
K, K_s = hydraulic conductivity of media or transmission zone [L T^{-1}]
$K_{avg}(\theta)$ = average unsaturated hydraulic conductivity [L T^{-1}]
k_c = crop coefficient
k_{cb} = basal crop coefficient
KD = transmissivity [L^2 T^{-1}]
k_e = soil evaporative coefficient
k_s = soil water stress
L = length [L]
M = soil moisture deficit
mg/L = milligrams per liter
mm/hr. = millimeters per hour
n = exponent related to the pore size distribution
N = newton [M]
N = north
n = number of samples collected.
n_i = number of samples from i^{th} test conducted
NTU = Nephelometric turbidity unit
$\bar{O}$ = mean of observed values
O = observed values
P = mass of glass beads in the pan [M]
P = precipitation directly on the pond [L]
P = predicted values
p = soil water depletion fraction
P_A = pond water surface area [L^2]
PD = percent difference to determine harvest safe yield [%]

PET = reference evapotranspiration [L T^{-1}]
P_P = pond water surface level perimeter [L]
q = Darcian velocity (flux rate) [L T^{-1}]
Q = quantity of flow [L^3]
Q_0 = flow out of the banks at x = 0 at any time t per foot of bank length [L T^{-1}]
Q_D = stormwater harvesting pond discharge [L T^{-1}]
Q_{GW} = groundwater seepage [L T^{-1}]
q_o = volumetric flow out of the banks at x = 0 at any time t per foot of bank length [L^3 T^{-1}]
q_s = total sink and/or source of water (rainfall, infiltration, or exfiltration) [L]
q_{SF} = silt fence flow-through-rate [L.T^{-1}]
R = rainfall volume [L]
R^2 = coefficient of determination
R_n = net radiation [M L^{-2} T^{-1}]
RO = surface runoff [L]
R_t = temperature correction factor
S = embankment slope
s = index for surface cover
S = pond storage [L^3]
s = seconds [T]
SC = sediment concentration in runoff [mg/L]
S_e = effective saturation
S_{ei} = initial effective saturation
S_{GW} = groundwater storage [L]
S_M = soil moisture storage [L]
$S_{M,IFD}$ = inflow and outflow difference when there is irrigation [L]
$S_{M,ZIFD}$ = inflow and outflow difference when there is no irrigation [L]
S_P = pond storage [L]
T = temperature [Θ]
T = total mass of glass beads passing through each specimen
T = turbidity [NTU]
T = unsaturated soil layer thickness [L]
T, t = time [T]
t_d = rainfall duration [T]
T_{hr} = mean daily temperature at 2 meter height [Θ]
T_i,= thickness of soil i^{th} layer [L]
t_p = time at surface ponding [T]
TS = total solids [mg/L]
U = Mann-Whitney tests statistics
u_2 = wind speed at 2 meter height [L T^{-1}]
u_{20} = water viscosity at 20ºC [L T^{-1}]

u_t = water viscosity at test temperature [L T^{-1}]
v = flow rate [L T^{-1}]
V = volume [L^3]
W = west
W = Wilcoxon signed-rank tests statistics
WM = weighted mean for the respective parameter
WMEC = weighted mean effluent concentration [mg/L]
WMET = weighted mean effluent turbidity [NTU]
WMIC = weighted mean influent concentration [mg/L]
WMIT = weighted mean influent turbidity [NTU]
x = distance [L]
X-machine = cross machine
z = depth in z-direction (positive downward) [L]
z = z-score
α = diffusivity [L T^{-1}]
α = significance level
γ = psychrometric constant [M L^{-2} Θ^{-1}]
Δ = slope vapor pressure curve [M L^{-2} Θ^{-1}]
θ = moisture content
θ_{FC} = moisture content at field capacity
θ_i, θ_r, θ_s = initial, residual, and saturated soil moisture content
λ = pore size distribution index
μ = population mean
σ = population standard deviation
ψ = effective suction at the wetting front
ψ = permittivity [T^{-1}]

INTRODUCTION

Problem Statement

Stormwater runoff is part of the natural hydrologic cycle in a watershed and can become a source of valuable water (Wanielista and Yousef 1993). However, stormwater runoff is a significant nonpoint pollution source to receiving surface water bodies (Beier 1992). The United States Environmental Protection Agency (USEPA 1996) estimates soil erosion to be the biggest contributor to nonpoint source pollution in the United States. Erosion from construction sites are 10 to 20 times the preconstruction, natural vegetative state (Fifield 2004). Runoff sediments from unprotected construction sites are about 150 to 200 tons per acre per year, and the average natural rate of soil losses is approximately 0.2 tons per acre per year (Smoot et al. 1992).

Sediments from stormwater runoff have been identified as a major contributor of pollutants to surface water and a dominant form of soil loss, by regulatory authorities (USEPA 1996). Surface water bodies across the United States are becoming more frequently damaged by sediment than any other pollutant (Hayes et al. 2005). It is estimated that over four billion tons of sediment are carried to ponds, rivers, and lakes with approximately one billion tons discharged into the ocean, and approximately 10 percent of this comes from erosion occurring at construction sites in the United States (USHUD 1970). Sediments are laden with pollutants which, when deposited, results in costly damage to aquatic areas, private and public lands. Sedimentation impairs the water quality in streams, rivers, reservoirs and lakes, and harm or kill fish and other wildlife, negatively affects recreation, wetlands, or other cultural resources (Peluso and Marshall 2002; Hayes et al. 2005).

The need to control pollution of natural water bodies and the consequent effect to aquatic life and recreation have led to increased concern by federal, state and local authorities. Thus, efforts have been geared towards the control of stormwater discharges with emphases on quantity (drainage and flood control) and quality (sediment and erosion control). These efforts are evident in the promulgation of the Federal Water Pollution Control Act of 1972, expanded by the Clean Water Act (CWA) in 1977 to regulate point source discharges. Subsequently, the Act was amended by the Water Quality Act in 1987 to establish the Nonpoint Source Management Program. In addition, the Environmental Protection Agency (EPA) requires state governments to set priorities for cleaning impaired waters by the establishment of the Total Maximum Daily Loads (TMDL). The TMDL is defined as the maximum amount of pollutant that can be discharged into receiving water body and still meet water quality standards (USEPA 2007). Both CWA and TMDL processes promote the concept and the practice for prevention of pollution at source and treatment of polluted runoff.

Silt Fence Fabrics and Polyacrylamide

The experimental research on sediment control was designed to reproduce silt fence application practices on construction sites. The goal was to provide performance standards to evaluate the use of silt fences as perimeter sediment barriers. Previous research studies do not provide a comprehensive performance evaluation of silt fence fabric installation and operational stability, and its effectiveness during and after a storm event or a series of storm events. Results from the experimentation program could potentially demonstrate filtration performance and hydraulic properties of silt fence under varying stress and site slope conditions. In addition, the

findings would shed light on the effects of installation and maintenance programs on silt fence to control runoff water quality.

There is seemly a relationship between the strain on the fabric, topography, particle size distribution, fabric pore opening, fabric type, fence installation, and the hydraulic properties to performance efficiency. Firstly, the research seek to establish all factors that influence the relationship in order to provide an enhanced analytical tool to aid in design, application and regulation. Secondly, silt fence fabric alone in its current practice does not always achieve the TMDL criteria for surface water discharge and may require secondary sediment control measures such as polyacrylamide (PAM) for erosion control and post-treatment of site runoff. Current regulatory requirements for PAM application rates are not supported by any comprehensive study on the site-specific dosage determination protocol. The study is designed to evaluate PAM testing protocol to determine dosage testing requirement that is capable of achieving target performance standards for pollution reduction. Finally, to determine an effective PAM application rate that can be achieved and deployed by operators in the field to enhance runoff water quality.

Model Development

Stormwater harvesting model development is based on previous studies and practices on the use of harvested stormwater from wet detention/retention ponds (Wanielista et al. 1988; Wanielista and Yousef 1993). The essence of these studies was to reduce pollutant discharged into receiving surface water bodies and the resultant economic benefits derived from the harvesting process. However, the current analysis and design approach is still under

development. The practice for stormwater harvesting pond analysis and design is based on regional historical rainfall data; it ignores contribution from groundwater, pond surface evaporation and rainfall; uses a constant harvesting rate; and is not site specific. The current practice can only achieve long-term averages because of different yearly rainfall data and does not provide means for the assessment on pollution reduction by volume.

The availability of water in the harvesting pond strongly influences the harvesting process. Thus, the mechanism of surface and subsurface water movement in the catchment area contributing to the pond needs a modeling tool that predicts accurate estimation of pond water volume available for harvesting and discharge to maintain pre-development water movement. The present state of science requires the use of numerical models for mapping the spatial characters of the catchment area and pond. However, economical and computational difficulties in sourcing the data needed to implement such an elaborate effort have discouraged research and application. The accurate prediction of the water movement through deterministic modeling processes become relevant when considering pond water harvesting as a stormwater management system. This study presents the development and application of a mathematical model for the stormwater harvesting pond with respect to examining the influence of both surface and subsurface water movement occurring in the catchment area.

The stormwater harvesting model developed demonstrated that the parameters of groundwater, rainfall, and evaporation cannot be eliminated, and that the harvesting of stormwater could potentially reduce the pollutant discharged. Secondly, the model revealed that there is a limit to the volume of stormwater that should be harvested from a given wet detention/retention pond, beyond which groundwater is depleted by the harvesting process.

There is a nonlinear relationship between the volume of stormwater harvested and the overflow discharged to surface water bodies. The relationship is not only a function of the harvesting volume but other factors, to be investigated, in varying degrees of influence. The goal is to establish all factors that influence this relationship in order to provide an enhanced design aid.

In summary, a research study was conducted to provide insight on silt fence fabrics effectiveness in sediment transport control; inherent problems associated with the performance of silt fence as a temporary sediment detention barrier. These problems include silt fence installation operationally stability; fabric apparent opening size, and flow-through-rate. The study was on the evaluation of the industry standard woven fabric and a nonwoven silt fence fabric, and comparison of both fabrics' performance standards. Furthermore, the research sought to provide PAM product dosage requirement limits; and its determination in the field. Finally, this study investigated the effects of stormwater harvesting to drawdown of groundwater (safe yield); the effect of harvesting rate to stormwater harvesting pond discharges; and the predictability of stormwater harvesting ponds performances and uses.

Research Objectives

The objectives of this research were to investigate the effectiveness of existing pollution control mechanisms separately, and the effectiveness of the combination as a treatment train to achieve the goal of pollution controlled discharges from construction sites. The research was separated into three specific pollution reduction treatment approaches. First was to conduct experimental studies, both in the laboratory to identify the index properties and field simulation of rainfall events for performance efficiency of silt fence fabrics. The results from both

laboratory and field-scale tests were evaluated to compare the performance efficiency of two silt fence fabrics separately. The second was to conduct laboratory tests on the efficiency of PAM and develop sediment removal efficiency and dosage determination testing protocols. And thirdly, to develop a deterministic model for a stormwater harvesting pond that simulate the runoff volume, harvesting rate, and storage volume based on the hydrologic cycle of the watershed with emphases on the pond water balance.

The first two sections of the study were intertwined into one and involve comprehensive experimental testing for a wide range of silt fence applications at construction sites. The silt fence fabrics investigated were the woven monofilament geosynthetic (ARS-1400) and belted silt retention fabric (BSRF) silt fence geotextiles. The ARS-1400 is the most commonly used silt fence fabric, while the BSRF is a new product expected to achieve higher performance standard. Further considered was the dosage determination for PAM products for use with silt fence to enhance the performance efficiency. The objectives of the combined section in the study are categorized as:

1) experimental evaluation of the index properties of geosynthetic silt fence fabrics and comparison to minimum specifications
2) field-scale testing of silt fence fabrics on a tilting test-bed using a rainfall simulator to evaluate the field performance, operational stability, filtration, and flow rate
3) relate field scale testing performance to index properties of silt fence fabrics
4) development of standard test procedure on PAM dosage in the field for site specific conditions.

The third section of this study is on the development and application of a mathematical model for a stormwater harvesting pond, when there is the potential for both surface and subsurface water movement occurring into and out of a pond in a catchment area. The model, Stormwater Harvesting and Assessment for Reduction of Pollution (SHARP) is based on the interaction between the pond water storage and subsurface water. The model is designed to simulate the interaction of the overall pond water balance and the catchment area geologic and hydrologic data; predict downstream flow; and account for the effect groundwater seepage on the pond water quality and quantity. In addition, the model aims to predict the percentage of runoff into a wet detention pond that is not discharged (capture volume) and the groundwater contribution to harvesting. Calibration and validation of the model was performed to assess the hydrologic behavior and performance by comparison of observed and simulated data at Miramar Lakes, Miramar, Florida.

Significance of the Study

The goal of this study was to develop an effective sediment treatment train that uses silt fence and/or PAM on construction sites that can reduce runoff pollutant loadings to meet the TMDL requirements. The study also aimed to establish the relationship between the flow rate and fabric performance over time. The findings of this research may be a valuable resource shedding light on the actual performance of silt fence fabric with or without PAM enhancement for the regulation and implementation of sediment control measures on construction sites vis-à-vis the current practices for both the research and engineering community. The solutions proffered will also be useful for upgrade to best management practices (BMPs), establish realistic performance standards, and improve training programs for consultants and contractors.

The research would further develop a stormwater harvesting model to simulate the hydrologic processes of water movement in a catchment area, establish the relationships that exist based on sound mathematical principles of surface and subsurface flow to predict stormwater discharge from stormwater harvesting ponds. The relevance of the model is that it offer an analysis and design aid for stormwater harvesting pond on the principle of the hydrodynamics in a porous media to describe stormwater discharge control.

The study combines non-structural and structural BMPs geared towards pollution prevention activities and habitat preservation. Non-structural refers to silt fence fabric and PAM use, while the structural refer to the stormwater harvesting pond. The combination of these BMPs would provide a sediment treatment-train to meet the necessary reduction in pollutant loading requirements and further reduce the damaging effects of discharging sediment pollutants into receiving water body. The reduction efficiency of the silt fence barrier combined with the effect of PAM would significantly reduce the sediment loading to the stormwater harvesting pond, which would make stormwater harvesting quality safe and discharges from the pond meet the TMDL requirements, both by quantity and quality, into water bodies.

Organization of the Dissertation

The research was designed to investigate the effectiveness of effluent control mechanisms and products from construction sites. In addition, to develop a mathematical model aimed at forecasting stormwater pond discharge volume by the harvesting of stormwater runoff stored in detention ponds for irrigation, and account for storage for specified time period in the pond, soil water and groundwater. To achieve the purposes of the research an introductory

chapter is presented that discusses the research problems, objectives, the significance of the study, and dissertation organization.

The second chapter provides extensive review of the relevant literature on stormwater harvesting pond, urban hydrologic modeling efforts, application and testing of polyacrylamide dosage requirements as an addition to sediment control barriers, and the application and performance efficiency of geotextile as sediment control barriers. The reviewed literature were on silt fence fabric types, textures, index properties, field and simulated tests, silt fence barrier designs, and operational stability of the system. Further literature reviews were on PAM products, testing protocols, dosage recommendation, and effectiveness in turbidity removal. And finally, detailed examination on hydrologic models, stormwater harvesting studies and modeling efforts, and operation of stormwater harvesting ponds. The purpose for the review was to provide insight on the researched topics to establish or confirm findings of previous studies and to relate the scientific facts to infer solutions to new problems, approach to existing problems, or to develop new theories associated to the study on hydrologic modification and effluent discharge.

After the literature review, the research is split into three chapters that presents and discusses independent but related studies on the effective reduction of pollutants discharged into receiving water bodies. The first study, which is presented in the third chapter, is on laboratory experiment on the index properties for both silt fence fabrics and to establish actual index properties for the field-scale testing. The second part of this chapter is on experimentation to develop a repeatable testing protocol to aid the determination of PAM dosage requirement by establishing the mixing energy through flow rate and contact time with the sediment-laden water. This involved the experimental investigation of various PAM products mixing rate and

performance efficiency for two sources of sediment-laden water – sandy and silty sand soil types. The variables for the PAM dosage testing were concentration, mixing rate and contact time related to flow rate, and filtration/non-filtration of PAM-mixed-with-sediment-laden water – to simulate filter fabric usage. The results were analyzed to establish recommended testing protocol for PAM dosage based on flow rate and contact time.

Chapter four discusses the field-scale testing on silt fence conducted on a tilting test-bed with simulated rainfall of different intensities to investigate performance efficiency and operational stability for both woven monofilament geotextile and nonwoven geotextile. The experimental study involves 96 series of field-scale tests for different rainfall intensities and events, and embankment slopes on non-cohesive soil. Records of field-scale test data and visual examination using photographic images, where necessary, are presented. Photographic visual evidence was inspected for fabric stress and system failures. A total of 1,745 water quality samples from field-scale experiments were analyzed for sediment concentrations and turbidity removal efficiency, and nonparametric statistical analyses conducted on all collected data. The findings from the tests were presented to evaluate the performance efficiency, determine the flow-through-rate of the filter fabrics, and compare both silt fence fabrics performance standards. Sensitivity analyses were conducted by varying the rainfall intensity, event, and embankment slope to investigate the parameter(s) that would significantly affect performance of the silt fence fabrics. Finally, the field-scale test findings and index properties were evaluated to test the validity of using index properties to classify and regulate silt fence fabrics.

The third independent study presented in chapter five discusses the design and development of stormwater harvesting model that provide a real time forecasting tool to estimate

impervious runoff volume, pond storage volume, and the volume of harvesting water required. The model is based on the hydrologic cycle of the watershed with emphases on the pond water balance to aid design. The model is capable of controlling pond discharge; predicting the volume of water available for harvesting and the subsequent discharge volume; and simulating runoff volume, harvesting rate, and storage volume.

The mathematical model predicts the percentage of runoff into a wet detention pond that is not discharged (capture volume) based on the water budget of the contributing area. The model was calibrated and validated to evaluate its capability to simulate measured parameters and evaluate the model performance evaluation. Model evaluation was conducted by using the root mean square error (RMSE), mean absolute error (MAE) and Index of agreement (d). Presented to evaluate the model efficiency and predictability of actual measurement of pond parameters were time-series plots and scatter graphs of observed data and simulated values. Further presented in this chapter were model graphic outputs on pond discharge volume reduction, harvesting rate and volume, and the effect of drawdown on groundwater.

Chapter six presents a general discussion to relate the three independent studies presented and discusses the combined effects of silt fence fabrics and PAM in pollutant reduction. Additionally, it discusses the combination of factors that compromise the operational stability and performance of silt fence, the limitations and areas of improvements of the current practice of silt fence installation, use, and design. Furthermore in this chapter, there is a discussion on the establishment of a treatment train that links the performance of the silt fence and stormwater harvesting pond and evaluate the efficiency on performance standards.

The seventh and final chapter presents the conclusions and recommendations to assist regulators and designers to choose appropriate silt fences fabrics and applications for construction sites erosion and sediment control plans; the adoption of PAM enhanced silt fence practices; and the provision of a scientific modeling tool to predict the performance of stormwater harvesting pond and safely plan the harvesting of the stormwater. It also presents recommendations for future work on these topics.

LITERATURE REVIEW

The problems associated to stormwater runoff (erosion and sedimentation) have led to the development of numerous best management practices (BMPs). The use of any one or combination of any BMP depends on site conditions and the objective(s) such as: water quality protection, flood control, aquifer recharge, and/or volume control. This study looks at a mix of a hydrologic modification approaches related to the amount of water on a watershed (irrigation) and effluent control from construction sites to target performance standards in pollutant reduction.

Stormwater ponds are one of many effective techniques adopted for pollutant removal from the collected runoff prior to discharge into receiving water body (Wanielista et al. 1988; FDEP 2007). Stormwater ponds are structural stormwater controls that allows for the detention or retention and slow release of stormwater runoff from a pond into surface water bodies. The detention of the stormwater runoff allows for settling of the suspended pollutants to the pond bed prior to release through a control mechanism (FDEP 2010). The various types of the stormwater ponds available are extended dry, wet detention pond, and retention pond. These ponds are designed to remove pollutants and control flooding among other benefits. Researchers have shown pollutant removal effectiveness of urban stormwater treatment practices (Schueler 1994; Schueler 1996; Harper and Baker 2007) limitations in removal of specific pollutants (Kehoe 1993; Kehoe et al. 1994) community acceptance as aesthetics and longevity.

In addition, ponds mitigate downstream flooding problems by attenuation of the peak rate of flow. However, the ever increasing rate of urbanization and the consequent construction activities results in increased watershed imperviousness (Heitz et al. 2000; Elliott and Trowsdale

2007). Impervious surfaces result in increased volume of runoff, pollutant mass to the pond, and subsequent discharged downstream. Schueler (2000) listed the associated environmental impacts on the receiving water bodies as downstream temperature regimes, downstream bed load movement, downstream dry weather water quality, downstream tropic shifts, upstream fish passage, upstream channel degradation, and destruction of riparian cover and wetlands.

The mitigation of some problems listed above involves a likely modification of the hydrology of the watershed by detaining the water prior to discharge. Hydrologic modification of the watershed may include the harvesting of some of the detained pond water for irrigation and infiltration of pervious areas in the contributing watershed. Wanielista (1993) describes the basic process of stormwater harvesting as the capture and storage of stormwater runoff in a harvesting pond and pumped back gradually to irrigate adjacent pervious areas. Water from stormwater harvesting is proven as environmentally and economically beneficial (Wanielista and Yousef 1993). Harvesting ponds reduce the volume of discharge and consequently release less pollutant load downstream. Furthermore, it increases pollutant removal efficiencies and groundwater recharge as substantial volume of annual stormwater runoff is returned to the watershed.

In addition to modeling stormwater harvesting pond, it is equally essential to prevent or reduce the sediment loading from construction sites within a pond contributing area. To achieve the reduction of sediment loading from disturbed lands various construction site BMPs are available and in use to limit surface runoff volumes and reduce water runoff pollution loadings. The combination of adequate site control BMPs and an effective stormwater harvesting pond would effectively reduce the pollutants discharged to surface water bodies in any watershed. Commonly used erosion and sediment control measures are erosion control blankets (ECB),

temporary vegetation, mulch, silt fences, straw bales, rock filter dams, and sediment ponds. The minimal erosion and sediment control measures required in most instances are perimeter controls (silt fences and straw bales) and tracking pads (crushed stone or gravel at vehicle access points) (FDEP 2008).

A silt fence, one of the temporary sediment controls, is a geosynthetic material installed to control sheet flow from disturbed lands by the creation of a small containment system that reduces the runoff velocity and allows for the deposition of suspended particles (Wanielista and Chopra 2010). There are numerous silt fence fabrics available, but the commonly available and accepted silt fence is the traditional monofilament geosynthetic used at most sites having construction activities shown in Figure 1. Studies on this type of silt fence have shown frequent failure to achieve the required performance target (Barrett et al. 1998; Wishowski et al. 1998; Faucette et al. 2009).

Figure 1 Woven silt fence fabric installed on a tilted test bed

In response to these findings, a nonwoven belted silt retention fabric (BRSF) is introduced by Silt Savers, Inc., shown in Figure 2. The BSRF is designed to retain more silt and reduce turbidity and suspended solids than the traditional woven monofilament silt fence fabric (Risse et al. 2007). However, proper installation and regular maintenance are essential to successful removal of sediment from runoff by any type of silt fence (Kouwen 1990; Barrett et al. 1998).

Figure 2 Nonwoven (BSRF) silt fence fabric installed on a tilted test bed

Efficiency performance evaluations proves that silt fence, a temporary sediment control, alone is not effective in removing sediment from runoff waters, especially clay and fine silt particles, due to inadequate detention time for settling (Arjunan et al. 2005). The performance efficiency can be improved upon by properly applying site-specific polymers to surrounding area drain and covering the soil with a layer of jute fabric; installing polymers inside and/or upstream

of water conveyance devices to treat runoff after passing through temporary barriers; allowing runoff water flow over and around polymers placed within drainage channel with check structures; and covering rock check structures with jute fabric that has been applied with site-specific polymer (Wanielista and Chopra 2010).

Silt Fence

Studies have demonstrated that the amount of sediment transported by stormwater runoff from large construction sites with no erosion control practices in place is significantly greater than from sites with erosion controls (USEPA 1999). This is not only true for large construction sites but is also evident in small construction sites (less than five acres). Research shows that during active construction, the average event mean concentration (ECM) of solids increased dramatically when compared to pre-construction and post construction, which is an indication that the construction phase is the most active phase (Owens et al. 2000).

To minimize soil losses regulatory agencies require erosion and sediment control at construction sites and post construction plans. Operators of construction sites engaged in clearing, grading, and excavating activities that disturb one acre or more are required to obtain the National Pollutant Discharge Elimination System (NPDES) permit for their stormwater discharge (USEPA 2009). Silt fence is a perimeter control intended to intercept and retain small amounts of sediment from disturbed areas during construction operations prior to off-site discharge. It is one of the most visible and maintenance-intensive best management practice (BMP) on an active construction site (Kouwen 1990).

A silt fence is a vertical temporary barrier made of geosynthetic filter fabric installed along the perimeter of disturbed lands or exposed surfaces to control sediment-laden sheet flow from leaving the site (FDEP 2008). The geosynthetic filter fabric is stretched across and attached to supporting wooden or steel posts and entrenched vertically into the soil. The function of silt fence is to decrease the velocity of sheet flow or site runoff, detain the water to allow for settling of suspended solids, and retain sediment on site. Silt fence does not filter sediment out of runoff water except for larger particles of sand (Barrett et al. 1998). However, its effectiveness is dependent on the ability to create small containment system to allow for deposition of suspended particles in the water (Risse et al. 2007; FDEP 2008). To achieve an acceptable level of effectiveness, proper installation and maintenance is important to reduce the chances of failure such as undercutting, end runs, holes and tears, over-topping, and fence collapse (Kouwen 1990; Henry et al. 1999).

Geotextile Testing Methods

Geotextiles are flexible and porous fabrics made by weaving (woven geotextiles) or by matting (nonwoven geotextiles) of synthetic fibers (Koerner 1997). Geotextiles are designed to enhance soil stability, flow through, media separator, and soil reinforcement. However, the role of geotextiles for erosion and sedimentation control barriers changes to filtration of suspended particles, damming of flowing water to allow for particle settling and yet allow water to flow through (McCarthy 1995). The initial standard test methods adopted were from textiles but have been modified and are continually revised to acceptable field practices (Fannin et al. 1996; Koerner 1997). ASTM D6461 (2007) provide a list of current standard test methods to determine the index properties of silt fence fabrics, namely grab strength (ASTM D4632), permittivity

(ASTM D4491), apparent opening size (ASTM D4751), and ultraviolet stability (ASTM D4355). However, the standard test method (ASTM D5141) for determining filtration efficiency and flow rate could practically predict field performances of geotextiles as silt fence filter fabrics. Research studies on different test methods aimed at the prediction of field performances of geotextiles have been reported and are considered by the relevant ASTM committee on geosynthetics. Available research studies have focused on the ultraviolet exposure, puncture resistance, filtration capability and strength of geotextiles in the field. Geosynthetic material selection and testing method should be based on the application and performance requirements, functions, design method, required geosynthetic properties, and specifications.

Narejo (2003) showed that the ability of a geotextile to retain fines depends primarily on its apparent opening size (AOS), and the AOS recommendations of AASHTO's M288 specification may be unsuitable for proper geotextile application. Study on the relationship between soil uniformity coefficient, particle size, and pore size observed formation of soil particle bridges on the surface of geotextiles as a function of the uniformity coefficient (Watson and John 1999). It is therefore suggested that pore opening size should be a function of the soil particle size, and the opening area influences the clogging potential and flow rate of a filtration system (Faure et al. 2006; Wu et al. 2006).

Geotextiles may not drain water as the index test results shows because laboratory test conditions are different from field conditions (Fourie and Addis 1999). The flow rate through silt fences under field conditions were two orders of magnitude less than would be calculated using the ASTM index property tests (Barrett et al. 1998). The difference in permittivity observed in the flow rate through a silt fence is attributed to the sediment clogging the fabric and from

turbulent flow through the fabric openings at hydraulic heads on the fabrics during use (Henry et al. 1999). In the study on clogging of nonwoven geotextiles under leachate flow, geotextile markedly lost permittivity due to biological clogging which is consistent with the observed biological mechanisms in silt fence (Palmeira et al. 2008). The results suggest that neither the geotextile thickness nor the distance between fibers affected the development of biological clogging.

In other studies on the effect of tensile strain on geotextiles, it was shown that the increase in uniaxial tensile strain increases the pore size distribution and the mean flow rate through geotextiles (Fourie and Addis 1999), and is more pronounced in nonwoven geotextile (Wang et al. 2008). Further research on weathering of textiles demonstrates that degradation is material dependent and not on the thickness of the material. Results reported indicate that weather affects the tensile properties and mass of the materials while thickness remains unaltered (Dierickx and Berghe 2004).

The stability of geotextiles subjected to non-uniform flow and/or puncture is of utmost importance for erosion and sediment control fabrics. Fourie and Addis (1999) discussed silt fence geotextiles that have been exposed to various types of loading and overburden stresses caused by erosion, installation, and during operation. It is generally assumed that the flow through the openings of geotextiles is uniformly one-dimensional, and the retention criterion depends only on geometrical parameters. However, studies show that geotextile filters depend on the applied hydraulic gradient and on the normal effective stress (Cazzuffi et al. 1999), and reveals that the soil particle motion by cyclic loading is different from uni-directional wave loading (Chew et al. 2003). Though, both studies were on buried geotextile for filtration and

simulated cyclic wave regime at coastal revetment application, the direction of loading on silt fence barriers subjected to turbulent flows from runoff is similar a cyclic loading formation.

Silt fence testing should be based on the design, construction, and durability properties and evaluated based on their ability to perform. The quality of the geosynthetic filter material is dependent on the general and physical, index, and performance properties. The general and physical properties of geosynthetic materials are: material type and construction, polymer(s), mass, thickness, roll dimensions, specific gravity, absorption, surface characteristics, and isotropy (McCarthy 1995). These properties characterize the geosynthetic filter material and help define the index and performance properties. General and physical properties can be obtained from the manufacturers and from tests performed using the relevant ASTM standard methods. The index properties are defined as the mechanical strength (uniaxial/asymmetric and rupture), endurance, and hydraulics. The performance (soil/fabric) properties are the stress-strain response under static, dynamic and cyclic loading, creep, friction and adhesion, soil retention, and filtration. Some of these properties may not be relevant to silt fence materials based on its intended use.

Silt Fence Fabric Testing

Geotextiles as erosion and sediment control barriers play the role of providing filtration of soil particles from leaving a site and yet allow the flow of water through them. The effectiveness of geotextile filters depends on the granularity of the protected soil, hydraulic conditions, geometry of the pore network or size distribution of the geotextile, and fabric thickness (Crebbin 1988; Fannin et al. 1996). In addition, certain variables such as strength,

durability and weathering degradation have been of concern to the users of these products. The need to understand the mechanism of geotextiles in erosion prevention and sediment control functions and to adequately predict the field performances of geotextiles has led to studies on the available test methods' ability to predict performance (Fannin et al. 1996; Barrett et al. 1998; Chew et al. 2003; Narejo 2003; Suits and Hsuan 2003; Risse et al. 2007; Chopra et al. 2010). The index properties of interest in a silt fence are: grab tensile strength, ultraviolet (UV) stability, apparent opening size (AOS), and permittivity tests. The geosynthetic industry has found that the determination of strength based on ASTM Standard index test methods adopted in the 1970s could not provide reliable prediction of a geosynthetic field performance (Crebbin 1988; Barrett et al. 1998; TenCate 2009).

Research on the effectiveness of silt fence has demonstrated the strong need for further studies on field-scale performances. Laboratory studies by Wyant (1981) showed no observable trend of water permeability and filtration efficiency for seven filter fabrics. The filter fabrics acted like dams and cannot be subjected to high flow rates. The silt fence losses functionality after three storm events greater than 12.7 mm (0.5 inch) rainfall and most clay-sized particles passed through because the particle settling rate is approximately 0.14 m/hr. These results suggest that the filter fabrics acted more of a dam than a filtering device. However, nearly 100 percent of sand-sized particles were retained on all fabrics, and the accumulation of the soil particles influenced the retention ability of every fabric. Kouwen (1990) describes geotextiles as effective filtration fabric, and less permeable fabrics results in greater efficiencies with potential for clogging and over-topping. Generally, Fisher and Jarrett (1984) concluded that a compromise is necessary between a fabric's ability to retain soil particles while transmitting water for any

fabric system in contact with detached soil particles. A fabric filtration efficiency is a function of both the geotextile characteristics and suspended sediments, as apparent opening size does not effectively indicate the filtration efficiency performance of silt fence fabrics (Crebbin 1988).

Previous field investigations on the performance of silt fences as sediment control systems demonstrated the effectiveness of silt fence fabric in reduction of total suspended solids (TSS), but it was found to be less effective for settleable solids and turbidity (Horner et al. 1990). On the other hand, Barrett et al. (1998) showed that filtration was insignificant in the removal of solids concentrations, and the removal was mainly due to the particle settling behind the silt fence. In addition, efficiency performance was mainly due to detention time, which is a function of the geometry of the upstream pond, fabric hydraulic properties, and silt fence maintenance. Wishowski et al. (1998), showed that sediment transport is initiated at the commencement of inflow which significantly clogged the fabric and results in rapid rise in backwater height. The trap efficiency decreased as particle size became smaller and was not significantly affected by flow rate but by influent concentration.

Most of the previous studies were performed using flumes; test beds with fixed slopes; or monitored storm events. For the monitored storm events, samples were collected after each storm event from standing pool upstream and downstream of the silt fence. While these studies have provided insight into the performance of silt fence fabrics, an active storm event would definitely impact the performance of the fabrics in turbidity and sediment concentration reduction. To this end, the present study investigated active rainfall events at different intensities and embankment slopes to evaluate the real time performances of silt fences.

Silt Fence Review Summary

Review of literature related to silt fences demonstrated that these fabrics remove solids by sedimentation and filtration and their efficiency performance is a function of the particle size distribution of the runoff characteristics, fabric properties, and installation and maintenance. The flow rate through a nonwoven geotextile is further influenced by the porosity of the material and tortuosity of the flow path, which becomes meandering and thus, longer.

Generally, silt fence materials are characterized by their permittivity and apparent opening size measured using the ATSM standard methods, but researchers have shown the limitations of these standard methods. The ASTM standard test methods are not appropriate for field estimation of sediment removal or hydraulic performance due to clogging and flow characteristics at the field. It is imperative to note that loading on the silt fence fabric induces strain that results in larger pore opening and influences the flow rate through the silt fence. This would eventually affect the sediment particle size that passes the silt fence and generally the performance efficiency. Finally, silt fence was unable to attain the 75 percent removal efficiency recommended (FDOT 2006) and would therefore need additional treatment measures to combine with it in order to achieve this target. One such treatment measure considered in this research is polyacrylamide, which is recommended as a secondary treatment train for sediment removal (Hayes et al. 2005; Iwinski 2010).

Polyacrylamide Application and Dosage Testing

Exposed land surfaces in construction sites increase the potential for soil erosion, high runoff volumes and velocities, and sediment losses. FDEP (2008) listed control measures for the

mitigation against soil losses, by increasing infiltration and decreasing erosion, as follows: mulches, erosion control blankets, hydroseed, and other soil amendments that cover and protect the exposed soil surface. Polyacrylamide (PAM) is one of such products introduced to increase infiltration, reduce runoff volume and eventually decrease soil erosion. PAM use on construction sites have been shown to reduce runoff sediment by 60 to 70 percent (Roa et al. 1998), is effective at 5 parts per million (ppm) sediment concentration and exhibits more than 90 percent reduction in runoff sediment (Orts et al. 2000), and can be used on steep slopes to reduce runoff and erosion (Flanagan et al. 2002).

PAM is a high molecular weight polymer and is widely used to control erosion in furrow irrigated agriculture (Lentz et al. 2000). It is currently recommended by local agencies to reduce turbidity of runoff water from construction sites (FDEP 2007). PAM increases cohesion, strengthens soil particles bonding and flocculates the suspended particles in the solution; thereby creates larger aggregates and as a result decreases the transportability and facilitates settling of suspended particles (Soupir et al. 2004). Flocculation is essentially an aggregation process assisted by organic electrolytes such as polymers (Iwinski 2010). The main intent is to settle the suspended colloidal particles in water/wastewater quickly, which typically settle slowly under normal conditions.

Numerous investigations on the application of polyacrylamide (PAM) for sediment reduction reveal varying results, but collectively allude to the need to change the dosage recommendation of State and/or manufactures to achieve effective turbidity removal efficiency. Hayes et al. (2005) showed that the isolated application of PAM (APS 705) or the combined application of PAM and mulch have no statistically significant effects on turbidity and runoff for

any storm event, even though increasing the rate of application tend to lessen turbidity and sediment loss. However, McLaughlin et al. (2009) found that PAM (APS 705) combined with fiber check dams (FCD) resulted in significant reductions in total suspended solids (TSS) and turbidity, which was well below 50 and 10 Nephelometric turbidity units (NTU) for powdered PAM and granulated PAM, respectively. The study by Faucette et al. (2009) on the effectiveness of PAM combined with compost filter socks sediment improved the performance efficiencies with respect to TSS and turbidity. Soupir et al. (2004) stated that the most effective TSS concentration removal treatment, in order of efficiency, are straw mulch, hydro-seeding and dry PAM, but that increasing the dosage of aqueous PAM reduced the runoff volume while dry PAM increased the runoff volume. Ersoy et al. (2009) study indicated that more PAM dosage does not translate to higher turbidity reduction, but that minimal dosage is more efficient (Arjunan et al. 2005) which is related to the ionic charges of the polymer and the soil water.

The application of PAM on soil surfaces for erosion control improves infiltration rate by increasing inter-particle bonding resulting from long polymer chains (Yu et al. 2003). The improvement in aggregate stability at low PAM dosage is attributed to polymer charge density, soil moisture content, and the type of exchangeable ion (Soupir et al. 2004). In addition, PAM does strengthen soil aggregates and flocculates suspended particles which create larger aggregates to settle down out of solution faster (Barvenik 1994; Trout et al. 1995).

PAM used for water clarification essentially causes suspended particles, bacteria, and viruses in water to aggregate into clumps or masses that falls to the bottom of the water column. The aggregate clumps or masses can be removed by filtration or other means considered necessary and effective. This process is described as coagulation which is the removal of

colloidal particles and subsequently flocculation, the aggregation of smaller particles into larger mass that can be readily removed. The typical intent is to settle the suspended colloidal particles in water/wastewater faster than the rate of settlement under normal conditions. In the process of coagulation positive charged ion is introduced into water to reduce the repulsion of surface charge particles (Trout et al. 1995; Lentz et al. 2000; Soupir et al. 2004). PAM, an anionic polymer, act as a coagulant that neutralizes the cationic molecules without the aquatic toxicity potential associated with some other cationic coagulants (FDEP 2007).

Polymers have been included in recently developed specification for erosion and sediment control in Canada and similar specifications have been adopted in the United States. Studies have determined that polymers are effective for several applications related to erosion and sediment control and are recommended for use on construction sites (Flanagan et al. 2002; Arjunan et al. 2005; FDEP 2007; Iwinski 2010). In view of this recommendation, there is a need to conduct index testing related to the performance of polymers dosage specification. The performance is evaluated by measuring turbidity, in terms of Nephelometric turbidity units (NTUs), for determining the polymers' effectiveness in the reduction of turbidity.

PAM Application Review Summary

The understanding from the review of the literature on polyacrylamide points to the observation that it does reduce turbidity and sediment load, increases infiltration, and reduces runoff and erosion. However, the application rate recommended by regulatory agencies may not be adequate for the effective performance of PAM. In addition, there may be an optimal PAM application rate beyond which there will be no significant gains in efficiency, but rather an

increased possibility for higher toxic effects. The increasing popularity of PAM within the industry forces the need for a more regulated implementation. By doing so, one can associate PAM reaction (contact) durations and dosages to obtain a desired turbidity removal efficiency. This brings up the questions of the dosage that is adequate for certain application purpose and is also safe to the environment when discharged.

Urban Hydrologic Model Development

Urbanization involves the physical growth of a habitat that results in more impervious surfaces with the consequent adverse effects of increase flooding, loss of vegetation, erosion, and water quality degradation (Hammer 1972; Schueler 2000; Paul and Meyer 2001; USEPA 2010). To address these problems, several urban water management tools are developed and used to bring about improvement in the environment and socio-economic life. The increase rate of urbanization and the consequent construction activities results in increased watershed imperviousness. Imperviousness results in an increased volume of runoff and pollutant mass to the pond and subsequent discharged downstream. This section of the study reflects on the stormwater management tools designed to mitigate the damaging effects on water quality and quantity. Furthermore, it considers modeling efforts geared towards combating the associated problems from urbanization, using structural BMPs such as retention/detention ponds.

Watershed Models

Hydrologic models of one-, two, and three-dimensions are designed with different approaches to modeling a watershed in order to mitigate against the adverse hydrologic and water quality effects of urbanization (Elliott and Trowsdale 2007). Most watershed models are

based on distributed hydrologic and hydraulic parameters. Hydrologic models apply the fundamental physical relationships based on theoretical concepts for the hydrology of a watershed. This approach to modeling tends to provide more information on the variability in the movement of water in both space and time within a watershed. Watershed models are typically designed to describe the physical and chemical processes of hydrology, environmental pollution, erosion and sedimentation, and/or agriculture by water based concepts (Schroeder et al. 1994; Ahuja et al. 2000; Elliott and Trowsdale 2007). The watershed models are driven by precipitation, land-use, impervious areas, slope, soil characteristics, and drainage (USEPA 2010). Models of the nature described above provide platforms for the study of hydrologic impact from changes in land uses and climate; and are effective tools to forecast pollutant and sediment movements.

Elliott and Trowsdale (2007) reviewed and compared the relevance of ten models to low impact development urban stormwater drainage systems and recommended the need for further modeling efforts in stormwater models. Recommendations included are to broaden the range of contaminants; and consider the transport and treatment of contaminants, baseflow and runoff components, and catchment scale testing of model prediction. Brief descriptions of some of the commonly used hydrologic and water balance models by the United States Environmental Protection Agency (USEPA) are presented.

Better Assessment Science Integrating point and Nonpoint Sources (BASINS) is an open source multipurpose environmental analysis system for water quality assessment model (USEPA 2007). It is developed to describe the process of watershed nonpoint and point source pollution transport and fate by the integration of geographical information system (GIS), watershed data,

and high-tech environmental assessment and modeling tools. The Watershed Assessment Model (WAM) assesses watershed related properties such as land-use, soils, climate, topography, hydrograph, basin and sub-basin boundaries, and point source and service coverage areas to simulate a variety of physical and chemical processes (USEPA 2010). Next, the Watershed Modeling System (WMS) is a tool that provides a comprehensive graphical modeling environment for all phases of watershed hydrology and hydraulics. The WMS interface is separated into modules that allow for the creation and manipulation of several data types.

Another model by USEPA (2010) is the Storm Water Management Model (SWMM), which is a dynamic rainfall-runoff simulation model used for single event or long-term simulation of runoff quantity and quality from primarily urban areas. SWMM runoff component operates on a collection of sub catchment areas that generates rainfall and runoff, and tracks the quantity and quality, flow rate and depth, and quality of water in the conveyance during a simulation period. The model accounts for time-varying rainfall, standing water evaporation, infiltration into unsaturated soil layers, percolation into groundwater layers, interflow between groundwater and drainage system, and nonlinear reservoir routing of overland flow.

The United States Geologic Services (USGS 2012) have different models that simulate watershed hydrology namely PRMS and HSPF. Precipitation-Runoff Modeling System (PRMS) is a modular-design, deterministic, distributed-parameter modeling system. PRMS evaluates the impacts of various combinations of precipitation, climate, and land use on streamflow, sediment yields, and general basin hydrology on soil-water relationships, sediment yields, and groundwater recharge. The HSPF (Hydrological Simulation Program—Fortran) is designed to simulate the hydrologic processes on pervious and impervious land surfaces, streams, and well-

mixed impoundments for extended time periods. HSPF uses rainfall and meteorological data to account for soil moisture, surface runoff, interflow, base flow, evapotranspiration, and groundwater recharge in the watershed area.

Other models designed to simulate and accounts for surface runoff in a watershed are HEC-1 (HMS), TR-20, TR-55, and GSSHA. HEC-1 is a lumped parameter model designed to simulate surface runoff from a single precipitation event with options for modeling rainfall, losses, unit hydrographs, and stream routing. TR-20 and TR-55 are designed by National Resources Conservation Service (NCRS) to estimate surface runoff from natural or synthetic rainstorm events, or surface runoff in small, urbanized watersheds, respectively. TR-55 utilizes the soil conservation services (SCS) runoff equations to predict the peak runoff rate and the total volume, provides a simplified tabular method for the generation of complete hydrograph based on the TR-20 calculation techniques (USDA 2008). Gridded Surface Subsurface Hydrologic Analysis (GSSHA) is a two-dimensional model designed for analysis of surface runoff, channel hydraulics, and groundwater interaction, and supports water quality and sediment transport (USACE 2011). GSSHA simulates the different processes of runoff generation and determines the controlling physical processes in a watershed, such as infiltration, saturated source areas, and groundwater discharge.

Stormwater Harvesting Process

Stormwater harvesting is the process of harvesting of detained/retained stormwater runoff within a watershed pond for irrigation and infiltration into adjacent pervious area. Frequently these areas are within the same watershed. It further has the potential to increase groundwater

recharge as a substantial volume of annual stormwater runoff is returned to the watershed. There are other uses for harvested stormwater that do not return water to the pond, such as cooling tower make-up, car washing, and other waste water carriage. A stormwater harvesting pond is designed to harvest the fraction of runoff volume in a wet detention pond for non-potable uses (Wanielista and Yousef 1993). The fraction available for harvesting (harvested volume) is considered the temporary storage volume and is below the flood control discharge invert elevation. It is necessary to note that the harvesting system is likely to deplete the permanent pool volume below a discharge control elevation, and at some times, supplementary water volume may be required to maintain the volume. Presented in Figure 3 is the schematic of a typical stormwater harvesting pond cross section. Wanielista and Yousef (1993) presented the methodology and design criteria for the harvesting volume.

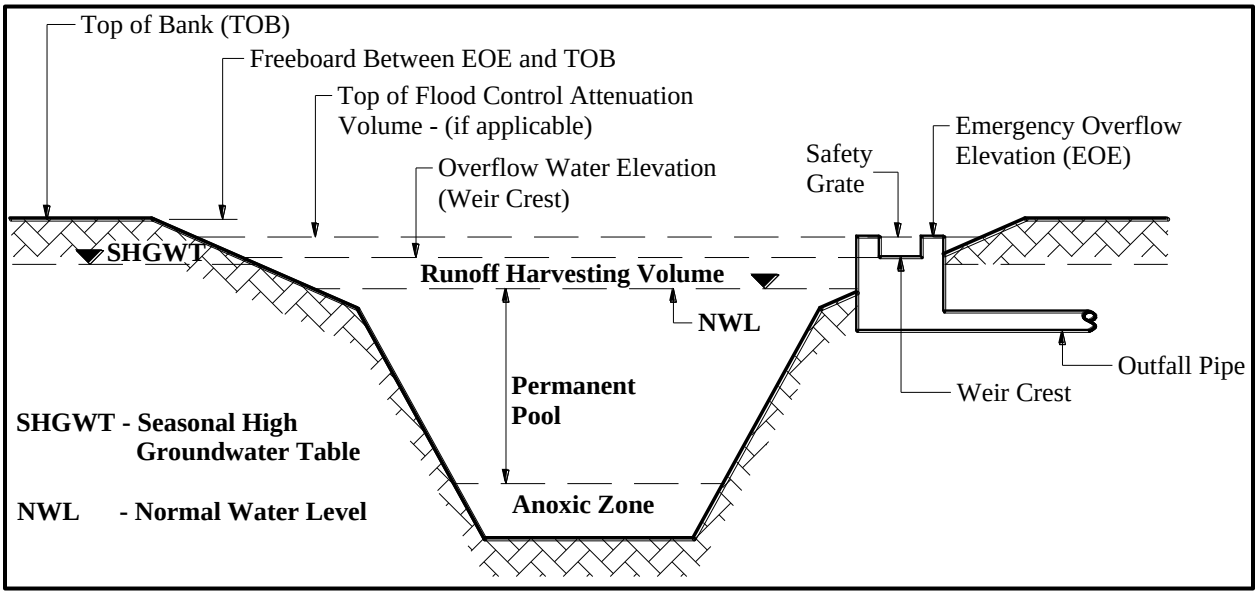

Figure 3 Schematic of stormwater harvesting pond

Stormwater Harvesting Pond

Numerous studies have been conducted on the need to use stormwater runoff and the benefits from such activity (Heitz et al. 2000; Clark et al. 2002; Jaber and Shukla 2005; Seymour 2005; Hwang and Draper 2006). However, only few publications useful in predicting the percent of runoff water captured using harvesting methods are available. The design and analysis model (Wanielista and Yousef 1993) provide series of rate-efficiency-volume (REV) curves to aid the design of harvesting ponds under the assumptions that there is minimal groundwater input and output to the pond. The primary use of the REV curves and the proposed model is to retain surface runoff water within a watershed and to reduce the mass of pollutants in the discharges to surface water bodies.

Harvesting Pond Simulation Model

The development and validation by Wanielista and Bradner (1992) and calibration by Wanielista (1993) showed that mathematical mass balance model can simulate the operation of a stormwater harvesting pond that has minimal groundwater exchange. The mass balance for the harvesting pond is based on inflow from rainfall events, discharge from the pond, and a harvesting volume rate. Water is discharged from the pond when the temporary storage volume exceeds the available storage. A relationship between the efficiency or runoff capture (note that this is runoff not discharge), harvesting rate and harvesting volume of the pond for a continuous time model was established from a simulation for specified period. Using local rainfall data, the simulation process provided the tools for the creation of charts of the harvesting rate, efficiency and harvesting volume (REV) for different rainfall regions. A chart for Orlando area in Florida is presented in Figure 4.

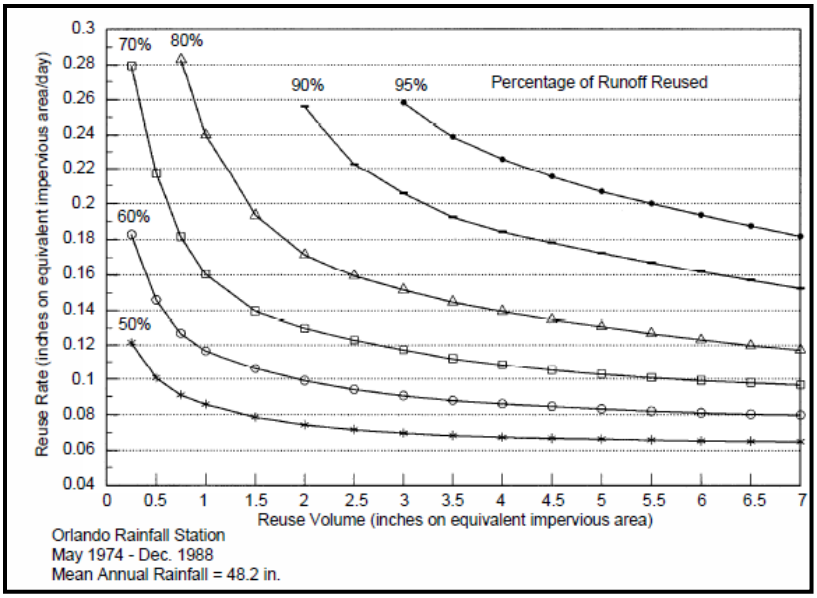

(Wanielista and Yousef 1993)

Figure 4 REV charts for Orlando, Florida

A mass balance for the harvesting pond was calculated based on the inflow and outflow from rainfall events, surface runoff, and harvested volume to the pond storage. Water is allowed to discharge from the pond when the temporary storage volume exceeds available storage. When the pond water goes below the permanent pool level, supplemental water was used to replenish the permanent pool volume. The model is based on the continuity equation for mass balance. Considering all potential water movement, Equation 1 expresses a complete hydrologic balance.

$$Input - Output = \Delta S \tag{1}$$

$$RO + G + P \pm F - H_{AR} - D - ET = \Delta S \tag{2}$$

where *RO* is the surface runoff; *G* is the supplemental water (groundwater); *P* is the precipitation directly on the pond; *F* is the water movement through the sides of the pond; H_{AR} is the harvested volume, *D* is the discharge; *ET* is the evapotranspiration; and *S* is the pond storage. Surface runoff volume was estimated based on known precipitation and watershed data, while the

harvesting rate was a controlled variable. The supplemental water and discharge were functions of the pond storage volume or water level of the pond. Supplement water was applied according to the rate of depletion of the permanent pool with maximum rate equal to the harvesting rate. In the REV model, the net flow of groundwater into a pond was assumed to equal zero and the average evaporation rate for a pond in Florida was considered approximately equal to the average precipitation on the pond in a one-year period. These terms were removed from the previous mass balance equation and are demonstrated in Equation 3.

$$RO + G - H_{AR} - D = \Delta S \tag{3}$$

It is important to factor in the availability and nearness of the water use facility in the design considerations for a stormwater harvesting pond, as there may be more water available. Additionally, when located near sensitive streams, pumping rates of the water should be controlled so as not to diminish or eliminate downstream flows needed to sustain aquatic life (Wanielista 1993). If located next to wetlands, it is desirable to show the impact on the wetland. Other than these, the use of stormwater within a watershed should be encouraged for the following beneficial reasons: it is cost effective, preserves potable water sources, maintains hydrologic balance, uses natural soil cleansing processes, and provides better water quality than reclaimed water. Harvested stormwater water can be used for multiple reasons, such as aquifer recharge, supplement water use for certain industrial purposes, source of irrigation for agricultural farms, and to enhance and even create wetlands (Wanielista 2007).

Hydrologic Model Review Summary

Reviews of available literatures on stormwater management systems showed the availability of several models, both lumped and distributed, for stormwater management systems in a watershed. Most of these models are designed to target specific hydrologic processes in a watershed or combination of two or more, while some others target the environmental impacts associated with stormwater. Models designed to include all the hydrologic processes for pond water harvesting are seldom found in literature. There is therefore a need to develop a comprehensive model for the entire processes of water movement, storage, and harvesting in a watershed area. The goal is to model the wide range of interactions of hydrologic processes of water movement, storage, and harvesting in stormwater management systems of a watershed. A model that simulate the integration of the physical processes of water movement in a pond, the atmosphere, soil surface, and subsurface within the unsaturated and saturated zones in order to quantify discharge and harvesting water volume from a watershed pond. Such a model is developed in this study.

EFFLUENT CONTROL LABORATORY TESTING

Index Property Testing

Silt fence materials index property tests and polyacrylamide dosage determination tests were performed at the Stormwater Management Academy laboratory (SMARTL) to correlate with field performances and applications. In addition to testing erosion and sediment control products on the test beds in the field-scale laboratory, this study conducted tests on the index properties of these products in a controlled laboratory environment, using the relevant American Society for Testing and Materials (ASTM) and/or American Association of State Highway and Transportation Officials (AASHTO) standard methods. The goals for these tests were to confirm manufacturer product data (if available) or determine new properties for silt fence fabrics; and develop sediment removal efficiency and testing protocols for polyacrylamide (PAM).

Silt Fence Fabric Testing

In accordance to ASTM standard test methods laboratory tests were conducted on the new product and the existing, a nonwoven belted silt retention fabric (BSRF) and woven monofilament silt fence (ARS-1400), respectively, to evaluate the index properties. Absolute Erosion Control, Incorporated and Silt Saver, Incorporated donated the ARS-1400 and BSRF silt fence fabrics, respectively, for the tests conducted at SMARTL. The following ASTM standard test methods were conducted on both fabrics to confirm the manufacturers' claims and establish the index properties in the laboratory.

- D4632-08 Grab Breaking Load and Elongation of Geotextiles

- D4491-99A (rev. 2004) Water Permeability of Geotextiles by Permittivity.
- D4833-00 Standard Test Method for Index Puncture Resistance of Geomembranes and Related Products
- D4751-04 Standard Test Method for Determining Apparent Opening Size of a Geotextile

ASR-1400 is an engineered geotextile, a circular woven polypropylene fabric, stabilized to resist degradation due to ultraviolet exposure, non-biodegradable and resistant to chemicals, mildew and insects usually encountered in soils (Assurence Corp. 2006). On the other hand, BSRF is a nonwoven biodegradable spun-bound polyester reinforced with coarse mesh-like fiberglass scrim sandwich between layers (Risse et al. 2007). Table 19 through Table 21 in Appendix A present the manufacturer's physical properties for ASR-1400 – minimum average roll values (MARV), physical and hydraulic properties for BSRF and ASTM D6461 standard specification for silt fence materials, respectively.

Testing Procedures and Discussions

The tests were independent of one another but related to the overall classification for a silt fence geotextile in accordance to ASTM specifications. Thus, the discussions were presented separately and a complete tabulation of the index properties of both geotextiles was listed along with the relevant ASTM specification.

Grab Strength Testing

Laboratory tests on the grab breaking load and elongation on BSRF and Type III silt fence materials were conducted in accordance with the ASTM D-4632-08 standard test method, in both dry and wet conditions. The breaking load is the maximum force in a tensile test applied to a specimen that results in rupture, and the elongation at break is the corresponding elongation. The ASTM D4632 is used to determine the strength of the fabric strands in a specific width and the strength contributed by adjacent strands (effective strength).

Specimen Preparation and Conditioning

ASTM D4632 (2008) requires that, where there is no reliable estimate available for the grab strength, tests should be conducted on 10 specimens (4 in. × 8 in.) for the machine direction and another 10 specimens for the cross-machine direction. The grab tests were conducted using the constant-rate-of-traverse (CRT) machine with the longer dimension parallel to the direction of load application for each silt fence. There were four groups of ten specimens classified as: DMD – dry condition with the longer dimension parallel to the machine direction; DCMD – dry condition with the longer dimension parallel to the cross-machine direction; WMD – wet condition with the longer dimension parallel to the machine direction; and WCMD – wet condition with the longer dimension parallel to the cross-machine direction.

Tests conducted in the wet condition were immersed in water at room temperature (70 ± 4ºF) to sufficiently soak the fabric. A minimum of 20 minutes was sufficient to thoroughly wet the specimens. The breaking load was calculated by averaging the values of the breaking load for all accepted specimens of that group. The apparent elongation is the average extension at the

breaking load for any specimen and is expressed as the percentage increase in length based on the initial nominal gage length of the specimen.

Grab Strength Testing Procedure

The apparatus used for the test is UNITED Tensile Testing Machine of constant-rate-of-traverse (CRT) type interfaced with a computer and clamps having jaw face measuring 2 in. by 3 in. with the longer dimension parallel to the direction of load application. The testing started by the attachment of a load cell with maximum capacity of 1000 pounds, and the clamps set at 3±0.5 inches apart and at operating speed of 12±0.5 inches per minute. The test specimen was then firmly secured in the clamps with the longer dimension parallel to the direction of load application, and centrally located in the widthwise direction of the clamps. A pretension load of 0.5 pounds is applied on the specimens before loading commences.

The CRT machine starts and runs until rupture of the material; and then the machine stopped and reset to the initial gage position for the next specimen in the same category. The autographic recorder measures and records the breaking load and elongation for every specimen for each direction and moisture conditioning. The tests were continued until ten acceptable specimen breaks were observed. Most breaks occurred above ¼ inch from the clamp edge and for more than 80 percent of the average break load for the corresponding silt fence material, which is within the acceptable criteria (ASTM D4632). Figure 5(a) through (d) show the testing machine with BSRF silt fence specimen placed in the clamp before and after rupture, and the interfaced computer.

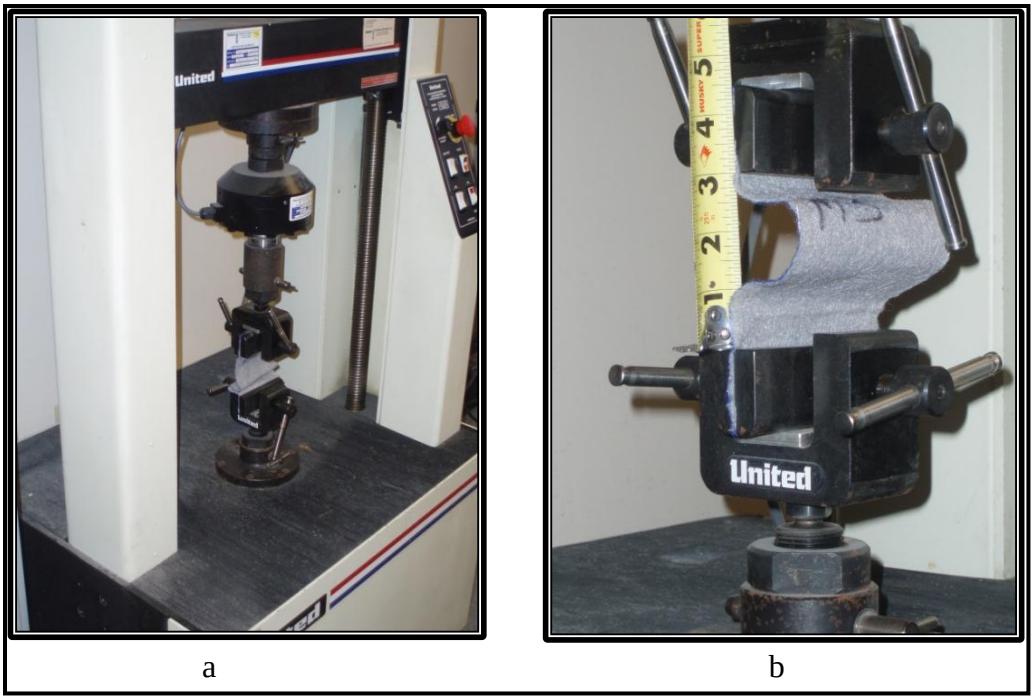

a b

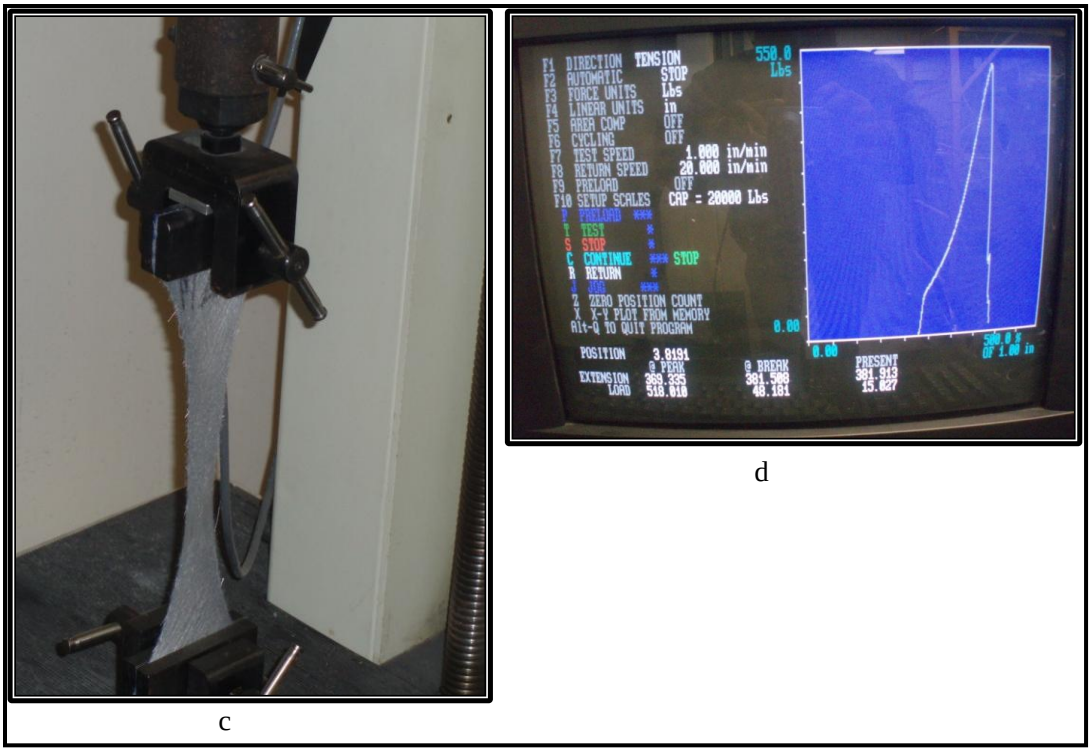

c d

Figure 5 Grab test apparatus with BSRF sample before and after load application

Grab Strength Results and Discussions

Detailed results for both silt fence fabrics are in Table 22 in Appendix B. However, a summary of the results for average breaking loads, elongations and strains are presented in Table 1, and Figure 6 and Figure 7 for the four groups: DMD, DCMD, WMD and WCMD of both BSRF and ARS-1400 silt fence fabrics.

Table 1 Average breaking loads and strain values for both BSRF and ARS-1400

Silt Fence Fabric	Testing Direction	Testing Condition	Load (lbs.)	Elongation (in.)	Strain (%)
BSRF	Cross-machine	Dry	163.2	1.32	38.3
		Wet	173.2	1.14	32.6
	Machine	Dry	129.9	1.35	39.8
		Wet	132.9	1.26	36.6
ARS-1400	Cross-machine	Dry	143.3	0.25	7.4
		Wet	122.8	0.24	7.1
	Machine	Dry	145.5	0.28	8.2
		Wet	121.2	0.27	7.6

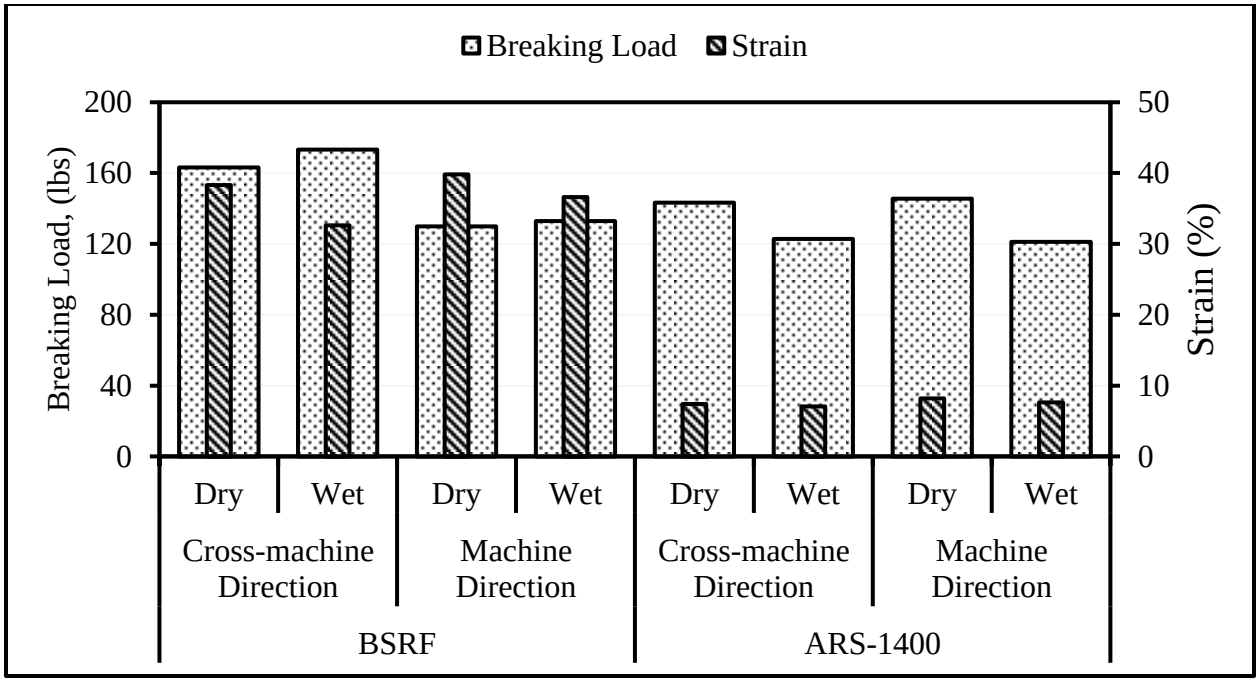

Figure 6 Average breaking loads and strain (%) for both BSRF and ARS-1400

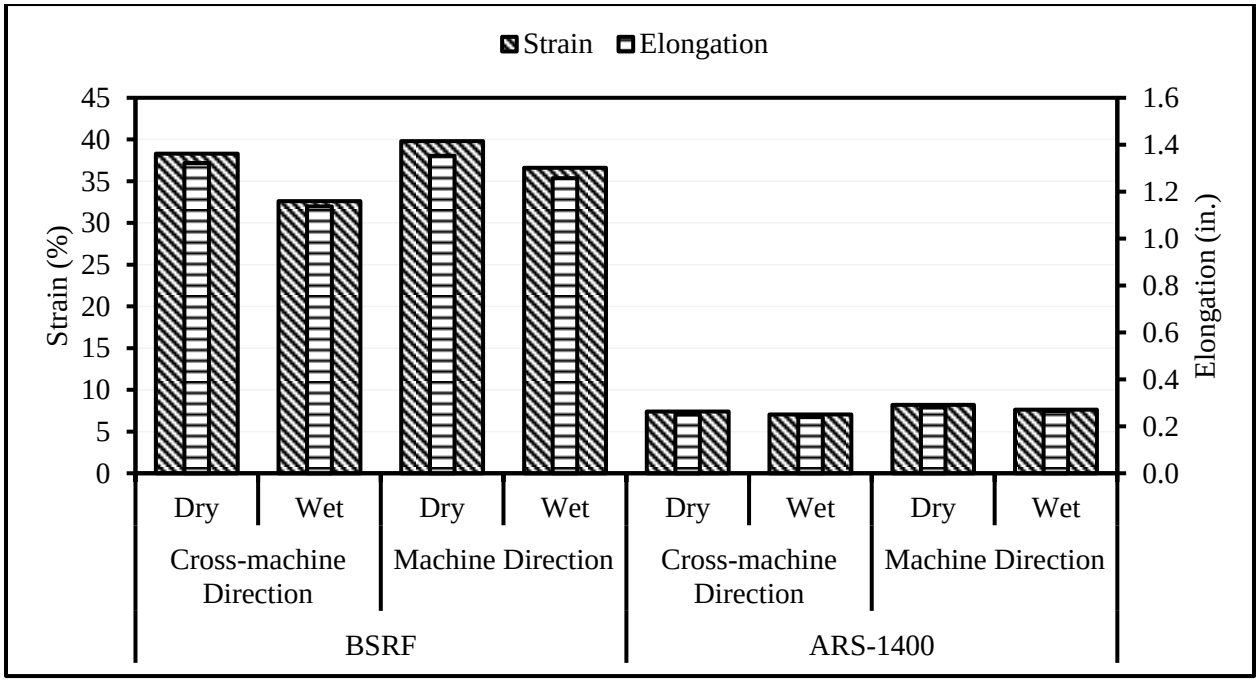

Figure 7 Average strain (%) and elongation for both BSRF and ARS-1400

To explain the fabric orientation and moisture conditions prior to testing, nonparametric statistical analyses (Mann-Whitney tests for two independent samples) were performed to test for significant differences for the four different testing conditioning on each fabric. Results showed that the moisture condition of BSRF prior to testing have no significant effect on the breaking load for both machine and cross-machine directions. However, comparisons between testing in machine and cross-machine directions have significant effect on the breaking load. The effect is due to the 0.5 in. × 1.0 in. rectangular orientation of the sandwich network of the reinforcing fiber in BSRF; the longer dimension is parallel to the cross-machine direction. It is, therefore reasonable to assume that the moisture conditionings of BSRF do not affect the grab strength, but the direction of installation of the fabric on site would significantly be affected at 95 percent confidence interval.

Also analyzed (statistically) is the effect of fabric orientation and moisture conditioning to strain of the fabric fibers of BSRF. The moisture conditioning significantly affected the strain values at break load in the cross machine direction and not in the machine direction. In the fabric orientation testing conditions the effects were reversed. There was no significant effect on strain between cross machine and machine directions for the dry condition, but wet condition significantly affected the strain at break loads in both testing directions. Unlike the effects on the grab strength, the corresponding strain values do not have same responses. Thus, an investigation of the correlation between grab strength and strain at peak load for the different moisture conditions and orientation were performed. The correlation results are shown in Table 2.

Table 2 Correlation between grab strength and strain at peak load for both silt fence fabrics

Silt Fence Material	Condition	Pearson Correlation, R	R-squared
BSRF	DCMD	0.2259	0.0510
	DMD	0.8395	0.7048
	WCMD	0.2549	0.0650
	WMD	0.6314	0.3987
ARS-1400	DCMD	0.4602	0.2117
	DMD	0.2849	0.0811
	WCMD	0.0318	0.0010
	WMD	0.2220	0.0493

Table 2 demonstrated that there is a higher correlation for BSRF silt fence when dry than wet in the machine direction, but the correlation is very weak in the cross machine direction. That is 70 percent of the strain at peak load is explained by the grab strength for DMD and 40 percent for WMD. However, only 5 percent and 7 percent of the variation in grab strength and strain at peak load is explained for the DCMD and WCMD. High grab strength does not necessarily translate to high strain at peak load. This explains why the statistical tests for grab strength and strain at peak load do not have similar responses.

Statistical analyses (Mann-Whitney Tests) on ARS-1400 test results revealed that the break load is not significantly affected by the fabric moisture conditioning and orientation, neither is the strain at peak load affected. These findings are supported by the configuration of the fabric; the orientation of the weaves is not substantial different – woven synthetic materials of equal arrangement in both machine and cross machine directions. There was no significant correlation between the grab strength and strain at peak load for the ARS-1400 fabric, see Table 2. It can be stated that high grab strength does not necessarily correspond to high strain nor low

grab strength to low strain at peak load. The strain of any fabric is dependent on the elasticity (brittle or ductile) of the component materials. Mann-Whitney test results are presented in Table 23 through Table 26 of Appendix B

Acceptance test on mean values

Statistical tests were conducted to show if there were significant differences in the grab strength and the corresponding grab elongations, see Table 3. The coefficients of variation were less than 1.0 for the different conditions and orientations of the BSRF silt fence, which indicates that the distribution has low-variance. That is, the dispersion of the test values from the calculated mean is minimal and the mean values truly represent the test results.

Table 3 Actual proportion within two standard deviations from the mean

Silt Fence	Condition	Grab strength		Strain at peak load	
		$\bar{y} \pm 2s$	Actual proportion	$\bar{y} \pm 2s$	Actual proportion
BSRF	DMD	(107.10, 152.61)	1.00	(32.58, 47.05)	1.00
	DCMD	(142.05, 1184.30)	1.00	(33.18, 43.45)	1.00
	WMD	(117.22, 148.59)	1.00	(30.60, 42.64)	1.00
	WCMD	(152.49, 193.87)	1.00	(27.14, 38.08)	1.00
ARS-1400	DMD	(111.23, 179.78)	1.00	(5.00, 8.10)	1.00
	DCMD	(112.30, 174.32)	1.00	(2.49,12.30)	1.00
	WMD	(65.60, 176.81)	1.00	(3.43, 11.82)	1.00
	WCMD	(57.47, 188.12)	1.00	(4.02, 10.11)	1.00

An analysis of the coefficients of variation showed that for BSRF the specimen data variations are similar, 6 percent, except for DMD having 9 percent data variation. The coefficients of variation on the ARS-1400 silt fence fabric show a distribution of low-variance; for the machine and cross-machine directions, these are 11 and 12 percent, and 27 and 23 percent, for dry and wet conditions, respectively. Figure 8 presents the comparison of the

average grab strength to the ASTM minimum requirement, and shows that both silt fence fabrics are above the minimum specifications. There are no minimum specifications for the elongation and strain at peak load for silt fence fabrics (ASTM D6461).

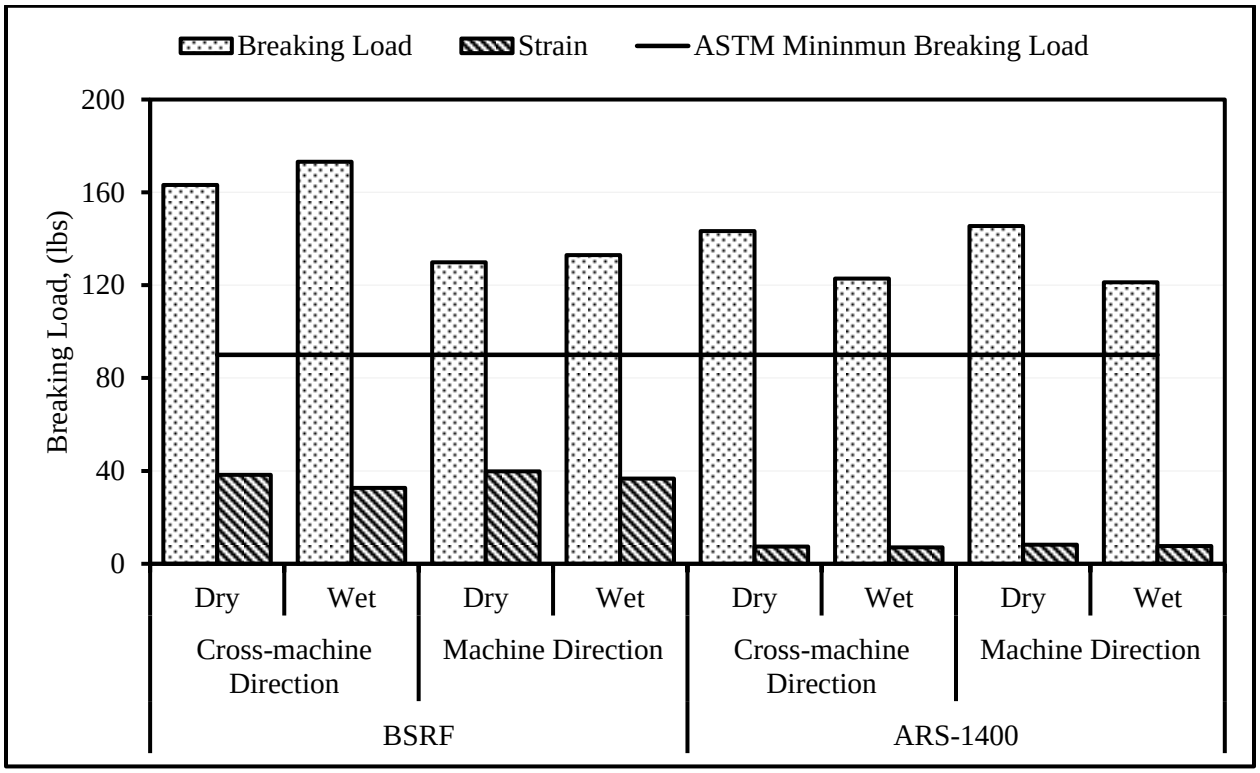

Figure 8 Comparisons of average grab strength results to ASTM minimum specifications

Permittivity Testing

Permittivity is defined as the "volumetric flow rate of water per unit cross sectional area per unit head under laminar flow conditions, in the normal direction through a geotextile;" and is an indicator of the quantity of water that can pass through a geotextile in an isolated condition (ASTM D4491 2009). The permittivity of the geotextile is determined by this expression in Equation 4 as

$$\psi = QR_t / hAt \tag{4}$$

$$R_t = u_t / u_{20^\circ C} \tag{5}$$

where ψ = permittivity, sec^{-1}; Q = quantity of flow, mm^3; h = head of water on the specimen, mm; A = cross-sectional area tested area of specimen, mm^2; t = time of flow, sec; R_t = temperature correction factor determined using Equation 5; u_t = water viscosity at test temperature, millipoises; and $u_{20^\circ C}$ = water viscosity at 20˚*C*, millipoises.

Test on the water permeability by permittivity of silt fence materials is in accordance with the ASTM D4491 standard test method. Permittivity test evaluates the volume of water that would pass through a geotextile under a given head over a particular cross-sectional area. The nominal coefficient of permeability is derived from the multiplication of permittivity by the thickness of the geotextile. Mathematical dimension of permittivity is presented in Equation 6 as

$$\psi = \frac{\left(L^3/T\right)/L^2}{L} = \left(\frac{L}{T}\right)\cdot\left(\frac{1}{L}\right) = \frac{1}{T} = T^{-1} \tag{6}$$

Permittivity of a geotextiles can be determined from the constant-head or falling-head test procedures. The falling head test is used for slow flow rate through the geotextile to allow the reading of head changes with time. However, constant head test is used when the flow rate is fast that makes measurement of head change with time difficult. The constant head test was performed on both BSRF and ARS-1400 silt fence fabrics.

Test Specimen Preparation and Conditioning

Water from the mains in the laboratory is passed through a de-airing device under a vacuum of 28-inch of mercury to bring down the dissolved oxygen content and reduce

experimental errors due to dissolved air in water, and reproducible test results. Prepared test water was drained slowly from the de-airing chamber into a 6-gallon plastic container, which was then lifted up using a pulley device and discharged into a storage tank. Four 75 millimeter (3.0-inch) diameter specimens from each of the silt fence fabrics were cut to fit the testing apparatus, see Figure 9. The cut geotextile specimen is placed in a sample holder and secured tightly between the holder top and base, then immersed in de-aired water at room temperature (70 ± 4ºF) for 2-hours prior to testing.

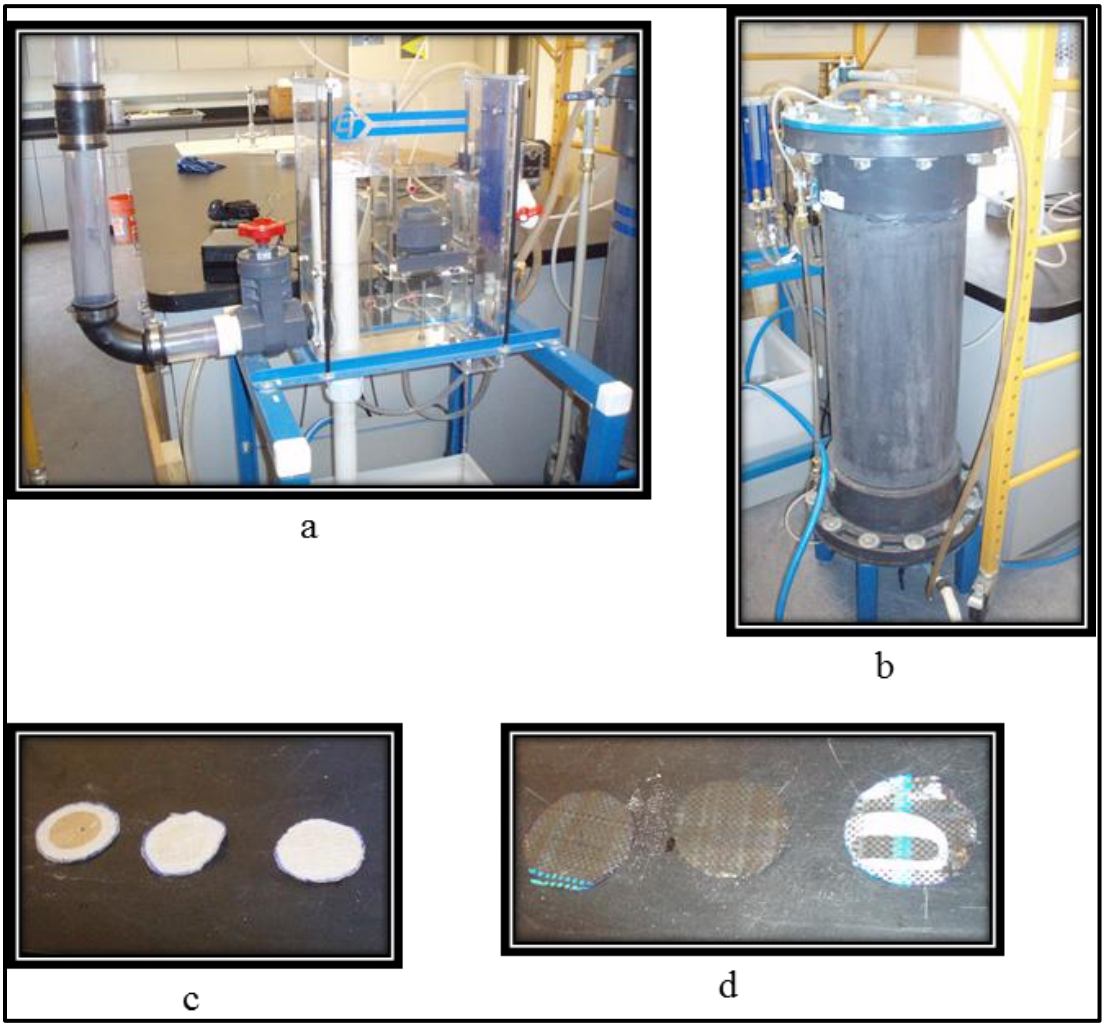

Figure 9 Permittivity testing apparatus, de-airing device and cut test specimens

Permittivity Testing Procedure

The permittivity testing device was assembled according to the manufacturer's specifications. In Figure 10, the upstream head tube was raised above the level of the downstream threshold and allows de-aired water to flow into the permittivity device enclosure and fill-up to its threshold (overflow). The soaked sample in the sample holder was quickly, but carefully, removed from de-aired water and inserted perpendicular into the water surface. The fitted sample holder with the specimen was securely screwed into the mount in the downstream sample area of the permittivity.

De-aired water flowed into the system through the water inlet; the upstream tube and the inlet throttle valve were continually adjusted to produce a 50 mm (2-inch) head of water on the geotextile. Flow through the geotextile was allowed to stabilize after the establishment of the 50 mm (2-inch) head differential. Thereafter, water flow through the geotextile and out of the permittivity device enclosure was collected for 30 seconds and the quantity of water measured. The following values were recorded: time (t), quantity of flow (Q) as collected from the drainage outlet and water temperature (T) for every specimen. Five readings per specimen were recorded for the four samples of each geotextile.

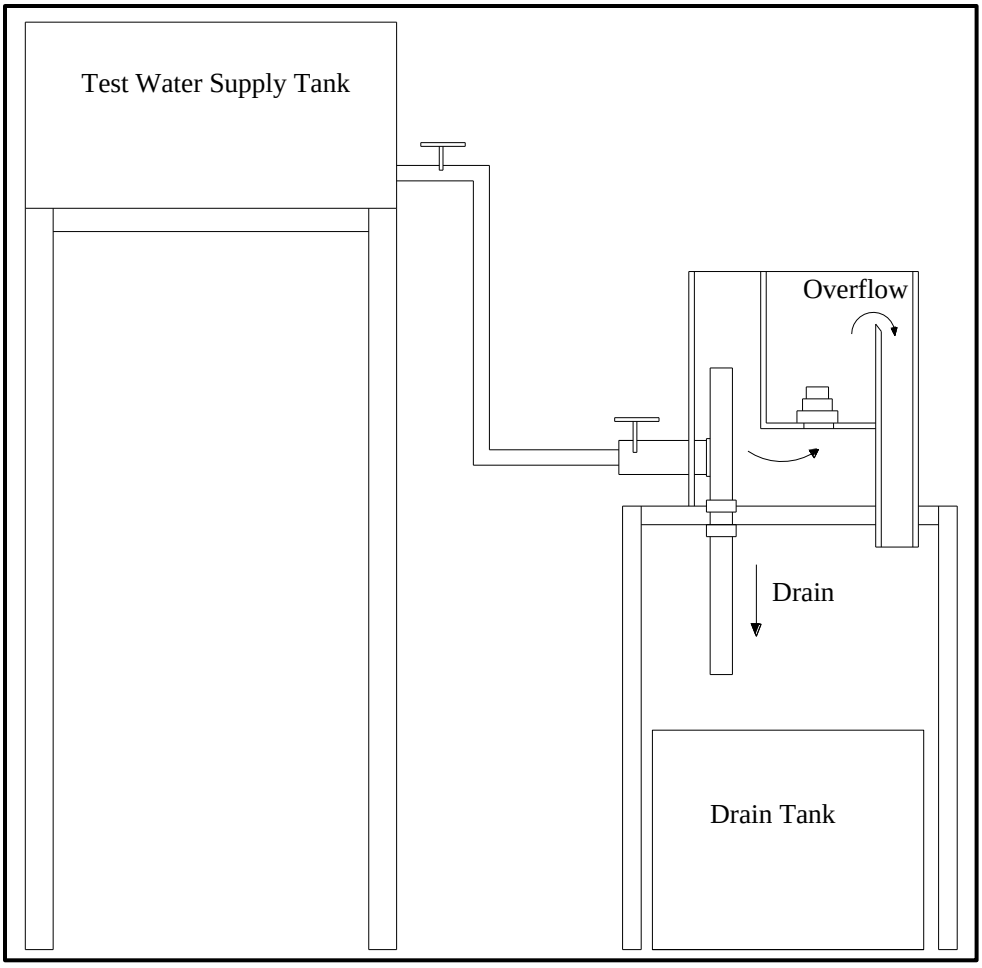

Figure 10 Constant head test setup of the permittivity device

After the first test specimen measurements were completed, the differential water head on the geotextile specimen was increased to 10 mm (⅜-inch) and the water was collected for 30 seconds and measured. The differential water head was further increased by 5 mm (3/16-inch) and the test procedure repeated until 75 mm (3-inch) of water head on the geotextile specimen in the permittivity device was attained. The volumetric flow rates versus head differentials is plotted to determine the region of laminar flow, which is the initial straight line portion of the plot, see Figure 11 for the ARS-1400 silt fence fabric.

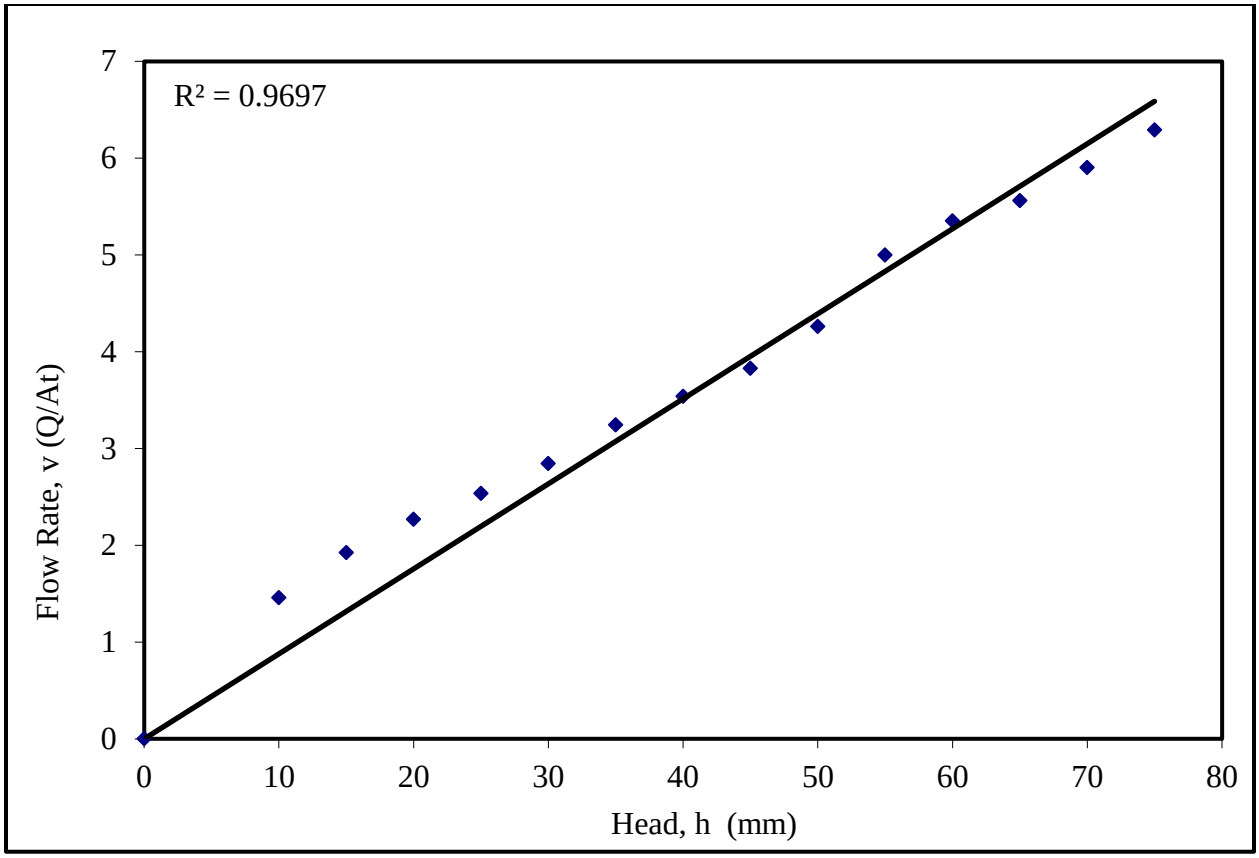

Figure 11 Calibration curve to determine region of laminar flow for ARS-1400 fabric

Permittivity Test Results

Computation of the permittivity of every geotextile specimen is based on the measured quantity of for each specimen and testing sequence. Permittivity and flow rate computations are dependent on specimen cross-sectional area of 2027 mm^2, 50 mm head of water on the specimen, test duration of 30 seconds, and temperature correction factor of 1.11 and 1.05 for BSRF and ARS-1400, respectively. Detailed result from the tests, and computed values are presented in Table 27 of Appendix C. Presented in Table 4 are the computed average permittivity, flow rate, and volumetric flow rate for BSRF and ARS-1400.

Table 4 Summary results of permittivity and flow rates

Parameters	Units	Fabrics		Average values
Permittivity	sec^{-1}	BSRF	Test result	2.50
			Manufacturer	--
		ARS-1400	Test result	0.11
			Manufacturer	0.05
Flow Rate	$m^3/m^2/min$ ($gal/ft^2/min$)	BSRF	Test result	1.88 (46.20)
			Manufacturer	0.512 (12.60)
		ARS-1400	Test result	0.08 (1.96)
			Manufacturer	--

The permittivity values for both silt fence fabrics are in the range of values calculated in an ASTM inter-laboratory test program conducted in 1999 for woven and nonwoven geotextiles (ASTM D4491 2009). There are no flow rate values in the ASTM manual, but based on the minimum permittivity value flow rates were computed from the sample size and test water temperature correction factors, and are presented in Figure 12. The observed permittivity and flow rate for both silt fence fabrics are above the ASTM minimum specifications. The permittivity and flow rate of ARS-1400 is approximately twice the minimum specification, but the permittivity and flow rate of BSRF is two orders of magnitude more than the ASTM specification.

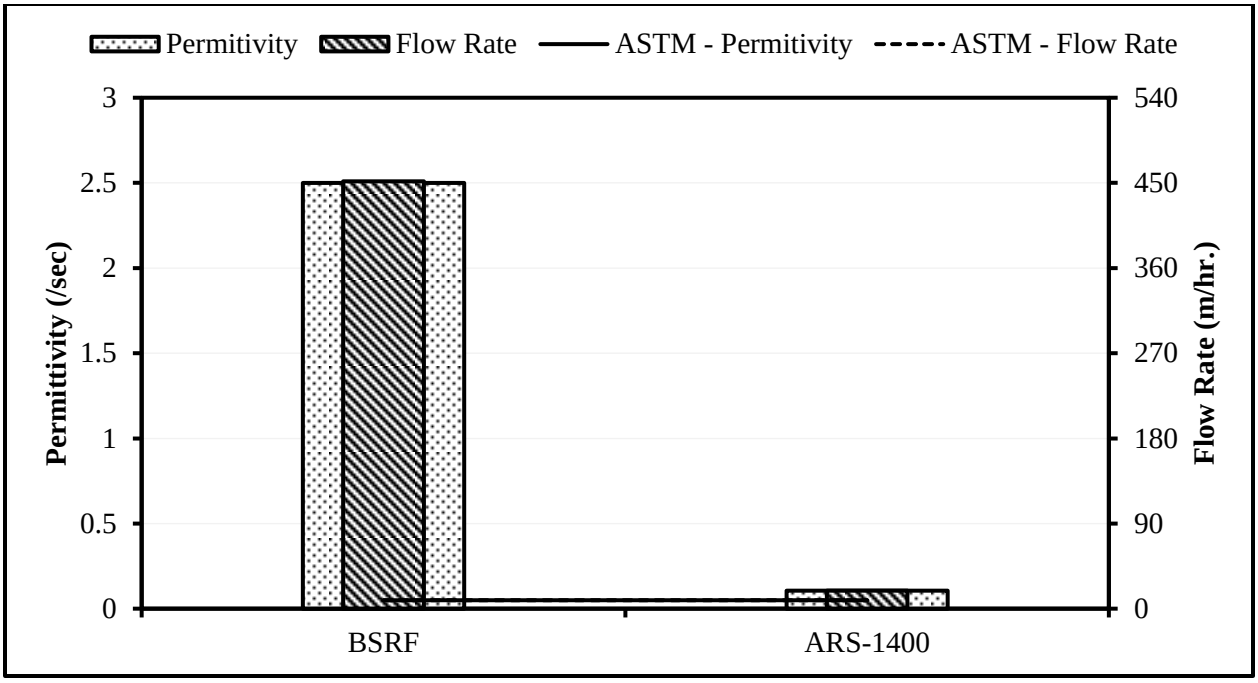

Figure 12 Comparisons of permittivity and flow rate values to ASTM minimum specifications

Apparent Opening Size Testing

The index test is designed to determine the apparent opening size (AOS) of a geotextile by sieving glass beads through it. The AOS becomes the approximate largest opening dimension available for soil to pass through (ASTM D4751). Equation 7 is used in the computation of the percentage of beads passing through each specimen

$$B = 100(P/T) \tag{7}$$

where B = percentage of beads passing through specimen; P = mass of glass beads in the pan, grams; and T = total mass of glass beads used in grams.

AOS Testing Procedure

Test on the apparent opening size (AOS) was conducted in accordance of the ASTM D-4751 standard test method. Five specimens per geotextile were selected and testing conducted on all specimens to determine the percent of glass beads passing through a geotextile. The average percent of glass beads passing through the specimen and the percent retained on the specimen were computed from the five samples for each geotextile at every bead diameter.

A mechanical sieve shaker is used to induce lateral and vertical particle motion on the fabric in the sieve. The induced motions enable the glass beads to generate different orientations to the sieve surface for easy passage of particles smaller than the opening on the geotextile. Other apparatus used were sieve cover, five sieve frames consisting of 8-inch diameter pans and sieves, spherical glass beads of different sizes, and Explorer Pro (EP4102D) balance having accuracy of 0.01 grams. See Figure 13 for AOS test apparatus and materials.

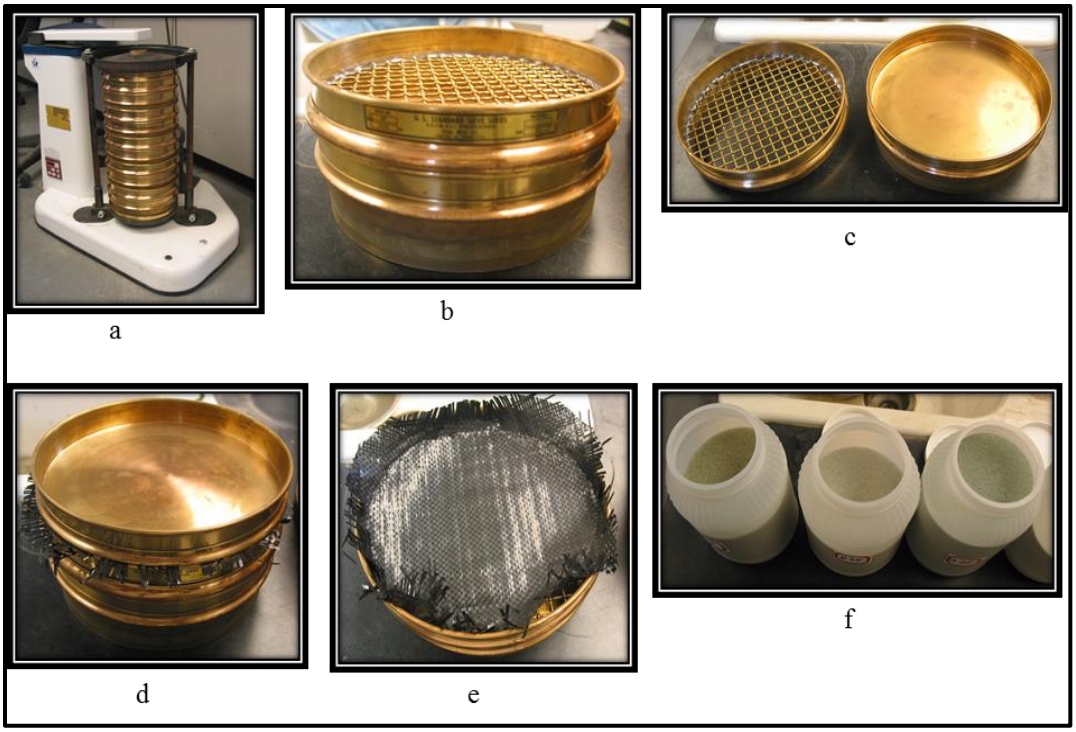

Figure 13 AOS sieve shaker, sieve frame, glass beads and ARS-1400 silt fence fabric

To determine the apparent opening size of silt fence fabrics, five samples from each silt fence material were cut and secured between sieve frames, held tautly and without wrinkles or bulges. Verified sizes of glass beads, weighing approximately 50 grams and starting with the smallest diameters, were placed at the center on the geotextile samples in the sieve frame. The sieve frames were then covered and placed in the mechanical sieve shaker and vibrated for 10 minutes to induce jarring motion that forces the glass beads to pass through the geotextile samples. Measurements of the weights of the glass beads retained on the specimen and those that passed through were recorded and the percentages of retained and passing computed. This process was repeated with larger glass bead sizes until the weight of beads passing through the specimen is 5 percent or less, for all five geotextile samples of both BSRF and ARS-1400 silt fence fabrics.

AOS Test Results and Discussion

The AOS is determined from a plot of the percentage of beads passing specimen versus the bead size on each geotextile. From each plot in Figure 14, the observed AOS for BSRF is 0.212 mm (Sieve #70) and for ARS-1400 is 0.70 mm (Sieve #25).

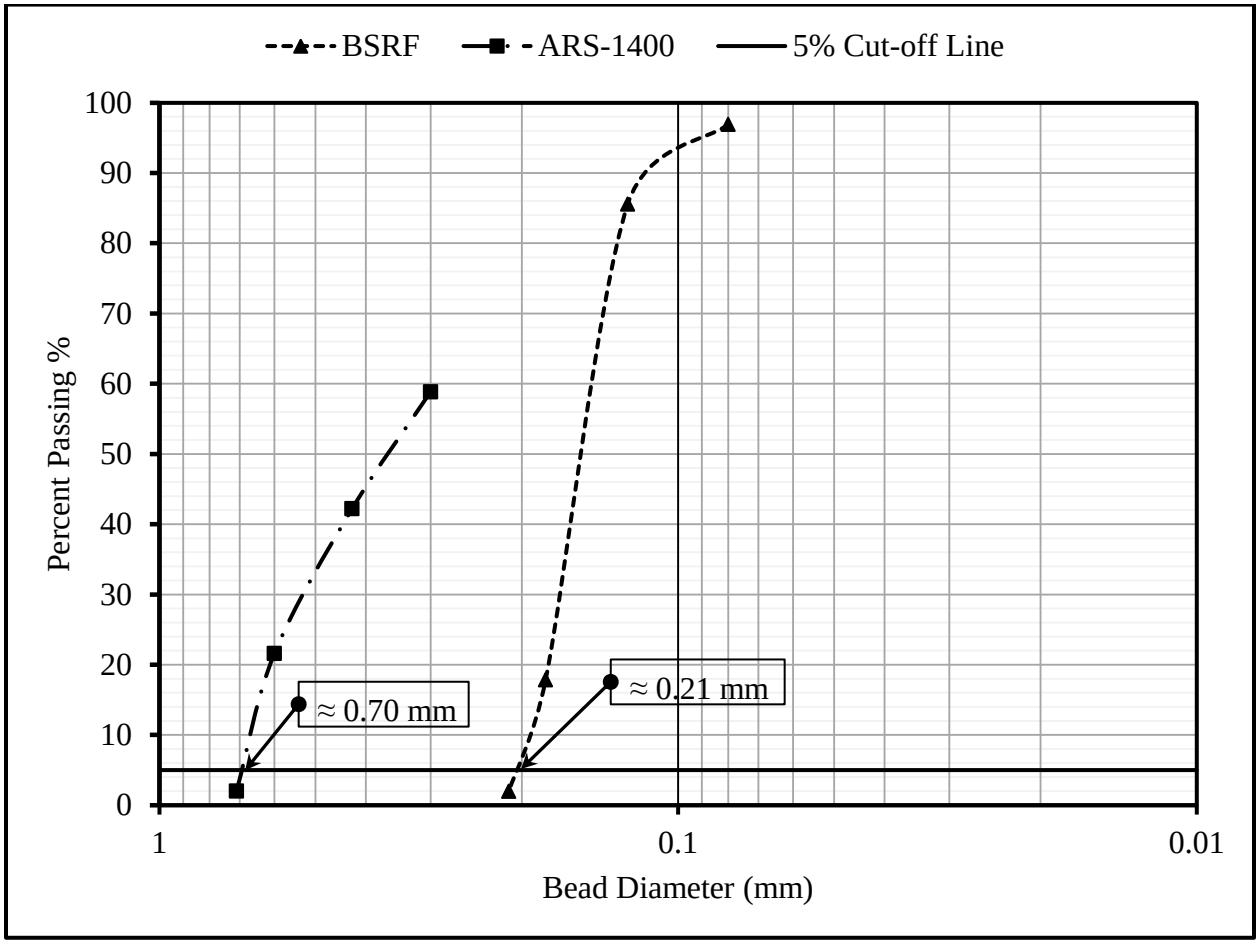

Figure 14 Sieve sizing on percent passing through BSRF and ARS-1400 geotextiles

Figure 15 shows the comparison between the average test results and the ASTM specification for silt fence fabrics. The AOS values determined from the tests for BSRF was below ASTM minimum recommendation of U.S. Sieve #30, but ARS-1400 was slightly less than the minimum (U.S. Sieve #25).

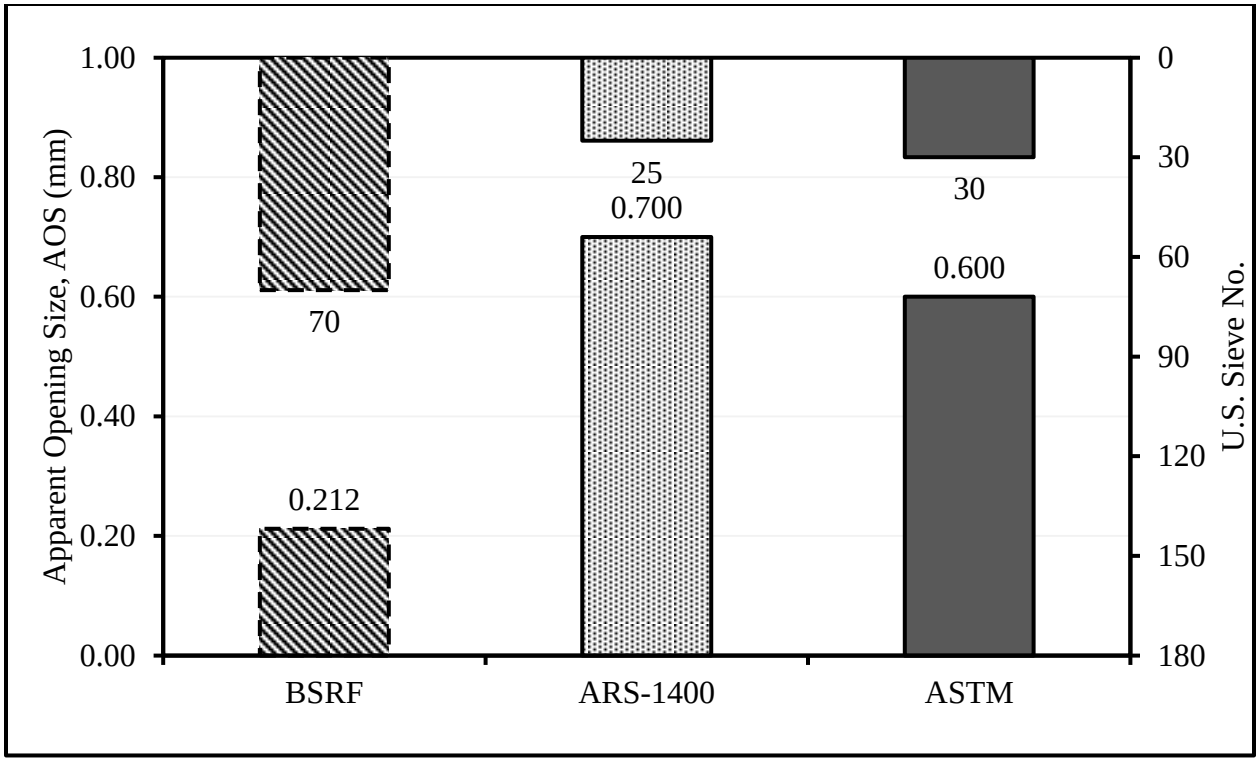

Figure 15 AOS for both geotextiles and ASTM specification

Puncture Resistance Testing

ASTM D4833 (2007) is designed to establish an index value by specifying standard criteria and a basis for uniform reporting. However, it is inappropriate for woven materials having large openings.

Puncture Resistance Testing Procedure

The test was conducted on two groups of 15 rectangular specimens cut 4.5 in. × 8 in. for the index puncture loads in a CRT machine for each geotextile. The groups were classified based on the moisture conditions as dry and wet. Wet specimens were immersed in water at room temperature (70 ± 4ºF) to sufficiently soak the fabric for at least 20 minutes. The puncture test equipment for this experiment is the UNITED tensile testing machine of constant-rate-extension

(CRE) type interfaced with a computer, and rectangular clamps attachment having internal opening diameter of 1.8 inches capable of preventing slippage. The test started by firmly securing the test specimen between the holding ring clamps attached to the CRE machine. The clamps are operated by pneumatic system with air pressure and have grooves on opposing surfaces to firmly secure the geotextile. Connected to the CRE machine is a solid steel rod with a diameter of 0.315 inch having a flat end with 45º chamfered edge.

For this test, the operating speed of the CRE machine was 12 ± 0.5 inches per minute with a load cell of 1000 pounds and a pretension load of 0.5 pounds applied by the steel rod on the test specimen. The CRE machine was then set to run until penetration of the test specimen and allowed to move 2 inches further downward. The machine was stopped and returned to the initial gage position for the next specimen of the same grouping. The interface computer records the resistance force per specimen extension until rupture for every specimen. This process was repeated for every specimen and in both dry and wet conditions. The peak resistance force observed was recorded as the puncture resistance. Figure 16(a), (b) and (c) show the clamping arrangement, for BSRF silt fence specimen placed in the clamp during test, and the interfaced computer, respectively.

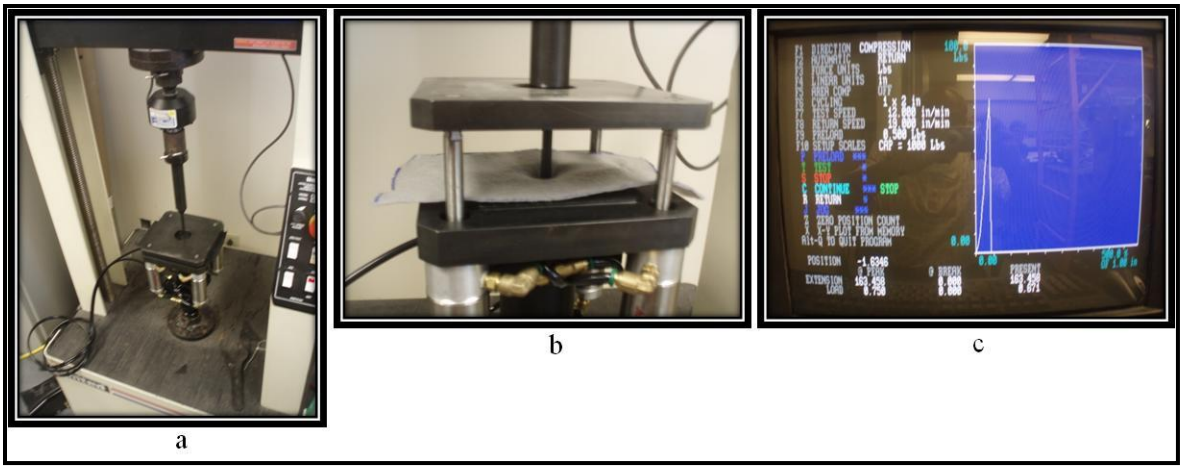

Figure 16 Index puncture resistance test set-up and fixtures

Puncture Test Results and Discussions

Tests on the BSRF silt fence specimens produced double peaks because of the composite nature of the geotextile – the fiber mesh reinforcement. However, only the initial peak resistance force is recorded as the puncture resistance even when the second peak resistance force was observed to be higher. The puncture load for each moisture condition is determined by averaging the computer output of resisting force versus extension through the test until failure, and is presented in Figure 17. There is no ASTM specification on puncture load for silt fence fabrics. Detailed results of the individual test specimen results are shown in Figure 54 and Figure 55 of Appendix D for both moisture conditions of dry and wet, respectively.

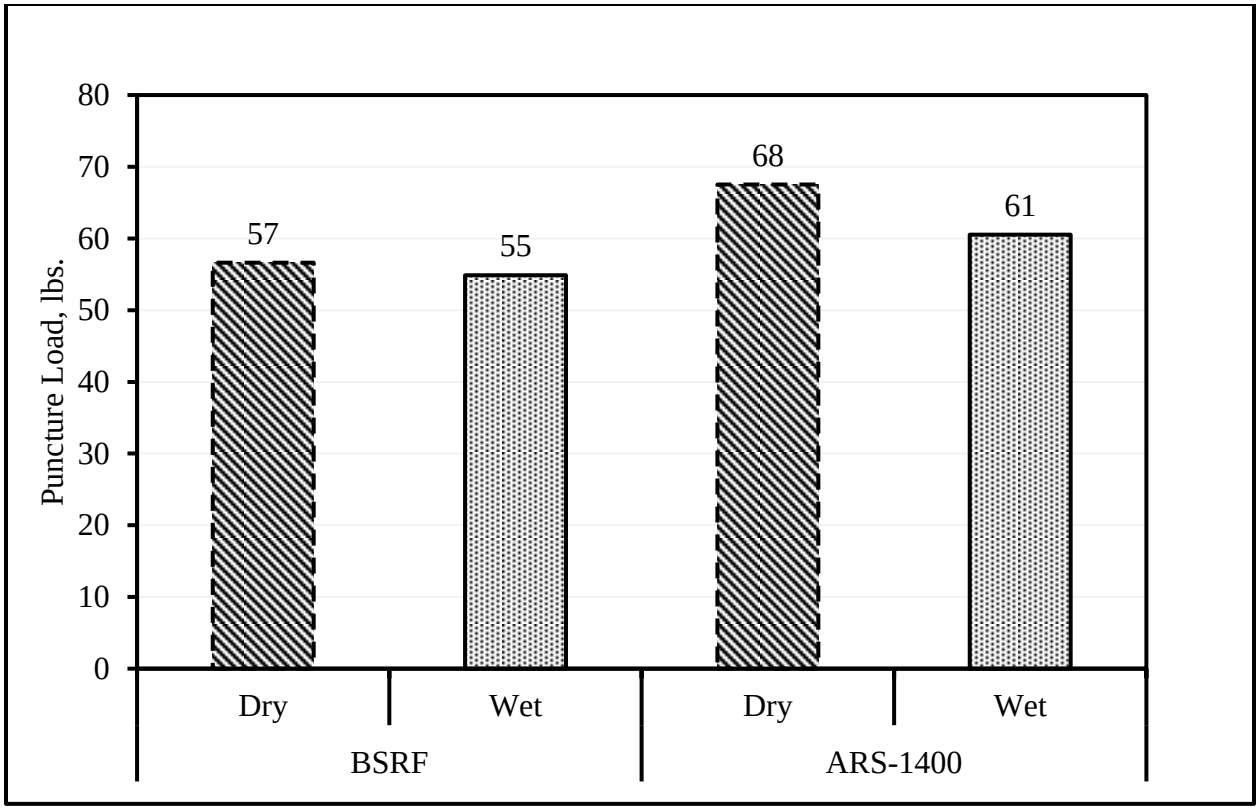

Figure 17 Average puncture resistance of BSRF and ARS-1400 geotextiles

The average puncture resistance, standard deviation and coefficients of variation were determined for both moisture conditions, separately. These statistical parameters for the puncture resistance are presented in Table 5. All observed puncture resistances of the specimens of both silt fence materials were within two standard deviations from their respective mean values. This acceptance is above the expected 95 percent based on the empirical rule and 75 percent based on the Chebyshev's rule for interpretation of standard deviation. Thus, confirms that the test data variations are within probability theorem acceptance limits and the mean values are true representations of the tests.

Table 5 Puncture resistance summary results for BSRF and ARS-1400 geotextiles

Statistical Parameters	BSRF		ARS-1400	
	Dry	Wet	Dry	Wet
Mean	56.6	54.9	67.5	60.5
Standard Deviation	7.10	6.49	4.62	8.56
Standard Error, ±	1.83	1.68	1.24	2.21
Coefficient of Variation	0.13	0.12	0.07	0.14
Minimum	44.95	44.95	59.83	50.61
Maximum	65.70	65.70	74.96	76.49
Count	15	15	14	15

The coefficients of variation for the BSRF fabric are 14 and 13 percent in the dry and wet moisture conditions, respectively. For ARS-1400 fabric, the coefficient of variation is 6.8 percent in the dry moisture condition and 14.1 percent in the wet condition (twice that of the dry). Variations of the puncture resistance are partly attributable to the point of penetration of the steel rod through the BSRF geotextile. The puncture resistance is higher when the steel rod makes contact with the fiberglass reinforcement, but lower puncture resistance when it contacts the polyester. The immersion in water tends to ease penetration through the woven strands of the ARS-1400 geotextile.

To evaluate the effect of moisture on the puncture resistance, Mann-Whitney tests on independent samples (nonparametric) were performed to evaluate the null hypotheses that the moisture condition does not have any effect on the puncture resistance at a significance level of 5 percent ($\alpha = 0.05$). The statistical analysis revealed that the moisture condition does not significantly affect the puncture resistance of BSRF geotextile, but showed significant effect on the ARS-1400 geotextile. The significant effect of moisture observed on ARS-1400 may have

resulted from loose strands and slippage due to the presence of water on the geotextile surface. Slippage may have forced the strands to move and allow the penetration rod to pass between strands instead of through the strand. The statistical test computations and decisions made on the effect of moisture condition on silt fence fabrics are presented in Table 30 of Appendix D.

Summary of Index Testing of Silt Fence Fabrics

Table 6 presents the summarized index properties for BSRF and ARS-1400 silt fence fabrics in comparison with the ASTM specifications. Both geotextiles index properties were above the ASTM minimum grab strength and permittivity values. BSRF was less than the ASTM maximum apparent opening size specification for silt fence material property requirements, but the ARS-1400 was slightly greater than specification. No test was performed on the ultraviolet stability property for both silt fence materials because the economic cost of having the equipment or even sending out to a qualified laboratory. For a conservative estimate, only the minimum value for the grab strength results in both moisture conditions (dry and wet) is presented as the breaking loads for both geotextiles.

Table 6 Comparison of ASTM index property specifications to BSRF and ARS-1400 fabrics

Property	Direction	ASTM Test Methods	Units	ASTM D6461	BSRF	ARS-1400
Grab Strength	Machine	D 4632	N	400	591	539
	X-Machine			400	726	637
Permittivity		D 4491	sec^{-1}	0.05	2.50	0.11
AOS		D 4751	mm	0.600	0.212	0.700
Ultraviolet stability[(a)]		D 4355	% retained strength	70% after 500 hr. of exposure	-	-

[(a)] – ASTM D4355 was not conducted for both silt fence fabrics in this research

Polyacrylamide Dosage Testing

Polyacrylamide has been shown as an effective erosion and sediment control product, capable of stabilizing exposed soil surfaces and clarifying sediment-laden runoff (Barvenik 1994; Flanagan et al. 2002; Arjunan et al. 2005; Iwinski 2010). However, there is no standard or repeatable testing method to estimate dosage requirements. The current practice involves empirical and subjective methods prescribed by the manufacturers with high probability of testing errors and uncertainty. Thus, an index test was conducted to determine PAM dosage estimation to achieve certain preset turbidity reduction efficiency. This would require establishing a repeatable testing method that combines the mixing flow velocity, mixing duration, and quantity of PAM to minimize the uncertainty in the testing method.

Dosage Determination Testing Method

To perform the test at SMARTL, five grams of clayey sand with a distribution of 60 percent coarse particles and 40 percent fines was mixed with 180 millimeter (mL) of de-ionized (DI) water to create a turbid mixture. After the settled solid particles have been removed from the mixed solution, the turbid water was measured to determine the initial turbidity using a Hach 2100P Turbidimeter. The turbid solution was poured into a 200 milliliter beaker that has a predetermined PAM dosage of 25, 50, 100, 150, 200 or 250 milligrams (mg) introduced earlier. The beaker was then placed on a stir plate with a stir bar in the solution to introduce mixing speed at predetermine revolutions of 125, 350, or 700 revolution per minute (rpm) for set mixing duration of 30, 45, 60, 75, 90, or 120 seconds. The polymer enhanced solution was removed from the stir plate and allowed to settle for a minute. Sample from the settled solution was collected to test for the final turbidity before and after the solution has been passed through a 35

or 64 micron filter. The process was repeated three times for every combination of dosage quantity, mixing speed, and mixing duration. Figure 18 shows sample water prior to treatment and after treatment with PAM product.

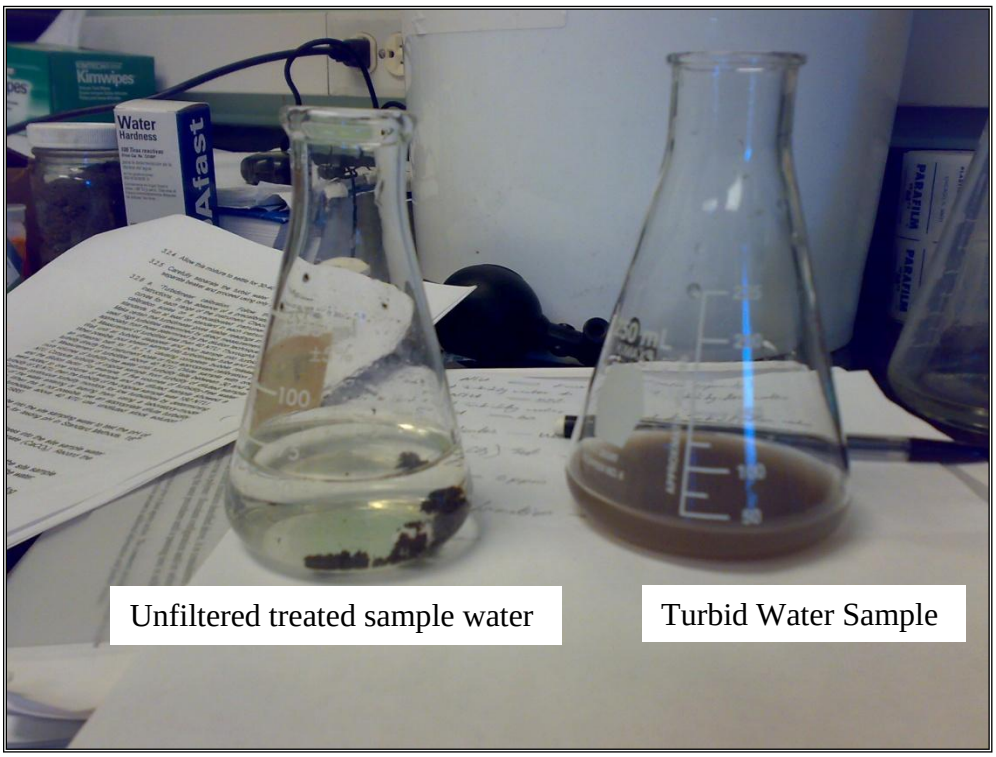

Figure 18 PAM treated and untreated water samples in beakers

PAM Dosage Testing Results and Discussions

For field application, the PAM dosage quantity is converted to PAM concentration by the ratio of a specific PAM dosage mass (mg) to 180 mL of DI water – milligram per liter (mg/L) or parts per million (ppm). The revolution is converted to flow rate of discharges from construction sites by a conversion of 1.0 rpm to 12.0 meters per hour (m/hr). The mixing duration is dependent on the length of channel designed for treatment and velocity of flow. Thus, the conversion factors are expressed in flow rate and concentration, respectively.

$$1\,rpm = 12.0\,m/hr. \text{ and } 1\,mg/mL = 16.7\,mg/L \quad (8)$$

From Equation 8, the concentration of PAM in the mixed solution and flow rate are estimated and presented in Table 7.

Table 7 Converted flow rate and concentration for PAM dosage

Mass (mg)	Concentration (mg/L)	Revolutions (rpm)	Flow rate (m/hr.)
25	417	125	1496
50	833	238	2843
200	3333	350	4189
250	4167		

Turbidity removal efficiency for the polymer tested is calculated using Equation 9

$$PE_{ff} = \left[1 - \frac{NTU_{final}}{NTU_{initial}}\right] \times 100 \quad (9)$$

where PE_{ff} = performance efficiency (%); NTU_{final} = final turbidity measurement after PAM enhancement (NTU); and $NTU_{initial}$ = initial turbidity measurement of mixed solution before PAM enhancement (NTU). A summary of performance efficiency on a powdered PAM – APS 705 – using a concentration of 417 and 833 mg/L are shown in Figure 19 and Figure 20, respectively. Test results for three other PAM products (APS 745, 706b, and 703d) are presented in Figure 56 to Figure 63 of Appendix F. One clear observation on all the plots is the effectiveness of PAM in the reduction of turbidity of the mixed solution (turbid water). PAM significantly reduces the turbidity but is dependent on the type of PAM product, concentration,

flow rate (mixing energy), and mixing time. Flow rate and mixing time can be derived from the treatment channel length and slope.

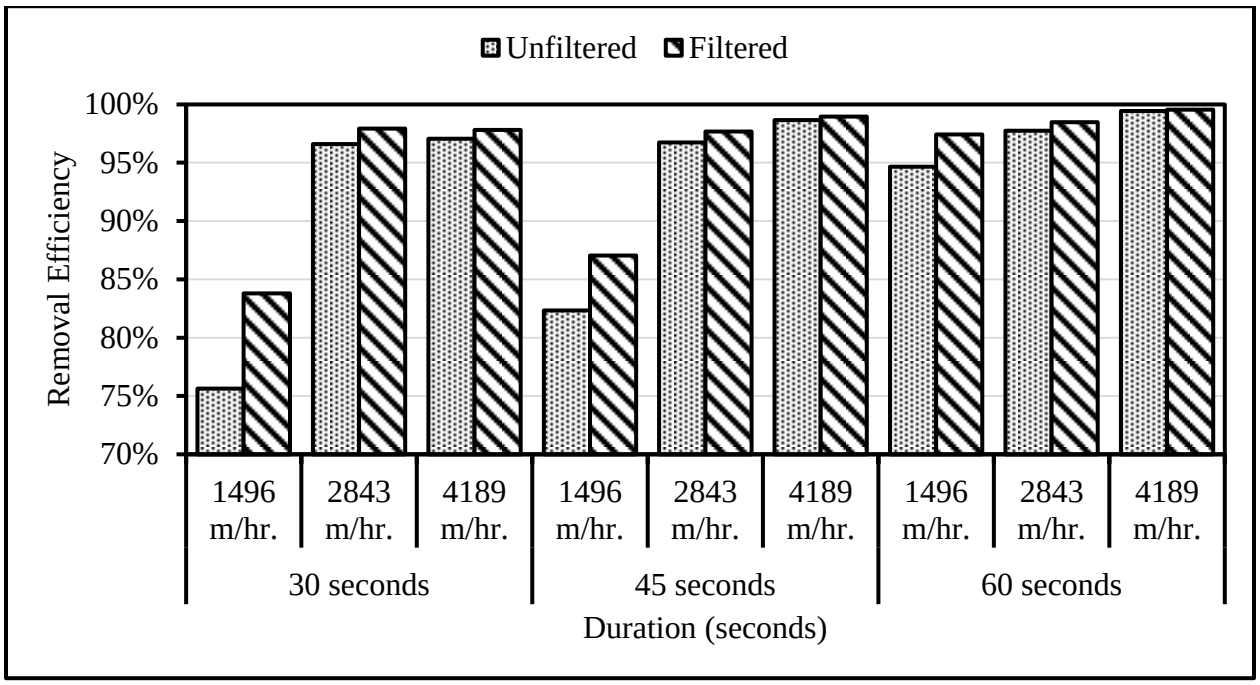

Figure 19 Plot of efficiencies for PAM APS 705 at a concentration of 417 mg/L

The lowest performance efficiency achieved in the laboratory tests for the soil-mixed solution using APS 705 was 76 percent, and with higher concentration, mixing energy, and mixing duration the efficiency increased to 99 percent. The observation revealed that to achieve higher performance efficiency, which translates to less turbidity, the reaction of PAM with the suspended sediment in the mixed solution should be enhanced. The enhancement can be achieved by increasing PAM concentration, mixing duration and/or mixing energy.

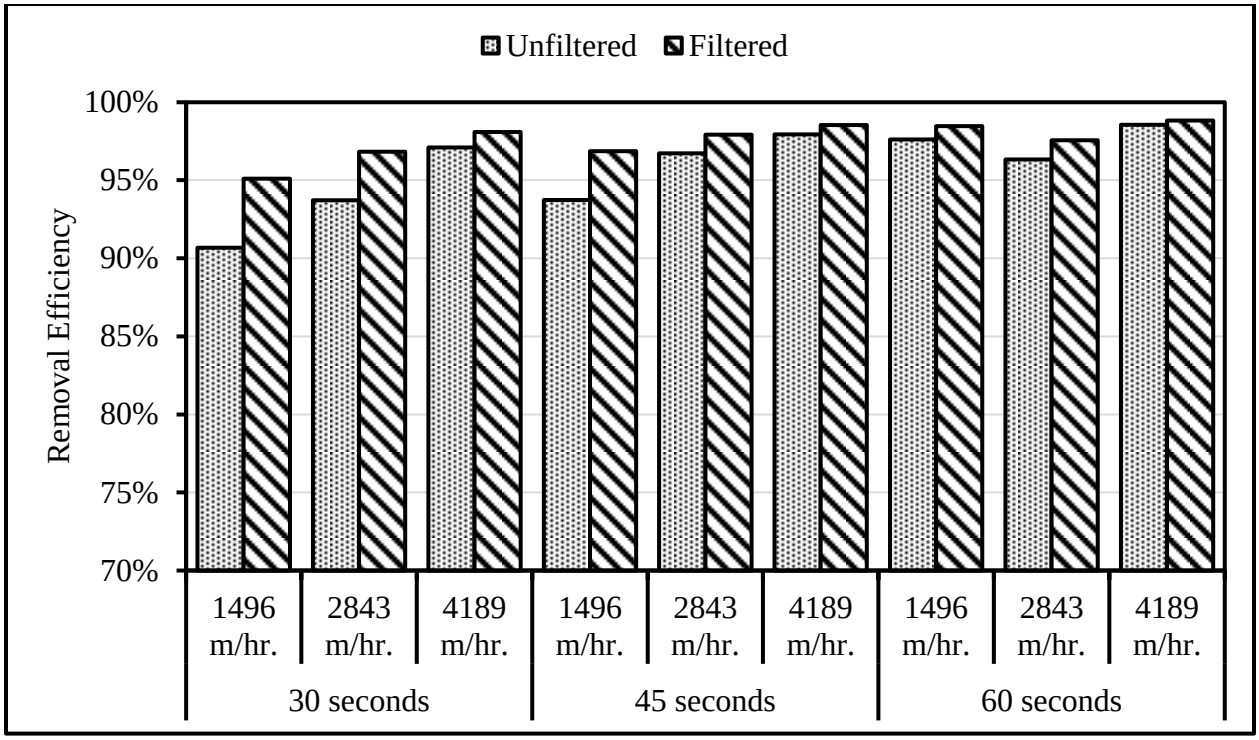

Figure 20 Plot of efficiencies for PAM APS 705 at a concentration of 833 mg/L

However, the plot for Figure 20 reveals that at certain level of PAM concentration there is no significantly observed improvement in performance efficiency. Thus, further increase in PAM concentration and mixing energy would not produce better results but only increases the possibility of higher levels of toxicity and more flocculants in the residual water discharged from the treatment channel. The observations from APS 705 PAM are similar to the other PAM products investigated and the results are shown in Appendix F.

Paired statistical tests were performed to investigate the effect of filtration of the residual water. The test conducted was the Wilcoxon Signed-Rank test on dependent parameters – unfiltered and filtered residual water. Test results showed significant effect on filtration of the residual water at 5 percent significance level for all four PAM products. Filtration did

significantly improve PAM performance efficiency and provided the means to hold down flocculants which eventually reduces the transport of PAM flocs to receiving water bodies. The Wilcoxon Signed-Rank test results for the four PAM products are presented in Table 31 to Table 38 of Appendix F.

In order to change the current practice of dependence on the manufacturer (Applied Polymer, Incorporated) for PAM dosage requirement for specific sites, the manufacturers guide is modified to fit the results from testing completed at SMARTL. The modification is derived from the current practice, but a methodological and repeatable procedure, aimed providing design tools for design and field engineers. The detailed modified procedure is shown in Appendix G.

Conclusions

The two silt fence fabrics, BSRF and ARS-1400 meet the ASTM specifications for the grab strength, permittivity and apparent opening size. Silt fence can be used to enhance PAM turbidity removal performance, and will significantly contribute in the reduction of sediment concentration of the discharge by trapping the flocculants. The dosage testing for turbidity removal using PAM reveals that as mixing speed and mixing time increase, the efficiency of the turbidity removal increases but that there is a threshold of mixing speed and time at which the efficiencies will plateau. At that dosage, the addition of PAM, mixing speed and/or mixing time will not significantly improve the performance standard.

EFFLUENT CONTROL FIELD-SCALE TESTING

Introduction

The two silt fence fabrics used for the tests are a nonwoven, polyester belted silt retention fabric (BSRF) and a woven monofilament polypropylene fabric (ARS 1400). The woven silt fence is described as a circular woven polypropylene geotextile in which individual filaments are woven into a regular pattern such that every filament retains dimensional stability relative to one another. It is designed to resist ultraviolet, biological, and chemical degradation normally found in soils. Assurene Corporation manufactured the woven silt fence fabrics identified as ASR-1400 and was donated for the study by Absolute Erosion Control, Inc. On the other hand, the nonwoven silt fence is a biodegradable, nonwoven, spun-bond, polyester geotextile reinforced with a fiberglass scrim (coarse mesh-like material) or net sandwiched in between the layers, which makes the geotextile and fiberglass materials act as a unit. This product identified as a Belted Silt Retention Fabric (BSRF) is manufactured and donated by Silt Saver, Inc. Georgia.

Field tests were designed to determine the field performance, installation, filtration capacity, and flow-through rates (herein referred to as flow rates) of woven and nonwoven silt fence barrier using a rainfall simulator on field scale testing bed. The study was intended to provide a better understanding of actual performance of silt fence in real-time operational conditions. Analysis of field scale testing results will further provide means of developing the relationship between the silt fence barrier flow rate and filtration efficiency. The tests involved series of field-scale tests of different rainfall intensities on compacted sandy soil embankment slopes. The research objectives are to conduct field-scale experimental studies on tilting test beds

with simulated rainfall to evaluate the effectiveness and efficiency; to determine the inherent problems in current practice; and to compute the flow through rate of silt fences as temporary sediment barriers.

Field-Scale Test Preparation

The investigations were conducted using the test beds and rainfall simulator available at the University of Central Florida (UCF) Stormwater Management Academy Research and Testing Laboratory (SMARTL). The aluminum test bed is 2.4 meter (8 feet) wide by 9.1 meter (30 feet) long by 12.7 centimeter (12 inches) deep and attached to a tilting system with a pivot at one end and a hydraulic mechanism to set different slopes (Wanielista and Chopra 2010). For the field-scale simulation, the test bed was modified by the construction of a plywood apron on its perimeter to increase the test bed depth to 50.8 centimeter (20 inches) to accommodate minimum depth of posts or stakes embedment – 45.7 centimeter (18 inches). The bed was then loaded with the sandy soil (93 percent sand and 7 percent silt, AASHTO Classification Type A-3) placed in three layers of 15.2 centimeter (6-inch), and compacted to achieve 95 percent Standard Proctor compaction effort of 1721 kilogram per cubic meter (107.4 pounds per cubic feet) maximum dry unit weight. Figure 21 shows the test bed modification to accommodate silt fence installation and soil placement.

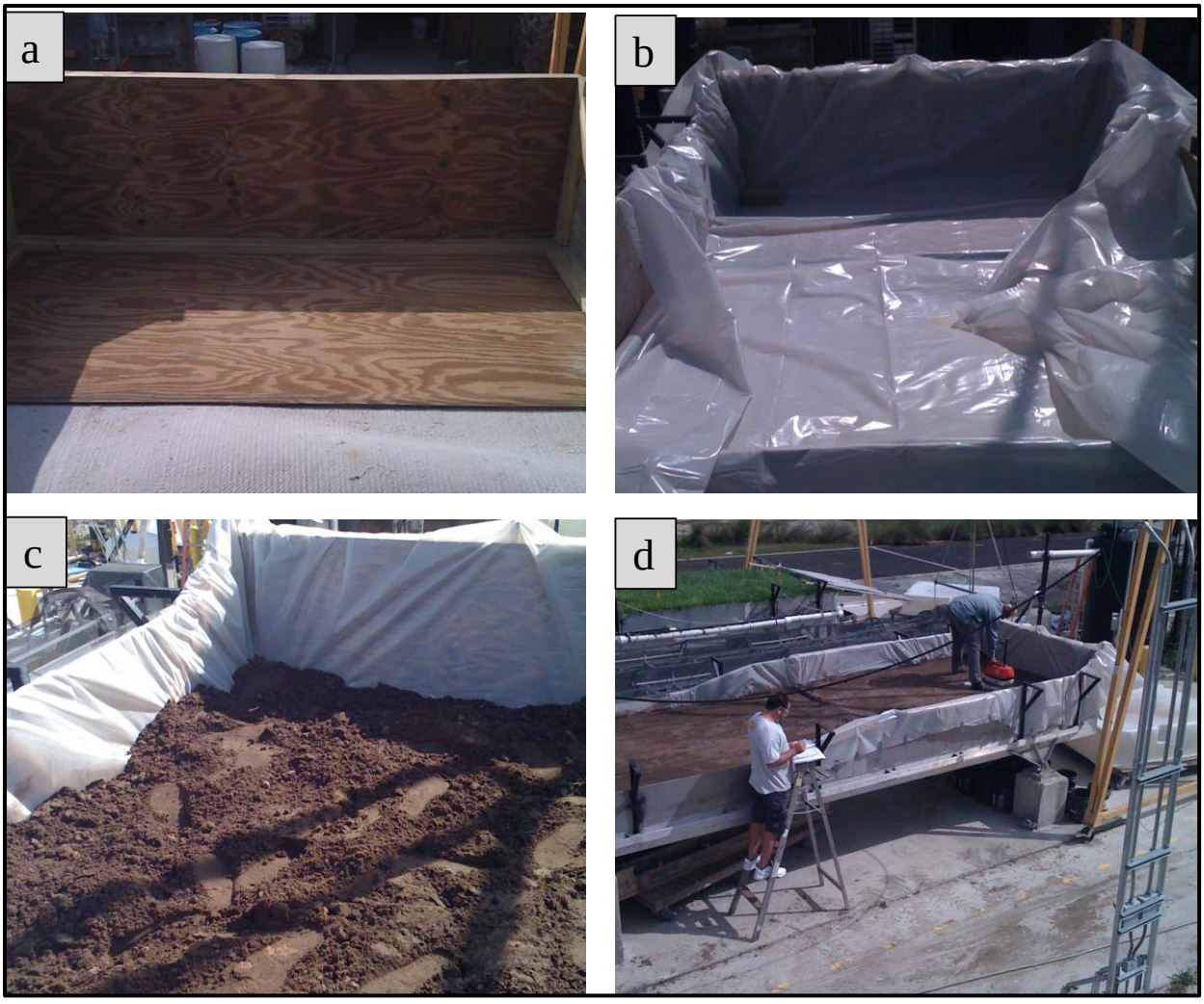

Figure 21 Pictures of test bed modification and preparation (a) plywood for depth, (b) Visqueen to protect plywood, (c) soil placement, and (d) soil density measurement

The silt fence posts (stakes) were spaced 1.5 meters (5 feet) and buried 45.7 centimeters (18 inches) deep into the soil. Trench of 15.2 by 15.2 centimeters (6 by 6 inches) was dug along the test bed perimeter and the silt fence placed in "L" shape, see Figure 22. The trench was then backfilled with the soil and compacted to achieve desired compaction level prior excavation. Figure 23 presents silt fence test setup for the two different fabrics for testing on the tilting test bed. Further details of the test bed setup may be found in this report, Index Testing to Support

the Stormwater Management Erosion and Sediment Control Laboratory (Chopra et al. 2010).

Figure 22 Silt fence installation on test-bed (a) 15 × 15 cm trench, and (b) BSRF silt fence installed

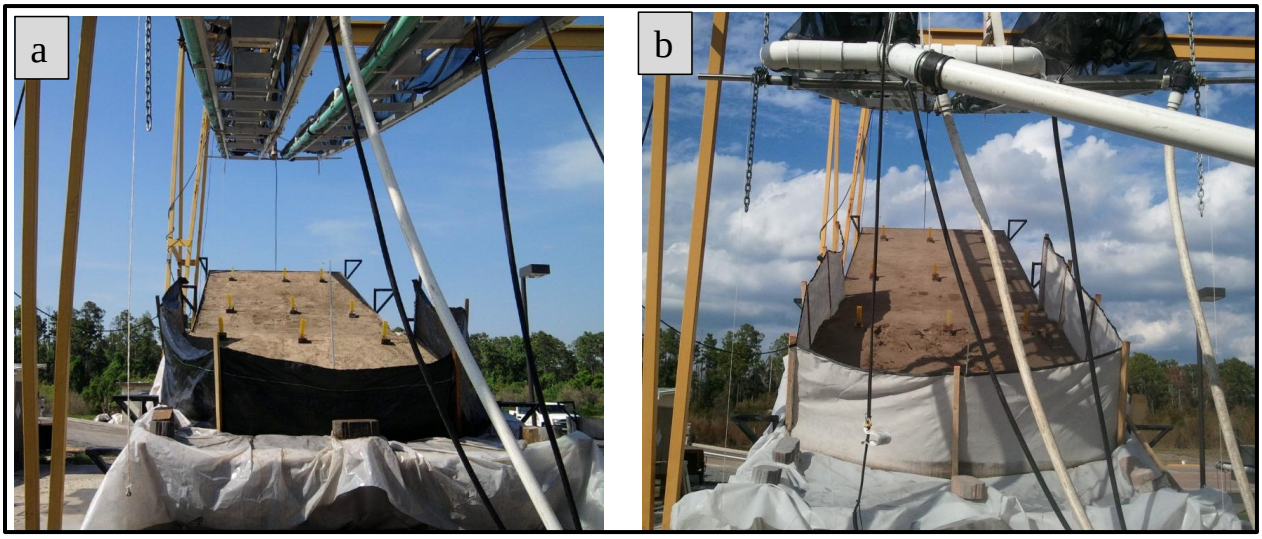

Figure 23 Rainfall simulator and test bed at SMART laboratory, UCF with (a) woven (ARS 1400) and (b) nonwoven (BSRF) silt fence fabrics installed and prepared for testing

Field-Scale Test Procedure

Both woven and nonwoven silt fence fabrics were installed on the tilting test bed and set to 3 different embankment slopes (33, 25, and 10 percent) and three simulated rainfall intensities

– 25.4, 76.4, and 127 millimeter per hour (1, 3, and 5 inches per hour, in./hr.). In addition, an extreme case of a very steep slope (50%) was also studied in order to determine the limits of the performance of these fabrics. It is not recommended that silt fences be used in situations with such steep slopes. The testing matrix for a typical case of 25% slope is shown in Figure 24.

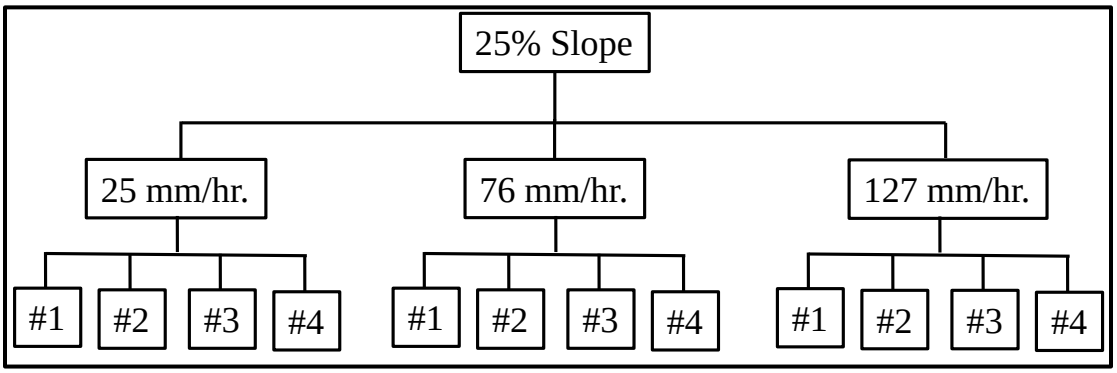

Figure 24 A sample field test matrix for 25 percent slope (repeated for 50, 33, and 10 percent slopes)

Four rainfall events were simulated for each pair of embankment slope and rainfall intensity. The duration of each simulated rainfall event was measured at the commencement of rainfall and continued for 30 minutes after initiation of runoff downstream of the silt fence. Downstream (effluent) runoff was collected at one-minute interval until runoff stopped for volume and mass measurement. In addition, grab samples were collected upstream (influent) of the silt fence and downstream at 5-minute intervals and continued until 30 minutes after every rainfall event or when there was no runoff downstream and/or upstream. The collected grab samples were tested for sediment concentration (total solids) and turbidity according to the Standard Methods for the Examination of Water and Wastewater (APHA et al. 2005).

During and after each simulated rainfall event, the installed silt fence was inspected for overtopping, tear or puncture on the fabric, and operational stability and resistance of the silt fence against the deposited soil and backwater loads. Any one of the aforementioned factors could lead to uncontrolled discharge which would eventual distort the results. Thus, samples were not collected from those tests that resulted in uncontrolled discharges. However, where none of these failures were observed, the rainfall was simulated again, after 3 hours or more interval, and testing continued with no maintenance or retrofit to the silt fence and soil surface after the previous rainfall event. The test was repeated one more time and after that, the silt fence was cleared of all debris and the soil on the test bed was flattened and compacted prior to the fourth simulated rainfall event to simulate maintenance. The rainfall events are numbered as #1, #2, #3, and #4, according to the sequence of testing for a set of rainfall intensity and embankment slope.

The entire test procedure was repeated for three embankment slopes and three simulated rainfall intensities. A total of 96 rainfall events were simulated, that is, 48 test events on each type of silt fence fabric. Tests were conducted over a span of one and half years, from December 8, 2009 through July 13, 2011. The total numbers of grab samples collected were 423 upstream and 376 downstream on the woven silt fence fabric. On the nonwoven silt fence fabric, the grab samples collected were 441 and 504 upstream and downstream, respectively.

A computer console attached to the rainfall simulator was utilized to preset rainfall intensity. The actual rainfall intensity was verified by direct measurement of volume and duration using rain gauges and stopwatch, for the respective rainfall event. The rainfall simulator was used to simulate rainfall for different rainfall intensities, which subsequently generated

runoff from the test bed. The rainfall simulator is fitted with pressurized distribution system with specialized water spray nozzles designed to produce drop sizes that is similar to natural rainfall. Wanielista and Chopra (2010) conducted drop size analysis from the rainfall simulator and showed how it effectively simulate natural rainfall.

Results and Discussion

Data for the rainfall intensity and duration, embankment slopes, rainfall events, and runoff samples from water that has pooled behind and in front of the silt fence were collected and measured. For both fabrics, data from the tests on embankment slopes of 33 and 50 percent were not analyzed as there were no water pools upstream of the nonwoven silt fence, and thus, no upstream grab samples. There were only downstream samples, which made it difficult to check the pre- and post-performance for these slopes. What actually occurred is the "flow" of soil towards the silt fence with no runoff. Submerged water did seep through the fabric and generated only downstream samples. For the woven silt fence, rainfall intensities of 76.4, and 127 mm/hr. (3 and 5 in./hr.) with 33 and 50 percent embankment slopes produced high volumes of upstream runoff and generated uncontrolled discharges such as overtopping and torn silt fence fabrics. This led to the stoppage of grab samples collection. In most of the uncontrolled discharge conditions, only about two to three pairs of samples were collected for a test, and these were considered too few for any meaningful further analysis. Based on the no sampling condition observed for nonwoven fabric and uncontrolled discharges in the woven fabric tests on 33 and 50 percent embankment slopes, the data collected are not included in the results discussed. Figure 25 shows factors that constitute uncontrolled discharges, namely overtopping, runoff gushing out of a torn fabric and the spill downstream.

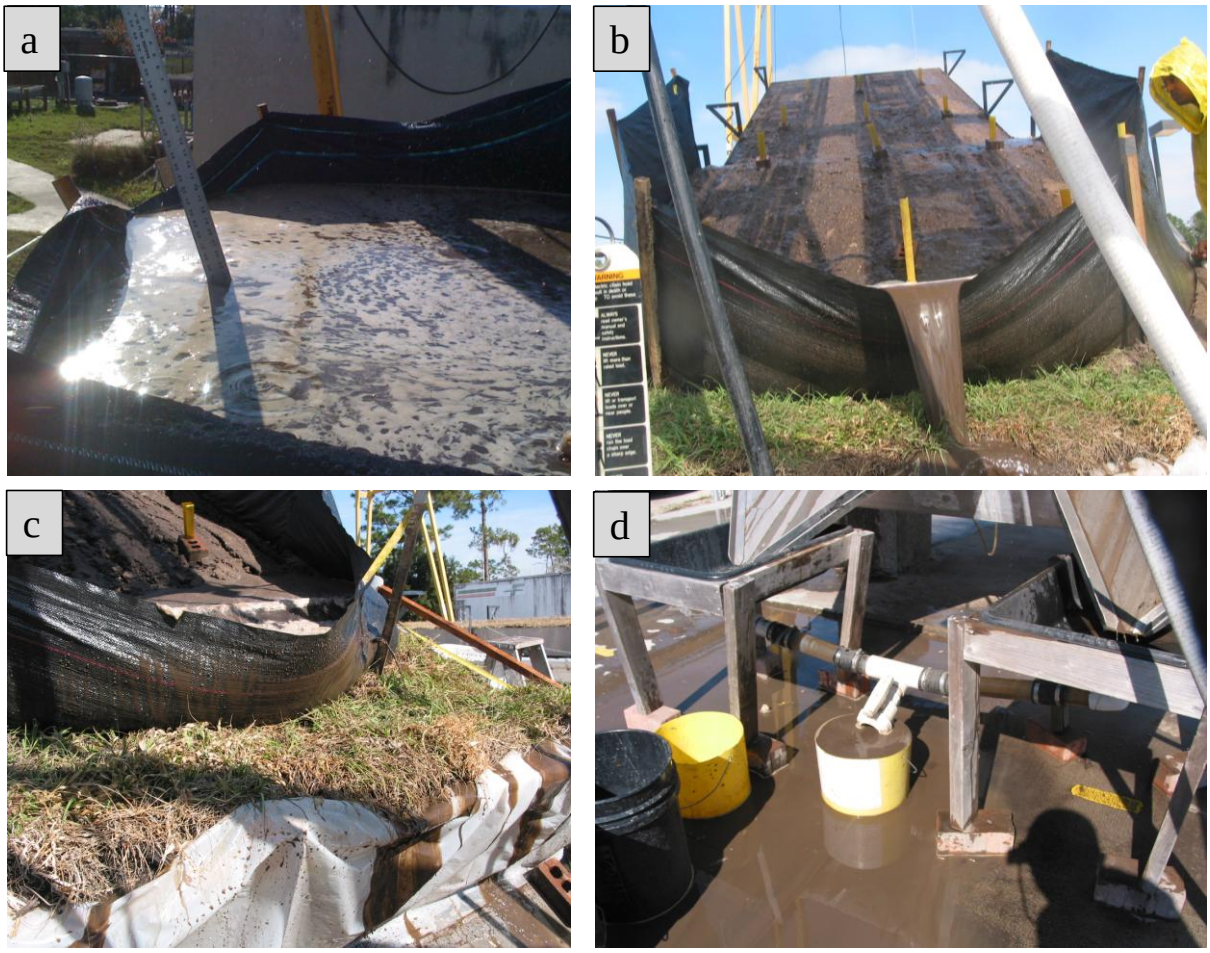

Figure 25 Uncontrolled discharge due to high slope and high intensity rainfall event (a) upstream flooding, (b) overtopping, (c) torn fabric, and (d) downstream spill

Grab samples (upstream and downstream) from 24 tests on the 10 and 25 percent embankment slopes for each silt fence fabric were analyzed for turbidity and sediment concentration. Sampling for the woven silt fence fabric resulted in 549 grab samples (295 upstream and 254 downstream) and for the nonwoven silt fence fabric it was a total of 543 grab samples (269 upstream and 274 downstream). On every test, both the turbidity and the sediment concentration values obtained from all collected grab samples are weighted by the volume of upstream and downstream water at 5-minute intervals to obtain representative characterization of

the turbidity and sediment concentration of both influent and effluent samples for that rainfall event. These computations are expressed in Equations 10 through 13

$$WMIC = \frac{\sum_{i=1}^{n}(SC)_{\text{inf}} \cdot \Delta V}{\sum \Delta V} \tag{10}$$

$$WMIT = \frac{\sum_{i=1}^{n}(T)_{\text{inf}} \cdot \Delta V}{\sum \Delta V} \tag{11}$$

$$WMEC = \frac{\sum_{i=1}^{n}(SC)_{eff} \cdot \Delta V}{\sum \Delta V} \tag{12}$$

$$WMET = \frac{\sum_{i=1}^{n}(T)_{eff} \cdot \Delta V}{\sum \Delta V} \tag{13}$$

where WMIC = weighted mean influent concentration (mg/L); WMEC = weighted mean effluent concentration (mg/L); SC = sediment concentration in runoff (mg/L); WMIT = weighted mean influent turbidity (NTU); WMET = weighted mean effluent turbidity (NTU); T = turbidity (NTU); ΔV = change in volume (inf. – influent and eff. – effluent); and n = number of samples collected. Table 8 and Table 9 present the volume-weighted turbidity and sediment concentration and the respective performance efficiency for both ARS-1400 and BSRF silt fence fabrics.

Table 8 ARS-1400 fabric test volume-weighted turbidity and sediment concentration results

Slope % (Ratio)	Rainfall Intensity (mm/hr.)	Rainfall Events	Volume-Weighted Mean Turbidity			Volume-Weighted Mean SSC		
			Upstream (NTU)	Down stream (NTU)	Performance Efficiency (%)	Upstream (mg/L)	Down stream (mg/L)	Performance Efficiency (%)
25% (4:1) Slope	25	#1	12796	15179	-19	8761	10215	-17
		#2	6695	5623	16	5703	4948	13
		#3	4084	3410	17	3687	2901	21
		#4	11689	9475	19	9511	7424	22
	76	#1	14338	15886	-11	10816	9590	11
		#2	8008	5779	28	7848	4981	37
		#3	10448	6749	35	10413	4359	58
		#4	6537	4937	24	4937	4623	6
	127	#1	11014	9905	10	10302	8564	17
		#2	9696	6405	34	10398	5910	43
		#3	10724	5486	49	11898	5362	55
		#4	8814	7909	10	8195	6784	17
10% (10:1) Slope	25	#1	903	473	48	844	763	10
		#2	790	615	22	990	735	26
		#3	695	525	25	1107	670	39
		#4	750	810	-8	1319	970	26
	76	#1	858	816	5	1065	863	19
		#2	705	566	20	778	793	-2
		#3	331	311	6	659	546	17
		#4	1118	1223	-9	1147	791	31
	127	#1	573	611	-7	718	515	28
		#2	558	505	9	776	599	23
		#3	425	528	-24	602	488	19
		#4	615	534	13	820	705	14

Table 9 BSRF fabric test volume-weighted turbidity and sediment concentration results

Slope % (Ratio)	Rainfall Intensity (mm/hr.)	Rainfall Events	Volume-Weighted Mean Turbidity			Volume-Weighted Mean SSC		
			Upstream (NTU)	Down stream (NTU)	Performance Efficiency (%)	Upstream (mg/L)	Down stream (mg/L)	Performance Efficiency (%)
25% (4:1) Slope	25	#1	1691	602	64	2984	660	78
		#2	2480	988	60	2113	695	67
		#3	1692	634	63	1892	512	73
		#4	2287	1154	50	1663	817	51
	76	#1	3510	1805	49	2064	1166	44
		#2	1835	837	54	1448	642	56
		#3	1546	554	64	1131	467	59
		#4	1896	670	65	1226	502	59
	127	#1	3472	2186	37	2228	1346	40
		#2	1835	655	64	1480	547	63
		#3	1060	232	78	593	147	75
		#4	2009	621	69	1201	475	60
10% (10:1) Slope	25	#1	502	141	72	2052	908	56
		#2	407	112	73	884	337	62
		#3	561	95	83	1298	219	83
		#4	200	92	54	315	299	5
	76	#1	497	291	42	820	375	54
		#2	257	131	49	406	245	40
		#3	143	64	55	326	183	44
		#4	198	71	64	400	274	31
	127	#1	208	124	40	387	278	28
		#2	231	127	45	403	300	26
		#3	61	45	26	286	251	12
		#4	241	93	61	431	340	21

Change in influent volume was calculated from the measured depth of ponded water upstream and effluent volume from the collected samples downstream. The influent volume was calculated as the product of the depth and length of backwater (pond behind the silt fence) and the width of the test-bed at 5-minute intervals. The volume of the effluent runoff was measured directly from the runoff collected from the collection bin downstream. To obtain paired

representation of both upstream and downstream turbidity and sediment concentration, the measured turbidity and sediment concentration at each time step was weighted with the corresponding change in influent and effluent volumes.

The performance efficiency for total solid removal (E_{TS}) and turbidity reduction (E_T) for each rainfall event were computed as expressed in Equations 14 and 15, respectively.

$$E_{TS}(\%) = 100 \cdot \left[1 - \frac{WMEC}{WMIC} \right] \tag{14}$$

$$E_T(\%) = 100 \cdot \left[1 - \frac{WMET}{WMIT} \right] \tag{15}$$

Presented in Table 10 and Table 11 are statistical analysis on the volume-weighted mean turbidity and sediment concentration on 10 and 25 percent embankment slopes for woven and nonwoven silt fence fabrics, respectively. Turbidity reduction efficiency ranged from -24 to 53 percent with a mean and median of 13 percent for the woven silt fence fabric. For the nonwoven fabric, the range for turbidity reduction efficiency varied between 26 and 83 percent with mean and median of 58 and 61 percent, respectively. However, based on standard errors obtained, the accuracy of the sample mean as a predictor of the true mean is approximately 31 and 5 percent for the woven and nonwoven silt fence fabrics, respectively.

Similarly, the sediment concentration removal efficiency for both silt fence fabrics ranged between -17 to 58 percent with a mean and median of 22 and 20 percent; and from 5 to 84 percent with mean and median of 49 and 55 percent for woven and nonwoven silt fence fabrics, respectively. The relative standard error indicates sample mean prediction error of 16

and 8 percent for the woven and nonwoven silt fence fabrics, respectively. The percentage of prediction error was calculated from the ratio of standard error and mean.

Table 10 Summary of basic statistics for woven (ARS 1400) silt fence

	Volume-weighted Mean Turbidity (NTU)				Volume-weighted Mean Sediment concentration (mg/L)			
Parameters	Up-stream	Down-stream	Diff.	Efficiency (%)	Up-stream	Down-stream	Diff.	Efficiency (%)
Mean	5132	4344	788	13	4721	3504	1216	22
Standard error	1012	954		4.0	876	662		3.5
Median	2601	2317	173	15	2503	1936	353	20
Standard Deviation	4959	4678	1635	19	4289	3257	1947	17
Minimum	331	311	20	6	602	488	114	19
Maximum	14338	15886	-1548	-11	11898	10215	1683	14
Weight-average	4295	3819	476	11	3758	3008	750	20

Table 11 Summary of basic statistics for nonwoven (BSRF) silt fence

	Volume-weighted Mean Turbidity (NTU)				Volume-weighted Mean Sediment Concentration (mg/L)			
Parameters	Up-stream	Down-stream	Diff.	Efficiency (%)	Up-stream	Down-stream	Diff.	Efficiency (%)
Mean	1201	513	687	58	1168	669	677	49
Standard Error	217	101		2.7	157	55		4.1
Median	810	261	647	61	1166	421	694	55
Standard Deviation	1064	564	555	14	767	309	558	21
Minimum	61	45	16	26	286	147	139	49
Maximum	3510	1805	1324	38	2984	1166	1638	55
Weight-Average	1413	617	796	56	1218	538	681	56

Equation 16 shows a computation for the weighted average of each silt fence volume-weighted mean turbidity and sediment concentration, based on the percentage of the prediction accuracy of the sample mean. It is computed as the ratio of sum-product of the weighted mean (WM) for the respective parameter – turbidity and sediment concentration – and the number of

samples (n_i) from each test conducted, and the sum of the number of samples. The weighted mean obtained from Equations 10 through 13 are multiplied by the number of grab samples and summed for the 24 tests; the sum-product was then divided by the sum of the grab samples for either upstream or downstream samples.

$$E_{mean} = \frac{\sum_{i=1}^{n}\left[(WM)_i \cdot n_i\right]}{\sum_{i=1}^{n} n_i} \tag{16}$$

The efficiency is computed as expressed in Equations 14 and 15 for turbidity and sediment concentrations, respectively. The calculation yielded 11 and 56 percent turbidity reduction efficiency, and 20 and 56 percent reduction efficiency in sediment concentration for woven and nonwoven fabrics, respectively. The difference between the upstream and downstream grows exponentially with the embankment slopes for turbidity and sediment concentration. The mean absolute deviation, which is a measure of accuracy of the fit to the observed data with less influence from outliers, ranged between 3.4 and 4.5 percent. The different embankment slope results are presented in Figure 26 through Figure 33 as bar chart plots for paired upstream and downstream volume-weighted mean turbidity and sediment concentration, at 10 and 25 percent embankment slopes for the woven and nonwoven silt fence fabrics.

Nonwoven Silt Fence Fabric Performance Evaluation

The volume-weighted mean turbidity for the nonwoven silt fence fabric at 10 percent slope revealed that there is a statistically significant effect in the reduction of turbidity between the upstream and downstream samples shown in Figure 26. The difference in turbidity

measurement ranged between 16 to 466 NTU, which translate to an average percent difference of 55 percent and standard deviation of 15 percent for the three rainfall intensities. On the other hand, for the same slope and fabric shown in Figure 27, the sediment concentration showed a significant reduction. The volume-weight mean solid concentration difference ranged between 16 and 1144 mg/L having an average performance efficiency of 39 percent and standard deviation of 21 percent. The wide range for both parameters of turbidity and solid concentration may be due to combination of the three rainfall intensities and four rainfall events, and sampling error during sample collection.

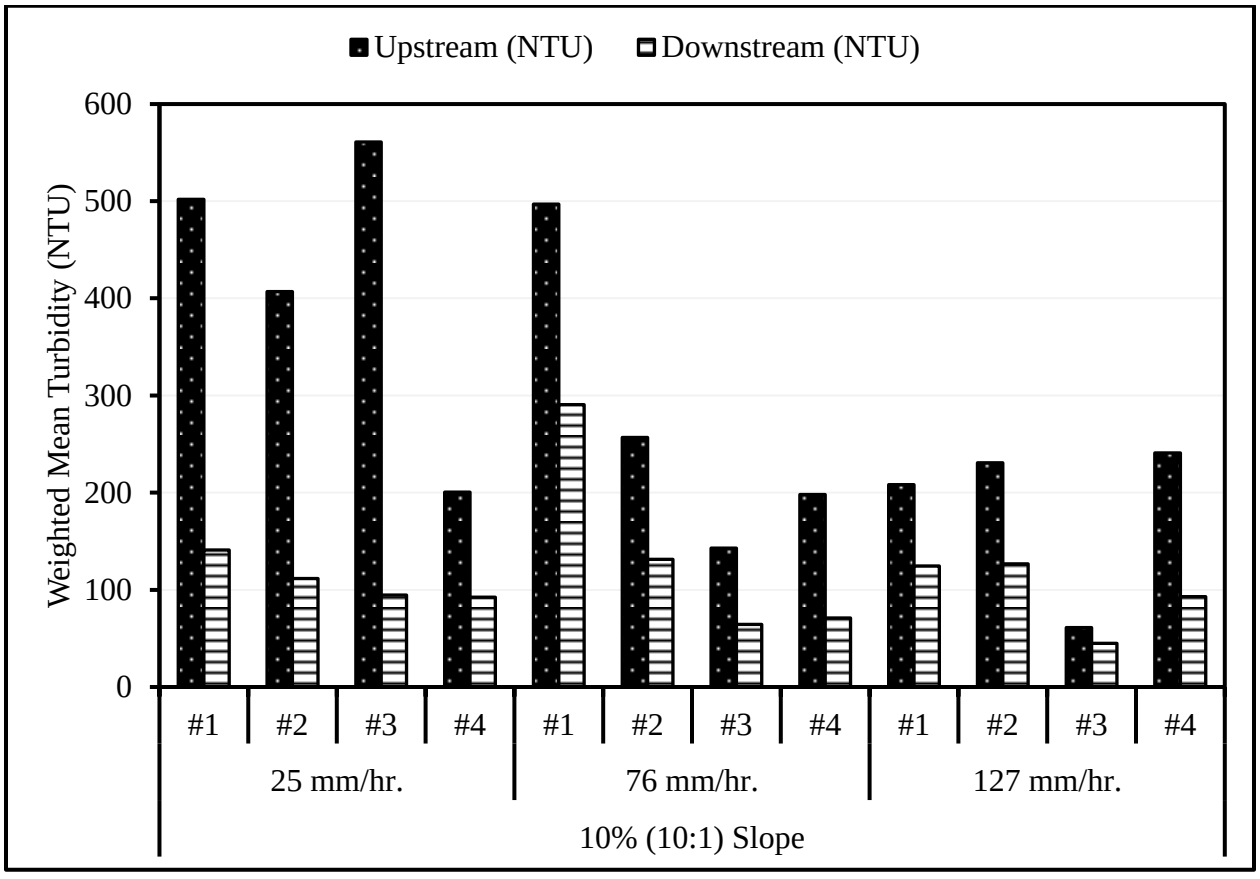

Figure 26 Volume-weighted mean turbidity for nonwoven silt fence at 10% slope

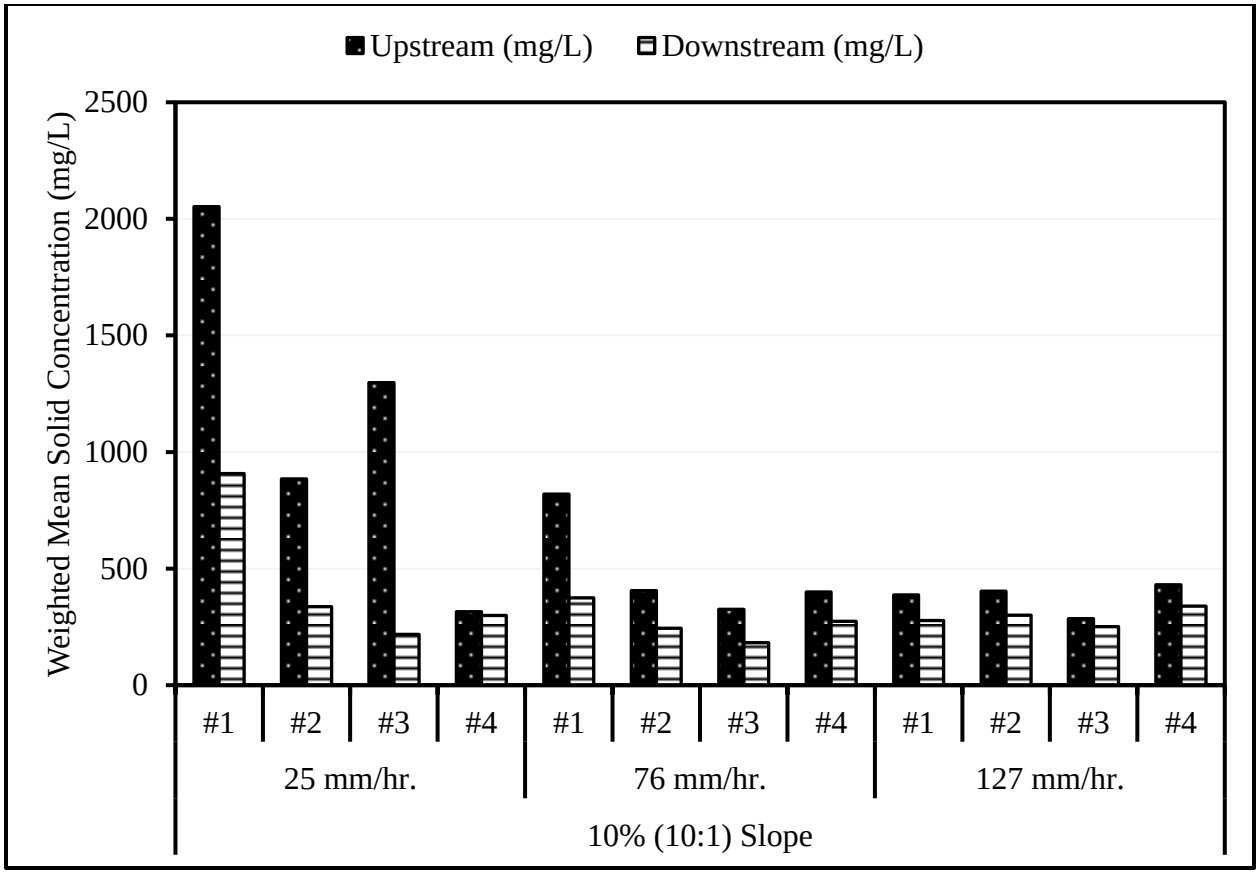

Figure 27 Volume-weighted mean sediment concentration for nonwoven silt fence at 10% slope

Both Figure 28 and Figure 29 for turbidity and solid concentration efficiency evaluations on 25 percent slope showed similar trend as was in 10 percent slope for the nonwoven silt fence fabric. That is, the silt fence significantly reduced the turbidity and sediment concentration of the samples collected from the upstream and downstream. The range for the difference in weighted mean turbidity is between 828 and 1705 NTU and an average performance efficiency of 60 percent at standard deviation of 10 percent. The volume-weighted mean sediment concentration ranged between 446 and 2325 mg/L, the average performance efficiency of the silt fence at this slope is 60 percent with a standard deviation of 11 percent.

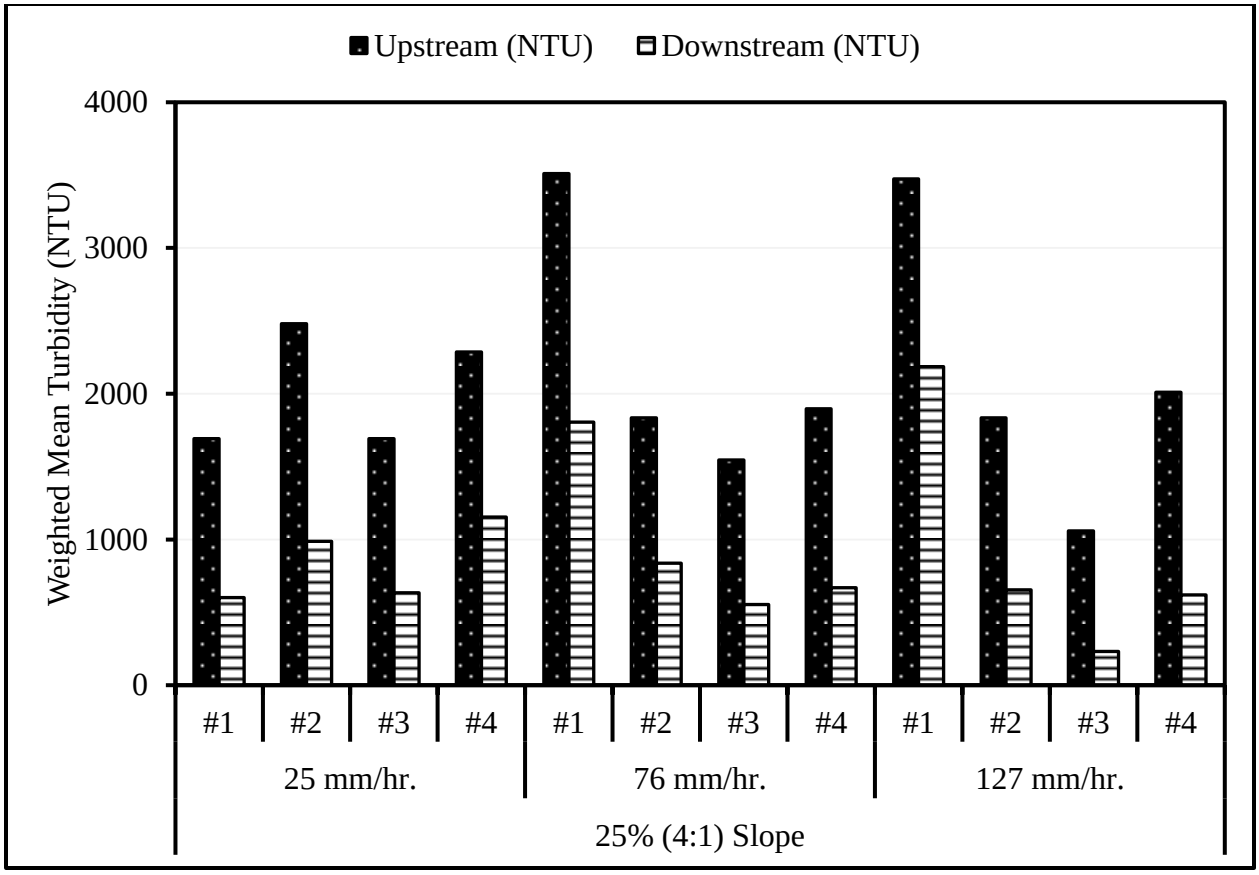

Figure 28 Volume-weighted mean turbidity for nonwoven silt fence at 25% slope

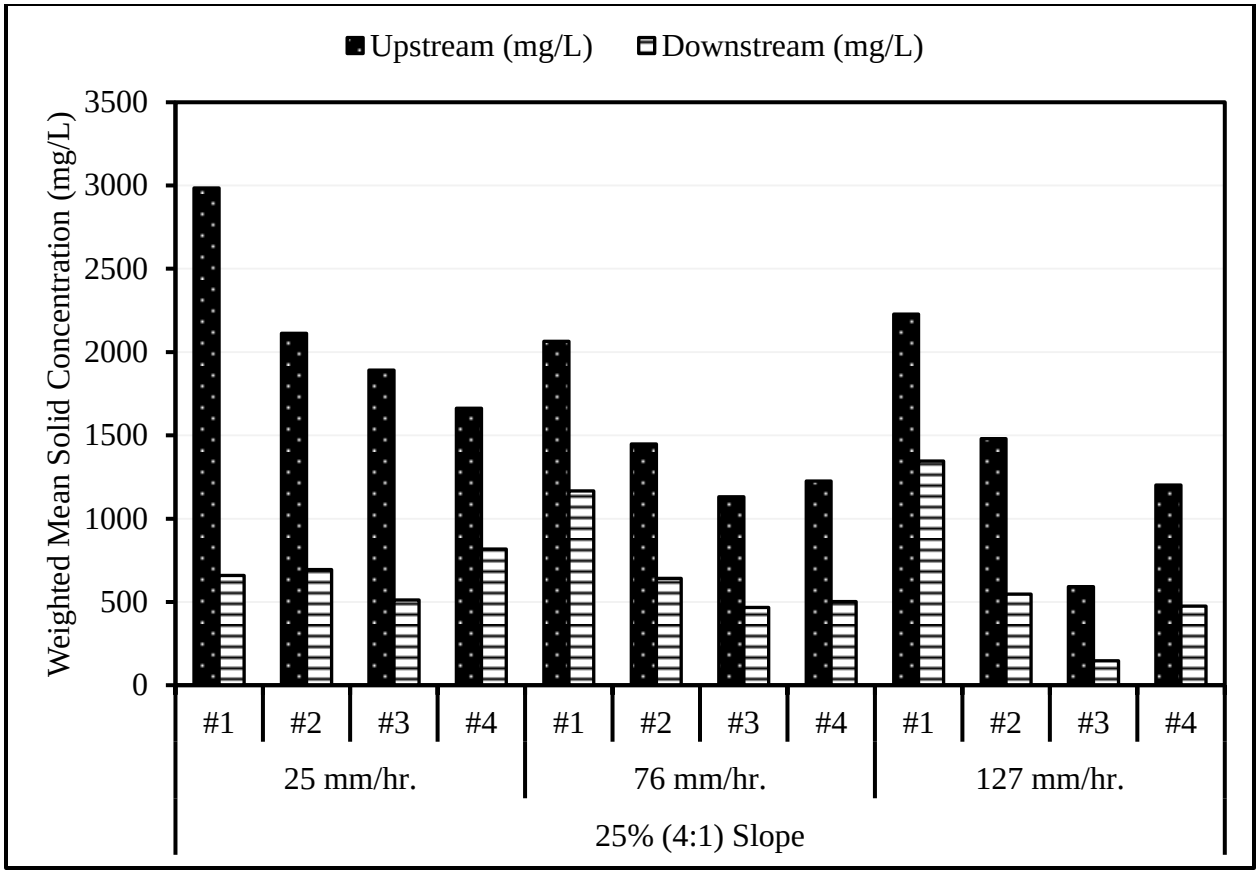

Figure 29 Volume-weighted mean sediment concentration for nonwoven silt fence at 25% slope

Woven Silt Fence Fabric Performance Evaluation

Figure 30 presents a bar chart for the upstream and downstream volume-weighted mean turbidity test results of the woven silt fence fabric installed on a 10 percent slope. The difference in the volume-weighted mean turbidity ranged between -105 and 429 NTU, and the average performance efficiency for turbidity reduction is 8 percent with a standard deviation of 18 percent. The volume-weighted sediment concentration in Figure 31 showed the range for the difference at upstream and downstream locations between -15 and 436 mg/L. The average and standard deviation for the silt fence performance in sediment concentration reduction are 21 and 10 percent, respectively. In spite of the low performance efficiencies observed, statistical

analyses showed that the silt fence has significant effect in the reduction of turbidity and solid concentration.

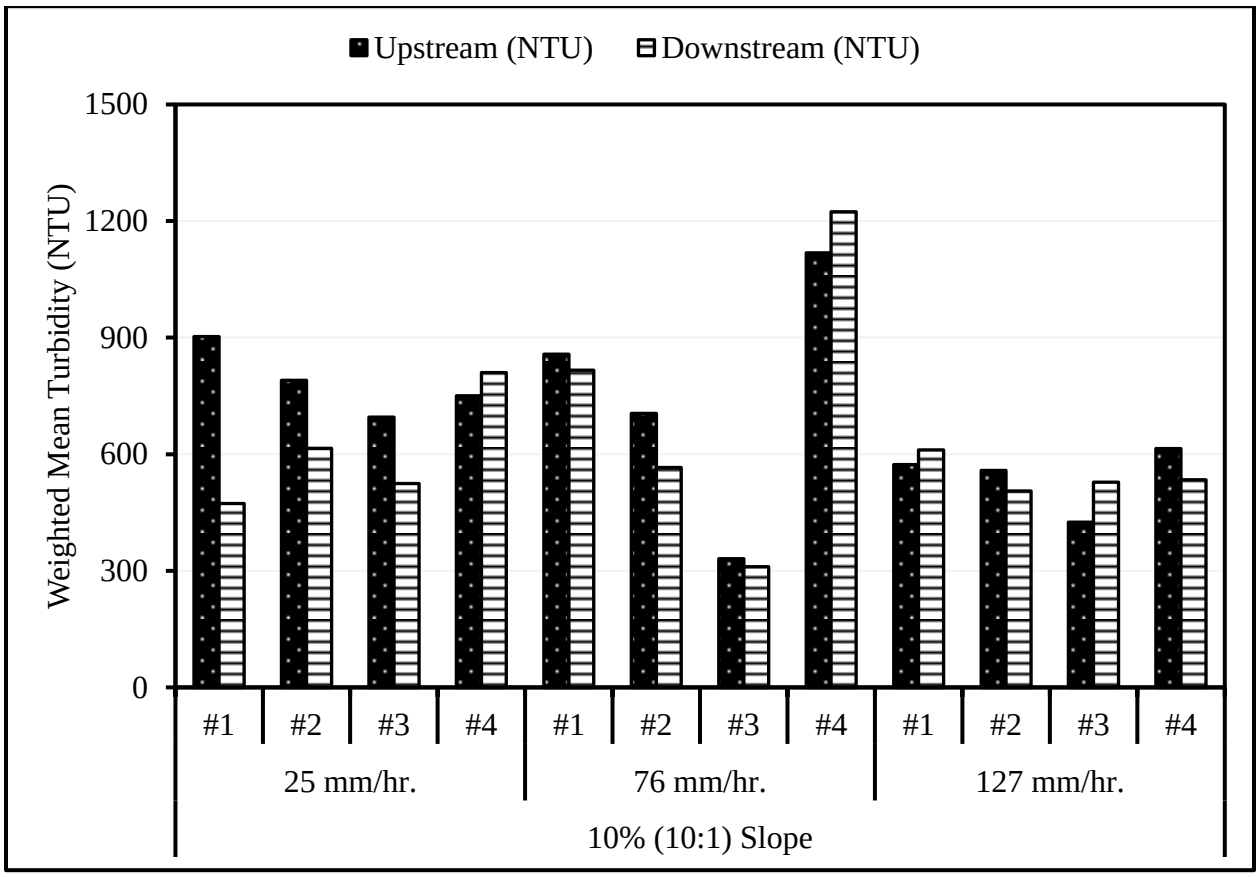

Figure 30 Volume-weighted mean turbidity for woven silt fence at 10% slope

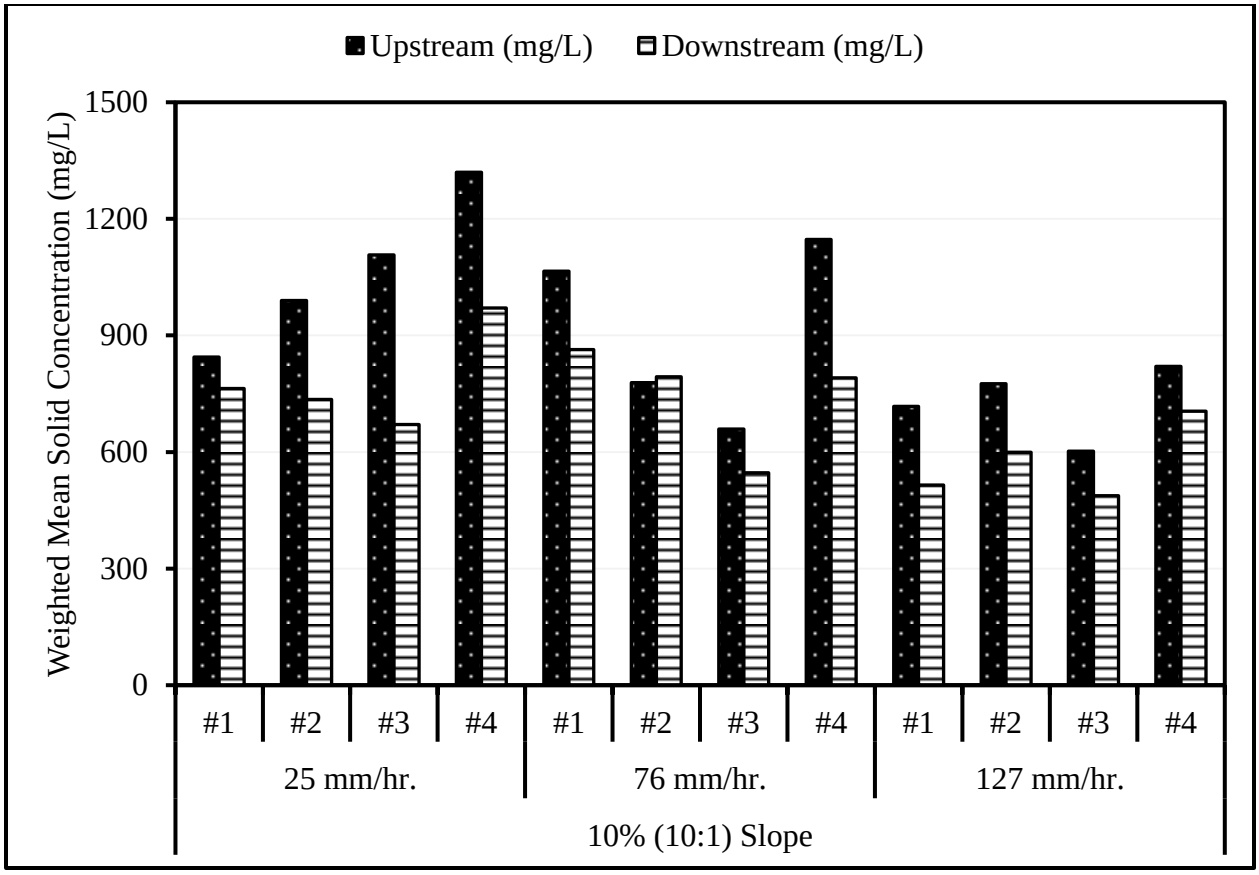

Figure 31 Volume-weighted mean sediment concentration for woven silt fence at 10% slope

The negative values observed for the woven fabric is explained by the volume-weighted mean turbidity and sediment concentration for downstream samples been higher than the paired upstream samples. In such cases, the downstream samples were more turbid or have more sediment concentration than the paired upstream sample. On the other hand, negative differences may have resulted due to sampling error, release of trapped particles in the fabric, and/or the effect of damming by the silt fence which resulted in settling of the particles in suspension after the simulated rainfall was stopped and grab samples were still collected. Thus, the grab samples collected from the water pool upstream had fewer sediment concentrations in suspension than the downstream samples.

For the woven silt fence fabric installed on 25 percent embankment slopes, the differences between the upstream and downstream samples in the volume-weighted mean turbidity and sediment concentration are statistically significant. However, there were observed negative differences, which can be attributed to the factors mentioned in previous paragraph. For Figure 32, the observed difference in volume-weighted turbidity is between -2383 and 5238 NTU. Both the average performance efficiency and standard deviation are 18 percent. For the same slope and fabric, the upstream and downstream plots shown in Figure 33 revealed a volume-weighted sediment concentration difference of between -1454 and 6536 mg/L. The average performance efficiency and standard deviation are 24 and 20 percent, respectively.

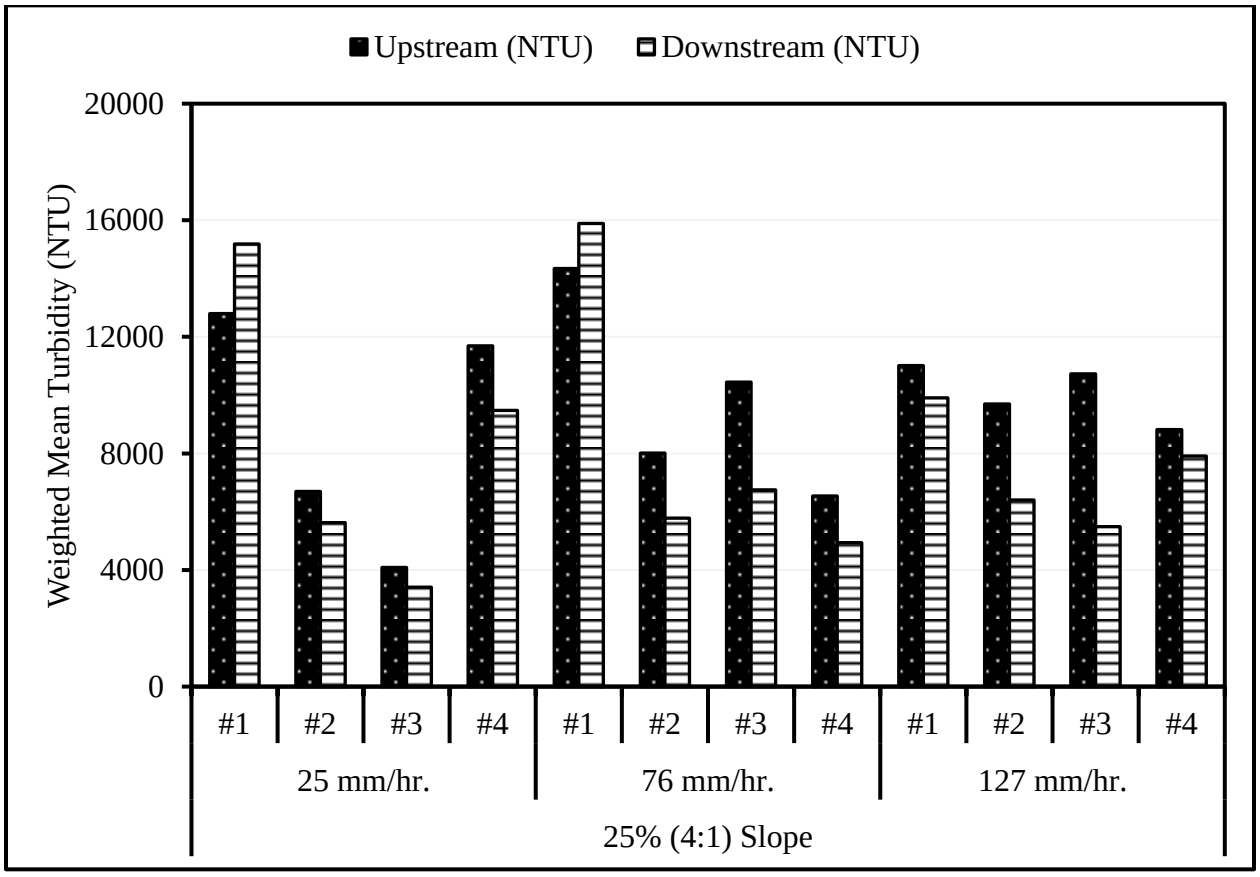

Figure 32 Volume-weighted mean turbidity for woven silt fence at 25% slope

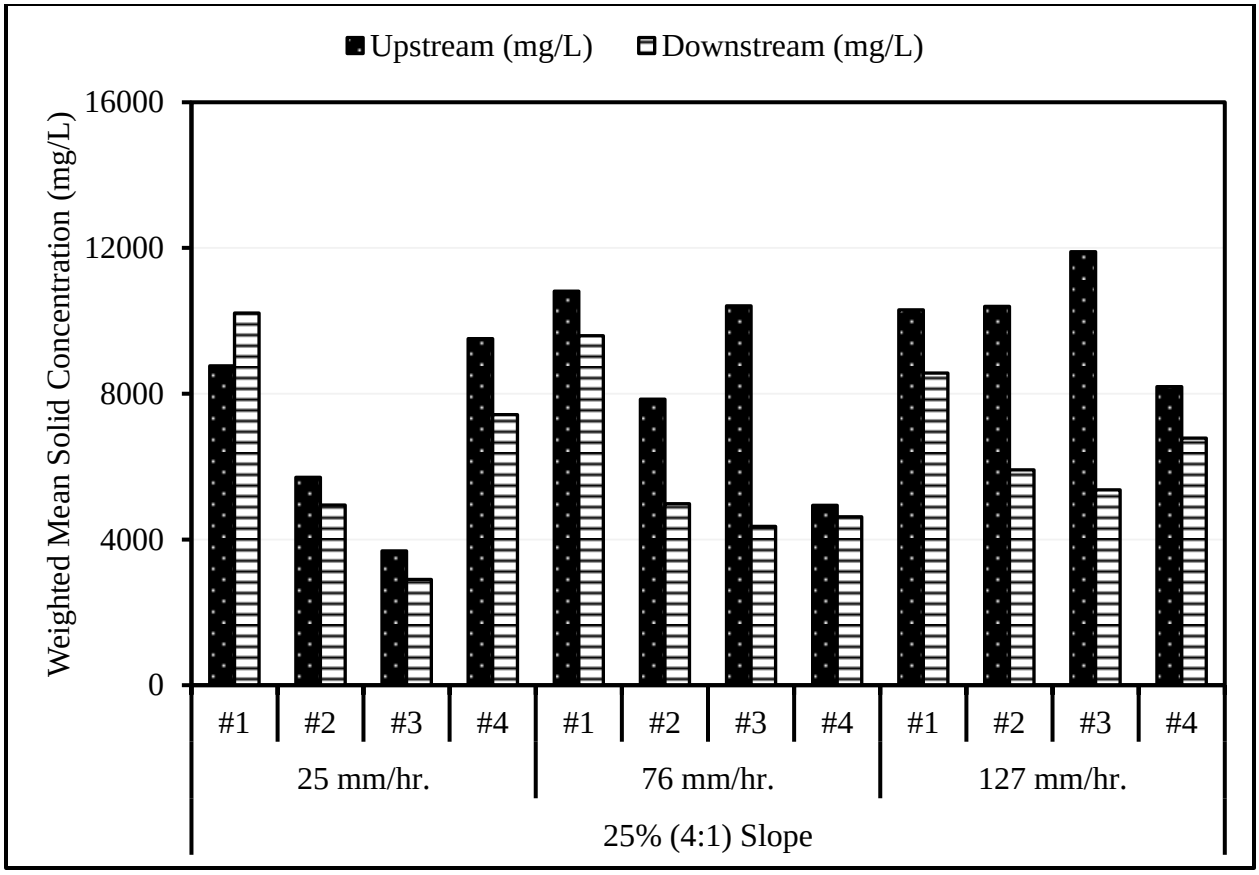

Figure 33 Volume-weighted mean sediment concentration for woven silt fence at 10% slope

Results from both silt fence fabrics showed observable differences in turbidity and sediment concentration values for the different slopes. The observed difference between slopes means higher slopes generated more suspended solids which translate to higher turbidity and sediment concentration at both upstream and downstream locations. The high suspended sediment values eventually resulted in higher performance efficiency and can be attributed to the erosion and transport of bigger sediment particles upstream. The big sediment particles were easily trapped and quickly settled down at the silt fence, but some particles traveled through the fabrics because of the increased flow rate upstream due to higher slope.

Hypotheses Testing on Silt Fence Fabric Performance

Statistical analysis was also performed to test the significance in turbidity reduction and sediment concentration removal for each silt fence fabric. The observed turbidity and sediment concentration for both upstream and downstream samples have unequal variance, high standard deviation, and skewness (Table 10 and Table 11), non-normality distributions, and did not meet the assumption of equal interval between measures. Thus, the data were tested as a nonparametric set using the Wilcoxon Signed-Rank tests on paired samples and a two-factor analysis of variance (ANOVA) with repeated measures on ranks. The alternative hypotheses for the test is that the treatment of runoff water by silt fence fabric significantly reduced the turbidity and sediment concentration downstream of the silt fence at a significance level of 5 percent ($\alpha = 0.05$).

The tests were performed under three conditions: first, paired data for the combination of 10 and 25 percent slopes which includes all rainfall events; second, combination of all rainfall events for an embankment slope. And third, separate analysis for different rainfall intensity on a given slope, which in effect is a sensitivity analysis to test the effect of testing sequence on performance. The Wilcoxon Signed-Rank test was used for the first two conditions presented in Table 12 and the two-factor ANOVA with repeated measures on ranks for the third condition.

Table 12 Wilcoxon signed-rank test probability values at a significance level of 5 percent

Silt Fence Fabric	Embankment Slope (%)	p-value	
		Turbidity	Sediment Concentration.
ARS-1400	10 and 25	0.0051	0.0001
	10	0.0912	0.0014
	25	0.0249	0.0048
BSRF	10 and 25	<0.0001	<0.0001
	10	0.0011	0.0011
	25	0.0011	0.0011

The first test condition, which is a combination of all rainfall intensities and events on 10 and 25 percent embankment slopes combined, for both silt fence fabrics showed statistically significant effect in turbidity reduction and sediment concentration removal at 95 percent confidence interval. The probabilities (p-value) for falsely rejecting the null hypotheses were 0.0051 and 0.0001 for the woven silt fence fabric for turbidity and sediment concentration, respectively; and less than 0.0001 for the nonwoven silt fence fabric turbidity and sediment concentration removal efficiencies. That is, the combination of slope and rainfall events does significantly affect the removal efficiency. The significance effect on both silt fence fabrics may have resulted from several factors such slope, rainfall intensity, and/or testing sequence, singularly or collectively. Thus, the second condition was considered to test the significance on separate embankment slope.

The second condition considered the combination of three rainfall intensities and various rainfall events for an embankment slope for significant difference between upstream and downstream samples. The intention was to identify the effect of rainfall intensities and testing sequence within a slope, separately. The effects of both silt fence fabrics in turbidity and

sediment concentration reduction efficiencies on 25 percent embankment slope were significant at 95 percent confidence interval. The probabilities for falsely rejecting the null hypotheses were 0.0249 and 0.0048 for the woven silt fence fabric for turbidity and sediment concentration, respectively, and 0.0011 for the nonwoven silt fence fabric turbidity and sediment concentration removal efficiencies (Table 12).

At 10 percent embankment slope, turbidity removal efficiency of the woven silt fence fabric was not significant at 95 percent interval, having a probability of 0.1047. Thus, there is about 10 percent chance that the test result could have been an error, so the null hypotheses cannot be rejected. On the other hand, it showed that rainfall intensity and testing sequence does not affect turbidity removal efficiency for woven on 10 percent slope. The sediment concentration removal efficiency was significant with a probability of 0.0014 for falsely rejecting the null hypotheses. The observed difference in effectiveness may be attributed to the apparent opening size (AOS) of the woven filter fabric, which is 0.60 millimeters and is much larger than the particles (silt and clay-size, less than 0.075 millimeters) that remain in suspension. For the nonwoven filter fabric, both turbidity and sediment concentration removal efficiencies were statistically significant at 95 percent confidence interval with the probability of 0.0001 for falsely rejecting the null hypotheses. Details of the Wilcoxon signed-rank test results are presented in Table 39 to Table 46 in Appendix H.

Further statistical tests to understand what factor on each slope contributed to the significant effect of the filter fabrics required the investigation of testing sequence for rainfall intensity on an embankment slope. However, the sample size of four events for rainfall intensity is less than the minimum sample size for the Wilcoxon Signed-Rank Table; thus, a two-factor

ANOVA test on ranks without repeat measure was performed. The results revealed that testing sequence in the three rainfall intensities for woven silt fence does not significantly affect the turbidity and sediment concentration removal efficiencies except for turbidity reduction at 25 mm/hr. and 76 mm/hr. (1 and 3 in./hr.) rainfall intensities for 25 and 10 percent slopes, respectively; and 127 mm/hr. (5 in./hr.) on 10 percent slope for sediment concentration reduction.

For the nonwoven silt fence on 10 and 25 percent slopes, turbidity and sediment concentration removal efficiencies were statistically significant at 76 and 127 mm/hr. (3 and 5 in./hr.) rainfall intensities except at 25 mm/hr. (1 in./hr.) for both turbidity and sediment concentration; and 127 mm/hr. (5 in./hr.) for turbidity only. The significant effects can be attributed to the performance of the silt fence fabrics rather than testing sequence. The no significant effect on turbidity reduction for 127 mm/hr. (5 in./hr.) rainfall on nonwoven fabric may be attributed to sampling errors or even the effect of erosion and condition on the soil surface before every rainfall event. Test soil surfaces that have been severely eroded in the previous rainfall event may result in high runoff volume because of the flow paths formed, but less fine particles in suspension for same rainfall intensity.

Sensitivity Analysis

The third condition is a sensitivity analysis on the responses of varying the slopes, rainfall intensities, and rainfall events on the removal efficiencies for both silt fence fabrics. The parameters varied for the sensitivity analysis are slope, rainfall intensity, and rainfall event. A two-factor ANOVA test on ranks with repeat measure was performed to determine the effect of

the factors and the interaction between factors. The significance level for the sensitivity analysis is 5 percent ($\alpha = 0.05$). The three combinations considered were intensity-slope-event (I-S-E), event-intensity-slope (E-I-S), and slope-event-intensity (S-E-I) as shown in Figure 34 (a) through (c) and detail discussions presented in subsequent sections.

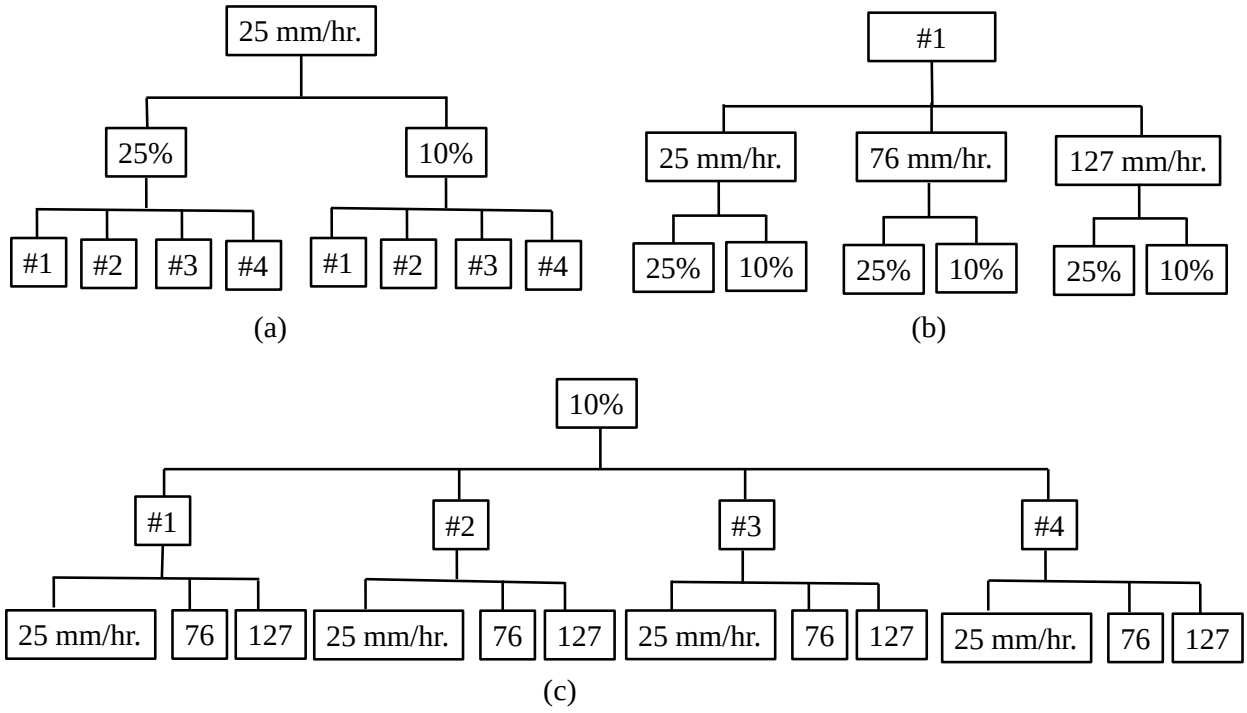

Figure 34 Sensitivity analysis matrices: (a) I-S-E, (b) E-I-S, and (c) S-E-I

Intensity-Slope-Event (I-S-E)

The first combination, I-S-E was designed to test the effect of slope for different rainfall events on silt fence performance, and the interaction between slope and silt fence removal efficiency. For the woven silt fence fabric, slope had significant effect on the performance of the silt fence in turbidity and sediment concentration removal. The silt fence does not significantly reduce turbidity and sediment concentration between upstream and downstream runoff. The interaction between slope and the woven silt fence for different rainfall event showed no

significant performance efficiencies for the three different rainfall intensities. That is, irrespective of the slope, the performance of the silt fence in turbidity and sediment concentration reduction was not affected by the rainfall event for the 5 percent significant level.

On the nonwoven silt fence fabric, the slope demonstrated significant effect on both turbidity and sediment concentration reduction for two rainfall intensities, but the sediment concentration reduction for 25 mm/hr. (1 in./hr.) rainfall intensity was not significant. For every rainfall event and intensity, the nonwoven silt fence significantly reduced both turbidity and sediment concentration from the upstream to the downstream runoff. The interaction between slope and nonwoven silt fence fabric for all rainfall events did not significantly affect the performances for both turbidity and sediment concentration reduction. There was significant effect on reduction performances at all rainfall intensities between rainfall events for the respective slopes for the nonwoven silt fence fabric. The two-way ANOVA on rank statistical analyses on the BSRF silt fence are presented in Table 47 to Table 52 of Appendix I.

For the woven silt fence fabric, the reduction performances between rainfall events were not significant. The different responses between silt fence fabrics can be attributed to trapped sediments clogging the fabric opening which resulted in better filtration in subsequent rainfall events for the nonwoven, but the woven had less trapped sediments because of the AOS for the fabrics. The sediment generated by the previous rainfall event, and possibly trapped in the fabric, were not available for subsequent events, unless the exposed surface is resurfaced before a rainfall event. Thus, the AOS, flow rate and filtration capacity of the fabrics controls filter fabrics performances. The two-way ANOVA on rank statistical analyses on the ARS-1400 silt fence are presented in Table 53 to Table 58 of Appendix I.

Event-Intensity-Slope (E-I-S)

The second combination of factors evaluated the effect of rainfall intensity on silt fence reduction performance on a combination of different slopes for individual rainfall event (#1 through #4). The test analyzed the interaction between rainfall intensity and silt fence performance for all rainfall events. Both the woven and nonwoven silt fence fabrics exhibited no significant effect of rainfall intensity on the turbidity and sediment concentration removal performance at any of the rainfall events, neither was there any significant interaction effect between intensity and performance. Thus, whatever difference observed between upstream and downstream runoff was not due to the rainfall intensity, but likely to the silt fence filtration and damming effects, or soil surface density and flow path conditions before any rainfall event. Detailed two-way ANOVA on rank statistical analyses on both silt fence fabrics are shown in Table 59 to Table 74 of Appendix J.

Slope-Event-Intensity (S-E-I)

The third combination investigated the effect of rainfall events on silt fence fabrics effectiveness of as temporary sediment barrier for a combination of rainfall intensities for specified slopes. In addition, the test considered interaction between rainfall events and silt fence fabrics on the turbidity and sediment concentration reduction performances. There was no significant interaction effect between rainfall events and intensities on any slope for both silt fence fabrics. That is, any variety of combination for rainfall event and intensity would not have significant effect on the performance of the silt fence fabric removal efficiencies. The different rainfall events for varying rainfall intensities had significant effect on turbidity removal on 10 and 25 percent slopes for both silt fence fabrics. The significant effect may be attributed to the

intensity of rainfall which caused turbulent flow regime upstream, agitated more fine particles to remain in suspension through the duration of rainfall and obstructed the passage of light through the runoff column. The downstream runoff experienced laminar flow because of the effect of the silt fence in the reduction of runoff velocity and filtration/damming at the silt fence.

On the woven silt fence fabric, there was no significant difference between upstream and downstream runoff for the variety of rainfall intensity for different rainfall events. That is, the performance of the silt fence at any rainfall event was not influenced by the rainfall intensity, but was significantly affected by changes made on the soil surface due to resurfacing and maintenance of silt fence. Maintenance does re-introduced fine particles to the soil surface upstream of the silt fence when the silt fence was cleared of debris and the soil surface compacted. Details of the two-way ANOVA on ranks statistical analyses on the ARS-1400 are shown in Table 75 to Table 78 of Appendix K.

However, on the nonwoven silt fence fabric, the response varied for different slopes. At 10 percent slope, there was no significant effect on sediment concentration removal by the silt fence for the variation of rainfall intensities on the different rainfall events, but at 25 percent slope it was significant. Higher embankment slopes tended to increase the runoff volume and velocity and thus, the erodibility of the soil surface which is shown in the results (Figure 26 through Figure 32). Particle sizes prevalent in sediment concentration analysis were easily trapped by the fabrics and, rainfall events did not significantly change the physics of erosion and sediment transport. However, rainfall intensity increased erosion and the consequent sediment transport from exposed soil surfaces. Details of the two-way ANOVA on ranks statistical analyses on the BSRF are shown in Table 79 to Table 82 of Appendix K.

Flow Rate

The flow rate through the silt fence fabrics is computed as the change in volume of runoff collected downstream divided by the average area of submerged silt fence as expressed in Equation 17. The calculated flow rate was converted to obtain a mean flow rate per hour for a rainfall event. Table 13 presents the summary of the flow rate between rainfall events for a rainfall intensity on each slope for both silt fence fabrics.

$$q_{SF} = \frac{2\Delta V}{(\Delta t)\cdot(h_{BW1} + h_{BW2})\cdot(b_{TB})} \tag{17}$$

where q_{SF} = silt fence flow-through-rate, ΔV = change in downstream volume, h_{BW} = depth of backwater upstream between time interval 1 and 2, b_{TB} = width of the test-bed, and Δt = time interval between 1 and 2.

Table 13 Summary of flow rate through silt fence fabrics

Silt Fence Fabric		Woven (ARS 1400)			Nonwoven (BSRF)		
Embankment Slope (%)	Rainfall Intensity (mm/hr.)	Flow Rate through Fabric (mm/hr.)			Flow Rate through Fabric (mm/hr.)		
		Mean	Median	Standard Deviation	Mean	Median	Standard Deviation
25	25	304	306	74	1848	1499	644
	76	144	151	42	967	1013	471.3
	127	378	371	49	882	782	341
10	25	373	346	78	2905	2189	2747
	76	1506	1540	250	1314*	1314*	*
	127	2119	2136	373	3282	3379	563

* insufficient data to effectively compute the mean and median flow-through-rate

The asteriks (*) is because of insufficient data to effectively compute the mean and median flow rate through nonwoven for 10 percent slope at 76 mm/hr. (3 in./hr.) – three out of

four missing flow data. Data for 10 percent slope at 76 mm/hr. (3 in./hr.) is not included in the statistical analysis performed to evaluate the flow rate for the nonwoven silt fence fabric. Typically, the nonwoven silt fence fabric had higher flow rate than the woven for all rainfall events, which confirm the difference in permittivity between both fabrics (Chopra et al. 2010). The variation observed in the mean flow rate data between intensity on same slope may be due to moisture condition of soil prior to any test, losses by infiltration, side flow losses from the test-bed, flow path under the silt fence, and losses and inaccurate measurements during experimentation.

Two-factor ANOVA without repeat measure statististical test was performed for significant differences between rainfall events and rainfall intensities, see details in Table 83 to Table 86 of Appendix L. As in previous statistical tests, the confidence interval was 95 percent ($\alpha = 0.05$). There was no significant difference in the flow rate between rainfall events on 10 and 25 percent slopes for both silt fence fabrics. The rainfall intensity significantly affected the flow rate through the woven silt fence fabric with probabilities of 0.0001 and 0.0067 for falsely rejecting the null hypotheses on 10 and 25 percent slopes, respectively. However, the rainfall intensity did not significantly influence the flow rate through the nonwoven silt fence fabric with probabilities of 0.0899 and 0.0512 for 10 and 25 percent slopes, respectively.

The different responses from both fabrics flow-through-rate due to changes in rainfall intensity may be attributed to the fabrics elongation (ductility) under stress. Tensile test on both fabric showed that nonwoven (BSRF) had greater ability to elongate without any significant effect to its apparent opening size, whereas woven (ARS-1400) comes to a sudden failure (Chopra et al. 2010). Higher rainfall intensity increases the upstream volume and velocity, and

thus, exerted higher pressure on the silt fence fabric. On the woven silt fence fabric, increased water pressure caused the AOS to increase and allowed more flow through, which was not observeable on the nonwoven fabric.

Conclusions

This study presents an investigation on active field-scale performance of two silt fence fabrics, woven (ARS 1400) and nonwoven (BSRF), turbidity and sediment concentration reduction efficiencies for different simulated rainfall events and embankment slopes using a tilting test-bed. Results and conclusions drawn from this study are presented in this dissertation.

It was observed that in general, silt fence fabrics installed at the toes of high embankment slopes (33 and 50 percent) easily develop problems such as overtopping, tearing off the stakes, and high deposits of eroded soil particles behind the silt fence. The problems resulted from the high runoff velocity and volume, which erodes the soil surface upstream and deposits the soil at the fence because of the damming condition. The issue with high slopes is evident in the sensitivity analyses conducted, which shows that slope have significant influence on the performance of the silt fabrics. At locations having high slopes such as 33 and 50 percent, it would be recommended that silt fence be installed after a change to a less steep slope of about 10 percent or less. The change in slope would reduce the runoff velocity and thus, the erodibility and subsequent deposits at the silt fence area.

Woven silt fence fabric displayed lower performance than the nonwoven with respect to both turbidity and sediment concentration reduction efficiencies. The woven fabric had average 11 and 20 percent, and nonwoven had 56 percent on both turbidity and sediment concentration

removal efficiencies, respectively. The performance was greatly influenced by the AOS and the response of AOS under increased soil-water pressure on the fence. Woven fabric low performance efficiency goes to show that it does not achieve good results by filtration, but by detention of runoff and sedimentation. On the other hand, the nonwoven fabric seems to achieve better filtration due to smaller AOS and tortuosity flow path. However, both fabrics could not achieve any higher percent removal as may be required by regulatory agencies because most suspended sediments have much smaller sizes than the AOS of both fabrics. Thus, other BMPs should be utilized along with silt fences as a treatment train to achieve the desired results.

Sensitivity analyses shows that the slope or rainfall intensity, and state of the installed silt fence rather than the number of repeat events have significant effect on performance. This would require that installed silt fence should be inspected regularly and maintained or replaced where problems are identified. Nonwoven silt fence fabric had higher flow-through-rate than the woven fabric for all rainfall intensities considered in the study. The flow-through-rate further confirms that the woven fabric achieve removal performance by interception and sedimentation as opposed to filtration. The sensitivity analysis on the flow-through-rate suggests that the rainfall intensity significantly affects the woven fabric and not the nonwoven one, because of the elongation capacity under increased runoff pressure.

Further testing is on-going on the both fabrics for a different soil type, namely silty sand (AASHTO type A-2-4) under similar testing conditions to investigate their removal performances. Results and comparisons between soil types will be presented in a future paper. It will be interesting to see if the results will vary substantially with soil type.

STORMWATER HARVESTING MODEL

Introduction

To predict the volume of water available for harvesting and subsequent discharge volume, a deterministic model was developed to simulate the runoff volume, harvesting rate, and storage volume based on the hydrologic cycle of the watershed with emphases on the pond water balance. A water budget model accounts for water movement in a pond, adjacent pervious area, evapotranspiration, and groundwater with time. This approach incorporates the different factors such as soil type, variable rainfall rates, variable irrigation rates, different turf grasses growth conditions, varying soil moisture conditions, groundwater table, water gradient, and watershed catchment characteristics. These parameters are incorporated into a water balance equation for the computation of the surface storage (harvesting pond), subsurface storage (soil water), and groundwater (aquifer) recharge to account for water storage and harvesting volumes available over time. The prediction model is based on classical surface and subsurface hydrologic equations which were simplified into numerical solutions with reasonable assumptions acceptable in practice.

Model Development

Several approaches have been developed to model various hydrologic processes of watersheds (Jaber and Shukla 2005; Elliott and Trowsdale 2007). The processes of water movement on the surface and in the unsaturated and saturated zones of the subsurface often require rigorous analyses. Therefore, simplification of the concepts into a mass balance approach with accountability of water is helpful in the development of adequate representation of water

volumes in mathematical models (Skaggs and Khaleel 1982; Tindall and Kunkel 1999). The simplifications in water movement on the surface and subsurface within a watershed model would reduce the rigorous analysis required to model the interaction between rainfall, runoff, infiltration, evapotranspiration, vadose zone water redistribution, groundwater flow, and seepage to open free-water bodies. Accurate simulation of the various processes based on the fundamental principles is essential in whatever simplifications and assumptions made in a model.

The goal of the study was to develop a model that simulates the interactions of hydrologic processes of water movement, storage, and harvesting in stormwater management systems of a watershed. A model was developed that simulates the integration of the physical processes of water movement in a pond, the atmosphere, soil surface, and subsurface within the unsaturated and saturated zones in order to quantify discharge and harvesting water volume from a watershed pond. Stormwater Harvesting and Assessment for Reduction of Pollution (SHARP) model is based on the analysis of stormwater harvesting with the option for groundwater input to and from a harvesting pond based on the principles of mass balance on pond storage and groundwater movement in a catchment area.

The SHARP model is deterministic but variable in time. It is a mass balance model designed to simulate the impact of harvesting pond water in regions where there is a possibility of sub surface inflow to and outflow from the pond while predicting the discharge and harvesting volume for any time period of interest. The model uses equations for the hydrologic and hydraulic processes of stormwater in a watershed, both in surface and subsurface phases (Skaggs and Khaleel 1982; Smajstral 1990; Allen et al. 1998; Shuttleworth 2007; Tadav et al. 2009). The SHARP model is programmed to accept watershed data generally available in most watershed

management and local authorities. The model is structured to reduce the number of calibrated parameters by the use of readily available measurable physical parameters and, when appropriate, empirical data. The development of the SHARP model is governed by mathematical deterministic relationships as conceptual components.

Development of Model Components

The water dynamics in a catchment at the surface-subsurface interface and pond water-groundwater interface modeling are critical in providing predictive tool for effectively evaluating the management needs of harvesting available pond water and controlling the discharge from pond. Determination of the saturated contributing surfaces and their evolution in time and space, and the relative contributions of the surface and subsurface to stream flow and pond are important issues in stormwater harvesting in a catchment area hydrology. Richard's equation is used to describe the water dynamics in the three physical domains of the land surface, vadose zone, and saturated zone with domain dependent parameters. Adopted in the development of the model components are contributive effects of the three physical domains to the pond, which flows are dominated by harvesting and discharge characteristics.

Model Basic Concepts

Richard's equation was solved in lumped form for the different model components. The model components were developed to describe the hydrologic processes inherent in the movement of water on the surface and in the subsurface. The basic governing processes for the surface and subsurface movement were expressed in the combination of continuity and water

budget equations for the pond storage (S_P), soil moisture storage (S_M), and groundwater recharge (S_{GW}).

Hydrologic Model

The hydrologic process involves interrelated sub-components of physical processes such as rainfall, irrigation, infiltration, surface runoff, subsurface water redistribution, and groundwater flow. Fundamentally, the change in storage within the hydrologic components for surface, soil moisture, and saturated groundwater flows as expressed in Equations 18 through 20.

$$\Delta S_P = R + RO - H_{AR} - E - D \pm Q_{GW} \tag{18}$$

$$\Delta S_M = R + I_{IRR} - RO - AET - DP \tag{19}$$

$$\Delta S_{GW} = DP \pm Q_{GW} \tag{20}$$

where ΔS_P = change in surface storage; ΔS_M = change in soil moisture; ΔS_{GW} = change in groundwater storage; AET = actual evapotranspiration; R = rainfall; RO = runoff; H_{AR} = harvesting volume; E = free surface evaporation; D = pond discharge; I_{IRR} = irrigation volume; DP = deep percolation; and Q_{GW} = groundwater seepage. The SHARP model loops the hydrologic processes of a detention pond to the adjacent land surface and subsurface dependent of the climatic conditions in the watershed. Schematic of a hydrologic cycle is shown in Figure 35.

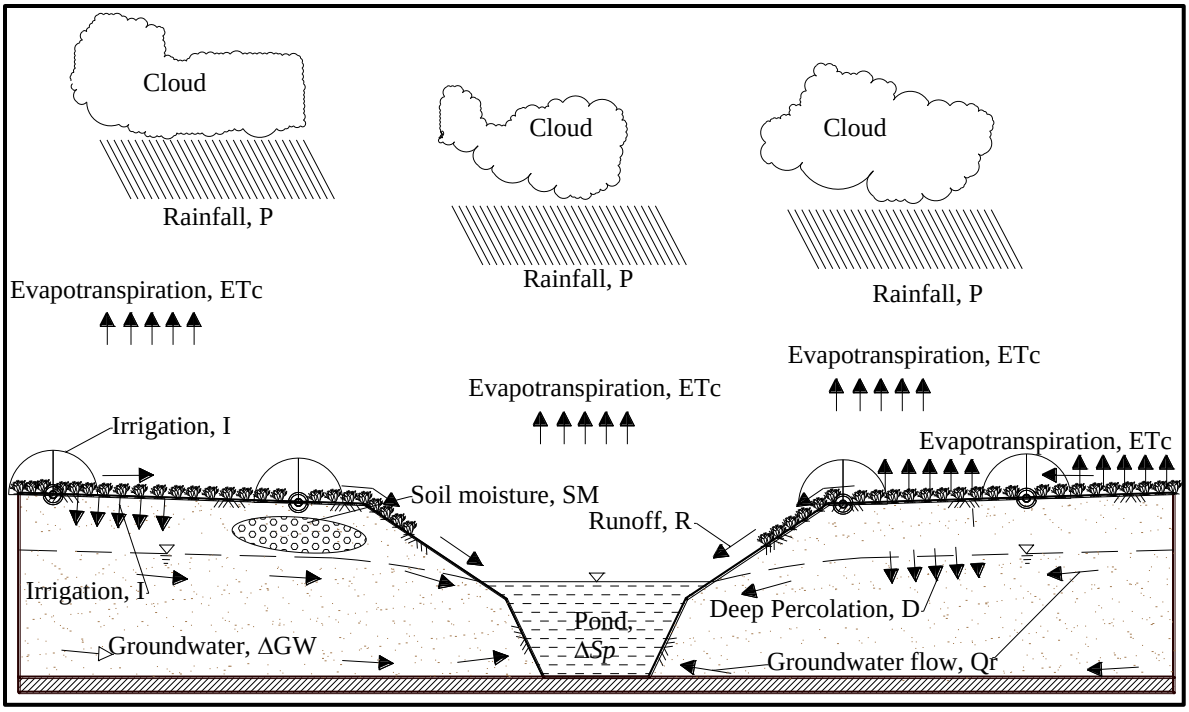

Figure 35 Typical hydrologic cycle

Model Operation

SHARP model, driven by precipitation, simulates the flow interactions of land surface and subsurface vadose zones, and the free-water surface and saturated zones. SHARP is an urban hydrology model with an hourly time step which integrates variety of soil characteristics, soil cover, surface slopes, rainfall and irrigation rates, fluctuations in groundwater levels, and water gradient. The relevance of the model is limited by the size of the watershed, as it is developed for pond catchment in a watershed. The model is a periodic loop of sequential computational processes of all the components in the hydrologic cycle. Preceding the loop are input parameters, boundary and initialization conditions followed by the model interactions to produce simulated monthly or yearly hydrologic values and graphic outputs.

SHARP model was developed using Microsoft Window-Excel interface to facilitate data entry, parameterization, characterization, and generation of numerical and graphical outputs. The model is composed of five modules, namely: LAND, ET, INFIL, SEEP, and POND. Brief descriptions of the five modules and, where necessary, the basic equations are presented in the following sections. Figure 36 presents the basic flow chart for SHARP model.

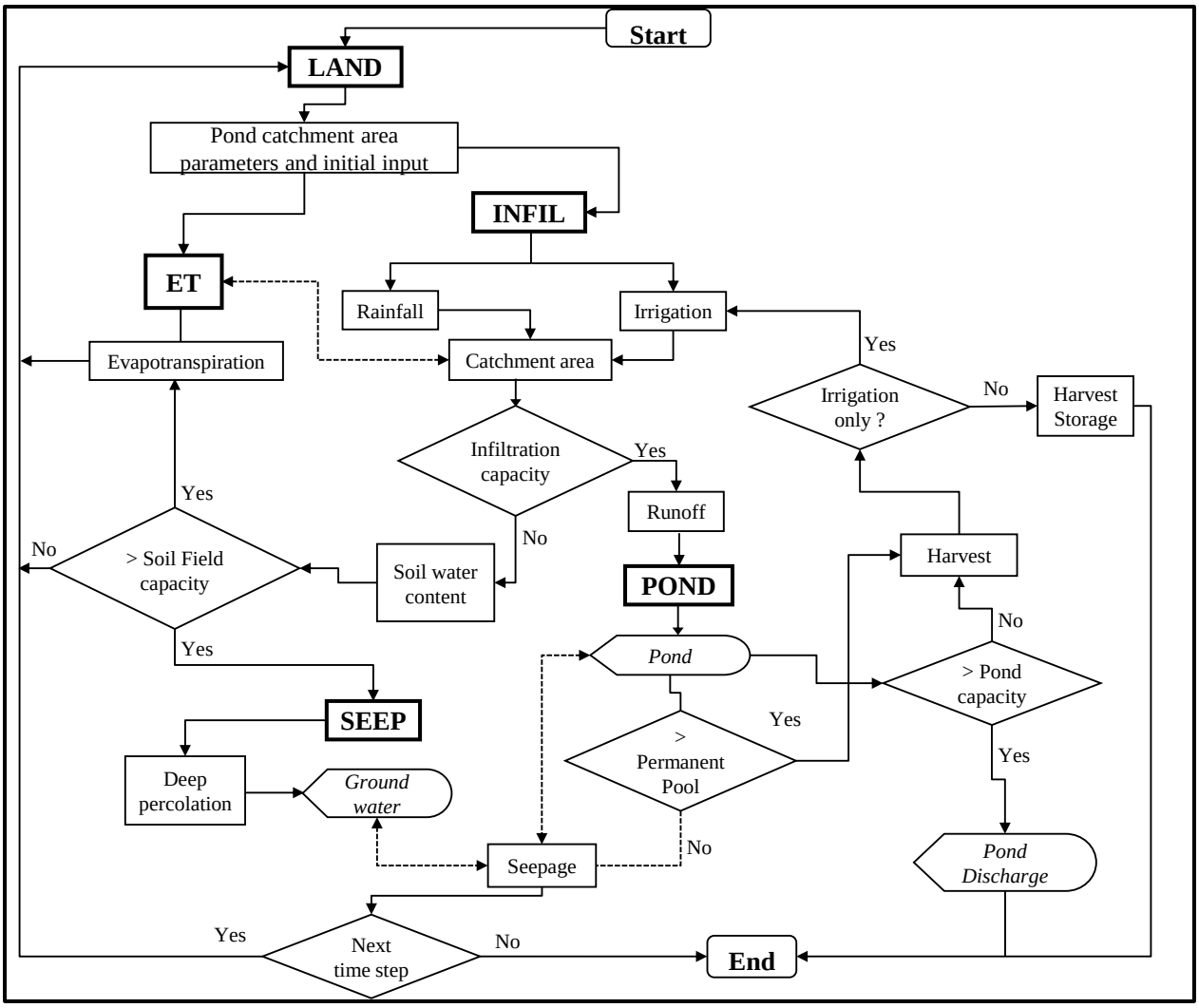

Figure 36 SHARP model basic flow chart

LAND Module

LAND module is the input unit that allows the user to specify watershed parameters, land uses and management, soil properties, and seasonal variations on weather data. The location inputs are geographic data such as the longitude, latitude, and elevation for the watershed location and pond catchment area. This allows for the definition of appropriate boundary for accurate simulation of water movement in the system. Meteorological parameters are essentially measured data or estimated from relevant formulations available in literatures and sourced from the National Weather Services (NWS) or local agencies. In addition, topographic description of the study area is relevant for selecting the hydrologic soil group that helps in identifying the soil types and defines the land use, percent imperviousness, urbanization level, slope, and vegetative cover and type. Finally, the control parameters are essentially system management controls to regulate the irrigation process frequency, volume, turfgrass water needs, required harvesting volume, and pond storage capacity. Table 14 presents the control parameters, calibrated values, and other regulations that may have to be incorporated into the model simulation.

Table 14 Model control parameters and calibrated values for the study area

Turfgrass Parameters			Management Allowed Depletion (MAD)			
Soil cover	Argentine Bahia		MAD during Initial Stage		70	%
Maximum grass height, H	0.30	m	MAD after Initial Stage		45	%
Mean maximum grass height, h_{crop}	0.08	m	Maximum Irrigation Depth, I_{max}		9.5	mm
Lower Limit of Evaporation, $K_{c\ min}$	0.15		Irrigation duration, t		0.5	hr.
Wetted Soil Fraction, f_w	1		Irrigation Interval, T_i		24	hr.
Evaporation zone depth, Z_e	0.1	m	Irrigation application rate		Variable	
Total Evaporable Water, TEW	191	mm	Time Step, Δt		1.0	hr.
Readily Evaporable Water, REW	5	mm	Harvest Storage Control		Irrigation Only	
Initial Depletion, D_e	13	mm	Harvesting Period per Day	Start Time	6:00	hrs.
Minimum Root Depth, $Root_{min}$	0.08	m		Stop Time	18:00	hrs.
Maximum Root Depth, $Root_{max}$	0.30	m	Irrigation Control		Water volume	
Available Water	62.5	mm/m	Pond Discharge Weir Configuration →		Pump	
Soil Water Depletion Fraction, p	0.5	No stress	Discharge Pumping Rate		37,854	m^3

ET Module

The ET module simulates the reference and crop evapotranspiration process by energy balance and turf grass needs for computing the actual evapotranspiration (AET) based on the FAO equation (Allen et al. 1998). Vegetation parameters for turfgrass in Florida were obtained from literature (Morton 1990), and Argentine Bahia was the dominant turfgrass in catchment area. The ET module model the irrigation needs of turfgrass, schedule the irrigation quantity and timing from the antecedent soil-moisture content and evapotranspiration. The potential evapotranspiration is expressed in Equation 21.

$$PET = \frac{0.408\Delta(R_n - G) + \gamma \frac{37}{T_{hr} + 273} u_2 \left[e^o(T_{hr}) - e_a\right]}{\Delta + \gamma(1 + 0.34u_2)} \quad (21)$$

A crop evapotranspiration, ET_c, is then calculated under standard conditions, that is assuming disease-free, well-fertilized crops, grown in large fields, under optimum soil water conditions, and achieving full production under the given climatic conditions (Allen et al. 1998). Equation 22 demonstrates an expression for the adjustment of the potential evapotranspiration by combination of basal crop coefficient (k_{cb}) and evaporation coefficient (k_e) expressed in Equation 23.

$$ET_c = k_c \times PET \quad (22)$$

$$k_c = k_{cb} + k_e \quad (23)$$

The actual evapotranspiration (*AET*) is adjusted for non-standard condition by a soil-water stress coefficient (k_s) for all kinds of stresses and environmental constraints. Evapotranspiration estimates were based on the FAO Penman-Montieth method (Allen et al. 1998) and expressed in Equation 24.

$$AET = (k_{cb}k_s + k_e) \times PET \quad (24)$$

where *PET* = reference evapotranspiration (mm day^{-1}); R_n = net radiation (MJ m^{-2} hr^{-1}); G = soil heat flux density (MJ m^{-2} hr^{-1}); T_{hr} = hourly mean daily temperature at 2 m height (°C); u_2 = wind speed at 2 m height (m s^{-1}); $e^o(T_{hr})$ = saturation vapor pressure curve at T_{hr} (kPa); e_s =

saturation vapor pressure (kPa); e_a = actual vapor pressure (kPa); Δ = slope vapor pressure curve (kPa °C^{-1}); γ = psychrometric constant (kPa °C^{-1}); and ET_c = crop evapotranspiration (mm day^{-1}).

Free-Water surface evaporation

Penman approached the estimation of evaporation from a free-water surface by a combination of the energy-budget and mass-balance methods (Penman 1948) expressed in Equation 25. The modified version of the Penman equation for free-water surface evaporation (Shuttleworth 2007) is defined as

$$E = \frac{\Delta R_n + \gamma(6.43)(1+0.536u_2)(e_s - e_a)}{\lambda(\Delta+\gamma)} \tag{25}$$

INFIL Module

INFIL module simulates the processes of infiltration, surface runoff, and soil water storage. SHARP model uses the Green and Ampt model for the infiltration computation (Skaggs and Khaleel 1982) as expressed in Equation 26

$$F = \begin{cases} R & for\ i \le K_s \\ \dfrac{\psi M}{(i/K_s)-1} & for\ i > K_s \end{cases} \tag{26}$$

where F = cumulative infiltration; ψ = suction at wetting front; M = soil water deficit; K_s = saturated hydraulic conductivity; and i = rainfall intensity. estimation of the surface runoff is by a water budget equation or the soil conservation service (SCS) curve number (Cronshey et al.

1986). Using the water budget model, permeable and impermeable surface runoffs are computed by Equations 27 and 28, respectively. Initial abstraction (I_a) is taken as 2.54 mm (0.1 inch) (Harper and Baker 2007). The conditions for infiltration and surface runoff after precipitation are presented in Table 15

$$RO = R + I_{IRR} - E - F \tag{27}$$

$$RO = R - I_a \tag{28}$$

Table 15 Runoff and infiltration response to precipitation

Conditions	Runoff Potentials	Descriptions
$i < K_s$	$RO = 0$ and $\theta_s < 1$	Rainfall infiltrates the soil; no runoff
$K_s < i < f_p$	$RO = 0$ and $\theta_s \Rightarrow 1$	Rainfall infiltrates the soil and the soil moisture increases to near surface saturation but no runoff
$K_s < f_p \leq i$	$RO = R - E - F$ and $S_e = 1$	Infiltration rate attains full capacity and starts decreasing, the near surface soil is becomes saturated and then generates runoff

where f_p = infiltration rate at ponding and S_e = effective saturation.

SEEP Module

The SEEP module simulates the process of water movement in the soil subsurface by water redistribution, deep percolation, and groundwater seepage. Infiltrated water is redistributed downward by soil matric and gravity potentials and upwards into the atmosphere by evapotranspiration in the soil subsurface. Estimation of the redistributed water is based on the rectangular profile (Tindall and Kunkel 1999). Soil-water above the field capacity in the root

zone drains to the groundwater as deep percolation and is governed by the soil characteristics. Flow is assumed as one-dimensional, so lateral flow in the vadose zone is ignored. Estimation for deep percolation is based on both steady and unsteady state flow processes in the soil during and after precipitation, respectively (Bethune et al. 2008). The steady-state flow is expressed in Equation 29 as

$$DP_{SS} = f \cdot t_d \tag{29}$$

where f = infiltration rate, t_d is the duration of the precipitation, and DP_{SS} = deep percolation in steady state. Deep percolation from on steady-state flow is gravity driven and is calculated when the soil moisture content is equal or greater than the moisture content at field capacity of the root zone or unsaturated layer. The unsteady-state flow in the unsaturated zone is the Darcian velocity (flux rate) based on the rectangular soil-moisture redistribution profile with the assumption that the initial soil-water content corresponds to the residual soil-water content (θ_r) or effective antecedent saturation (S_{ei}) (Tindall and Kunkel 1999) as expressed in Equation 30.

$$q = \frac{K_s}{\left(S_{ei}\right)^{-n} + \frac{nK_s t}{F}} \tag{30}$$

where q = flux rate; S_{ei} = initial soil saturation; and n = exponent related to the pore-size distribution index λ, (3 + 2/λ), for different soil characteristics and are available in literature (Brooks and Corey 1966). Deep percolation is computed for the pervious area only as the combination of both steady-state and unsteady-state flow processes expressed in Equation 31.

$$DP = DP_{SS} + q \tag{31}$$

Soil moisture in the unsaturated zone is influenced by moisture losses from actual evapotranspiration within the root zone and deep percolation. The soil moisture content is estimated based on the mass balance of flow in the unsaturated zone for each layer of soil as expressed by Equation 32.

$$\theta_i = \frac{S_{M,i-1} + R + I_{IRR} - RO - AET - DP}{T} \tag{32}$$

where T = unsaturated soil layer thickness. The estimated soil moisture content is substituted into Equations 33 and 34 for the corresponding negative pressure head, $h(\theta)$ and unsaturated hydraulic conductivity, $K(\theta)$ (Brooks and Corey 1966; Rawls et al. 1982).

$$h(\theta_i) = \frac{h_{cb}}{\left(\frac{\theta_i - \theta_r}{\theta_s - \theta_r}\right)^{1/\lambda}} \tag{33}$$

$$K(\theta_i) = K_s\left(\frac{\theta_i - \theta_r}{\theta_s - \theta_r}\right)^n \tag{34}$$

where h_{cb} = bubbling pressure head; θ_i = soil moisture content; θ_r = residual soil moisture content; and θ_s = saturated soil moisture content. The estimated hydraulic conductivity as a function of soil moisture is used to compute the groundwater recharge based on the deep percolation formulation.

Groundwater seepage equation is based on Darcy's law for porous media flows and it is a function of the water gradient and soil characteristics. In this study, seepage is related to bank flow condition resulting in the rise and fall of stream stages (Glover 1963). The rise and fall of

the pond stage over time describes the flow to and return from the pond based on the relative water level difference between the groundwater and pond water, and reservoir storage. The flow q_o out of the banks at distance $x = 0$ at any time t per foot of bank length is expressed in Equation 35.

$$q_{x=o} = \frac{HkD}{\sqrt{\pi \alpha t}} \tag{35}$$

where H = initial drainage depth; kD = transmissibility of an aquifer; t = time; and α = diffusivity. The flow out of the reservoir bank is expressed in volumetric flow units (L^3/T) per length of the reservoir bank. For consistency in units with other parameters such as rainfall, irrigation, and runoff volumes, the flow in Equation 35 is converted to unit volume (L) by the multiplication of the perimeter (P_P) of the pond water surface level per the surface area (P_A) as expressed in Equation 36.

$$Q_{x=0} = q_{x=0}\left(\frac{P_P}{P_A}\right) \tag{36}$$

POND Module

POND module simulates the pond storage using outputs from ET, INFIL, and SEEP modules, and rainfall data. Pond storage volume computation is based on Equation 18 (repeated below), which accounts for the initial volume, rainfall on the pond and seepage from groundwater into the pond as inputs; and pumped irrigation volume, discharge volume, evaporation, and seepage to the surrounding soil as output. This is computed for hourly time step to provide a real time simulation of water available for irrigation. Pond storage volume is

controlled by the setup of minimum and maximum storage volumes. At the minimum storage volume mark, the release of water for irrigation is stopped and at the maximum storage volume mark discharge of pond water commences.

$$\Delta S_P = R + RO - H_{AR} - E - D \pm Q_{GW}$$

Input and Output

SHARP model is a continuous simulation model designed to perform simulation in response to the periodic needs for stormwater management. Outputs from the model consist of periodic plots of rainfall and irrigation characterization, pond storage volume, harvesting storage volume, pond discharge volume, soil water volume, and groundwater volume. Basic data inputs in the model are used to develop periodic water storage in the pond, vadose (unsaturated) zone, and saturated zone to predict pond water harvesting volume availability and needs, total discharge volume, and percentage of surface runoff discharged. The movement of water in the watershed is synthesized from the model and inputted automatically within the model for specified hourly time step. The watershed characteristics and initial soil properties are used to set the initial boundary conditions of the model, shown in Table 14 above. SHARP model user and input interfaces are shown in Figure 37 below, and Figure 64 through Figure 73 in Appendix M.

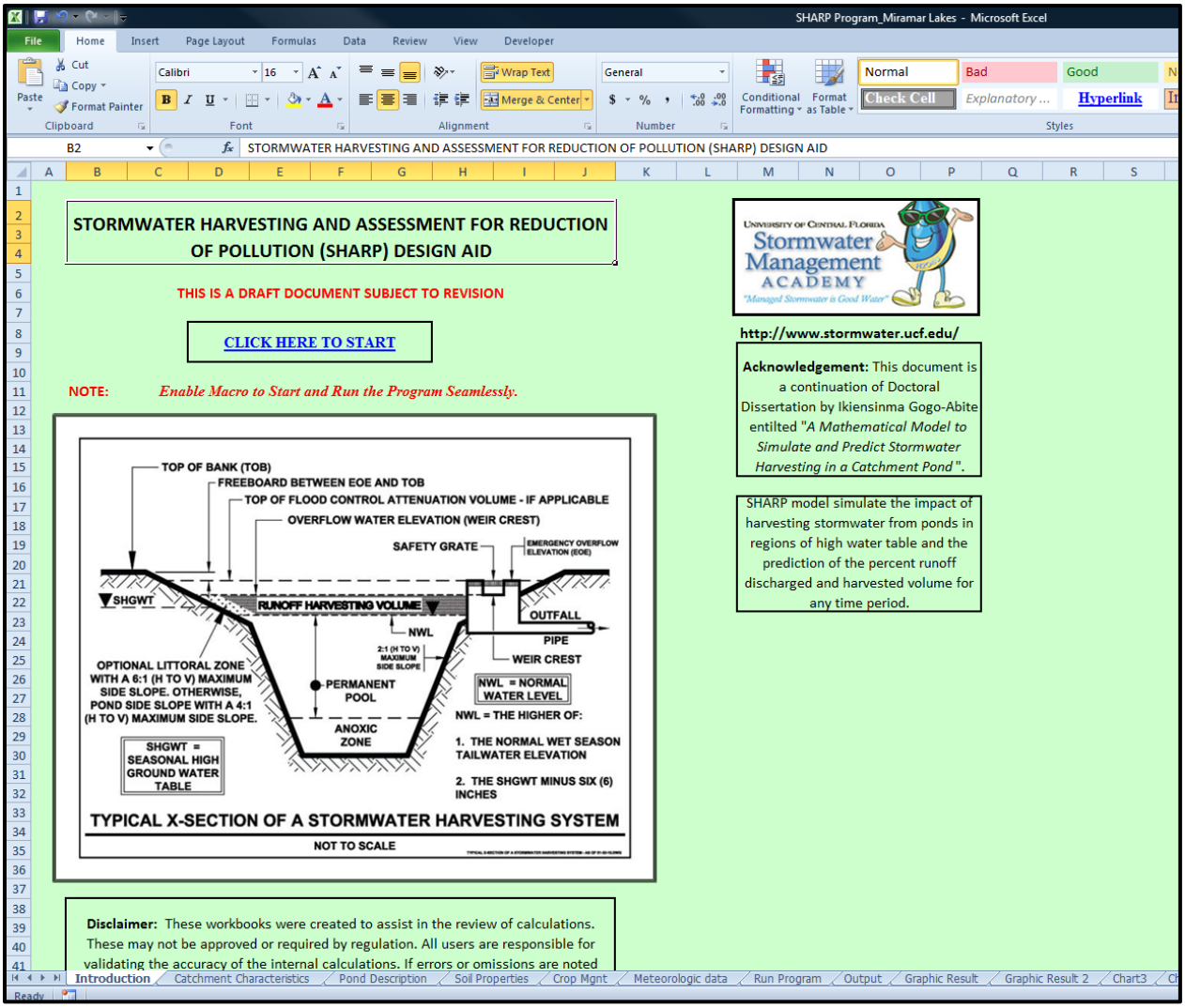

Figure 37 SHARP program user welcome interface

Model Parameters

SHARP model consists of specific watershed parameters that provide the mechanism to adjust the simulation for the given catchment area topographic, hydrologic, soil, and landscape and management conditions. It is designed to be used in a wide range of pond catchment areas, which must be evaluated for every model application. Some of these parameters could be evaluated from known watershed characteristics, while others that could not be precisely determined would be evaluated through calibration with existing data or laboratory analyses.

These are categorized as system, meteorological, and control parameters described in the LAND module. The following parameters are defined by calibration, experimentation, or from published data: hydraulic conductivity, porosity and void ratio, initial water content, residual water content, saturation water content, and the initial depth of groundwater table. Constants and exponential parameters are used to aid calculation of other model parameters through the simulation process. Data for the pond's sediment, permanent pool, harvesting volume, and overflow volumes were management decisions provided by City of Miramar and adapted to simulate the pond storage.

SHARP Model Application

The model is applied to a catchment area to verify its functionality, performance, and reliability. A simulation for SHARP model calibration and validation was performed on pond water level for the years 2009 and 2008, respectively. The pond is located at the North West corner of the Miramar Parkway and Interstate 75 Expressway (25.98° N, 80.36° W and 2.12 m (7 feet) elevation) in the City of Miramar, Broward County, Florida, shown in Figure 38. The catchment area is an industrial and commercial zone of approximately 80 hectare (197 acre), and has a directly connected impervious area (DCIA) of 38 hectare (94 acre) and an irrigable area of 25.5 hectare (63 acre). The stormwater pond surface area is 16 hectare (40 acre) and is at elevation 2.12 m (7.0 feet) and an average pond bottom elevation at -2.12 m (-7.0 feet). According to the soil investigation report by Ardaman & Associates (2007), the general soil profile has a top layer of silty sand with rock fragments to sand from the ground surface to 1.2 m (4 feet) depth and limestone below the top layer.

Figure 38 Satellite imagery of the pilot site (Miramar Lakes)

In this study, the rainfall and meteorological data for year 2008 and 2009 were obtained for the weather station at North Perry Airport (KHWO), Hollywood, Florida (26.00° N, 80.24° W) having a 2.44 m (8 feet) surveyed elevation, which is about 11.27 km (7 miles) East of the experimental site in Miramar shown in Figure 39. The weather station records rainfall, temperature, relative humidity, wind speed and direction, atmospheric pressure, sky cover for radiation analysis; and the historical data were obtained from Weather Underground website (Wunderground.com 2010). Data from this site was used as inputs in both ET and INFIL modules of the SHARP model.

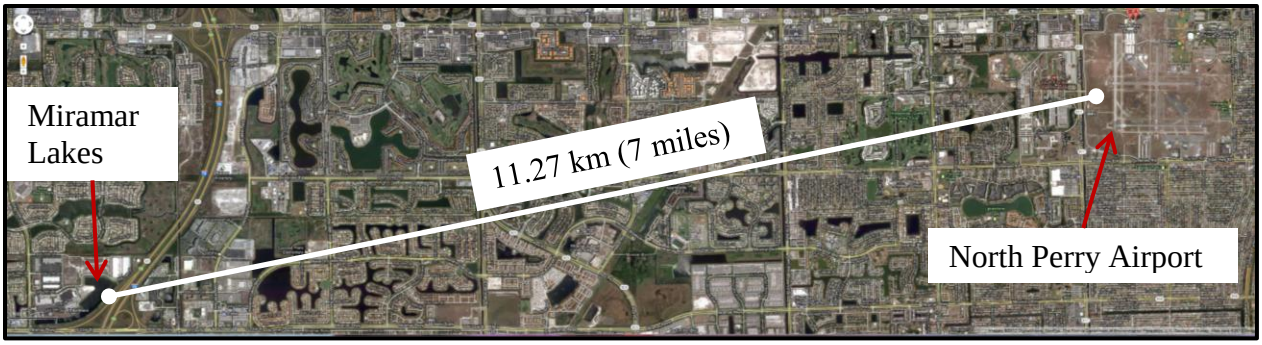

Figure 39 Distance between the pilot site location and nearest weather station

The City of Miramar provided the pond water elevations for years 2008 and 2009 (January through December each year). The start and end elevations for year 2008 were 0.78 m and 0.82 m (2.55 and 2.70 feet), and for year 2009 were 0.82 m and 0.88 m (2.70 and 2.89 feet), respectively, at 10 minutes interval. However, SHARP model used hourly time step hourly (Δt = 1 hr.) for simulation of pond water elevation. Model calibration period was from January 1, 2009 at 00:00 hours to December 31, 2009 at 23:59 hours. The validation period was from January 1, 2008 at 00:00 hours to December 31, 2008 23:59 hours. The pond water elevation was the control parameter for the calibration of SHARP model at the pilot site. Table 16 presents the initial hydraulic properties for the pilot study.

Table 16 Model initial input and boundary parameters for the soil layers

Soil Hydraulic Properties			
Description	Units	First Layer	Second Layer
Soil type		Loamy Sand	Limestone
Initial water content, θ_i	cm/cm (in./in.)	0.100	0.100
Residual saturation, θ_r	cm/cm (in./in.)	0.030	0.020
Water content at saturation, θ_s	cm/cm (in./in.)	0.300	0.200
Moisture content at field capacity, θ_{FC}	cm/cm (in./in.)	0.170	0.180
Pore size distribution index, λ		0.553	0.165
Bubbling pressure, h_{cb}	cm (in.)	14.20 (5.59)	1.00 (2.54)
Saturated hydraulic conductivity, k_s	cm/hr. (in./hr.)	6.11 (2.41)	12.70 (5.0)
Layer Depth, d	cm (in.)	124 (48)	425 (168)

In addition, the City of Miramar provided the management information for the pilot site. Harvesting volume was set at 113.6 m^3 per day (30000 gallons per day) for six days of the week in the year, except in the winter months (December through March) when only half of this volume was harvested. No harvesting was done when the catchment area received rainfall above 12.7 mm (0.5 in.). The pond discharge mechanism is a pump set at a rate of 37,854 m^3 per day (10 million gallons per day) at a discharge elevation of 0.97 m (3.2 feet). However, the City reported that the discharge rate and discharged level were varied through the year and do not have records of these variable rates and levels.

Results and Discussion

Groundwater models are qualitatively analyzed for overall performance using efficiency criteria for error measurements, calibrations and validation of the model. Commonly used goodness-of-fit tests for hydrologic model performance and reported in literature are, but not limited to, root mean square error (*RMSE*), mean absolute error (*MAE*), coefficient of

determination (R^2), scatter plot of observed versus simulated variables, time series plot for both observed and simulated variables, Nash-Sutcliffe coefficient (E), and the index of agreement (d) (Krause et al. 2005; Harmel et al. 2010). However, none of these criteria is singularly sufficient to provide objective assessment of model ability to reproduce observed measurements and simulated behavior. Krause et al. (2005) showed that the different criteria reflects systematic errors for varying conditions of flow volume, and recommended "a combination of different efficiency criteria complemented by the assessment of the absolute or relative volume error." Both *RMSE* and *MAE* measure the average magnitude of error in the dimension of the continuous variable measured, and ranges between zero and infinity (∞) with lower values as better forecasting model. Study showed that *MAE* is an unambiguous measure of average error and is the "most natural measure of average error magnitude" (Willmott and Matsuura 2005).

The coefficient of determination, which is the squared ratio of the covariance and the multiplied standard deviations of the observed and predicted values, explains only the extent of dispersion between the observed and predicted to the combined dispersion. R^2 is reported to be insensitive to models which systematically over- or under-predict all the time (Krause et al. 2005) and is insensitive to bias between predicted and observed values (Jaber and Shukla 2004). Instead, the Nash-Sutcliffe efficiency and the index of agreement are used for better evaluation of hydrologic models. According to Krause et al. (2005), both E and d quantify the difference between observation and prediction by the absolute deviation, thus higher values have greater influence than lower ones, and are not sensitive to systematic over- or under-prediction by model during low flows. A relative deviation modification was applied to counteract problems identified in both E and d as shown in the Equations 37 and 38, respectively (Krause et al. 2005).

$$E_{rel} = 1 - \frac{\sum_{i=1}^{n}\left(\frac{O_i - P_i}{O_i}\right)^2}{\sum_{i=1}^{n}\left(\frac{O_i - P_i}{\overline{O}}\right)^2} \quad (37)$$

$$d_{rel} = 1 - \frac{\sum_{i=1}^{n}\left(\frac{O_i - P_i}{O_i}\right)^2}{\sum_{i=1}^{n}\left(\frac{\left|P_i - \overline{O}\right| + \left|O_i - \overline{O}\right|}{\overline{O}}\right)^2} \quad (38)$$

where O_i = i^{th} term of the observed value; P_i = i^{th} term of the predicted value; n = total number of observations; and $\bar{O}$ = mean of the observed values. Using the relative deviations significantly reduces the influence of absolute deviations during high flow regimes, and is more sensitive on systematic model over- or under-prediction during low flow regimes.

Parameters calibrated for SHARP model in this study were saturated hydraulic conductivities, pore size distribution, turfgrass growth parameters, soil field capacity, discharge pumping rate, infiltration capacity, and surface storage. Values for some these parameters are shown in Table 15 and Table 16. Both discharge pumping rate and discharge level were calibrated because the operational rate and discharge level varied at every use as opposed to the use of a fixed rate through the calibration period in this study. The discharged was manually operated and the actual values were not available.

SHARP model evaluation was conducted by pairwise comparison of observed measurement and simulated output of pond water level for both the calibration and validation periods, and with graphical comparisons. In this study, both *RMSE* and *MAE* were used for average error measurements and the relative forms index of agreement (d_{rel}) for efficiency

criteria of SHARP performance. The index of agreement is dimensionless term that measures degree of error free in model predictions and ranges between zero (no correlation) and 1.0 (perfect fit) between measured and simulated pond water level. Results of these three measures and the means and variances of the observed measurements and simulated values of the pond water level for both the calibration and validation periods are presented in Table 17.

Table 17 Statistical performance indicators of the observed and simulated pond water elevation

Efficiency Criteria Symbol			$\mu^{(a)}$ (m)	$s^{(b)}$ (m)	$C_v^{(c)}$	RMSE m (ft.)	MAE m (ft.)	d_{rel}
Yearly Observation	Jan - Dec, 2008 Validation	Observed	0.86	0.12	0.14	0.07 (0.24)	0.05 (0.16)	0.91
		Predicted	0.82	0.10	0.12			
	Jan - Dec, 2009 Calibration	Observed	0.87	0.14	0.17	0.08 (0.26)	0.06 (0.21)	0.92
		Predicted	0.87	0.14	0.17			
Seasonal Observation	2008 Validation period Dry	Observed	0.81	0.08	0.09	0.021 (0.07)	0.018 (0.06)	0.98
		Predicted	0.81	0.07	0.09			
	Wet	Observed	0.93	0.14	0.15	0.12 (0.38)	0.10 (0.32)	0.85
		Predicted	0.93	0.14	0.15			
	2009 Calibration period Dry	Observed	0.80	0.10	0.12	0.07 (0.24)	0.06 (0.20)	0.89
		Predicted	0.81	0.13	0.16			
	Wet	Observed	1.03	0.10	0.09	0.09 (0.30)	0.07 (0.24)	0.74
		Predicted	1.00	0.07	0.07			

[(a)] = sample mean; [(b)] = sample variance; [(c)] = coefficient of variation

Calibration Period Simulation Results

The model showed good prediction of the pond water elevations with efficiency criteria of 0.07 m (*RMSE*), 0.06 m (*MAE*) and 0.89 (d_{rel}) during the dry months and 0.09 m (*RMSE*), 0.07 m (*MAE*) and 0.74 (d_{rel}) in the wet months. Index of agreement of 0.74 and 0.89 are very good values for error-free model predictions evaluation. The overall calibration period model simulation has d_{rel} = 0.92, *RMSE* = 0.08 m., and *MAE* = 0.0.06 m. Figure 40 presents a time

series plot for the observed and predicted pond water elevation and the corresponding rainfall data. The break in the observed pond water elevation is due to missing data for the period (06/20/2009 to 08/14/2009); no readings were recorded because of equipment malfunction. The difference in the elevations is explained by the lack of accurate discharge pumping rate and elevation. SHARP model imposed fixed discharge rate and elevation through the calibration period. Thus, the model may over- or under-estimate the volume of discharge from the pond, especially during high inflow volumes. In addition, there is the issue of backflow from adjacent ponds to equalize the pond elevations, which were not simulated due to lack of adequate data.

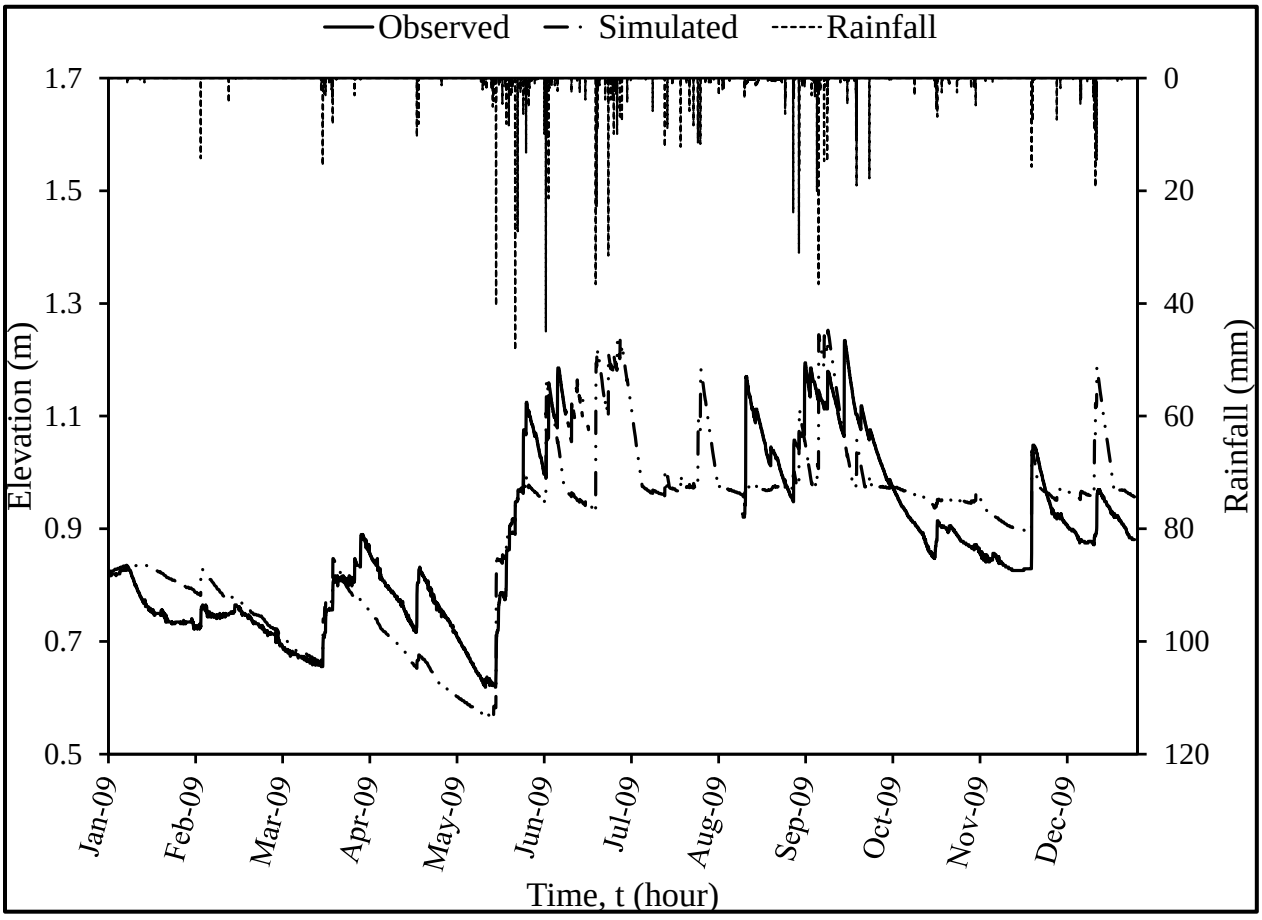

Figure 40 Observed and predicted pond water elevation for calibration period of January through December 2009

Figure 41 presents scatter-graph plotted for the pond water elevation between the observed values and predicted data for the calibration period. The plot showed the R^2 = 0.74 and the linear regression line equation with a gradient, b = 1.03. Value of 1.0 for R^2 means dispersion in prediction is equal to observation, and gradient b = 1.0 and intercept, a = 0 signifies perfect agreement. For proper model assessment, Krause et al. (2005) recommended that the R^2 should be weighted with the gradient (b) by the expressions in Equations 39 for an all-inclusive evaluation of model results.

$$wR^2 = \begin{cases} |b| \cdot R^2 & \text{for } b \le 1 \\ |b|^{-1} \cdot R^2 & \text{for } b > 1 \end{cases} \tag{39}$$

The weighted coefficient of determination (wR^2) becomes 0.76 that is the model had a 24 percent under-prediction of the measured data for the calibration period. In addition to the reasons given for the model prediction accuracy, the differences between the measured and predicted may be due to averaging of the initial parameters for the catchment area, soil properties, land covers and slopes, and rainfall and meteorological data obtained from the nearest weather station, about 11 km (7 miles) east of the catchment location.

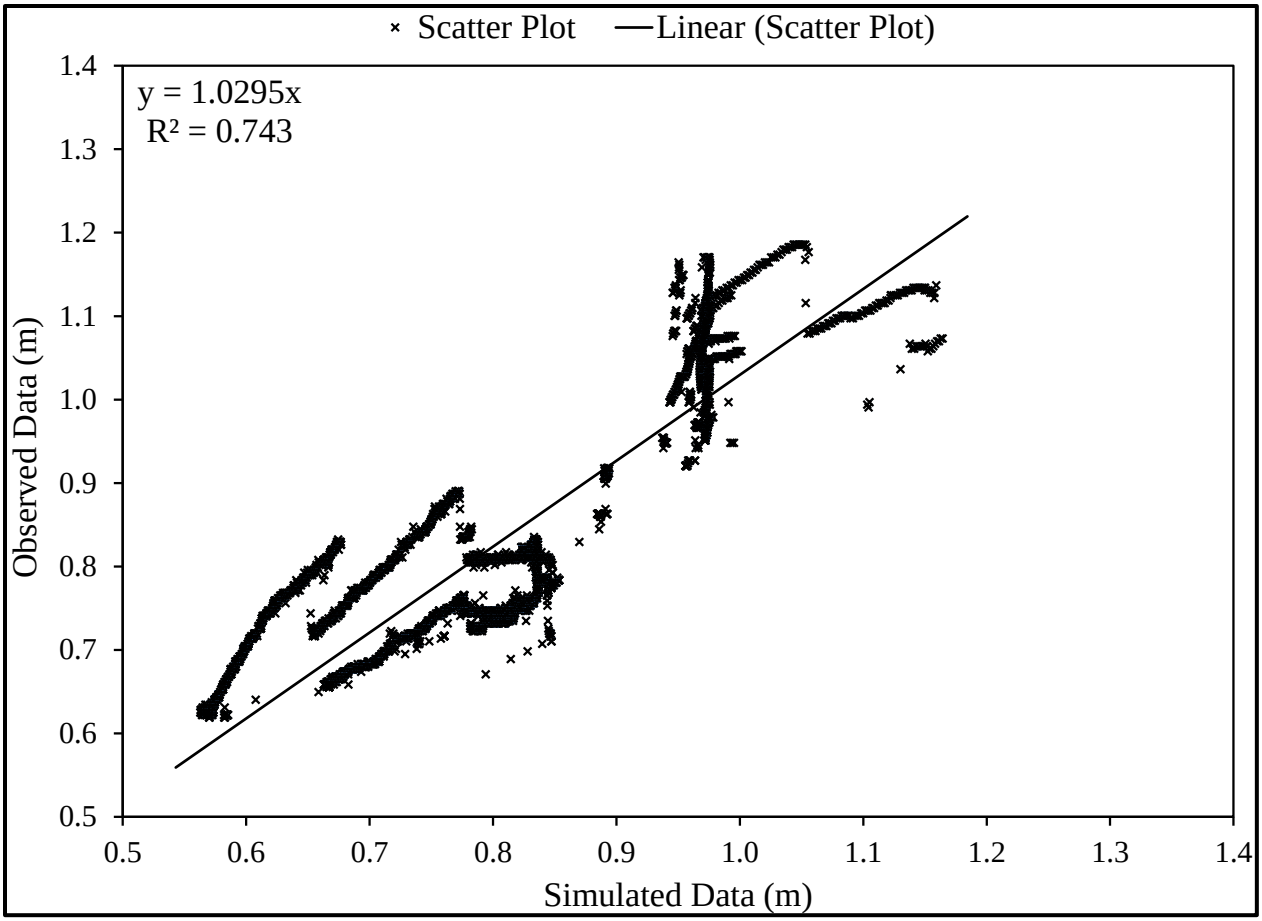

Figure 41 Scatter plot of observed versus simulated pond water level from January through December, 2009

Validation Period Simulation Results

After the calibration of SHARP model, evaluation to validate the model was conducted using parameters from the calibration period of January through December, 2009 to set the discharge pumping rate, discharge elevation, irrigation scheduling, and land cover. Breaks in the observed pond water elevation are also noticeable for the validation period in Figure 42, from 08/20/2008 to 09/05/2008 due to the effect of tropical storm Fay in August 2008. The validation period showed that the model closely predicted the pond water elevations, especially during the

dry months of January through May and November to December with efficiency criteria of *RMSE* = 0.02 m, *MAE* = 0.018 m, and d_{rel} = 0.98.

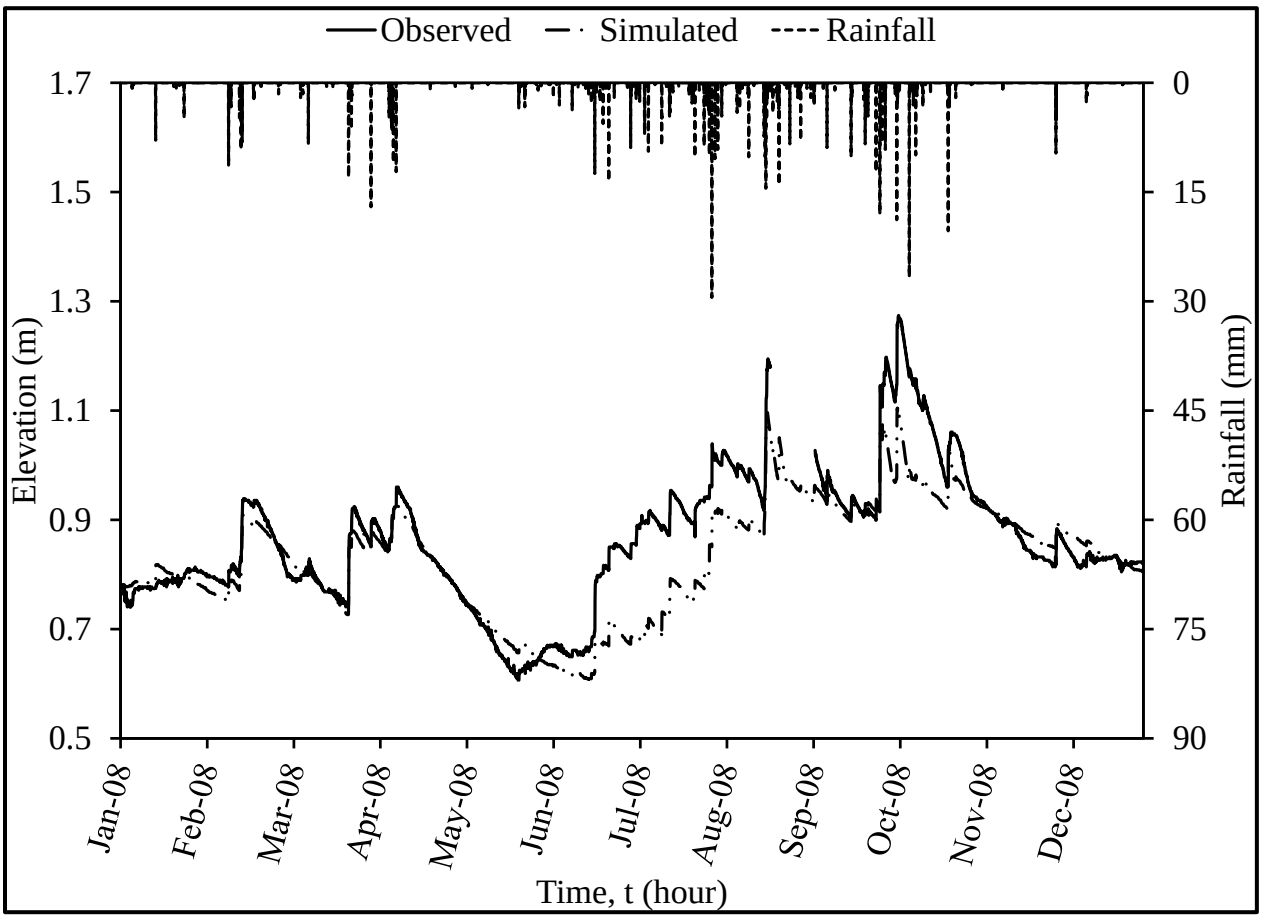

Figure 42 Observed and predicted pond water elevation for the validation period of January through December 2008

The simulated pond water elevation during the wet season (June through October) dropped in elevation but followed the same trend. The efficiency criteria for the wet months (Table 17) were 0.12 m (*RMSE*), 0.1 m (*MAE*) and 0.85 (d_{rel}) which shows that the simulated values acceptably matched the observed data for the wet period of the validation year. Again, the reasons for the under-prediction during the wet months are explained in the lack of data on the varied discharge pumping rate and elevations for the pond. For the whole validation period, the

efficiency criteria are *RMSE* = 0.07 m, *MAE* = 0.05 m, and d_{rel} = 0.91. In addition to the goodness-of-fit indicators are scatter-graphs of observed measurement and predicted values of the pond water elevation for the validation periods shown in Figure 43.

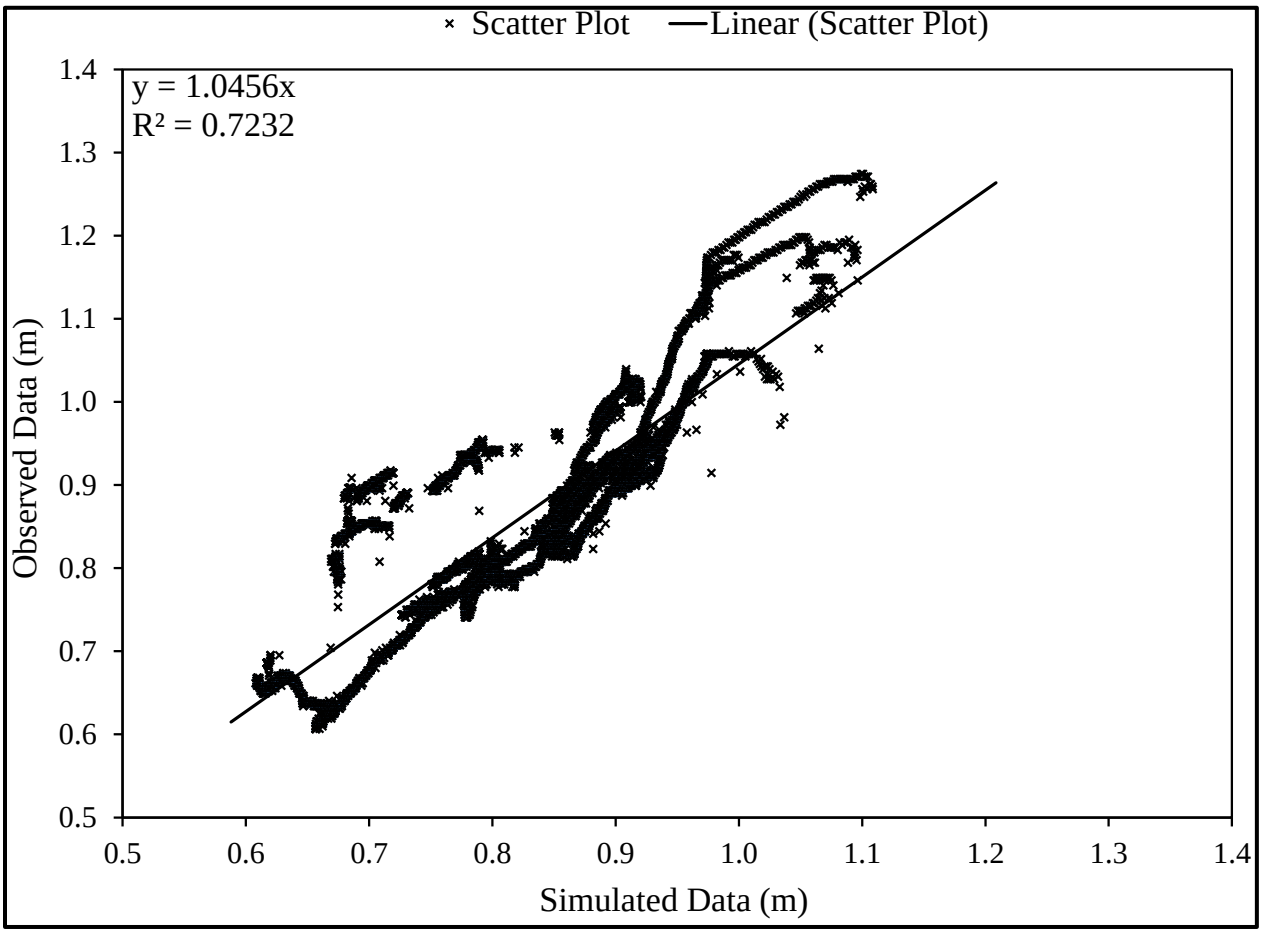

Figure 43 Scatter plot of observed versus simulated pond water level from January through December, 2008

The plot showed the R^2 = 0.72 and the linear regression line equation with gradient, *b* = 1.04. The weighted coefficient of determination (wR^2) becomes 0.69 that is the model had a 31 percent under-prediction of the measured data in the validation period. The realization that R^2 is less in the validation period than the calibration period when all other efficiency criteria showed

better goodness-of-fit goes to reveal the problem of using R^2 alone for model prediction accuracy. For the seasonal scatter-graphs (Figure 44 and Figure 45), R^2 = 0.92 and 0.78, and wR^2 = 0.92 and 0.70 for the dry and wet months of the validation period, respectively, which are in agreement with the other efficiency criteria for the same period. The weighted coefficient of determination for the wet months significantly affected the entire validation period.

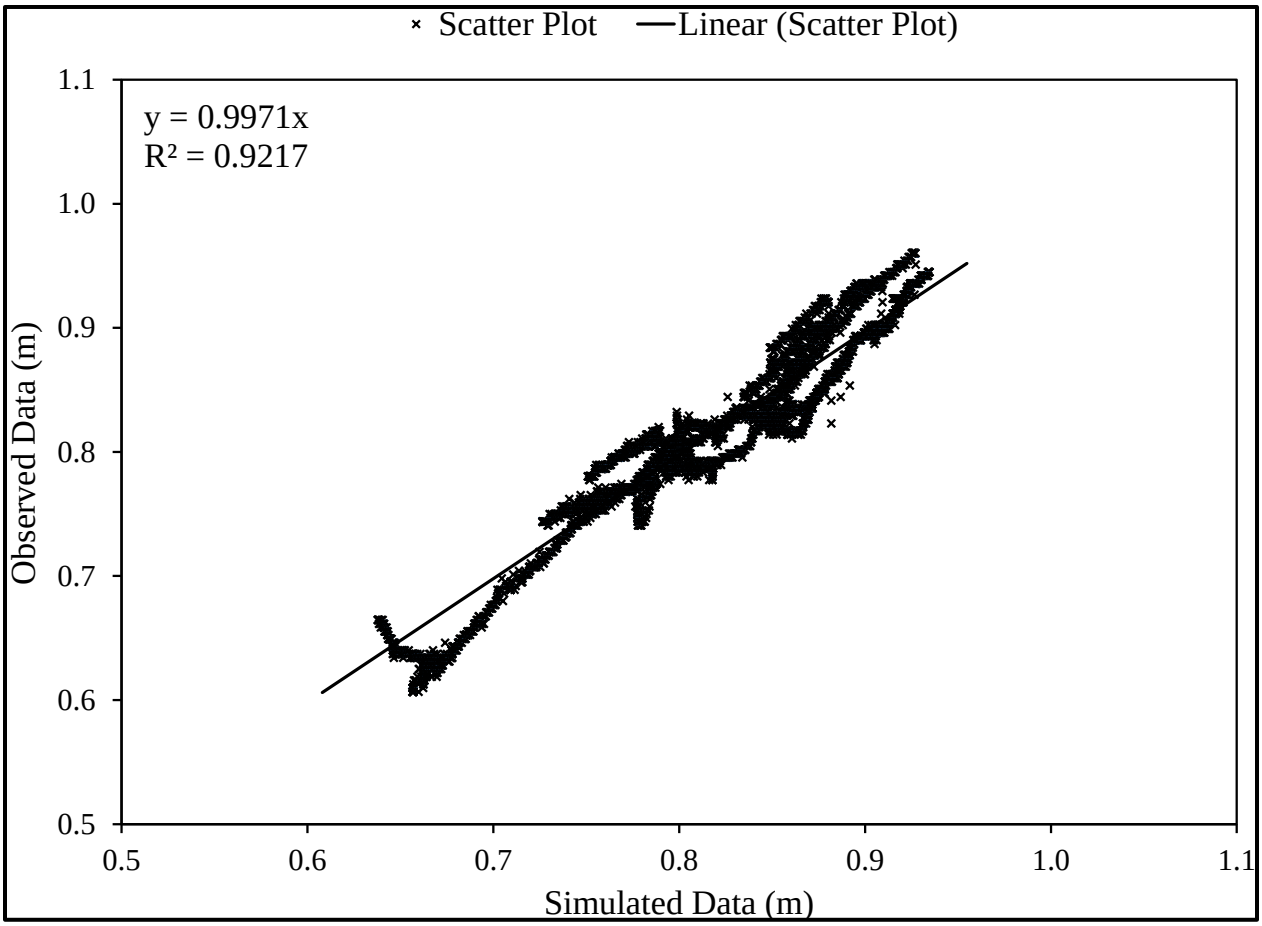

Figure 44 Scatter plot of observed versus simulated pond water level dry months in 2008

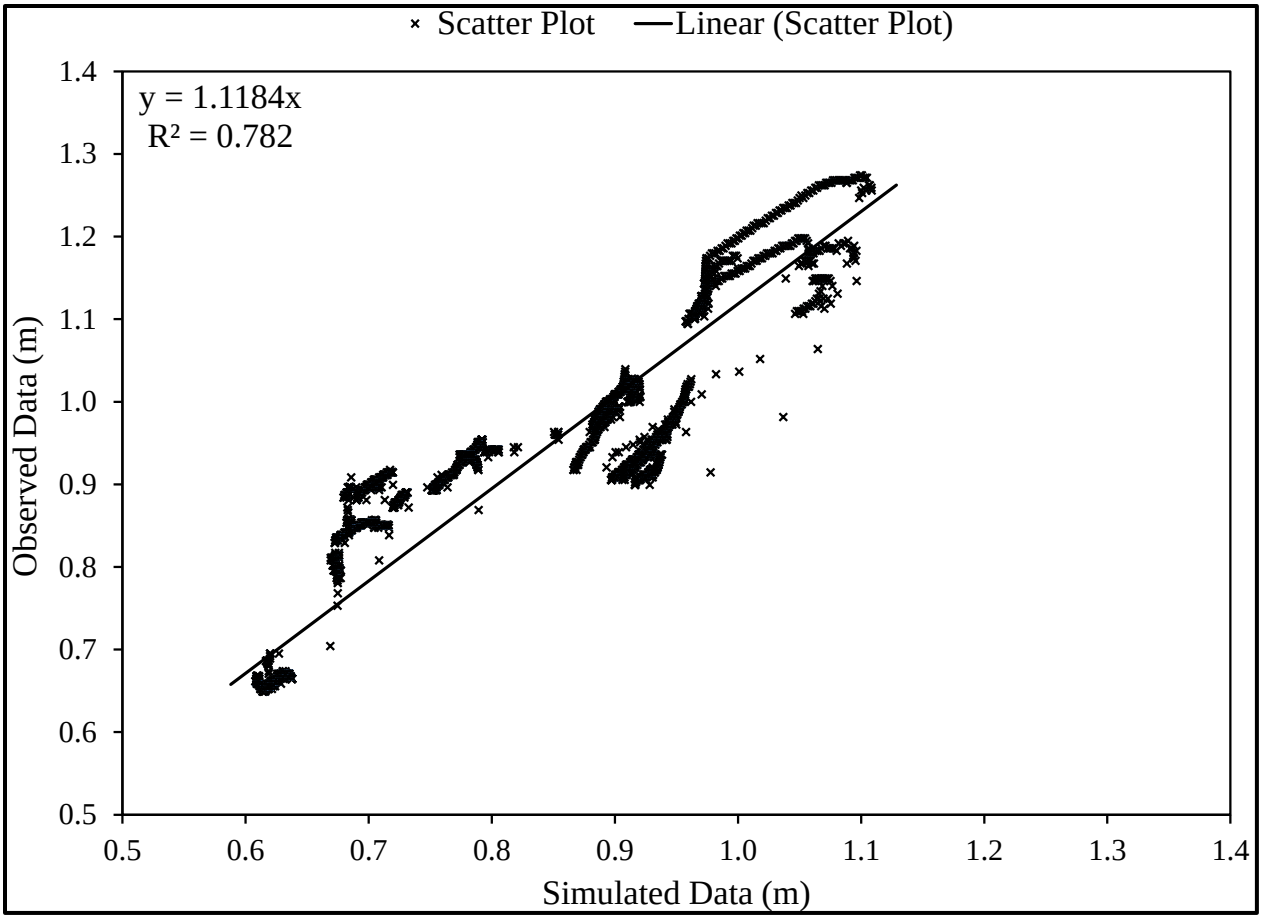

Figure 45 Scatter plot of observed versus simulated pond water level dry months in 2008

SHARP Output Results

The SHARP model has the additional capability to display graphically the effect of stormwater harvesting to the groundwater drawdown, pond discharge volume, and stormwater runoff contribution to harvesting. In Figure 46 is presented a plot of the percentage of runoff discharged against increase in the weekly harvesting volume for each simulation period of one year. The trend reveals an exponential decrease in percentage of runoff volume discharged with an intercept value equivalent to no harvesting.

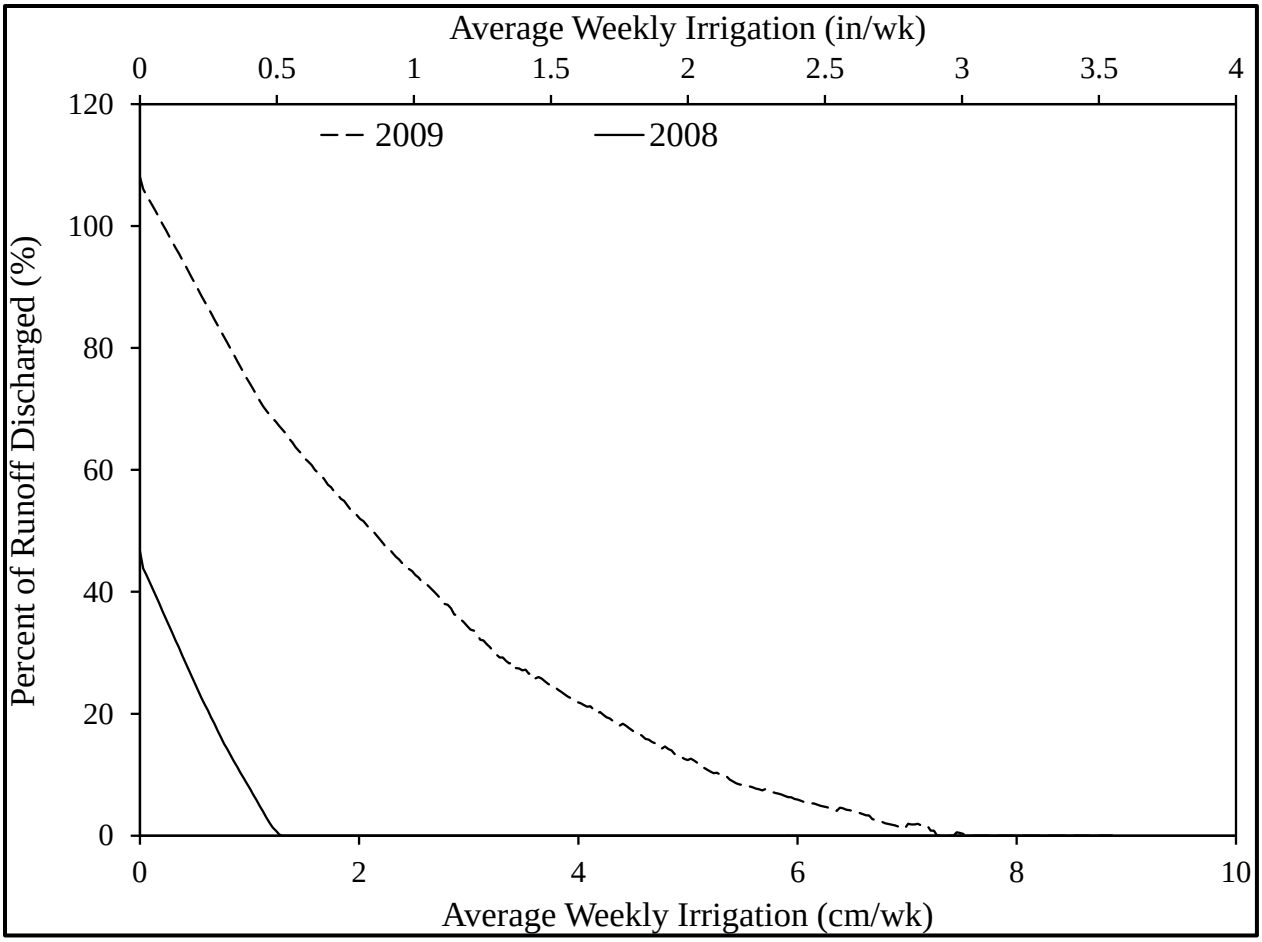

Figure 46 Percent of runoff discharged at permeability of 12.7 cm/hr. (5in/hr.)

Figure 46 explains that the discharge from the harvesting pond is about 108 percent of the runoff or 8 percent more water than the runoff contribution is discharged for 2009. The source of this excess water could be attributed to groundwater seepage, direct rainfall on the pond, and equalization flow from adjacent ponds. However, for the year 2008, only about 48 percent of the runoff is discharged. Subsequent increase in the weekly harvest volume showed an exponential decline in the percent of runoff discharged, which eventually decreased to zero runoff volume discharged. This gives credence to the fact that stormwater harvesting will reduce the discharge from ponds to adjacent surface water, which in effect achieves reduction in the total maximum

daily load (TMDL) by volume. The plots further reveal that harvesting can significantly reduce the quantity of pollutant discharged to receiving bodies by the reduction of the volume of discharge.

However, the increases on the weekly harvest rate generate a drawdown effect on the adjacent groundwater level. At a low rate or no irrigation from the wet detention pond, the percent of groundwater contribution to the pond is about 12 and 6 percent for year 2009 and 2008, respectively, but this increased with increasing weekly harvesting rate, as shown in Figure 47. This is due to the control mechanism set in the pond to regulate any undesirable effect on groundwater and the surrounding environment. The control mechanism is a permanent pool level or safe yield level, below which no harvesting is permitted. The harvest safe yield is the volume of water harvested from the pond without unacceptable effects on the groundwater. So, even when the weekly rate is increased at the same regular interval the corresponding change in the annual harvest volume is minimal thus, groundwater contribution to the pond is regulated.

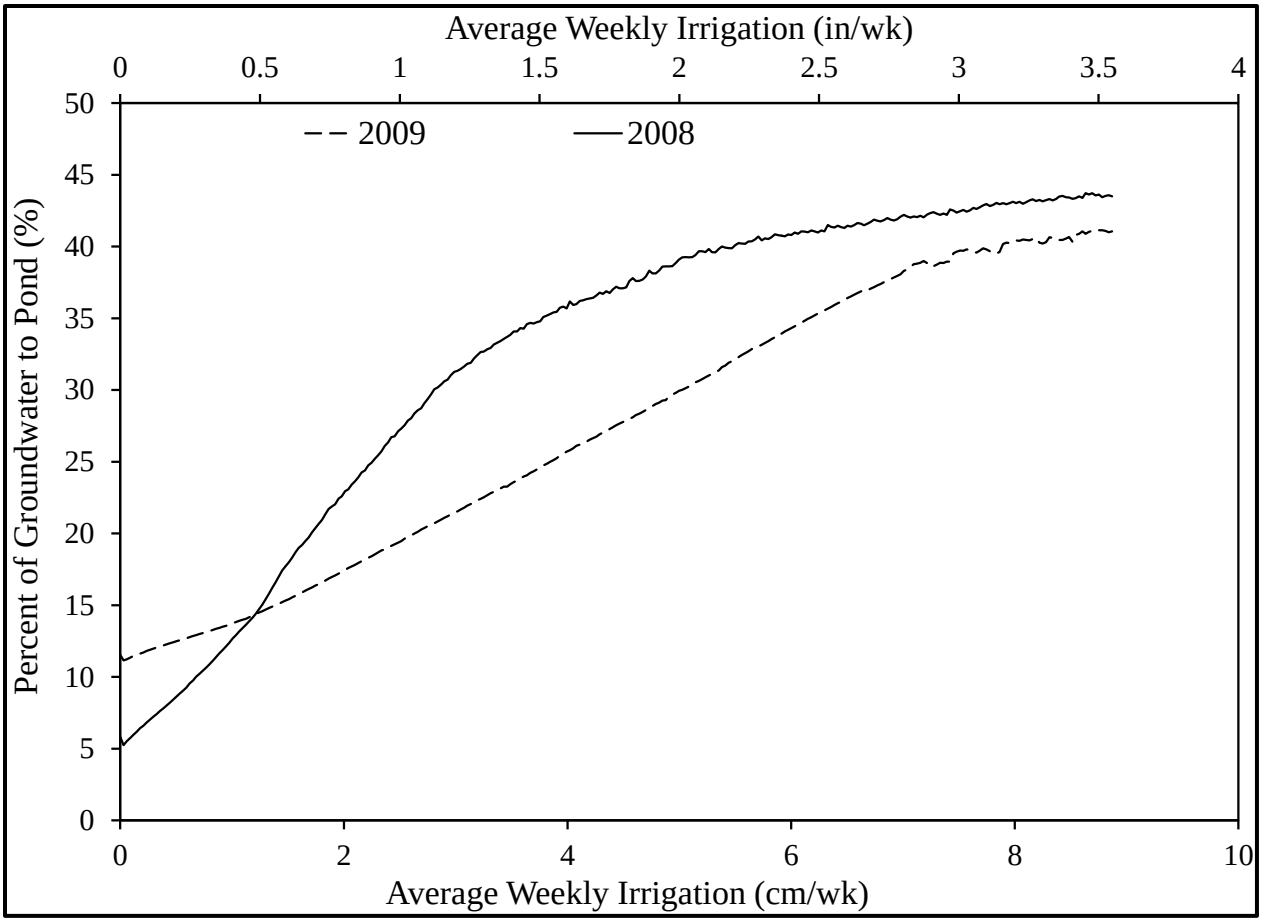

Figure 47 Percent of groundwater contribution to pond at permeability of 12.7 cm/hr. (5 in./hr.)

The percent of groundwater component is obtained from the fraction of groundwater seepage to the total intake of the pond per volume of weekly irrigation rate. The groundwater seepage to the pond increases as the weekly irrigation volume increases, but this is used as harvesting volume rather than discharge volume, which meets one of the reasons for the establishment of stormwater harvesting pond as a best management practice (BMP). This is expected due to the fact that a drawdown of the pond water level will significantly lead to increased seepage from the effective groundwater within the zone of influence.

The concerns on the effect of harvesting from wet detention pond on groundwater are addressed by the SHARP model in its capability to predict a safe yield to determine an acceptable maximum harvesting rate. In Figure 48 is shown the plot of the cumulative pond inflow (rainfall, runoff, and groundwater) and outflow (discharge, harvest, and evaporation) at weekly average harvesting rate of 0.17 cm/wk. (0.02 in./wk.). In the first five months of simulation (January to May 2009) the pond outflow is higher than inflow due to the low rainfall volume and constant harvesting from the pond. In the wet months of the simulation year, the inflow became higher because of the increased rainfall volume, less evaporation, and more groundwater available for seepage to the pond.

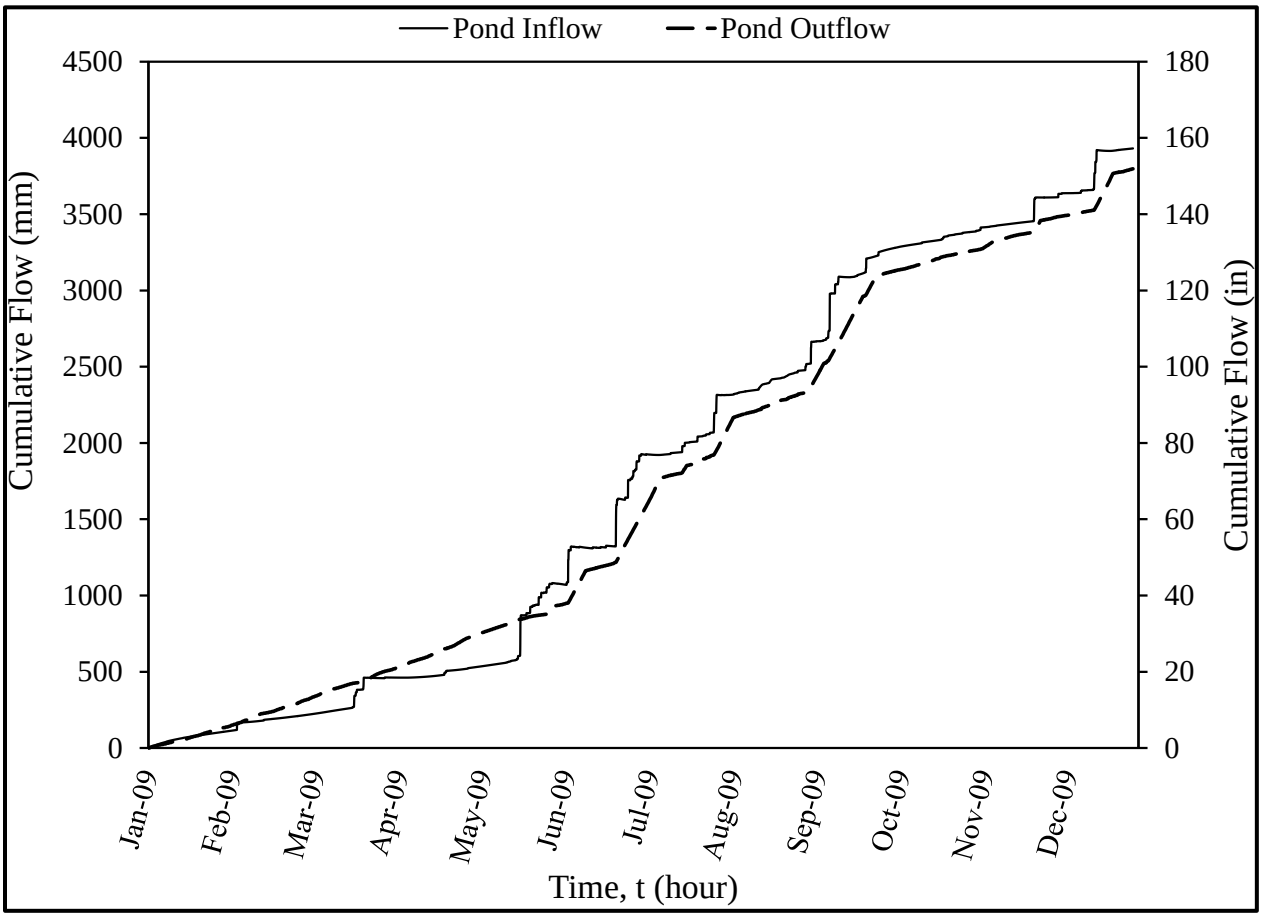

Figure 48 Cumulative inflow and outflow without irrigation in 2009

Furthermore, the percentage of groundwater contribution is also a function of the hydraulic properties of the pond boundary soil. High hydraulic conductivity, as in this study 12.7 cm/hr (5 in./hr) increases the groundwater seepage, which may eventually lead to total loss of pond water to the ground for the simulated period. In Figure 49 is presented a hypothetical case when the hydraulic conductivity of the pond soil liner is set at approximately 1.3 cm/hr (0.5 in/hr).

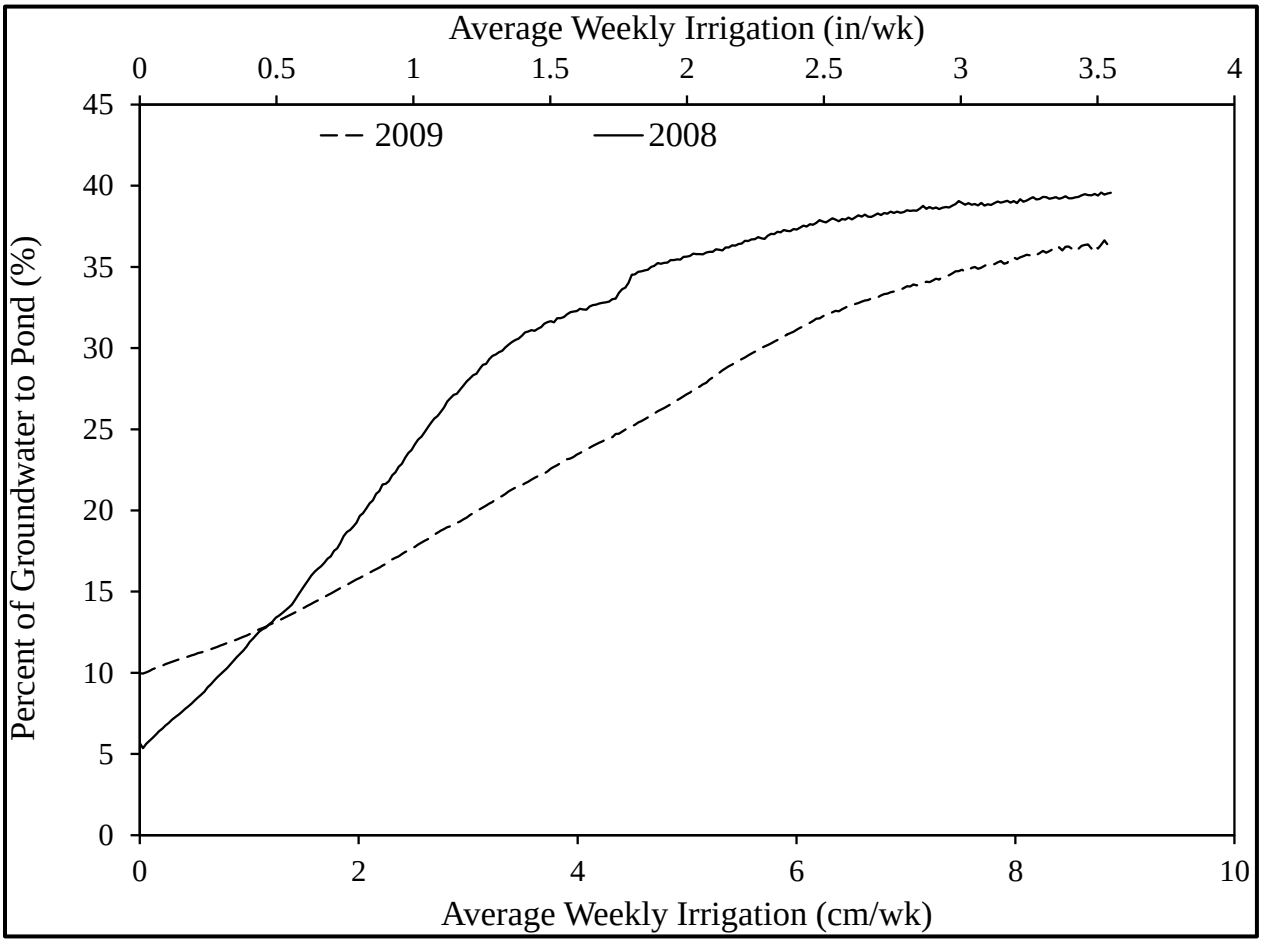

Figure 49 Percent of groundwater contribution to pond at permeability of 1.3 cm/hr. (0.5 in./hr.)

The percent of groundwater contribution to pond water started at low values of 10 and 5 percent and increased to 39 and 36 percent at 5.6 mm/hr. (2.2 in./hr) average weekly irrigation

rate for 2009 and 2008, respectively. The difference between percent of groundwater contribution to pond for both hydraulic conductivities (12.7 and 1.3 cm/hr) indicate that the hydraulic property of the pond soil liner will affect the seepage volume to the pond. The plots further revealed that harvesting can significantly reduce the quantity of pollutant discharged to receiving bodies by the reduction of the volume of discharge. The trend observed above is repeated for variable increments of average weekly irrigation to show the relative differences shown in Figure 50.

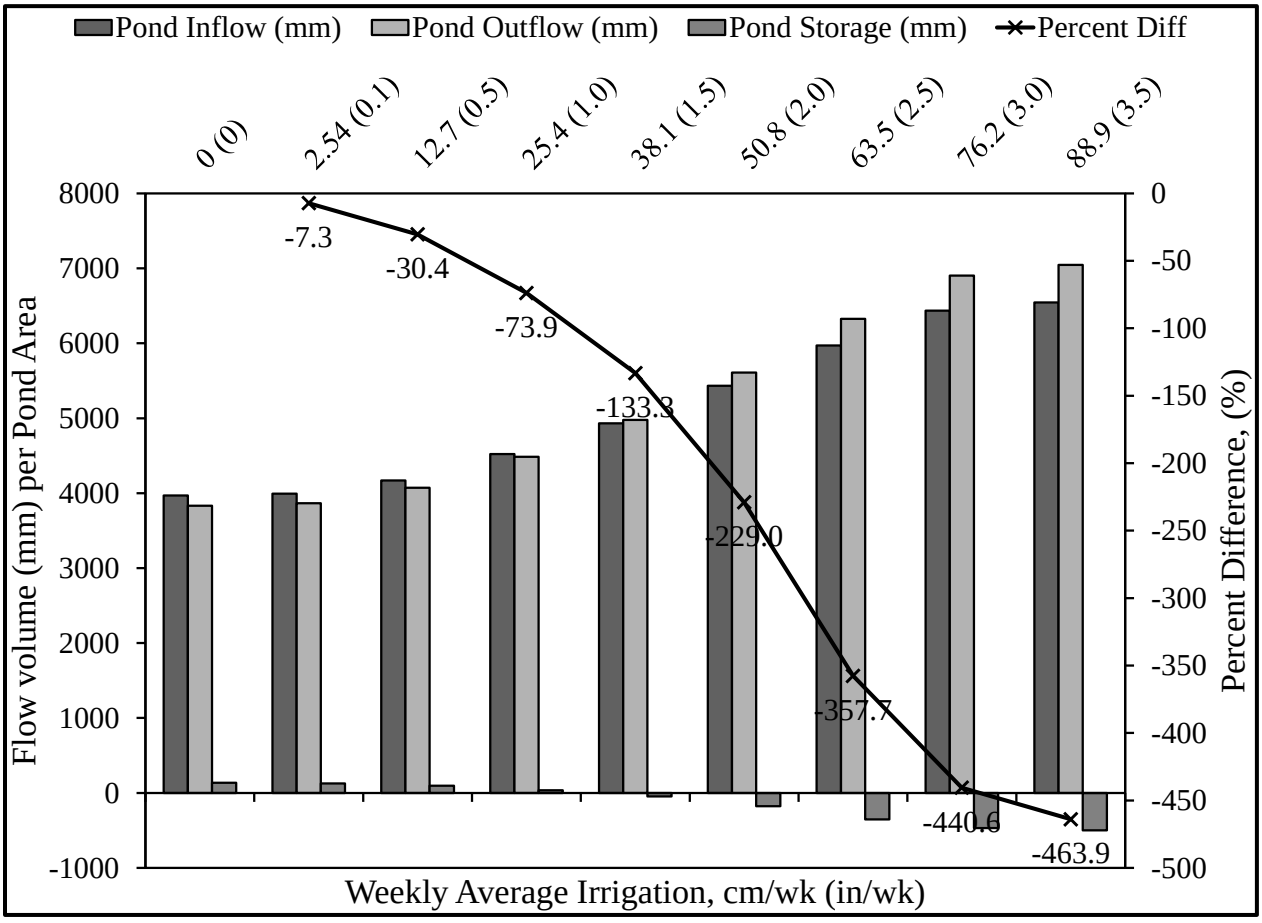

Figure 50 Percent differences relative to zero average weekly irrigation

As the harvesting volume is increased the percent difference in pond storage increases negatively, that is, there is a net loss in the water available for harvesting, which also means more groundwater seepage to the pond. In Figure 51 is shown the groundwater elevation around the perimeter of the pond and the safe yield level for the catchment area.

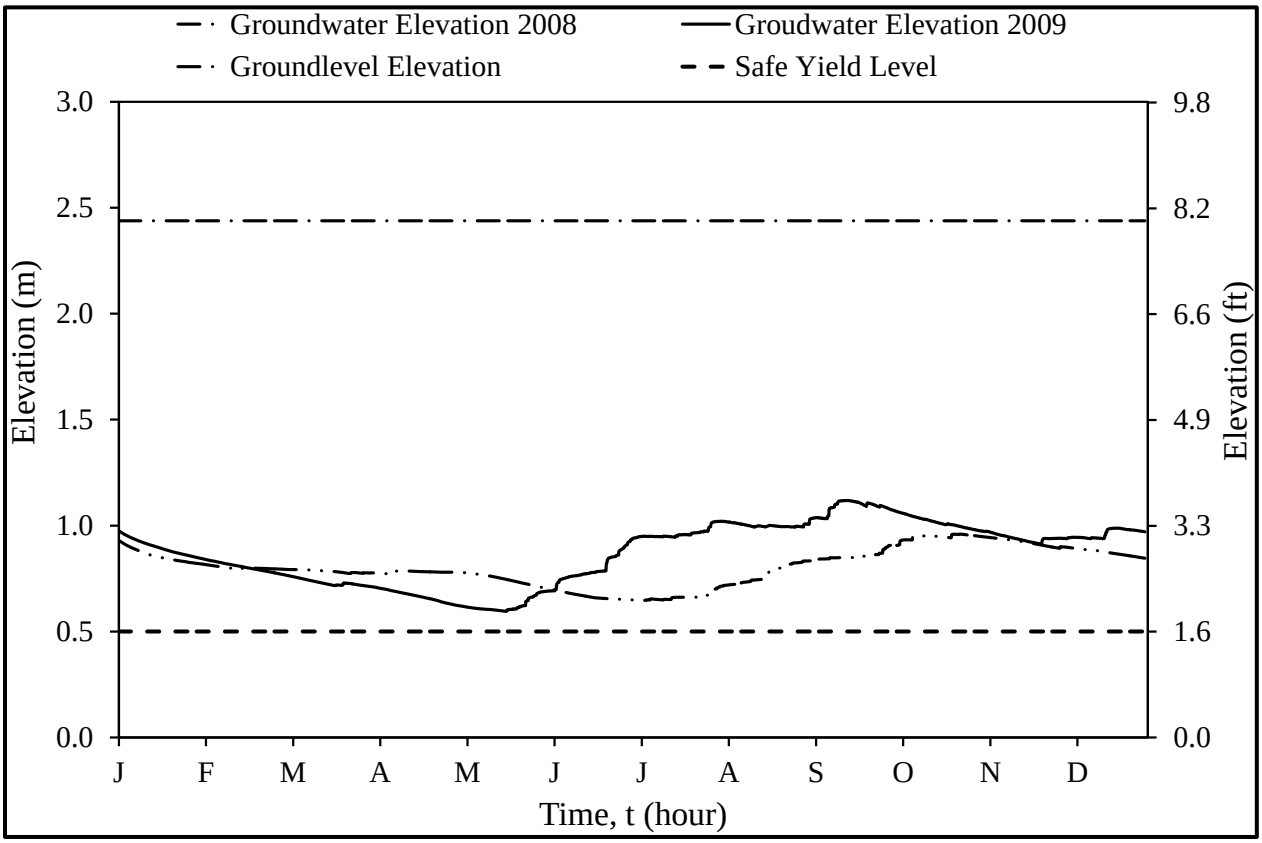

Figure 51 Groundwater elevations for the calibration and validation periods

As a check on mass balance consistency on the pond storage volume computation based on the pond surface area, the annual cumulative volumes of the factors in Equation 18 are presented in Table 18, which shows the inflow and outflow from the pond.

Table 18 Pond inflow and outflow parameter depths over the pond area for the simulated period

Year	Parameter	Input, mm (in.)	Output, mm (in.)
2008 (Validation period)	Rainfall (R)	1119.63 (44.08)	-
	Runoff (RO)	1250.95 (49.25)	-
	Harvest (H_{AR})	-	24.24 (0.95)
	Evaporation (E)	-	1897.54 (74.71)
	Discharge (D)	-	548.08 (21.58)
	Seepage (Q_{GW})	341.47 (13.44)	210.44 (8.28)
2009 (Calibration period)	Rainfall (R)	1611.88 (63.46)	-
	Runoff (RO)	1880.70 (74.04)	-
	Harvest (H_{AR})	-	22.96 (0.9)
	Evaporation (E)	-	1779.27 (70.05)
	Discharge (D)	-	1995.03 (78.54)
	Seepage (Q_{GW})	601.8 (23.69)	163.17 (6.42)

In the calibration period, net inflow and outflow for the pond is 133.96 mm (5.27 in.), which equals the difference between starting and ending pond water elevations of 2956.56 mm and 3090.42 mm (116.40 in. and 121.67 in.), respectively. Similarly, for the validation period, net inflow and outflow for the pond is 26.92 mm (1.06 in.), which equals the difference between starting and ending pond water elevations of 2910.84 mm and 2938.30 mm (114.60 in. and 115.68 in.), respectively. In addition to the pond water elevation, the model simulates the groundwater level (Figure 51) by the computation of the infiltration (Figure 74), evapotranspiration (Figure 75), runoff (Figure 76), deep percolation (Figure 77), lateral seepage (Figure 78), and total precipitation (Figure 79) in Appendix N. These interaction parameters are not validated in this study because of no available data for the pilot site. However, the predictability of the pond water elevation is evident that these parameters would be within statistically acceptable values.

Conclusions

The SHARP model developed for a stormwater harvesting pond uniquely accesses the interaction of surface water and groundwater in a catchment area and reasonably predicts the water movement through deterministic modeling process using basic mass balance principles of a catchment area hydrologic cycle. The model validation performed at the pilot site, on Miramar Lakes, Miramar, Florida water elevation predicts the general trend of the lake level fluctuations and shows no significant difference between the measured and simulated at 1% significance level. SHARP developed on Microsoft Excel platform convincingly simulated the pond water elevation at the pilot site within statistically acceptable level (R^2 greater than 0.72) for both the model calibration and validation.

In addition to the pond water elevation, the model simulates the groundwater level by the computation of the infiltration, evapotranspiration, runoff, deep percolation, lateral seepage, and total precipitation. These interaction parameters were not validated in this study because of no available data for the pilot site. However, the predictability of the pond water elevation is evident that these parameters would be within statistically acceptable values. The SHARP model provides a real-time forecasting tool to predict and plan pollutant loading reduction from the stormwater harvesting pond.

Furthermore, SHARP output provides the user(s) the capability to assess harvest safe-yield and flow between a pond and surrounding land with or without harvesting, and predict the percentage of runoff into a wet detention pond that is not discharged. This is relevant to stormwater management and planning due to the fact that the basic process of stormwater harvesting involves the capture and storage of stormwater runoff in a harvesting pond and

gradual use to irrigate adjacent pervious areas or for consumptive use (no return to the pond). The model confirms that harvesting ponds reduce the volume of discharge, and consequently, the pond releases less pollutant load downstream and increases groundwater recharge, as substantial volume of annual stormwater runoff is returned to the watershed.

GENERAL DISCUSSION

This chapter presents interrelationships based on the different studies conducted in this dissertation. In reference to the first objective, that is to relate the index properties of silt fence fabrics to field performances, three silt fence index properties namely grab strength, permittivity, and apparent opening size were correlated to the field performance of the fabrics in order to ascertain the relevance of using the index properties to specify minimum requirements. In pursuit of the second objective, the silt fence fabric sediment removal efficiency was combined with the stormwater harvesting pond reduction efficiency to create a potential treatment train aimed at achieving higher sediment removal efficiency. The treatment train approach is necessitated by the low performance efficiencies achieved by both silt fence fabrics in the field simulated rainfall events.

Field Hydraulic Properties

The index hydraulic properties of silt fence fabrics do not correlate to field performance, and is evident in the apparent opening size (ASTM D4751) and the permittivity (ASTM D4491) standard methods. Hydraulic properties relate the fabrics' abilities to conduct fluid and retain soil particles. Both fabrics have permittivity of 2.5 and 0.11 per second values which were greater than the minimum ASTM specification of 0.05 per second. The apparent opening sizes for both fabrics are 0.212 and 0.700 mm for BSRF and ARS-1400, respectively, and the maximum ASTM specification is 0.600 mm. The laboratory hydraulic properties obtained for both fabrics meets the ASTM specifications, and it is expected that field performance would replicate laboratory results. However, the flow rate obtained from the permittivity test tends to

overestimate the flow-through-rate of the silt fence fabrics over an actual field performance flow-through-rate.

Flow-Through-Rate

The average flow-through-rates obtained from the permittivity tests were 451.2 m/hr and 19.1 m/hr for BSRF and ARS-1400 silt fence fabrics (Table 4), respectively. These were significantly different when compared against the maximum flow-through-rates obtained from the simulated field performance (irrespective of slope or rainfall intensity) of 6.7 m/hr. and 2.5 m/hr for BSRF and ARS-1400 silt fence fabrics (Table 13), respectively. The laboratory test results are two and one order of magnitude greater than the respective fabrics' field flow-through-rate. For a conservative correlation between field and laboratory results flow-through-rates, the maximum field flow-through-rate is compared against the average laboratory test rates. Using the maximum values counteracts the influence of slope, rainfall intensities, silt fence maintenance, and antecedent soil conditions.

The factors that may have contributed to the difference in field and laboratory flow-through-rates are the moisture (humidity and wet/dry) condition and density of the soil surface, and the percentage of fines trapped in the fabric – which reduces the AOS, further slows down runoff velocity and eventually, the volume of downstream runoff. The moisture conditions affect how quickly upstream surface runoff is generated, the rate of runoff flow, and moisture losses through infiltration. A reduced runoff volume and slower velocity translate to less pressure on the fabric which eventually does not significantly alter the fabric opening (AOS). On the other hand, high flow rates upstream lead to more particles been trapped in the fabric which reduces

the apparent opening sizes and slows the flow-through-rate. The resultant effect may be considered as an advantage as it is likely to increase sediment removal efficiency, but also a disadvantage because it increases backwater build which may lead to overtopping and flooding problems. Figure 52 shows the effect of high backwater upstream of the silt fence, which includes flooding upstream, overtopping, fabric ripped off the stake at the staple connection, and stress on the fabric that led to larger fabric opening (AOS).

Figure 52 Effect of high backwater upstream of a silt fence: (a) flooding, (b) overtopping, (c) fabric ripped off the stake at the staple connection, and (d) larger fabric opening

Sediment Retention Performance Efficiency

The AOS test method estimates the largest opening and not the percentage of openings per square area of a fabric. Thus, it is purely a measure for soil retention capability upstream of the site. As is evident in the laboratory and field performance studies, the ARS-1400 has larger apparent opening than the BSRF. However, both permittivity and flow rate through the fabrics of BSRF are greater than what is obtained from the ARS-1400 (Table 4 and Table 13, and Figure 15). This may be attributed to the percent of opening per square area of each fabric, but this was not measured in the study. On the other hand, considering soil retention ability of the fabrics, the ARS-1400 having a larger AOS retained less suspended sediments when compared to the BSRF with smaller AOS (Figure 24 through Figure 33). The fabric with larger AOS allows nearly all the suspended sediments to pass through but retains soil particles that could not remain in suspension for a long period of time.

Most of the suspended sediments are silt- and clay-sizes with a maximum spherical diameter less than 0.075 mm, which is much smaller when compared to the apparent opening sizes of BSRF (0.212 mm), ARS-1400 (0.600 mm), and ASTM specification (0.600 mm). However, field test performance results showed that the BSRF achieved average suspended sediment concentration and turbidity reduction of 57 and 59 percent, respectively. This can be attributed to tortuous flow path within the fabric. The BSRF traps suspended sediments and reduces the AOS to achieve higher reduction performance efficiency without significantly affecting the flow-through-rate for the duration and number of rainfall events in this study.

The ARS-1400 achieved average suspended sediment concentration and turbidity reduction of 20 and 11 percent, respectively. This is because of the large AOS, though it equals

the ASTM minimum specification, does not have good reduction performance efficiency. ARS-1400 does function by effectively slowing down the runoff velocity to allow for particles to settle down. However, for clay- and silt-sized particles that takes longer time to settle down the water column, the ARS-1400 fabric does perform significantly less in sediment retention than what was obtained by the BSRF.

The different sediment retention abilities for both fabrics are evident in the field test results on performance evaluation. The ARS-1400 fabric turbidity reduction efficiency value was less than the suspended sediment concentration reduction, but remained approximately the same for the BSRF. Thus, runoff detention time does not directly explain the reduction performance efficiency of silt fence in the field. Longer detention time may likely results in overtopping and higher pressure on the silt fence which can cause failure of the stakes and tear or puncture of the fabric for long duration rainfall events, see Figure 52.

Field Mechanical Properties

The laboratory mechanical properties for silt fence fabrics are the grab strength and puncture resistance. There were no experiments conducted to directly correlate laboratory results to field performances for the mechanical properties. However, the water pressure upstream could be related to the applied load in the grab strength test. Briefly described, grab strength test uses a 101.6 mm wide by 203.2 mm length (4 by 8 in.) specimen clamped at both ends with a 25.4 mm (1 in.) smooth surface grip spaced 75 mm (3 in.) apart. Incremental tensile load is applied at a rate of 300 mm/min (12 in./min) to measure strain and determine the break load. In the field, the minimum spacing recommended by regulatory agencies between stakes (posts) is 1.2 m (4 ft.)

which is farther than the laboratory test set-up distance between clamps. The increased spacing and area would require higher break load value to strain the fabric and finally cause failure. Thus, instead of limiting the grab strength property to break load only, it should be related to the combination of break load and corresponding strain of the fabric. This is recommended as a procedure in grab strength test but not specified as a requirement for silt fence fabrics (ASTM D4632). In addition, the length and width of the test specimen should reflect the field condition, which will be similar to the breaking force and elongation of textile fabrics – strip method (ASTM 5035-06).

A significant difference between field application and grab strength test is the direction of loading for the grab strength test. The load is applied along the length of the specimen which only considers uniaxial strength, but in the field the loadings are biaxial. In the field, the water pressure exerts a force perpendicular to the length of the silt fence which then induces radial stresses along the length of the silt fence because it is attached between stakes. Thus, the uniaxial loading would not fully describe the strength of the fabric in the field. Furthermore, the radial stresses and strain causes the fabric to stretch and increases the apparent opening size, which would eventually lead to higher flow-through-rate and allow bigger sediment particles to pass through, see Figure 52(d). The increase in AOS is limited by the percentage of elongation allowed by the fabric for the applied loading. In this study, BSRF has higher strain capacity than the ARS-1400 (Figure 7) and thus have less significant effect on the increase of its AOS. The jet streams shown in Figure 53 is a resultant effect of higher upstream pressure on the silt fence which force an increase in the AOS, and thus more flow through. The strain capacity results are

reflected in the reduction performance efficiencies measured in field testing and the failure or tear observed in the ARS-1400 fabric.

Figure 53 Upstream runoff and soil pressure and resultant effect: jet stream flow

Treatment Train Approach

There is the possibility of a single stormwater treatment process not achieving the minimum requirements of most stormwater management agencies for pollution control. Thus, it is recommended, if that should be the case, that a treatment train approach be designed to effectively reduce generated pollutant loads in successive BMPs applied serially (Hayes et al. 2005; VNDCR 2006; FDEP 2007). The design of a treatment train approach that requires the combinations of structural and/or nonstructural BMPs in series should be dependent on proven effectiveness of the individual BMPs combined to meet local regulatory and physical site requirements. The efficiency of each of the treatment train component must account for the reduction of pollutant loading transferred to the subsequent component downstream in the series.

The reduction in pollutant loading of a stormwater runoff may be achieved quantitatively or qualitatively depending on the different BMPs combined. The added advantage of a BMP treatment train is that the series of BMPs provides a level of backup and redundancy, which will introduce another level of treatment if one within the train fails to function as designed.

Silt Fence and Polyacrylamide Treatment Train

In the course of this study, research conducted focused on effluent control from construction sites to establish the sediment reduction efficiency, and hydrologic modification of a catchment area to effectively predict the stormwater harvesting volume used for irrigation and discharge volume reduction. The performance standard obtained for both silt fence fabrics were less than the 85 percent reduction of the post-development average annual loading of nutrients required by local agencies (FDEP 2010). In addition, sediments are expected to be retained on site during the construction phase, but if discharged, must not constitute a violation of the turbidity standards (29 NTU above background in Florida). Therefore, both silt fence fabrics would require additional BMP to further improve removal in the final discharge.

In this study, silt fence enhanced by a potential combination with polyacrylamide to reduce construction site pollutant loadings was presented. The PAM products used in this study achieved minimum reduction efficiencies, without filtration, of between 18 and 76 percent for the four products tested. The low value (18 percent) shows that the PAM product used is not suitable for the soil type in the test. The minimum reduction efficiencies improved to between 40 to 95 percent when the PAM residue is filtered through a 35 micron filter (smaller than the AOS of both silt fence fabrics). Filtration of the PAM residue showed significant improvement in the

performance standard, which in some cases are above the minimum standard specification. The filter mimics a silt fence fabric, even though the AOS are significantly different, and showed a positive improvement in the performance of the combination of PAM and filter fabric. However, difference in AOS could also mean that both silt fence fabrics combined with PAM may not meet the required minimum standard. In addition, there are concerns on the toxic effect of PAM discharged directly into receiving water bodies. Thus, another treatment method may be required to further improve performance in reduction of pollutant loadings from construction sites and mitigate the concentration of PAM residue in the discharges.

Stormwater Harvesting Pond as Part of the Treatment Train

For the hydrologic modification, a second BMP, stormwater harvesting pond process was simulated to effectively predict stormwater discharge and use to aid planning and design of a treatment train. Thus, whatever loading of pollutant from construction sites which were not removed by the silt fence fabric would constitute the loading of pollutant that is discharged into the stormwater harvesting pond. Local regulatory agencies require that sediment accumulation in the stormwater system from construction activities be removed, so as not to cause loss in storage volume, protect wetlands, or prevent off-site flooding (FDEP 2010). With the capability to predict the inflow and outflow of the stormwater harvesting pond, planning and design engineers or management agencies will be better equipped to control residence time, harvesting volume, and discharge volume, especially during high volume inflows.

Removal efficiency of total nitrogen and total phosphorus is a function of the residence time (Harper and Baker 2007). Longer residence time in detention pond could achieve a

maximum of 90 percent total phosphorus removal and 45 percent total nitrogen reduction of the pond discharge. If the treated stormwater in the pond is harvested and used for irrigation, instead of been discharged, then approximately, 100 percent efficiency can be achieved in sediment reduction by volume. The SHARP model, developed as part of the research, provides a real-time forecasting tool to predict discharge volume and plan harvesting rate. The model can be used to control the percent removal efficiency to achieve targeted standards. A combination of the silt fence treatment and/or PAM treatment with a stormwater harvesting pond would further improve the performance standards of the treatment train. The advantage of the SHARP model is that sediment reduction performance efficiency can be predicted, planned, and executed in real-time.

CONCLUSIONS

In this research, pollutant reduction treatment methods used on construction sites were investigated to assess the effectiveness and performance standards under varying site conditions. For the effectiveness of effluent discharge controls, two silt fence fabrics real-time performance were evaluated on different slopes, rainfall intensities, and rainfall events with after-maintenance event. The field performances were related to the laboratory index properties of both silt fence fabrics to establish the correlation and predictability of field performance from index properties.

Polyacrylamide (PAM) dosage determination was conducted to scientifically perform repeatable laboratory tests and verify site-specific requirements in terms of PAM concentration, mixing energy and reaction time to achieve good performance standards in the field. Furthermore, experimental investigation of effluent discharges from construction sites treated with polyacrylamide (PAM) only, and combination with filter fabrics was performed to define PAM enhanced silt fence sediment reduction performance standards. Finally, a predictability stormwater harvesting pond model (SHARP) was developed that provides real-time assessment of pond inflow and outflows, assesses groundwater mound around the perimeter of the pond, and tool for planning and controlling of pond discharges. The SHARP model can be integrated with silt fence or combined silt fence and PAM treated site discharges in the form of BMP treatment train in series for pollutant reduction assessment.

One contribution of this research is that it provides tools to regulatory agencies, consultants and contractors on the relevance of geotextile index properties test methods for silt fence fabrics to real-time field performances. Unlike what is regulated and practiced, the tests conducted showed that the index properties do not adequately represent field performances.

Thus, the present test methods need reviews and updates to reproduce the field performances and/or the silt fence. The performance standards required for pollutant reduction should be revised to reflect site-specific conditions, location historical rainfall intensity, and fabric type. The research provided statistically satisfactory scientific findings that would aid regulatory agencies to specify realistic performance standards for silt fence fabrics. On the other hand, regulatory agencies now have scientific evidence to further study the control of construction site discharges using temporary sediment barriers, and the need for enhancement to guide practicable and result-oriented standards.

The research further developed, from current practice that is empirical and subjective, repeatable scientific PAM dosage determination test method. The method is aimed at achieving laboratory performance standards that could be used by contractors and designers in site-specific stormwater treatment plans required by regulatory agencies. The dosage determination test proved repeatability and the performance of PAM in sediment reduction from site runoff as a standalone product and/or combined with silt fence as a treatment train approach. The findings give local regulatory agencies and field practitioners the tools to determine performance standard for PAM used as a standalone treatment measure or combined with filter fabric as PAM-enhanced silt fence fabric.

The SHARP model developed in this research provided a tool that demonstrates the effect of interaction between pond water storage and subsurface water movement, including the overland flows (demonstration of how the interaction affects the overall pond water balance and the entire catchment area hydrologic cycle). The model integrates the flows and discharges from the catchment area, which may include PAM and silt fence treated runoff, to the treatment

achievable in the pond due to residence time; and controls harvesting and discharge volumes to meet required performance standards. SHARP model is readily available for the assessment of off-site discharges, downstream flooding, groundwater safe yield, harvesting rate by stormwater management agencies.

A combination of the silt fence, PAM, and stormwater harvesting model in a serial stormwater treatment train would effectively reduce pollutant loading from construction sites and within the catchment area to meet the required performance standards. The reduction efficiency achieved would significantly reduce the sediment loading to the stormwater harvesting pond. This would improve the quality of stormwater harvesting and discharge volumes from the pond and meet the TMDL requirements.

APPENDIX A
STANDARD SPECIFICATIONS

Table 19 Manufacturer Recommended Physical and Hydraulic Properties of ASR-1400

Property	Unit	Test Method	MARV (English)
Weight Unit Area gsm[(1)]	g/m^2	ASTM D-5261	70
Weave			10 × 10
Grab Tensile	lb	ASTM D-4632	100
% Grab Elongation @ Yield	%	ASTM D-4632	15
Mullen Burst	psi	ASTM D-3786	220
Puncture	lb	ASTM D-4833	40
Trapezoidal Tear	lb	ASTM D-4533	40
UV Resistance @ 500 hours	%	ASTM D-4355	80
AOS[(2)]	US sieve No.	ASTM D-4751	30
Permittivity	sec^{-1}	ASTM D-4491	0.05
Flow Rate	gal/min/ft	ASTM D-4491	6

Table 20 Manufacturers' Specification of Physical and Hydraulic Properties for BSRF

Property	Unit	Test Method	Manufacturers Specification
Grab Tensile Strength-warp	lb	ASTM D-4632	95
Grab Tensile Strength-sewn	lb	ASTM D-4632	95
Elongation	%	ASTM D-4632	68
Apparent Opening Size	US Sieve No.	ASTM D-4751	70
Permittivity	s^{-1}	ASTM D-4191	
Flow Rate/Flux	gpm	ASTM D-5141	185
Ultraviolet Stability	% at 500 hours	ASTM D-4355	26.3

Table 21 ASTM D 6461 Temporary Silt Fence Material Property Requirements

Property	Direction	Test Methods	Units	Supported Silt Fence	Unsupported Silt Fence	Type of Value
Grab Strength	Machine	ASTM D 4632	N (lbs)	400 (90)	550 (90)	MARV
	X-Machine			400 (90)	450 (90)	MARV
Permittivity		ASTM D 4491	sec^{-1}	0.05	0.05	MARV
Apparent Opening Size		ASTM D 4751	Mm (US Sieve #)	0.60 (30)	0.60 (30)	Max. ARV
Ultraviolet Stability		ASTM D 4355	% Retained Strength	70% after 500 hours of exposure	70% after 500 hours of exposure	Typical

APPENDIX B
GRAB STRENGTH TESTS

Table 22 ASTM D4632 (grab and elongation) test results for BSRF and ARS-1400

Measure	Specimen No.	BSRF				ARS-1400			
		Cross-machine Direction		Machine Direction		Cross-machine Direction		Machine Direction	
		Dry	Wet	Dry	Wet	Dry	Wet	Dry	Wet
Peak (Breaking) Load (lbs.)	1	155	167	112	134	152	107	112	117
	2	168	163	143	132	137	98	134	84
	3	148	164	130	119	145	99	154	132
	4	161	172	132	131	159	87	158	84
	5	174	179	110	128	118	88	127	119
	6	155	188	139	141	123	135	145	123
	7	178	190	133	137	133	129	162	139
	8	171	181	135	143	149	168	163	174
	9	171	163	123	124	150	179	159	142
	10	151	166	141	141	167	139	140	99
Elongation at Peak Load (in.)	1	1.30	0.99	1.18	1.42	0.32	0.20	0.33	0.31
	2	1.17	1.18	1.47	1.23	0.26	0.30	0.28	0.14
	3	1.39	1.21	1.37	1.12	0.23	0.32	0.25	0.37
	4	1.32	1.17	1.45	1.14	0.39	0.14	0.29	0.37
	5	1.36	1.03	1.15	1.23	0.13	0.24	0.26	0.26
	6	1.38	1.20	1.29	1.28	0.32	0.26	0.32	0.22
	7	1.43	1.10	1.49	1.32	0.14	0.23	0.24	0.31
	8	1.43	1.07	1.39	1.22	0.19	0.23	0.26	0.24
	9	1.28	1.12	1.28	1.17	0.29	0.24	0.34	0.27
	10	1.16	1.28	1.47	1.44	0.25	0.23	0.24	0.18
Strain at Break Load (%)	1	38.62	28.63	35.49	40.69	9.31	5.95	9.71	9.06
	2	33.99	33.17	44.23	35.79	7.62	8.77	8.09	4.20
	3	40.09	35.49	39.87	32.81	6.65	9.70	7.35	10.85
	4	38.12	33.57	41.91	33.25	11.51	4.13	8.52	9.69
	5	39.99	29.40	33.61	36.28	3.82	7.24	7.74	7.51
	6	39.67	34.44	37.93	37.26	9.49	7.83	9.26	6.41
	7	40.70	31.44	44.04	38.73	4.07	6.78	6.92	9.16
	8	40.90	30.71	40.37	35.66	5.54	6.51	7.45	6.77
	9	37.09	31.88	37.67	34.03	8.48	7.03	9.92	7.57
	10	33.97	37.38	43.03	41.70	7.48	6.69	7.04	5.06

Table 23 Mann-Whitney Tests on breaking load for BSRF and ARS-1400 in dry conditioning

Cross-machine Direction				Machine Direction			
BSRF	ARS-1400	Rank U (1)	Rank D (2)	BSRF	ARS-1400	Rank U (1)	Rank D (2)
155	152	11	10	112	112	2	3
168	137	16	4	143	134	14	9
148	145	6	5	130	154	6	16
161	159	14	13	132	158	7	17
174	118	19	1	110	127	1	5
155	123	12	2	139	145	11	15
178	133	20	3	133	162	8	19
171	149	17.5	7	135	163	10	20
171	150	17.5	8	123	159	4	18
151	167	9	15	141	140	13	12
n1 =	10	n2 =	10	n1 =	10	n2 =	10
R1 =	142	R2 =	68	R1 =	76	R2 =	134
U =	13	μ_U =	50.00	U =	79	μ_U =	50.00
z =	2.835	σ_U =	13.23	z =	-2.154	σ_U =	13.23
z crit =	1.645	α =	0.05	z crit =	1.645	α =	0.05
$R1_{mean}$ =	105	$R2_{mean}$ =	105	$R1_{mean}$ =	105	$R2_{mean}$ =	105
z1 =	2.835	z2 =	-2.835	z1 =	-2.154	z2 =	2.154
Lower Limit	23	Upper Limit	77	Lower Limit	23	Upper Limit	77
p-value =	0.0058			p-value =	0.0340		
Decision (z-value):		Reject Ho		Decision (z-value):		Reject Ho	
Decision (p-value):		Reject Ho		Decision (p-value):		Reject Ho	
Decision (U-limits):		Reject Ho		Decision (U-limits):		Reject Ho	

Table 24 Mann-Whitney Tests on strain at peak load for BSRF and ARS-1400 in dry conditioning

Cross-machine Direction				Machine Direction			
BSRF	ARS-1400	Rank U (1)	Rank D (2)	BSRF	ARS-1400	Rank U (1)	Rank D (2)
38.62	9.31	15	8	35.49	9.71	12	9
33.99	7.62	12	6	44.23	8.09	20	6
40.09	6.65	18	4	39.87	7.35	15	3
38.12	11.51	14	10	41.91	8.52	17	7
39.99	3.82	17	1	33.61	7.74	11	5
39.67	9.49	16	9	37.93	9.26	14	8
40.70	4.07	19	2	44.04	6.92	19	1
40.90	5.54	20	3	40.37	7.45	16	4
37.09	8.48	13	7	37.67	9.92	13	10
33.97	7.48	11	5	43.03	7.04	18	2
n1 =	10	n2 =	10	n1 =	10	n2 =	10
R1 =	155	R2 =	55	R1 =	155	R2 =	55
U =	0	μ_U =	50.00	U =	0	μ_U =	50.00
z =	3.817	σ_U =	13.23	z =	3.817	σ_U =	13.23
z crit =	1.645	α =	0.05	z crit =	1.645	α =	0.05
$R1_{mean}$ =	105	$R2_{mean}$ =	105	$R1_{mean}$ =	105	$R2_{mean}$ =	105
z1 =	3.817	z2 =	-3.817	z1 =	3.817	z2 =	-3.817
Lower Limit	23	Upper Limit	77	Lower Limit	23	Upper Limit	77
p-value =	0.0002			p-value =	0.0002		
Decision (z-value):		Reject Ho		Decision (z-value):		Reject Ho	
Decision (p-value):		Reject Ho		Decision (p-value):		Reject Ho	
Decision (U-limits):		Reject Ho		Decision (U-limits):		Reject Ho	

Table 25 Mann-Whitney Tests on breaking load for BSRF and ARS-1400 in wet conditioning

Cross-machine Direction				Machine Direction			
BSRF	ARS-1400	Rank U (1)	Rank D (2)	BSRF	ARS-1400	Rank U (1)	Rank D (2)
167	107	13	5	134	117	13	4
163	98	9	3	132	84	12	1
164	99	11	4	119	132	6	11
172	87	15	1	131	84	10	2
179	88	17	2	128	119	9	5
188	135	19	7	141	123	16	7
190	129	20	6	137	139	14	15
181	168	18	14	143	174	19	20
163	179	10	16	124	142	8	18
166	139	12	8	141	99	17	3
n1 =	10	n2 =	10	n1 =	10	n2 =	10
R1 =	144	R2 =	66	R1 =	124	R2 =	86
U =	11	μ_U =	50.00	U =	31	μ_U =	50.00
z =	2.986	σ_U =	13.23	z =	1.474	σ_U =	13.23
z crit =	1.645	α =	0.05	z crit =	1.645	α =	0.05
$R1_{mean}$ =	105	$R2_{mean}$ =	105	$R1_{mean}$ =	105	$R2_{mean}$ =	105
z1 =	2.986	z2 =	-2.986	z1 =	1.474	z2 =	-1.474
Lower Limit	23	Upper Limit	77	Lower Limit	23	Upper Limit	77
p-value =	0.0041			p-value =	0.1868		
Decision (z-value):		Reject Ho		Decision (z-value):		Do Not Reject Ho	
Decision (p-value):		Reject Ho		Decision (p-value):		Do Not Reject Ho	
Decision (U-limits):		Reject Ho		Decision (U-limits):		Do Not Reject Ho	

Table 26 Mann-Whitney Tests on strain at peak load for BSRF and ARS-1400 in wet conditioning

Cross-machine Direction				Machine Direction			
BSRF	ARS-1400	Rank U (1)	Rank D (2)	BSRF	ARS-1400	Rank U (1)	Rank D (2)
28.63	5.95	11	2	40.69	9.06	19	7
33.17	8.77	16	9	35.79	4.20	15	1
35.49	9.70	19	10	32.81	10.85	11	10
33.57	4.13	17	1	33.25	9.69	12	9
29.40	7.24	12	7	36.28	7.51	16	5
34.44	7.83	18	8	37.26	6.41	17	3
31.44	6.78	14	5	38.73	9.16	18	8
30.71	6.51	13	3	35.66	6.77	14	4
31.88	7.03	15	6	34.03	7.57	13	6
37.38	6.69	20	4	41.70	5.06	20	2
n1 =	10	n2 =	10	n1 =	10	n2 =	10
R1 =	155	R2 =	55	R1 =	155	R2 =	55
U =	0	μ_U =	50.00	U =	0	μ_U =	50.00
z =	3.817	σ_U =	13.23	z =	3.817	σ_U =	13.23
z crit =	1.645	α =	0.05	z crit =	1.645	α =	0.05
$R1_{mean}$ =	105	$R2_{mean}$ =	105	$R1_{mean}$ =	105	$R2_{mean}$ =	105
z1 =	3.817	z2 =	-3.817	z1 =	3.817	z2 =	-3.817
Lower Limit	23	Upper Limit	77	Lower Limit	23	Upper Limit	77
p-value =	0.0002			p-value =	0.0002		
Decision (z-value):		Reject Ho		Decision (z-value):		Reject Ho	
Decision (p-value):		Reject Ho		Decision (p-value):		Reject Ho	
Decision (U-limits):		Reject Ho		Decision (U-limits):		Reject Ho	

APPENDIX C
PERMITTIVTY TESTS

Table 27 ASTM D4491 (permittivity) test results for BSRF and ARS-1400

Fabric	BSRF				ARS-1400			
Specimen	1	2	3	4	1	2	3	4
Quantity of Flow, (mL)	8081	6754	9135	9002	378	252	307	404
	7271	6821	9391	8436	357	242	307	399
	7121	6549	8802	8214	352	236	299	399
	6758	6449	8547	7548	352	234	298	396
	6305	6283	8214	6926	331	234	294	394
Permittivity, (sec^{-1})	2.6473	2.2128	2.9928	2.9492	0.1244	0.0829	0.1009	0.1330
	2.3819	2.2346	3.0764	2.7637	0.1175	0.0795	0.1009	0.1313
	2.3328	2.1455	2.8837	2.6910	0.1158	0.0778	0.0985	0.1313
	2.2139	2.1128	2.8001	2.4728	0.1158	0.0771	0.0981	0.1303
	2.0655	2.0582	2.6910	2.2691	0.1089	0.0771	0.0968	0.1296
Flow rate, (m/hr.)	478.43	399.90	540.86	532.98	22.38	14.92	18.15	23.93
	430.46	403.84	555.98	499.46	21.14	14.30	18.15	23.62
	421.58	387.74	521.15	486.32	20.83	13.99	17.72	23.62
	400.09	381.82	506.03	446.89	20.83	13.86	17.66	23.44
	373.28	371.97	486.32	410.08	19.58	13.86	17.41	23.31
	Specimen Area =		2026.83	mm^2	Test Duration =		30	seconds
	BSRF Temperature correction factor			1.11	ARS-1400 Temperature correction factor			1.05

APPENDIX D
APPARENT OPENING SIZE TESTS

Table 28 ASTM D4751 (AOS) test results for BSRF and ARS-1400

Fabric	U.S. Sieve No.	Bead diameter, (mm)	Percent passing	Percent retained	Percent loss
BSRF	180	0.080	96.92	2.37	0.71
	120	0.125	85.56	13.99	0.45
	80	0.180	17.83	82.07	0.10
	70	0.212	1.96	97.83	0.21
ARS-1400	50	0.300	58.83	41.19	-0.02
	40	0.425	42.20	57.64	0.16
	30	0.600	21.61	67.54	10.86
	25	0.710	2.01	97.79	0.20

Table 29 Glass bead sizes (ASTM D4751)

Bead Size Range				Bead Size Designation	
Passing		Retained			
Opening size, mm	Sieve Number	Opening size, mm	Sieve Number	Opening size, mm	Sieve Number
2.00	10	1.70	12	1.70	12
1.40	14	1.18	16	1.18	16
1.00	18	0.85	20	0.85	20
0.71	25	0.60	30	0.60	30
0.50	35	0.425	40	0.425	40
0.355	45	0.300	50	0.300	50
0.250	60	0.212	70	0.212	70
0.180	80	0.150	100	0.150	100
0.125	120	0.106	140	0.106	140
0.090	170	0.075	200	0.075	200

APPENDIX E
PUNCTURE LOAD TESTS

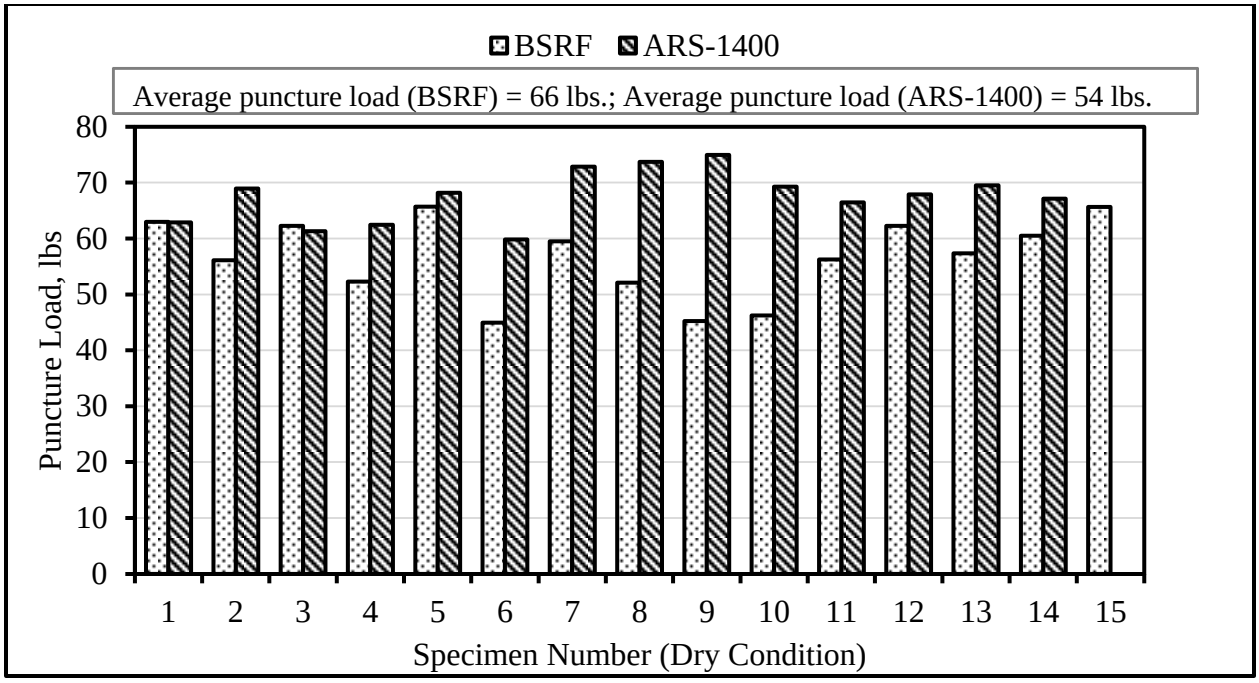

Figure 54 Puncture resistance for BSRF and ARS-1400 in dry condition

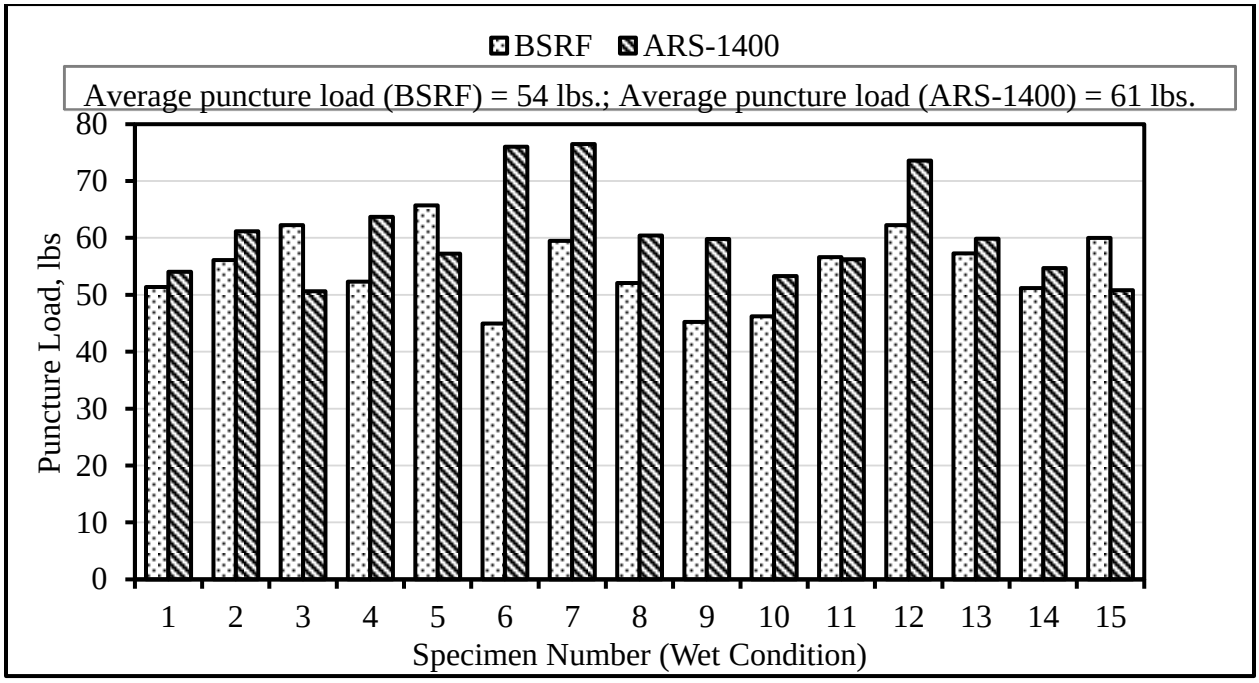

Figure 55 Puncture resistance for BSRF and ARS-1400 in wet condition

Table 30 Man-Whitney test results on Puncture resistance for BSRF and ARS-1400

BSRF				ARS-1400			
Dry	Wet	Rank U (1)	Rank D (2)	Dry	Wet	Rank U (1)	Rank D (2)
63	51	27	8	63	54	15	4
56	56	13.5	13.5	69	61	21	12
62	62	24	24	61	51	13	1
52	52	11.5	11.5	62	64	14	16
66	66	29.5	29.5	68	57	20	7
45	45	1.5	1.5	60	76	9	28
59	59	19.5	19.5	73	76	24	29
52	52	9.5	9.5	74	60	26	11
45	45	3.5	3.5	75	60	27	8
46	46	5.5	5.5	69	53	22	3
56	57	15	16	66	56	17	6
62	62	24	26	68	74	19	25
57	57	18	17	70	60	23	10
61	51	22	7	67	55	18	5
66	60	28	21		51		2
n1 =	15	n2 =	15	n1 =	14	n2 =	15
R1 =	252	R2 =	213	R1 =	268	R2 =	167
U =	93	μ_U =	112.50	U =	47	μ_U =	105.00
z =	0.830	σ_U =	24.11	z =	2.553	σ_U =	22.91
z crit =	1.645	α =	0.05	z crit =	1.645	α =	0.05
$R1_{mean}$ =	232.5	$R2_{mean}$ =	232.5	$R1_{mean}$ =	210	$R2_{mean}$ =	225
z1 =	0.830	z2 =	-0.830	z1 =	2.553	z2 =	-2.553
Lower Limit	64	Upper Limit	161	Lower Limit	59	Upper Limit	151
p-value =	0.4295			p-value =	0.0013		
Decision (z-value):		Do Not Reject Ho		Decision (z-value):		Reject Ho	
Decision (p-value):		Do Not Reject Ho		Decision (p-value):		Reject Ho	
Decision (U-limits):		Do Not Reject Ho		Decision (U-limits):		Reject Ho	

APPENDIX F
PAM DOSAGE TESTING RESULTS

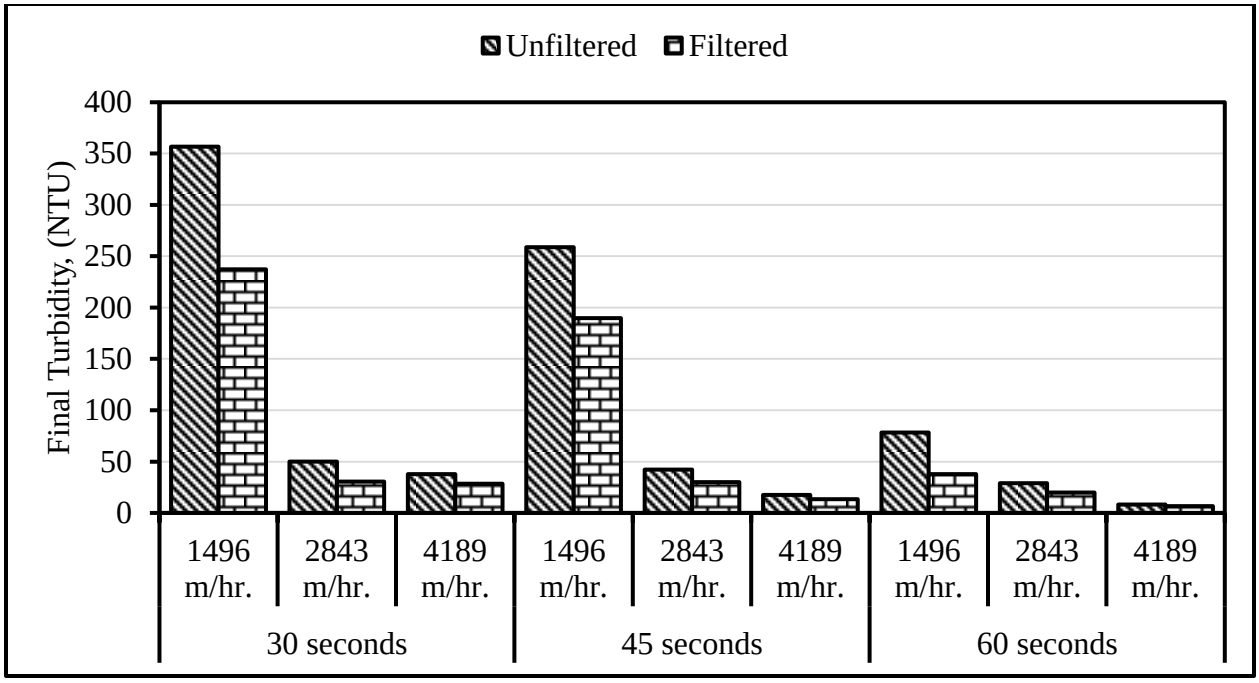

Figure 56 Final turbidity for PAM APS 705 at a concentration of 417 mg/L

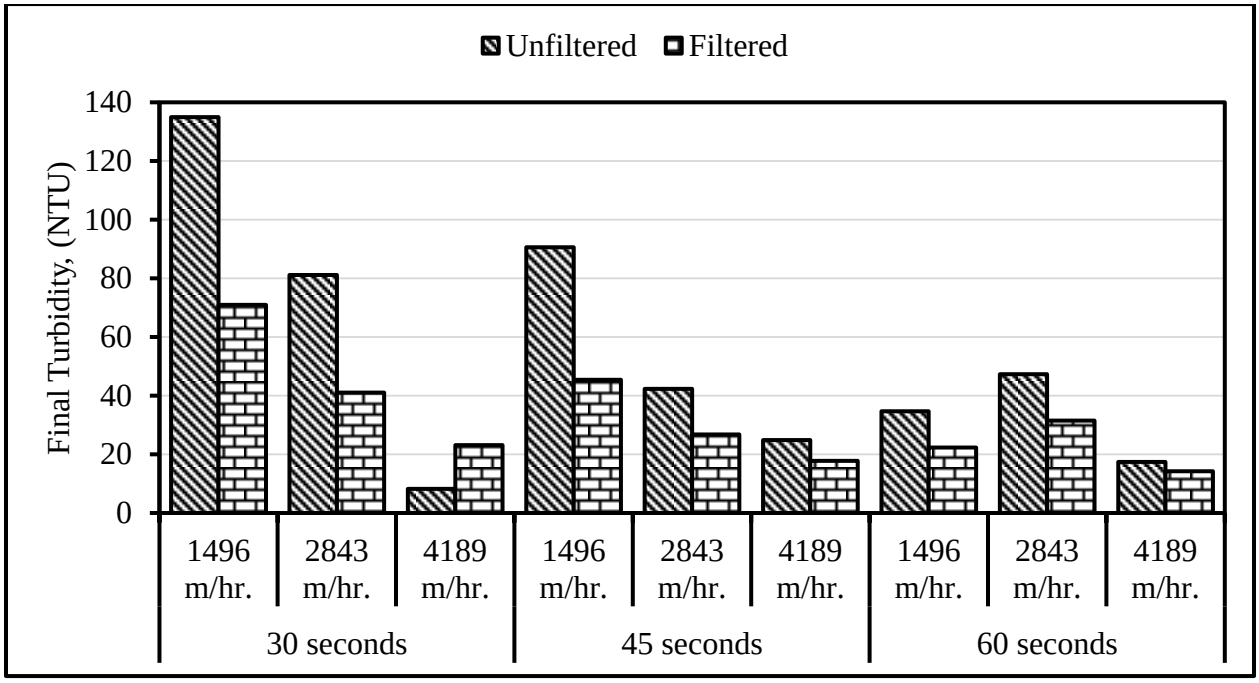

Figure 57 Final turbidity for PAM APS 705 at a concentration of 833 mg/L

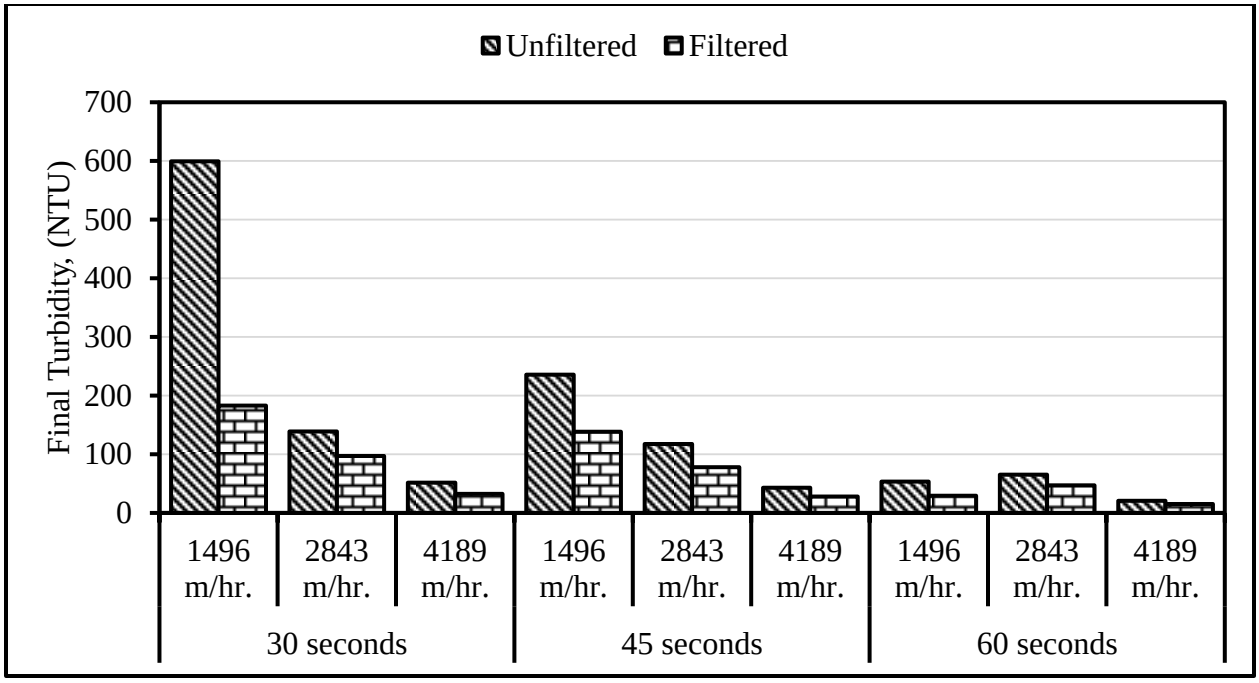

Figure 58 Final turbidity for PAM APS 745 at a concentration of 417 mg/L

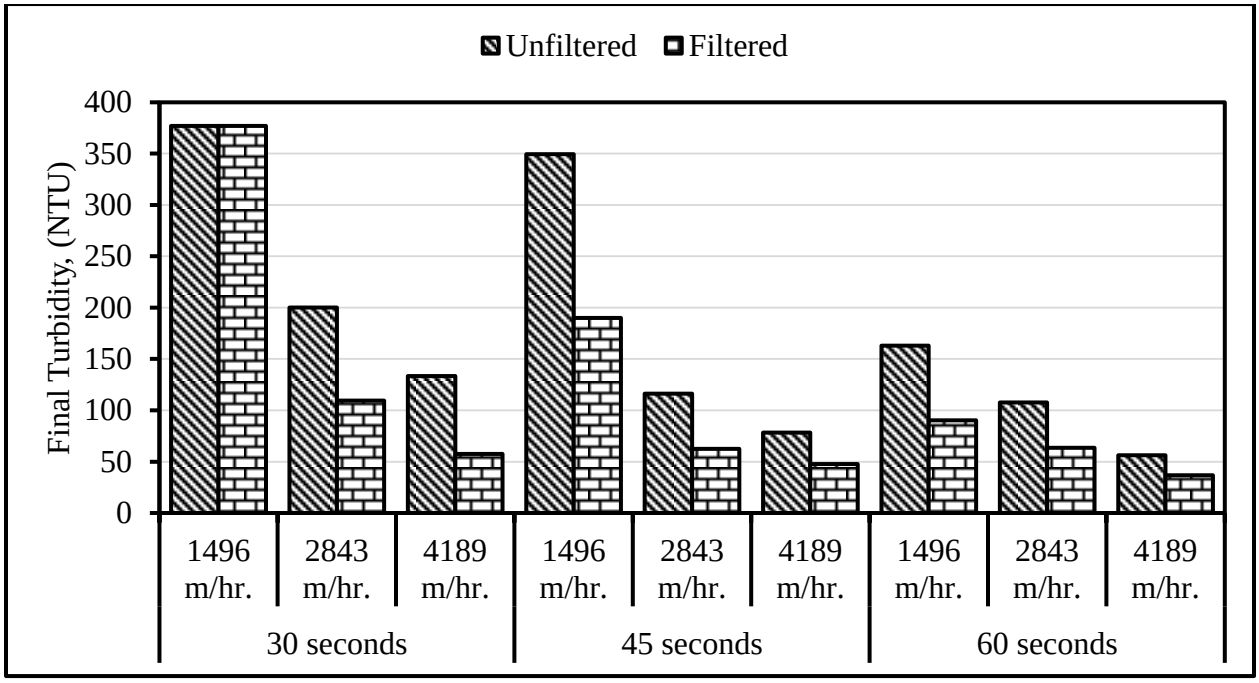

Figure 59 Final turbidity for PAM APS 745 at a concentration of 833 mg/L

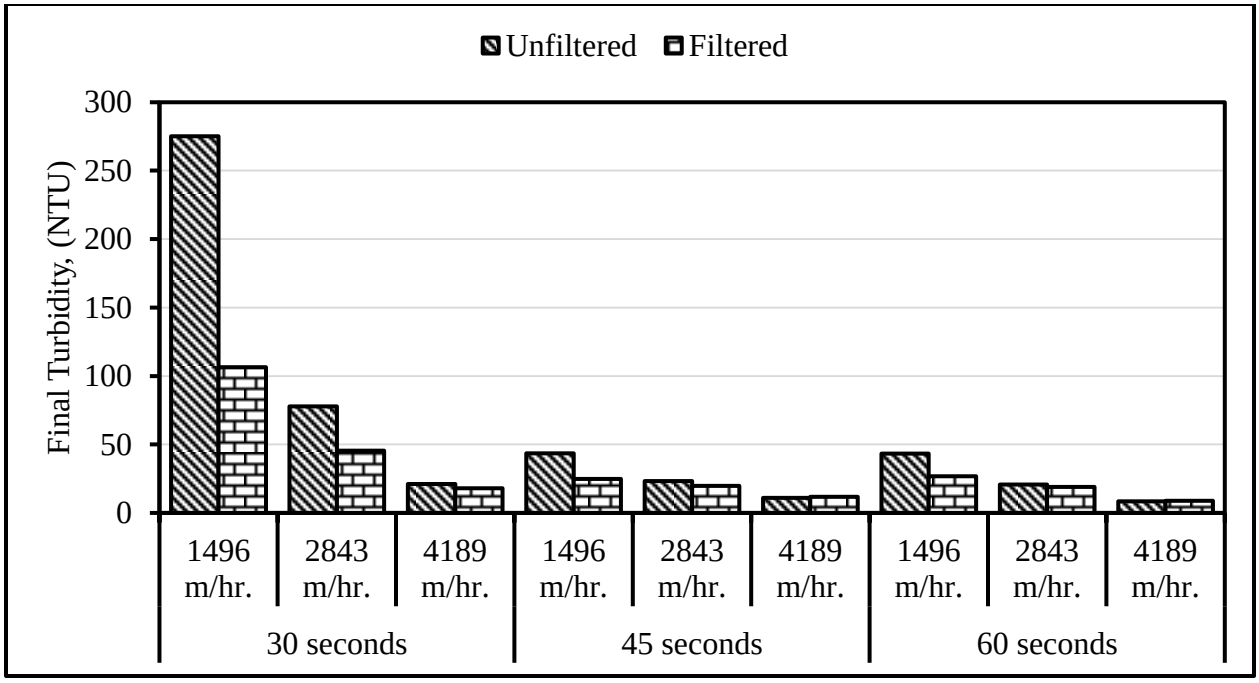

Figure 60 Final turbidity for PAM APS 706 at a concentration of 3333 mg/L

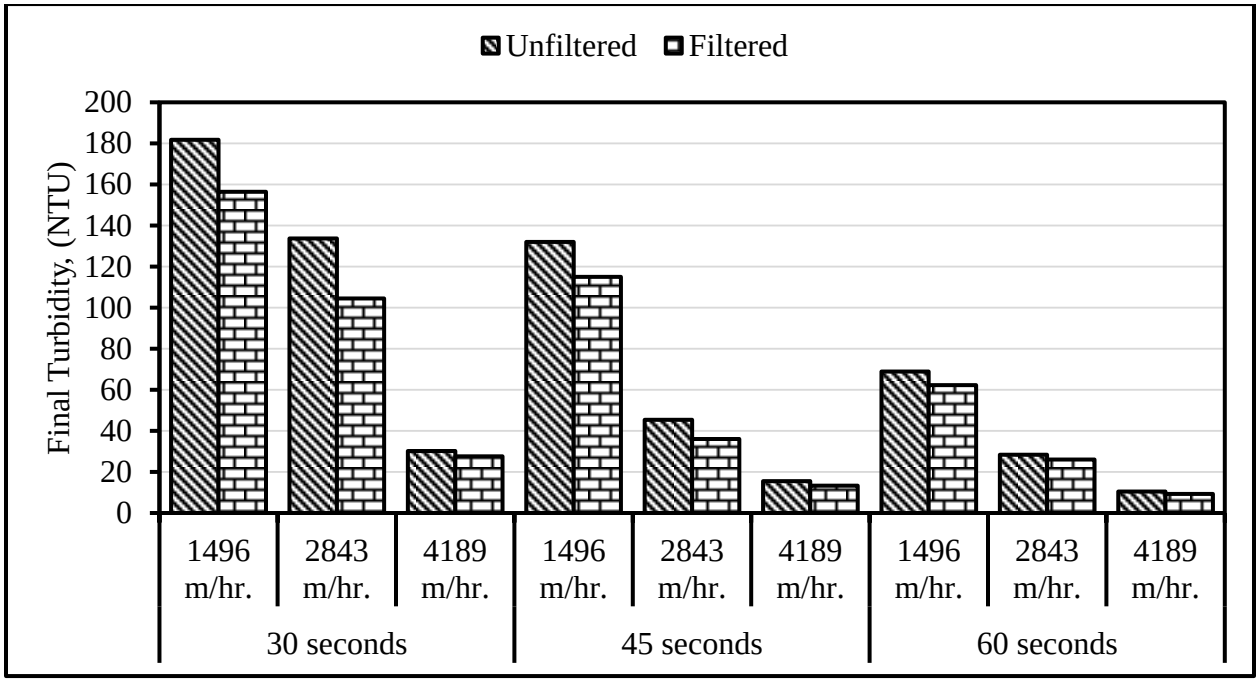

Figure 61 Final turbidity for PAM APS 706 at a concentration of 4167 mg/L

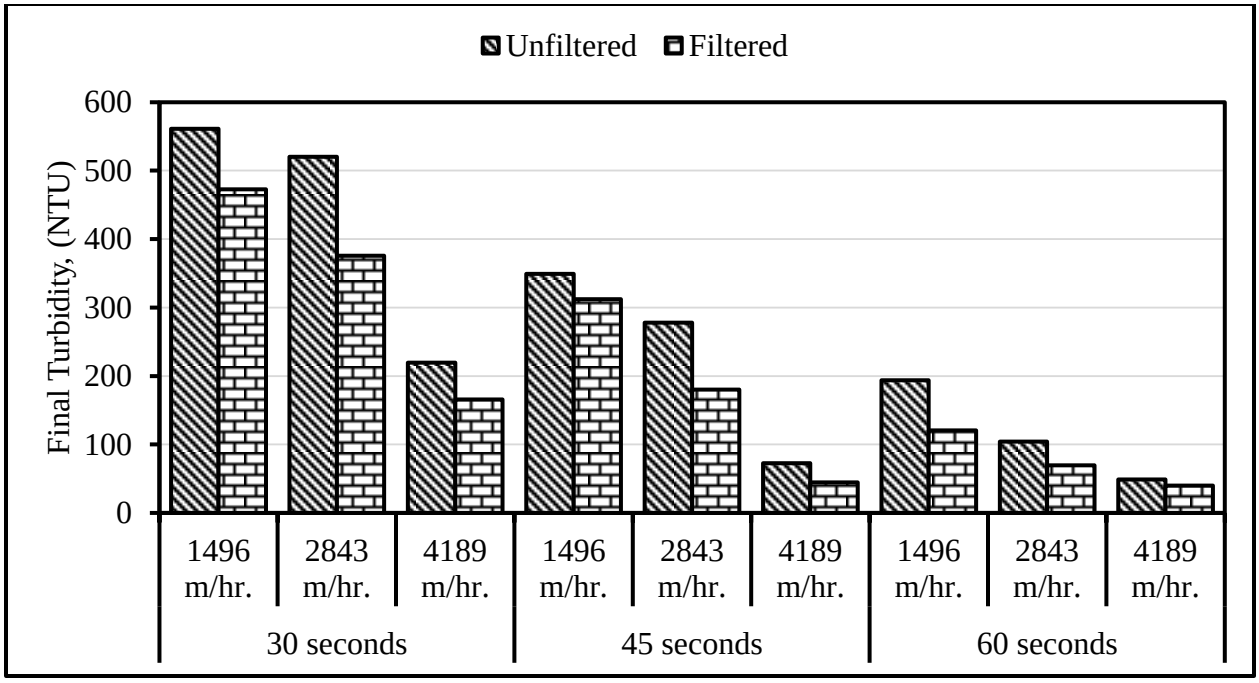

Figure 62 Final turbidity for PAM APS 703d at a concentration of 3333 mg/L

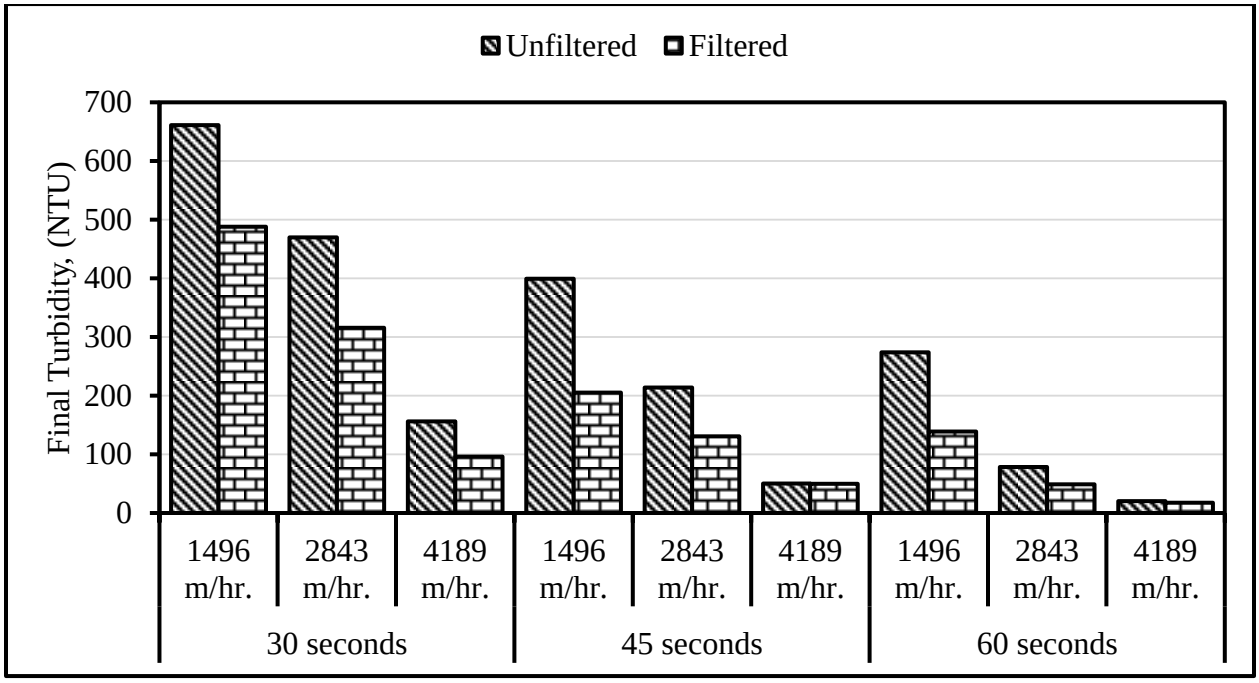

Figure 63 Final turbidity for PAM APS 703d at a concentration of 4167 mg/L

Table 31 Wilcoxon signed-rank test results for APS 705 417 mg/L concentration

Mixing time	Mixing speed	Unfiltered	Filtered	U - D	|U -D|	Rank of |U - D|	Signed Rank
30	125	357	237	119.33	119.33	9	9
	237.5	50	31	19.37	19.37	6	6
	350	38	28	9.57	9.57	4	4
45	125	259	190	69.00	69.00	8	8
	237.5	42	30	12.27	12.27	5	5
	350	18	14	4.03	4.03	2	2
60	125	78	38	40.47	40.47	7	7
	237.5	29	20	9.23	9.23	3	3
	350	8	7	1.54	1.54	1	1
W^+ =	0.0	σ_W =	16.88	W =	-45.0	z =	2.70
W^- =	45.0	α =	0.05	N =	9	zcrit =	1.64
μ_W =	0.00	W_{stat} =	0.0	p =	0.0038	Wcrit =	5.00
	Decision:			Reject Ho			

Table 32 Wilcoxon signed-rank test results for APS 705 833 mg/L concentration

Mixing time	Mixing speed	Unfiltered	Filtered	U - D	|U -D|	Rank of |U - D|	Signed Rank
30	125	135	71	64.03	64.03	9	9
	237.5	81	41	40.10	40.10	7	7
	350	8	23	-14.90	14.90	4	-4
45	125	91	45	45.17	45.17	8	8
	237.5	42	27	15.47	15.47	5	5
	350	25	18	7.17	7.17	2	2
60	125	35	22	12.33	12.33	3	3
	237.5	47	32	15.73	15.73	6	6
	350	17	14	3.20	3.20	1	1
W^+ =	41.0	σ_W =	16.88	W =	37.0	z =	2.22
W^- =	4.0	α =	0.05	N =	9	zcrit =	1.64
μ_W =	0.00	W_{stat} =	4.0	p =	0.0142	Wcrit =	5.00
	Decision:			Reject Ho			

Table 33 Wilcoxon signed-rank test results for APS 745 417 mg/L concentration

Mixing time	Mixing speed	Unfiltered	Filtered	U - D	|U -D|	Rank of |U - D|	Signed Rank
30	125	599	183	416.33	416.33	9	9
	237.5	139	97	41.80	41.80	7	7
	350	51	32	19.00	19.00	4	4
45	125	236	138	97.30	97.30	8	8
	237.5	118	78	39.87	39.87	6	6
	350	43	28	15.03	15.03	2	2
60	125	54	30	24.10	24.10	5	5
	237.5	65	47	18.33	18.33	3	3
	350	21	15	5.43	5.43	1	1
W^+ =	45.0	σ_W =	16.88	W =	45.0	z =	2.70
W^- =	0.0	α =	0.05	N =	9	zcrit =	1.64
μ_W =	0.00	W_{stat} =	0.0	p =	0.0038	Wcrit =	5.00
	Decision:			Reject Ho			

Table 34 Wilcoxon signed-rank test results for APS 745 833 mg/L concentration

Mixing time	Mixing speed	Unfiltered	Filtered	U - D	|U -D|	Rank of |U - D|	Signed Rank
30	125	377	377	0.00			
	237.5	200	109	90.60	90.60	7	7
	350	133	58	75.70	75.70	6	6
45	125	349	190	159.33	159.33	8	8
	237.5	116	62	53.97	53.97	4	4
	350	78	48	30.70	30.70	2	2
60	125	163	90	72.77	72.77	5	5
	237.5	108	64	44.00	44.00	3	3
	350	56	37	19.43	19.43	1	1
W^+ =	36.0	σ_W =	14.28	W =	36.0	z =	2.56
W^- =	0.0	α =	0.05	N =	8	zcrit =	1.64
μ_W =	0.00	W_{stat} =	0.0	p =	0.0059	Wcrit =	3.00
	Decision:			Reject Ho			

Table 35 Wilcoxon signed-rank test results for APS 706b 3333 mg/L concentration

Mixing time	Mixing speed	Unfiltered	Filtered	U - D	|U -D|	Rank of |U - D|	Signed Rank
30	125	275	106	168.60	168.60	9	9
	237.5	78	46	32.27	32.27	8	8
	350	21	18	3.10	3.10	4	4
45	125	44	25	18.59	18.59	7	7
	237.5	23	20	3.43	3.43	5	5
	350	11	12	-0.69	0.69	2	-2
60	125	43	27	16.40	16.40	6	6
	237.5	21	19	1.73	1.73	3	3
	350	9	9	-0.37	0.37	1	-1
W^+ =	42.0	σ_W =	16.88	W =	39.0	z =	2.34
W^- =	3.0	α =	0.05	N =	9	zcrit =	1.64
μ_W =	0.00	W_{stat} =	3.0	p =	0.0104	Wcrit =	5.00
	Decision:			Reject Ho			

Table 36 Wilcoxon signed-rank test results for APS 706b 4167 mg/L concentration

Mixing time	Mixing speed	Unfiltered	Filtered	U - F	|U -F|	Rank of |U - F|	Signed Rank
30	125	182	156	25.33	25.33	8	8
	237.5	134	104	29.20	29.20	9	9
	350	30	28	2.63	2.63	4	4
45	125	132	115	17.00	17.00	7	7
	237.5	45	36	9.23	9.23	6	6
	350	15	13	2.13	2.13	2	2
60	125	69	62	6.67	6.67	5	5
	237.5	28	26	2.40	2.40	3	3
	350	11	9	1.27	1.27	1	1
W^+ =	45.0	σ_W =	16.88	W =	45.0	z =	2.70
W^- =	0.0	α =	0.05	N =	9	zcrit =	1.64
μ_W =	0.00	W_{stat} =	0.0	p =	0.0038	Wcrit =	5.00
	Decision:			Reject Ho			

Table 37 Wilcoxon signed-rank test results for APS 703d 3333 mg/L concentration

Mixing time	Mixing speed	Unfiltered	Filtered	U - F	|U -F|	Rank of |U - F|	Signed Rank
30	125	561	473	88.33	88.33	7	7
	237.5	520	376	144.67	144.67	9	9
	350	219	166	53.67	53.67	5	5
45	125	349	312	36.67	36.67	4	4
	237.5	278	180	98.00	98.00	8	8
	350	73	45	28.03	28.03	2	2
60	125	194	121	73.00	73.00	6	6
	237.5	104	70	34.57	34.57	3	3
	350	49	40	8.73	8.73	1	1
W^+ =	45.0	σ_W =	16.88	W =	45.0	z =	2.70
W^- =	0.0	α =	0.05	N =	9	zcrit =	1.64
μ_W =	0.00	W_{stat} =	0.0	p =	0.0038	Wcrit =	5.00
	Decision:			Reject Ho			

Table 38 Wilcoxon signed-rank test results for APS 703d 4167 mg/L concentration

Mixing time	Mixing speed	Unfiltered	Filtered	U - F	|U -F|	Rank of |U - F|	Signed Rank
30	125	661	488	173.33	173.33	8	8
	237.5	470	316	154.00	154.00	7	7
	350	156	96	60.23	60.23	4	4
45	125	399	205	193.67	193.67	9	9
	237.5	214	130	83.53	83.53	5	5
	350	50	50	0.37	0.37	1	1
60	125	274	139	135.33	135.33	6	6
	237.5	79	49	29.83	29.83	3	3
	350	20	18	2.47	2.47	2	2
W^+ =	45.0	σ_W =	16.88	W =	45.0	z =	2.70
W^- =	0.0	α =	0.05	N =	9	zcrit =	1.64
μ_W =	0.00	W_{stat} =	0.0	p =	0.0038	Wcrit =	5.00
	Decision:			Reject Ho			

APPENDIX G
PAM DOSAGE DETERMINATION PROCEDURE

The following are procedural recommendations for testing PAM.

Materials/Apparatus

1. Five (5) grams site specific soil or 180 mL turbid site water
2. If site water is not available, approximately 237 mL de-ionized water
3. Two (2) clear/transparent beakers or glassware capable of holding at least 180 mL of water with the soil from the site)
4. Polymer sizes to be tested:
5. Blocks – 50, 100, 150, 200 and 250 mg
6. Powder – 25 and 50 mg
7. pH meter or litmus paper
8. Nephelometric Turbidity Meter (NTU meter)
9. Water Quality Test Strips or meter for testing Total Hardness
10. PO_4^{-3} test strips or meter to test for phosphate

Procedure

1. Water sample only
    1. Shake water sample to ensure water is uniformly mixed.
    2. Allow insoluble material to settle for 60 seconds before drawing samples.

ii. Carefully pour the muddy water into a second clear/transparent container taking care to not allow the sand and bulk of the heavier dirt to enter the second container.

iii. Pour approximately 60 mL of this muddy water into a clean transparent beaker or glassware to test the polymer block/log with.

iv. Turbidity measurement

v. Turbidimeter calibration – follow the manufacturer's operating instructions for the turbidimeter used.

vi. Measurement of turbidities above meter capacity – dilute sample with one or more volumes of de-ionized (DI) water until turbidity falls within the meter capacity. Compute turbidity of original sample from turbidity of diluted sample and the dilution factor used. For example, if five volumes of DI water were added to one volume of sample and the diluted sample showed a turbidity of 50 NTU, then the turbidity of the original sample is 300 NTU.

vii. Place the predetermined dosage of the PAM sample within beaker and then proceed to pour in 60 mL of the prepared sample water.

viii. Place the beaker with PAM and solution on stir plate at predetermined mixing speed and record the time in seconds that it takes to cause particulate formation.

ix. Filter the treated soil sample water through a predetermined filter media based on discharge requirements.

x. Take a final NTU reading of the filtered sample water by repeating step (1.2.vi) and record as NTU_f.

xi. If this test does not meet the water quality requirements for the specific site being tested, repeat the test process using a different polymer until the water quality requirements are met. Discharge should not violate the state of Florida's water quality standards (WQS); turbidity shall not be greater than 29 NTU above background.

2. Soil sample only

i. Take five (5) grams of the soil to be tested.

ii. Dry and mortar the five grams of soil to a fine dust and place into a transparent beaker or glassware capable of holding approximately 237 mL of de-ionized water or preferably water that is taken from the sampling site.

iii. Repeat steps 1.2.i to 1.2.x

iv. Repeat this entire process for each polymer block/log tested as required.

In order to obtain the proper polymer type, all variables need to be accounted for prior to requesting any polymers from manufacturers. High or low pH can greatly affect flocculation. Elevated calcium carbonate ($CaCO_3$) will affect polymer solubility. Cold temperatures may reduce reaction time and warm temperatures may increase reaction time. The subsequent steps are completed alongside turbidity removal to justify the polymer best suited for the site specific application.

1. Dip litmus paper or a pH probe into the site sampling water to test the pH of the water. Follow the procedure for testing pH in Standard Methods, 16th Edition, 1985. Record the value.

2. Dip a water quality test strip for total hardness into the site sample water for five (5) seconds to test for calcium carbonate ($CaCO_3$). Record the value.

Dip a water quality test strip for phosphate into the site sample water for five (5) seconds to test for the amount of phosphate in the water.

APPENDIX H
STATISTICAL ANALYSES TABLES FOR FIELD-SCALE TESTS

Table 39 Wilcoxon signed-rank test for ARS-1400 turbidity reduction at 25% slope

Slope % (Ratio)	Rainfall Intensity (mm/hr.)	Rainfall Events (#)	Volume-Weighted Mean Turbidity (NTU)					
			Upstream	Downstream	U - D	|U -D|	Rank of |U - D|	Signed Rank
25 (4:1)	25	1	12796	15179	-2383	2383	9	-9
		2	6695	5623	1072	1072	3	3
		3	4084	3410	674	674	1	1
		4	11689	9475	2214	2214	7	7
	76	1	14338	15886	-1548	1548	5	-5
		2	8008	5779	2229	2229	8	8
		3	10448	6749	3699	3699	11	11
		4	6537	4937	1599	1599	6	6
	127	1	11014	9905	1109	1109	4	4
		2	9696	6405	3291	3291	10	10
		3	10724	5486	5238	5238	12	12
		4	8814	7909	905	905	2	2
	σ_W =	25.50	W^+ =	64.0	W =	50.0	Decision:	
	α =	0.05	W^- =	14.0	N =	12	Reject H_o	
	μ_W =	0.00	W_{stat} =	14.0	z =	1.98		
	p =	0.0249	W_{crit} =	17.00	z_{crit} =	1.64		

Table 40 Wilcoxon signed-rank test for ARS-1400 sediment concentration removal at 25% slope

Slope % (Ratio)	Rainfall Intensity (mm/hr.)	Rainfall Events (#)	Volume-Weighted Mean Sediment Concentration (mg/L)					
			Upstream	Downstream	U - D	|U -D|	Rank of |U - D|	Signed Rank
25 (4:1)	25	1	8761	10215	-1454	1454	6	-6
		2	5703	4948	755	755	2	2
		3	3687	2901	786	786	3	3
		4	9511	7424	2088	2088	8	8
	76	1	10816	9590	1226	1226	4	4
		2	7848	4981	2867	2867	9	9
		3	10413	4359	6054	6054	11	11
		4	4937	4623	315	315	1	1
	127	1	10302	8564	1737	1737	7	7
		2	10398	5910	4488	4488	10	10
		3	11898	5362	6536	6536	12	12
		4	8195	6784	1412	1412	5	5
	σ_W =	25.50	W^+ =	72.0	W =	66.0	Decision:	
	α =	0.05	W^- =	6.0	N =	12	Reject H_o	
	μ_W =	0.00	W_{stat} =	14.0	z =	2.61		
	p =	0.0048	W_{crit} =	17.00	z_{crit} =	1.64		

Table 41 Wilcoxon signed-rank test for ARS-1400 turbidity reduction at 10% slope

Slope % (Ratio)	Rainfall Intensity (mm/hr.)	Rainfall Events (#)	Volume-Weighted Mean Turbidity (NTU)					
			Upstream	Downstream	U - D	|U -D|	Rank of |U - D|	Signed Rank
10 (10:1)	25	1	903	473	429	429	12	12
		2	790	615	175	175	11	11
		3	695	525	171	171	10	10
		4	750	810	-60	60	5	-5
	76	1	858	816	41	41	3	3
		2	705	566	139	139	9	9
		3	331	311	20	20	1	1
		4	1118	1223	-105	105	8	-8
	127	1	573	611	-38	38	2	-2
		2	558	505	53	53	4	4
		3	425	528	-103	103	7	-7
		4	615	534	81	81	6	6
	σ_W =	25.50	W^+ =	56.0	W =	34.0	Decision:	
	α =	0.05	W^- =	22.0	N =	12	Fail to Reject H_o	
	μ_W =	0.00	W_{stat} =	22.0	z =	1.35		
	p =	0.0912	W_{crit} =	17.00	z_{crit} =	1.64		

Table 42 Wilcoxon signed-rank test for ARS-1400 sediment concentration removal at 10% slope

Slope % (Ratio)	Rainfall Intensity (mm/hr.)	Rainfall Events (#)	Volume-Weighted Mean Sediment Concentration (mg/L)					
			Upstream	Downstream	U - D	|U -D|	Rank of |U - D|	Signed Rank
10 (10:1)	25	1	844	763	81	81	2	2
		2	990	735	255	255	9	9
		3	1107	670	436	436	12	12
		4	1319	970	349	349	10	10
	76	1	1065	863	202	202	7	7
		2	778	793	-15	15	1	-1
		3	659	546	113	113	3	3
		4	1147	791	356	356	11	11
	127	1	718	515	203	203	8	8
		2	776	599	176	176	6	6
		3	602	488	114	114	4	4
		4	820	705	115	115	5	5
	σ_W =	25.50	W^+ =	77.0	W =	76.0	Decision:	
	α =	0.05	W^- =	1.0	N =	12	Reject H_o	
	μ_W =	0.00	W_{stat} =	1.0	z =	3.00		
	p =	0.0014	W_{crit} =	17.00	z crit =	1.64		

Table 43 Wilcoxon signed-rank test for BSRF turbidity reduction at 25% slope

Slope % (Ratio)	Rainfall Intensity (mm/hr.)	Rainfall Events (#)	Volume-Weighted Mean Turbidity (NTU)					
			Upstream	Downstream	U - D	|U -D|	Rank of |U - D|	Signed Rank
25 (4:1)	25	1	1691	602	1089	1089	5	5
		2	2480	988	1492	1492	11	11
		3	1692	634	1058	1058	4	4
		4	2287	1154	1132	1132	6	6
	76	1	3510	1805	1705	1705	12	12
		2	1835	837	998	998	3	3
		3	1546	554	992	992	2	2
		4	1896	670	1227	1227	8	8
	127	1	3472	2186	1287	1287	9	9
		2	1835	655	1180	1180	7	7
		3	1060	232	828	828	1	1
		4	2009	621	1388	1388	10	10
	σ_W =	25.50	W^+ =	78.0	W =	78.0	Decision:	
	α =	0.05	W^- =	0.0	N =	12	Reject H_o	
	μ_W =	0.00	W_{stat} =	0.0	z =	3.08		
	p =	0.0011	W_{crit} =	17.00	z_{crit} =	1.64		

Table 44 Wilcoxon signed-rank test for BSRF sediment concentration removal at 25% slope

Slope % (Ratio)	Rainfall Intensity (mm/hr.)	Rainfall Events (#)	Volume-Weighted Mean Sediment Concentration (mg/L)					
			Upstream	Downstream	U - D	|U -D|	Rank of |U - D|	Signed Rank
25 (4:1)	25	1	2984	660	2325	2325	12	12
		2	2113	695	1418	1418	11	11
		3	1892	512	1380	1380	10	10
		4	1663	817	846	846	6	6
	76	1	2064	1166	899	899	8	8
		2	1448	642	806	806	5	5
		3	1131	467	665	665	2	2
		4	1226	502	723	723	3	3
	127	1	2228	1346	882	882	7	7
		2	1480	547	932	932	9	9
		3	593	147	446	446	1	1
		4	1201	475	727	727	4	4
	σ_W =	25.50	W^+ =	78.0	W =	78.0	Decision:	
	α =	0.05	W^- =	0.0	N =	12	Reject H_o	
	μ_W =	0.00	W_{stat} =	0.0	z =	3.08		
	p =	0.0011	W_{crit} =	17.00	z_{crit} =	1.64		

Table 45 Wilcoxon signed-rank test for BSRF turbidity reduction at 10% slope

Slope % (Ratio)	Rainfall Intensity (mm/hr.)	Rainfall Events (#)	Volume-Weighted Mean Turbidity (NTU)					
			Upstream	Downstream	U - D	|U -D|	Rank of |U - D|	Signed Rank
10 (10:1)	25	1	502	141	361	361	11	11
		2	407	112	295	295	10	10
		3	561	95	466	466	12	12
		4	200	92	108	108	5	5
	76	1	497	291	206	206	9	9
		2	257	131	125	125	6	6
		3	143	64	79	79	2	2
		4	198	71	127	127	7	7
	127	1	208	124	84	84	3	3
		2	231	127	104	104	4	4
		3	61	45	16	16	1	1
		4	241	93	148	148	8	8
	σ_W =	25.50	W^+ =	78.0	W =	78.0	Decision:	
	α =	0.05	W^- =	0.0	N =	12	Reject H_o	
	μ_W =	0.00	W_{stat} =	0.0	z =	3.08		
	p =	0.0011	W_{crit} =	17.00	z_{crit} =	1.64		

Table 46 Wilcoxon signed-rank test for BSRF sediment concentration removal at 10% slope

Slope % (Ratio)	Rainfall Intensity (mm/hr.)	Rainfall Events (#)	Volume-Weighted Mean Sediment Concentration (mg/L)					
			Upstream	Downstream	U - D	|U -D|	Rank of |U - D|	Signed Rank
10 (10:1)	25	1	2052	908	1144	1144	12	12
		2	884	337	547	547	10	10
		3	1298	219	1079	1079	11	11
		4	315	299	16	16	1	1
	76	1	820	375	445	445	9	9
		2	406	245	161	161	8	8
		3	326	183	143	143	7	7
		4	400	274	126	126	6	6
	127	1	387	278	109	109	5	5
		2	403	300	103	103	4	4
		3	286	251	35	35	2	2
		4	431	340	91	91	3	3
	σ_W =	25.50	W^+ =	78.0	W =	78.0	Decision:	
	α =	0.05	W^- =	0.0	N =	12	Reject H_o	
	μ_W =	0.00	W_{stat} =	0.0	z =	3.08		
	p =	0.0011	W_{crit} =	17.00	z crit =	1.64		

APPENDIX I
(I-E-S) SENSITIVITY ANALYSIS STATISTICAL RESULTS

Table 47 Two-way ANOVA on Ranks for BSRF turbidity reduction for 25 mm/hr.

Volume-Weighted Mean Turbidity (NTU)						
Rainfall Intensity	Rainfall Events (#)	Upstream	Downstream	Slope % (Ratio)	Rank U (1)	Rank D (2)
25 mm/hr.	1	1691	602	25% (4:1)	13	9
	2	2480	988		16	11
	3	1692	634		14	10
	4	2287	1154		15	12
	1	502	141	10% (10:1)	7	4
	2	407	112		6	3
	3	561	95		8	2
	4	200	92		5	1

Source of Variation	SS	df	MS	F	P-value	F crit
Sample	256	1	256	153.6	3.37E-08	4.7472
Columns	64	1	64	38.4	4.61E-05	4.7472
Interaction	0	1	0	0	1	4.7472
Within	20	12	1.667			
Total	340	15		α =	0.05	
Decision:	Reject Ho					
Decision:	Reject Ho					
Decision:	Fail to Reject Ho					

Table 48 Two-way ANOVA on Ranks for BSRF sediment concentration removal for 25 mm/hr.

Volume-Weighted Mean Sediment Concentration (mg/L)						
Rainfall Intensity	Rainfall Events (#)	Upstream	Downstream	Slope % (Ratio)	Rank U (1)	Rank D (2)
25 mm/hr.	1	2984	660	25% (4:1)	16	6
	2	2113	695		15	7
	3	1892	512		13	5
	4	1663	817		12	8
	1	2052	908	10% (10:1)	14	10
	2	884	337		9	4
	3	1298	219		11	1
	4	315	299		3	2

Source of Variation	SS	df	MS	F	P-value	F crit
Sample	49	1	49	4.5759	0.0537	4.7472
Columns	156.25	1	156.25	14.5914	0.0024	4.7472
Interaction	6.25	1	6.25	0.5837	0.4596	4.7472
Within	128.5	12	10.7083			
Total	340	15		α =	0.05	
Decision:	Fail to Reject Ho					
Decision:	Reject Ho					
Decision:	Fail to Reject Ho					

Table 49 Two-way ANOVA on Ranks for BSRF turbidity reduction for 76 mm/hr.

Volume-Weighted Mean Turbidity (NTU)						
Rainfall Intensity	Rainfall Events (#)	Upstream	Downstream	Slope % (Ratio)	Rank U (1)	Rank D (2)
76 mm/hr.	1	3510	1805	25% (4:1)	16	13
	2	1835	837		14	11
	3	1546	554		12	9
	4	1896	670		15	10
	1	497	291	10% (10:1)	8	7
	2	257	131		6	3
	3	143	64		4	1
	4	198	71		5	2

Source of Variation	SS	df	MS	F	P-value	F crit
Sample	256	1	256	65.3617	3.38E-06	4.7472
Columns	36	1	36	9.1915	0.0104	4.7472
Interaction	1	1	1	0.2553	0.6225	4.7472
Within	47	12	3.9167			
Total	340	15		α =	0.05	
Decision:	Reject Ho					
Decision:	Reject Ho					
Decision:	Fail to Reject Ho					

Table 50 Two-way ANOVA on Ranks for BSRF sediment concentration removal for 76 mm/hr.

Volume-Weighted Mean Sediment Concentration (mg/L)						
Rainfall Intensity	Rainfall Events (#)	Upstream	Downstream	Slope % (Ratio)	Rank U (1)	Rank D (2)
76 mm/hr.	1	2064	1166	25% (4:1)	16	13
	2	1448	642		15	10
	3	1131	467		12	8
	4	1226	502		14	9
	1	820	375	10% (10:1)	11	5
	2	406	245		7	2
	3	326	183		4	1
	4	400	274		6	3

Source of Variation	SS	df	MS	F	P-value	F crit
Sample	210.25	1	210.25	43.8783	2.45E-05	4.7472
Columns	72.25	1	72.25	15.0783	0.0022	4.7472
Interaction	0	1	0	0	1	4.7472
Within	57.5	12	4.7917			
Total	340	15		α =	0.05	
Decision:	Reject Ho					
Decision:	Reject Ho					
Decision:	Fail to Reject Ho					

Table 51 Two-way ANOVA on Ranks for BSRF turbidity reduction for 127 mm/hr.

Volume-Weighted Mean Turbidity (NTU)						
Rainfall Intensity	Rainfall Events (#)	Upstream	Downstream	Slope % (Ratio)	Rank U (1)	Rank D (2)
127 mm/hr.	1	3472	2186	25% (4:1)	16	15
	2	1835	655		13	11
	3	1060	232		12	8
	4	2009	621		14	10
	1	208	124	10% (10:1)	6	4
	2	231	127		7	5
	3	61	45		2	1
	4	241	93		9	3

Source of Variation	SS	df	MS	F	P-value	F crit
Sample	210.25	1	210.25	34.8	7.26E-05	4.7472
Columns	56.25	1	56.25	9.3103	0.0101	4.7472
Interaction	1	1	1	0.1655	0.6913	4.7472
Within	72.5	12	6.0417			
Total	340	15		α =	0.05	
Decision:	Reject Ho					
Decision:	Reject Ho					
Decision:	Fail to Reject Ho					

Table 52 Two-way ANOVA on Ranks for BSRF sediment concentration removal for 127 mm/hr.

Volume-Weighted Mean Sediment Concentration (mg/L)						
Rainfall Intensity	Rainfall Events (#)	Upstream	Downstream	Slope % (Ratio)	Rank U (1)	Rank D (2)
127 mm/hr.	1	2228	1346	25% (4:1)	16	14
	2	1480	547		15	11
	3	593	147		12	1
	4	1201	475		13	10
	1	387	278	10% (10:1)	7	3
	2	403	300		8	5
	3	286	251		4	2
	4	431	340		9	6

Source of Variation	SS	df	MS	F	P-value	F crit
Sample	156.25	1	156.25	17.4418	0.0013	4.7472
Columns	72.25	1	72.25	8.0651	0.0149	4.7472
Interaction	4	1	4	0.4465	0.5166	4.7472
Within	107.5	12	8.9583			
Total	340	15		α =	0.05	
Decision:	Reject Ho					
Decision:	Reject Ho					
Decision:	Fail to Reject Ho					

Table 53 Two-way ANOVA on Ranks for ARS-1400 turbidity reduction for 25 mm/hr.

Volume-Weighted Mean Turbidity (NTU)						
Rainfall Intensity	Rainfall Events (#)	Upstream	Downstream	Slope % (Ratio)	Rank U (1)	Rank D (2)
25 mm/hr.	1	12796	15179	25% (4:1)	15	16
	2	6695	5623		12	11
	3	4084	3410		10	9
	4	11689	9475		14	13
	1	903	473	10% (10:1)	8	1
	2	790	615		6	3
	3	695	525		4	2
	4	750	810		5	7

Source of Variation	SS	df	MS	F	P-value	F crit
Sample	256	1	256	43.2676	2.62E-05	4.7472
Columns	9	1	9	1.52113	0.241062	4.7472
Interaction	4	1	4	0.6761	0.426984	4.7472
Within	71	12	5.9167			
Total	340	15		α =	0.05	
Decision:	Reject Ho					
Decision:	Fail to Reject Ho					
Decision:	Fail to Reject Ho					

Table 54 Two-way ANOVA on Ranks for ARS-1400 sediment concentration removal for 25 mm/hr.

Volume-Weighted Mean Sediment Concentration (mg/L)						
Rainfall Intensity	Rainfall Events (#)	Upstream	Downstream	Slope % (Ratio)	Rank U (1)	Rank D (2)
25 mm/hr.	1	8761	10215	25% (4:1)	14	16
	2	5703	4948		12	11
	3	3687	2901		10	9
	4	9511	7424		15	13
	1	844	763	10% (10:1)	4	2
	2	990	777		6	3
	3	1107	670		7	1
	4	1319	971		8	5

Source of Variation	SS	df	MS	F	P-value	F crit
Sample	256	1	256	52.0678	1.06E-05	4.7472
Columns	16	1	16	3.2542	0.0964	4.7472
Interaction	9	1	9	1.8305	0.2010	4.7472
Within	59	12	4.9167			
Total	340	15		α =	0.05	
Decision:	Reject Ho					
Decision:	Fail to Reject Ho					
Decision:	Fail to Reject Ho					

Table 55 Two-way ANOVA on Ranks for ARS-1400 turbidity reduction for 76 mm/hr.

Volume-Weighted Mean Turbidity (NTU)						
Rainfall Intensity	Rainfall Events (#)	Upstream	Downstream	Slope % (Ratio)	Rank U (1)	Rank D (2)
76 mm/hr.	1	14338	15886	25% (4:1)	15	16
	2	8008	5779		13	10
	3	10448	6749		14	12
	4	6537	4937		11	9
	1	858	816	10% (10:1)	6	5
	2	705	566		4	3
	3	331	311		2	1
	4	1118	1223		7	8

Source of Variation	SS	df	MS	F	P-value	F crit
Sample	256	1	256	38.886	4.35E-05	4.7472
Columns	4	1	4	0.6076	0.4508	4.7472
Interaction	1	1	1	0.1519	0.7036	4.7472
Within	79	12	6.5833			
Total	340	15		α =	0.05	
Decision:	Reject Ho					
Decision:	Fail to Reject Ho					
Decision:	Fail to Reject Ho					

Table 56 Two-way ANOVA on Ranks for ARS-1400 sediment concentration removal for 76 mm/hr.

Volume-Weighted Mean Sediment Concentration (mg/L)						
Rainfall Intensity	Rainfall Events (#)	Upstream	Downstream	Slope % (Ratio)	Rank U (1)	Rank D (2)
76 mm/hr.	1	10816	9590	25% (4:1)	16	14
	2	7848	4981		13	12
	3	10413	4359		15	9
	4	4937	4623		11	10
	1	1065	863	10% (10:1)	7	6
	2	778	793		3	5
	3	659	546		2	1
	4	1147	791		8	4

Source of Variation	SS	df	MS	F	P-value	F crit
Sample	256	1	256	44.2014	2.37E-05	4.7472
Columns	12.25	1	12.25	2.1151	0.1715	4.7472
Interaction	2.25	1	2.25	0.3885	0.5448	4.7472
Within	69.5	12	5.7917			
Total	340	15		α =	0.05	

Decision:	Reject Ho
Decision:	Fail to Reject Ho
Decision:	Fail to Reject Ho

Table 57 Two-way ANOVA on Ranks for ARS-1400 turbidity reduction for 127 mm/hr.

Volume-Weighted Mean Turbidity (NTU)						
Rainfall Intensity	Rainfall Events (#)	Upstream	Downstream	Slope % (Ratio)	Rank U (1)	Rank D (2)
127 mm/hr.	1	11014	9905	25% (4:1)	16	14
	2	9696	6405		13	10
	3	10724	5486		15	9
	4	8814	7909		12	11
	1	573	611	10% (10:1)	6	7
	2	558	505		5	2
	3	425	528		1	3
	4	615	534		8	4

Source of Variation	SS	df	MS	F	P-value	F crit
Sample	256	1	256	46.9008	1.78E-05	4.7472
Columns	12.25	1	12.25	2.2443	0.1599	4.7472
Interaction	6.25	1	6.25	1.1450	0.3056	4.7472
Within	65.5	12	5.4583			
Total	340	15		α =	0.05	

Decision:	Reject Ho
Decision:	Fail to Reject Ho
Decision:	Fail to Reject Ho

Table 58 Two-way ANOVA on Ranks for ARS-1400 sediment concentration removal for 127 mm/hr.

Volume-Weighted Mean Sediment Concentration (mg/L)						
Rainfall Intensity	Rainfall Events (#)	Upstream	Downstream	Slope % (Ratio)	Rank U (1)	Rank D (2)
127 mm/hr.	1	10302	8564	25% (4:1)	14	13
	2	10398	5910		15	10
	3	11898	5362		16	9
	4	8195	6784		12	11
	1	718	515	10% (10:1)	6	2
	2	776	599		7	3
	3	602	488		4	1
	4	820	705		8	5

Source of Variation	SS	df	MS	F	P-value	F crit
Sample	256	1	256	87.7714	7.21E-07	4.7472
Columns	49	1	49	16.8	0.001476	4.7472
Interaction	0	1	0	0	1	4.7472
Within	35	12	2.9167			
Total	340	15		α =	0.05	
Decision:	Reject Ho					
Decision:	Reject Ho					
Decision:	Fail to Reject Ho					

APPENDIX J
(E-I-S) SENSITIVITY ANALYSIS STATISTICAL RESULTS

Table 59 Two-way ANOVA on Ranks for ARS-1400 turbidity reduction for rainfall event #1

Volume-Weighted Mean Turbidity (NTU)						
Rainfall Events	Slope % (Ratio)	Upstream	Downstream	Rainfall Intensity (mm/hr.)	Rank U (1)	Rank D (2)
#1	25 (4:1)	12796	15179	1	9	11
	10 (10:1)	903	473		6	1
	10 (10:1)	14338	15886	3	10	12
	25 (4:1)	858	816		5	4
	25 (4:1)	11014	9905	5	8	7
	10 (10:1)	573	611		2	3

Source of Variation	SS	df	MS	F	P-value	F crit
Sample	15.5	2	7.75	0.372	0.7042	5.1433
Columns	0.3333	1	0.3333	0.016	0.9035	5.9874
Interaction	2.1667	2	1.0833	0.052	0.949752	5.1433
Within	125	6	20.8333			
Total	143	11		α =	0.05	
Decision:	Fail to Reject Ho					
Decision:	Fail to Reject Ho					
Decision:	Fail to Reject Ho					

Table 60 Two-way ANOVA on Ranks for ARS-1400 sediment concentration removal for rainfall event #1

Volume-Weighted Mean Sediment Concentration (mg/L)						
Rainfall Events	Slope % (Ratio)	Upstream	Downstream	Rainfall Intensity (mm/hr.)	Rank U (1)	Rank D (2)
#1	25 (4:1)	8761	10215	1	8	10
	10 (10:1)	844	763		4	3
	10 (10:1)	10816	9590	3	12	9
	25 (4:1)	1065	863		6	5
	25 (4:1)	10302	8564	5	11	7
	10 (10:1)	718	515		2	1

Source of Variation	SS	df	MS	F	P-value	F crit
Sample	15.5	2	7.75	0.3974	0.6885	5.1433
Columns	5.3333	1	5.3333	0.2735	0.6197	5.9874
Interaction	5.1667	2	2.5833	0.1325	0.8784	5.1433
Within	117	6	19.5			
Total	143	11		α =	0.05	
Decision:	Fail to Reject Ho					
Decision:	Fail to Reject Ho					
Decision:	Fail to Reject Ho					

Table 61 Two-way ANOVA on Ranks for ARS-1400 turbidity reduction for rainfall event #2

Volume-Weighted Mean Turbidity (NTU)						
Rainfall Events	Slope % (Ratio)	Upstream	Downstream	Rainfall Intensity (mm/hr.)	Rank U (1)	Rank D (2)
#2	25 (4:1)	6695	5623	1	10	7
	10 (10:1)	790	613		6	4
	10 (10:1)	8008	5779	3	11	8
	25 (4:1)	705	583		5	3
	25 (4:1)	9696	6386	5	12	9
	10 (10:1)	558	505		2	1

Source of Variation	SS	df	MS	F	P-value	F crit
Sample	1.5	2	0.75	0.036	0.9648	5.1433
Columns	16.333	1	16.333	0.784	0.4099	5.9874
Interaction	0.1667	2	0.083	0.004	0.9960	5.1433
Within	125	6	20.833			
Total	143	11		α =	0.05	
Decision:	Fail to Reject Ho					
Decision:	Fail to Reject Ho					
Decision:	Fail to Reject Ho					

Table 62 Two-way ANOVA on Ranks for ARS-1400 sediment concentration removal for rainfall event #2

Volume-Weighted Mean Sediment Concentration (mg/L)						
Rainfall Events	Slope % (Ratio)	Upstream	Downstream	Rainfall Intensity (mm/hr.)	Rank U (1)	Rank D (2)
#2	25 (4:1)	5703	4948	1	9	7
	10 (10:1)	990	777		6	3
	10 (10:1)	7848	4981	3	11	8
	25 (4:1)	778	812		4	5
	25 (4:1)	10398	5719	5	12	10
	10 (10:1)	776	599		2	1

Source of Variation	SS	df	MS	F	P-value	F crit
Sample	1.5	2	0.75	0.0341	0.9667	5.1433
Columns	8.333	1	8.333	0.3789	0.5609	5.9874
Interaction	1.1667	2	0.583	0.0265	0.9740	5.1433
Within	132	6	22			
Total	143	11		α =	0.05	
Decision:	Fail to Reject Ho					
Decision:	Fail to Reject Ho					
Decision:	Fail to Reject Ho					

Table 63 Two-way ANOVA on Ranks for ARS-1400 turbidity reduction for rainfall event #3

Volume-Weighted Mean Turbidity (NTU)						
Rainfall Events	Slope % (Ratio)	Upstream	Downstream	Rainfall Intensity (mm/hr.)	Rank U (1)	Rank D (2)
#3	25 (4:1)	4084	3410	1	8	7
	10 (10:1)	695	525		6	4
	10 (10:1)	10448	6749	3	11	10
	25 (4:1)	331	311		2	1
	25 (4:1)	10724	5047	5	12	9
	10 (10:1)	425	528		3	5

Source of Variation	SS	df	MS	F	P-value	F crit
Sample	3.5	2	1.75	0.0772	0.9266	5.1433
Columns	3	1	3	0.1324	0.7285	5.9874
Interaction	0.5	2	0.25	0.0110	0.9891	5.1433
Within	136	6	22.667			
Total	143	11		α =	0.05	
Decision:	Fail to Reject Ho					
Decision:	Fail to Reject Ho					
Decision:	Fail to Reject Ho					

Table 64 Two-way ANOVA on Ranks for ARS-1400 sediment concentration removal for rainfall event #3

Volume-Weighted Mean Sediment Concentration (mg/L)						
Rainfall Events	Slope % (Ratio)	Upstream	Downstream	Rainfall Intensity (mm/hr.)	Rank U (1)	Rank D (2)
#3	25 (4:1)	3687	2901	1	8	7
	10 (10:1)	1107	670		6	5
	10 (10:1)	10413	4359	3	11	9
	25 (4:1)	659	546		4	2
	25 (4:1)	11898	5000	5	12	10
	10 (10:1)	602	488		3	1

Source of Variation	SS	df	MS	F	P-value	F crit
Sample	0	2	0	0	1	5.1433
Columns	8.333	1	8.333	0.3731	0.5637	5.9874
Interaction	0.667	2	0.3333	0.0149	0.9852	5.1433
Within	134	6	22.333			
Total	143	11		α =	0.05	
Decision:	Fail to Reject Ho					
Decision:	Fail to Reject Ho					
Decision:	Fail to Reject Ho					

Table 65 Two-way ANOVA on Ranks for ARS-1400 turbidity reduction for rainfall event #4

Volume-Weighted Mean Turbidity (NTU)						
Rainfall Events	Slope % (Ratio)	Upstream	Downstream	Rainfall Intensity (mm/hr.)	Rank U (1)	Rank D (2)
#4	25 (4:1)	11689	9475	1	12	11
	10 (10:1)	750	811		3	4
	10 (10:1)	6537	4937	3	8	7
	25 (4:1)	1118	1223		5	6
	25 (4:1)	8814	7909	5	10	9
	10 (10:1)	615	560		2	1

Source of Variation	SS	df	MS	F	P-value	F crit
Sample	8	2	4	0.1791	0.8403	5.1433
Columns	0.333	1	0.333	0.0149	0.9068	5.9874
Interaction	0.667	2	0.3333	0.0149	0.9852	5.1433
Within	134	6	22.333			
Total	143	11		α =	0.05	
Decision:	Fail to Reject Ho					
Decision:	Fail to Reject Ho					
Decision:	Fail to Reject Ho					

Table 66 Two-way ANOVA on Ranks for ARS-1400 sediment concentration removal for rainfall event #4

Volume-Weighted Mean Sediment Concentration (mg/L)						
Rainfall Events	Slope % (Ratio)	Upstream	Downstream	Rainfall Intensity (mm/hr.)	Rank U (1)	Rank D (2)
#4	25 (4:1)	9511	7424	1	12	10
	10 (10:1)	1319	971		6	4
	10 (10:1)	4937	4623	3	8	7
	25 (4:1)	1147	791		5	2
	25 (4:1)	8195	6784	5	11	9
	10 (10:1)	820	692		3	1

Source of Variation	SS	df	MS	F	P-value	F crit
Sample	14	2	7	0.3590	0.7124	5.1433
Columns	12	1	12	0.6154	0.4626	5.9874
Interaction	0	2	0	0	1	5.1433
Within	117	6	19.5			
Total	143	11		α =	0.05	
Decision:	Fail to Reject Ho					
Decision:	Fail to Reject Ho					
Decision:	Fail to Reject Ho					

Table 67 Two-way ANOVA on Ranks for BSRF turbidity reduction for rainfall event #1

Volume-Weighted Mean Turbidity (NTU)						
Rainfall Events	Slope % (Ratio)	Upstream	Downstream	Rainfall Intensity (mm/hr.)	Rank U (1)	Rank D (2)
#1	25 (4:1)	1691	602	1	9	7
	10 (10:1)	502	141		6	2
	10 (10:1)	3510	1805	3	12	10
	25 (4:1)	497	291		5	4
	25 (4:1)	3472	1576	5	11	8
	10 (10:1)	208	124		3	1

Source of Variation	SS	df	MS	F	P-value	F crit
Sample	9.5	2	4.75	0.2457	0.7897	5.1433
Columns	16.333	1	16.333	0.8448	0.3935	5.9874
Interaction	1.1667	2	0.583	0.0302	0.9704	5.1433
Within	116	6	19.333			
Total	143	11		α =	0.05	
Decision:	Fail to Reject Ho					
Decision:	Fail to Reject Ho					
Decision:	Fail to Reject Ho					

Table 68 Two-way ANOVA on Ranks for BSRF sediment concentration removal for rainfall event #1

Volume-Weighted Mean Sediment Concentration (mg/L)						
Rainfall Events	Slope % (Ratio)	Upstream	Downstream	Rainfall Intensity (mm/hr.)	Rank U (1)	Rank D (2)
#1	25 (4:1)	2984	660	1	12	4
	10 (10:1)	2052	964		9	6
	10 (10:1)	2064	1166	3	10	8
	25 (4:1)	820	375		5	2
	25 (4:1)	2228	983	5	11	7
	10 (10:1)	387	278		3	1

Source of Variation	SS	df	MS	F	P-value	F crit
Sample	10.5	2	5.25	0.3621	0.7105	5.1433
Columns	40.333	1	40.333	2.7816	0.1464	5.9874
Interaction	5.1667	2	2.583	0.1782	0.8411	5.1433
Within	87	6	14.5			
Total	143	11		α =	0.05	
Decision:	Fail to Reject Ho					
Decision:	Fail to Reject Ho					
Decision:	Fail to Reject Ho					

Table 69 Two-way ANOVA on Ranks for BSRF turbidity reduction for rainfall event #2

Volume-Weighted Mean Turbidity (NTU)						
Rainfall Events	Slope % (Ratio)	Upstream	Downstream	Rainfall Intensity (mm/hr.)	Rank U (1)	Rank D (2)
#2	25 (4:1)	2480	988	1	12	9
	10 (10:1)	407	112		6	1
	10 (10:1)	1835	837	3	11	8
	25 (4:1)	257	131		5	3
	25 (4:1)	1835	655	5	10	7
	10 (10:1)	231	127		4	2

Source of Variation	SS	df	MS	F	P-value	F crit
Sample	3.5	2	1.75	0.0946	0.9111	5.1433
Columns	27	1	27	1.4595	0.2725	5.9874
Interaction	1.5	2	0.75	0.0405	0.9605	5.1433
Within	111	6	18.5			
Total	143	11		α =	0.05	
Decision:	Fail to Reject Ho					
Decision:	Fail to Reject Ho					
Decision:	Fail to Reject Ho					

Table 70 Two-way ANOVA on Ranks for BSRF sediment concentration removal for rainfall event #2

Volume-Weighted Mean Sediment Concentration (mg/L)						
Rainfall Events	Slope % (Ratio)	Upstream	Downstream	Rainfall Intensity (mm/hr.)	Rank U (1)	Rank D (2)
#2	25 (4:1)	2113	695	1	12	8
	10 (10:1)	884	337		9	3
	10 (10:1)	1448	642	3	10	7
	25 (4:1)	406	245		5	1
	25 (4:1)	1480	547	5	11	6
	10 (10:1)	403	300		4	2

Source of Variation	SS	df	MS	F	P-value	F crit
Sample	13.5	2	6.75	0.5063	0.6264	5.1433
Columns	48	1	48	3.6	0.1066	5.9874
Interaction	1.5	2	0.75	0.0563	0.9458	5.1433
Within	80	6	13.33			
Total	143	11		α =	0.05	
Decision:	Fail to Reject Ho					
Decision:	Fail to Reject Ho					
Decision:	Fail to Reject Ho					

Table 71 Two-way ANOVA on Ranks for BSRF turbidity reduction for rainfall event #3

Volume-Weighted Mean Turbidity (NTU)						
Rainfall Events	Slope % (Ratio)	Upstream	Downstream	Rainfall Intensity (mm/hr.)	Rank U (1)	Rank D (2)
#3	25 (4:1)	1692	634	1	12	9
	10 (10:1)	561	96		8	4
	10 (10:1)	1546	554	3	11	7
	25 (4:1)	143	64		5	3
	25 (4:1)	1060	194	5	10	6
	10 (10:1)	61	45		2	1

Source of Variation	SS	df	MS	F	P-value	F crit
Sample	24.5	2	12.25	0.8077	0.4891	5.1433
Columns	27	1	27	1.7802	0.2305	5.9874
Interaction	0.5	2	0.25	0.0165	0.9837	5.1433
Within	91	6	15.167			
Total	143	11		α =	0.05	
Decision:	Fail to Reject Ho					
Decision:	Fail to Reject Ho					
Decision:	Fail to Reject Ho					

Table 72 Two-way ANOVA on Ranks for BSRF sediment concentration removal for rainfall event #3

Volume-Weighted Mean Sediment Concentration (mg/L)						
Rainfall Events	Slope % (Ratio)	Upstream	Downstream	Rainfall Intensity (mm/hr.)	Rank U (1)	Rank D (2)
#3	25 (4:1)	1892	512	1	12	8
	10 (10:1)	1298	214		11	2
	10 (10:1)	1131	467	3	10	7
	25 (4:1)	326	183		6	1
	25 (4:1)	593	259	5	9	4
	10 (10:1)	286	251		5	3

Source of Variation	SS	df	MS	F	P-value	F crit
Sample	19.5	2	9.75	1.1038	0.3907	5.1433
Columns	65.333	1	65.33	7.3962	0.0347	5.9874
Interaction	5.167	2	2.583	0.2925	0.7565	5.1433
Within	53	6	8.833			
Total	143	11		α =	0.05	
Decision:	Fail to Reject Ho					
Decision:	Fail to Reject Ho					
Decision:	Fail to Reject Ho					

Table 73 Two-way ANOVA on Ranks for BSRF turbidity reduction for rainfall event #4

Volume-Weighted Mean Turbidity (NTU)						
Rainfall Events	Slope % (Ratio)	Upstream	Downstream	Rainfall Intensity (mm/hr.)	Rank U (1)	Rank D (2)
#4	25 (4:1)	2287	1154	1	12	9
	10 (10:1)	200	92		5	2
	10 (10:1)	1896	670	3	10	8
	25 (4:1)	198	71		4	1
	25 (4:1)	2009	621	5	11	7
	10 (10:1)	241	93		6	3

Source of Variation	SS	df	MS	F	P-value	F crit
Sample	3.5	2	1.75	0.0938	0.9118	5.1433
Columns	27	1	27	1.446	0.2744	5.9874
Interaction	0.5	2	0.25	0.0134	0.9867	5.1433
Within	112	6	18.667			
Total	143	11		α =	0.05	
Decision:	Fail to Reject Ho					
Decision:	Fail to Reject Ho					
Decision:	Fail to Reject Ho					

Table 74 Two-way ANOVA on Ranks for BSRF sediment concentration removal for rainfall event #4

Volume-Weighted Mean Sediment Concentration (mg/L)						
Rainfall Events	Slope % (Ratio)	Upstream	Downstream	Rainfall Intensity (mm/hr.)	Rank U (1)	Rank D (2)
#4	25 (4:1)	1663	817	1	12	9
	10 (10:1)	315	299		3	2
	10 (10:1)	1226	502	3	11	8
	25 (4:1)	400	274		5	1
	25 (4:1)	1201	475	5	10	7
	10 (10:1)	431	340		6	4

Source of Variation	SS	df	MS	F	P-value	F crit
Sample	0.5	2	0.25	0.0125	0.9876	5.1433
Columns	21.333	1	21.333	1.0667	0.3415	5.9874
Interaction	1.167	2	0.583	0.0292	0.9714	5.1433
Within	120	6	20			
Total	143	11		α =	0.05	
Decision:	Fail to Reject Ho					
Decision:	Fail to Reject Ho					
Decision:	Fail to Reject Ho					

APPENDIX K
(S-E-I) SENSITIVITY ANALYSIS STATISTICAL RESULTS

Table 75 Two-way ANOVA on Ranks for ARS-1400 turbidity reduction for 10% slope

Volume-Weighted Mean Turbidity (NTU)						
Slope % (Ratio)	Rainfall Intensity (mm/hr.)	Upstream	Downstream	Rainfall Events	Rank U (1)	Rank D (2)
10% (10:1)	25	903	473	#1	22	4
	76	858	816		21	20
	127	573	611		10	12
	25	790	613	#2	18	13
	76	705	583		16	11
	127	558	505		8	5
	25	695	525	#3	15	6
	76	331	311		2	1
	127	425	528		3	7
	25	750	811	#4	17	19
	76	1118	1223		23	24
	127	615	560		14	9

Source of Variation	SS	df	MS	F	P-value	F crit
Sample	475.6667	3	158.5556	4.2901	0.0211	3.2389
Columns	60.16667	1	60.1667	1.6280	0.2202	4.4940
Interaction	22.83333	3	7.6111	0.2059	0.8908	3.2389
Within	591.3333	16	36.9583			
Total	1150	23		α =	0.05	
Decision:	Reject Ho					
Decision:	Fail to Reject Ho					
Decision:	Fail to Reject Ho					

Table 76 Two-way ANOVA on Ranks for ARS-1400 sediment concentration removal for 10% slope

Volume-Weighted Mean Sediment Concentration (mg/L)						
Slope % (Ratio)	Rainfall Intensity (mm/hr.)	Upstream	Downstream	Rainfall Events	Rank U (1)	Rank D (2)
10% (10:1)	25	844	763	#1	17	10
	76	1065	863		21	18
	127	718	515		9	2
	25	990	777	#2	20	12
	76	778	812		13	15
	127	776	599		11	4
	25	1107	670	#3	22	7
	76	659	546		6	3
	127	602	488		5	1
	25	1319	971	#4	24	19
	76	1147	791		23	14
	127	820	692		16	8

Source of Variation	SS	df	MS	F	P-value	F crit
Sample	301	3	100.333	2.6260	0.0860	3.2389
Columns	228.1667	1	228.1667	5.9716	0.0265	4.4940
Interaction	9.5	3	3.16667	0.0829	0.9684	3.2389
Within	611.3333	16	38.2083			
Total	1150	23		α =	0.05	
Decision:	Fail to Reject Ho					
Decision:	Reject Ho					
Decision:	Fail to Reject Ho					

Table 77 Two-way ANOVA on Ranks for ARS-1400 turbidity reduction for 25% slope

Volume-Weighted Mean Turbidity (NTU)						
Slope % (Ratio)	Rainfall Intensity (mm/hr.)	Upstream	Downstream	Rainfall Events	Rank U (1)	Rank D (2)
25% (10:1)	25	12796	15179	#1	21	23
	76	14338	15886		22	24
	127	11014	9905		19	16
	25	6695	5623	#2	9	5
	76	8008	5779		12	6
	127	9696	6386		15	7
	25	4084	3410	#3	2	1
	76	10448	6749		17	10
	127	10724	5047		18	4
	25	11689	9475	#4	20	14
	76	6537	4937		8	3
	127	8814	7909		13	11

Source of Variation	SS	df	MS	F	P-value	F crit
Sample	584.3333	3	194.778	7.7395	0.0020	3.2389
Columns	112.6667	1	112.667	4.4768	0.0504	4.4940
Interaction	50.33333	3	16.778	0.6667	0.5847	3.2389
Within	402.6667	16	25.167			
Total	1150	23		α =	0.05	
Decision:	Reject Ho					
Decision:	Fail to Reject Ho					
Decision:	Fail to Reject Ho					

Table 78 Two-way ANOVA on Ranks for ARS-1400 sediment concentration removal for 25% slope

Volume-Weighted Mean Sediment Concentration (mg/L)						
Slope % (Ratio)	Rainfall Intensity (mm/hr.)	Upstream	Downstream	Rainfall Events	Rank U (1)	Rank D (2)
25% (10:1)	25	8761	10215	#1	16	19
	76	10816	9590		23	18
	127	10302	8564		20	15
	25	5703	4948	#2	9	6
	76	7848	4981		13	7
	127	10398	5719		21	10
	25	3687	2901	#3	2	1
	76	10413	4359		22	3
	127	11898	5000		24	8
	25	9511	7424	#4	17	12
	76	4937	4623		5	4
	127	8195	6784		14	11

Source of Variation	SS	df	MS	F	P-value	F crit
Sample	291	3	97	2.7981	0.0736	3.2389
Columns	216	1	216	6.2308	0.0239	4.4940
Interaction	88.33333	3	29.44	0.8494	0.4871	3.2389
Within	554.6667	16	34.67			
Total	1150	23		α =	0.05	
Decision:	Fail to Reject Ho					
Decision:	Reject Ho					
Decision:	Fail to Reject Ho					

Table 79 Two-way ANOVA on Ranks for BSRF turbidity reduction for 10% slope

Volume-Weighted Mean Turbidity (NTU)						
Slope % (Ratio)	Rainfall Intensity (mm/hr.)	Upstream	Downstream	Rainfall Events	Rank U (1)	Rank D (2)
10% (10:1)	25	502	141	#1	23	12
	76	497	291		22	20
	127	208	124		16	9
	25	407	112	#2	21	8
	76	257	131		19	11
	127	231	127		17	10
	25	561	96	#3	24	7
	76	143	64		13	3
	127	61	45		2	1
	25	200	92	#4	15	5
	76	198	71		14	4
	127	241	93		18	6

Source of Variation	SS	df	MS	F	P-value	F crit
Sample	274	3	91.333	3.8728	0.0295	3.2389
Columns	486	1	486	20.6078	0.0003	4.4940
Interaction	12.667	3	4.2222	0.1790	0.9091	3.2389
Within	377.33	16	23.583			
Total	1150	23		α =	0.05	
Decision:	Reject Ho					
Decision:	Reject Ho					
Decision:	Fail to Reject Ho					

Table 80 Two-way ANOVA on Ranks for BSRF sediment concentration removal for 10% slope

Volume-Weighted Mean Sediment Concentration (mg/L)						
Slope % (Ratio)	Rainfall Intensity (mm/hr.)	Upstream	Downstream	Rainfall Events	Rank U (1)	Rank D (2)
10% (10:1)	25	2052	964	#1	24	22
	76	820	375		20	14
	127	387	278		15	6
	25	884	337	#2	21	12
	76	406	245		18	3
	127	403	300		17	9
	25	1298	214	#3	23	2
	76	326	183		11	1
	127	286	251		7	4
	25	315	299	#4	10	8
	76	400	274		16	5
	127	431	340		19	13

Source of Variation	SS	df	MS	F	P-value	F crit
Sample	241	3	80.333	2.9390	0.0649	3.2389
Columns	433.5	1	433.5	15.8598	0.0011	4.4940
Interaction	38.1667	3	12.722	0.4654	0.7104	3.2389
Within	437.33	16	27.333			
Total	1150	23		α =	0.05	
Decision:	Fail to Reject Ho					
Decision:	Reject Ho					
Decision:	Fail to Reject Ho					

Table 81 Two-way ANOVA on Ranks for BSRF turbidity reduction for 25% slope

Volume-Weighted Mean Turbidity (NTU)						
Slope % (Ratio)	Rainfall Intensity (mm/hr.)	Upstream	Downstream	Rainfall Events	Rank U (1)	Rank D (2)
25% (10:1)	25	1691	602	#1	14	3
	76	3510	1805		24	16
	127	3472	1576		23	13
	25	2480	988	#2	22	9
	76	1835	837		18	8
	127	1835	655		17	6
	25	1692	634	#3	15	5
	76	1546	554		12	2
	127	1060	194		10	1
	25	2287	1154	#4	21	11
	76	1896	670		19	7
	127	2009	621		20	4

Source of Variation	SS	df	MS	F	P-value	F crit
Sample	216.3333	3	72.111	5.244	0.0103	3.2389
Columns	704.1667	1	704.167	51.21	2.28E-06	4.4940
Interaction	9.5	3	3.167	0.230	0.8739	3.2389
Within	220	16	13.75			
Total	1150	23		α =	0.05	
Decision:	Reject Ho					
Decision:	Reject Ho					
Decision:	Fail to Reject Ho					

Table 82 Two-way ANOVA on Ranks for BSRF sediment concentration removal for 25% slope

Volume-Weighted Mean Sediment Concentration (mg/L)						
Slope % (Ratio)	Rainfall Intensity (mm/hr.)	Upstream	Downstream	Rainfall Events	Rank U (1)	Rank D (2)
25% (10:1)	25	2984	660	#1	24	9
	76	2064	1166		21	14
	127	2228	983		23	12
	25	2113	695	#2	22	10
	76	1448	642		17	8
	127	1480	547		18	6
	25	1892	512	#3	20	5
	76	1131	467		13	2
	127	593	259		7	1
	25	1663	817	#4	19	11
	76	1226	502		16	4
	127	1201	475		15	3

Source of Variation	SS	df	MS	F	P-value	F crit
Sample	266.33	3	88.778	7.9207	0.0018	3.2389
Columns	704.167	1	704.167	62.8253	6.25E-07	4.4940
Interaction	0.167	3	0.0556	0.0050	0.9995	3.2389
Within	179.33	16	11.2083			
Total	1150	23		α =	0.05	
Decision:	Reject Ho					
Decision:	Reject Ho					
Decision:	Fail to Reject Ho					

APPENDIX L
FLOW-THROUGH-RATE STATISTICAL ANALYSES

Table 83 Two-way ANOVA on ARS-1400 flow-through-rate at 25 percent slope

	Rainfall Intensity		
Rainfall Events (#)	1 in./hr.	3 in./hr.	5 in./hr.
1	10	7	17
2	14	3	13
3	15	6	13
4	9	6	16

Source of Variation	SS	df	MS	F	P-value	F crit
Rows	4.06	3	1.35	0.1984	0.8938	4.7571
Columns	176.32	2	88.16	12.9347	0.0067	5.1433
Error	40.89	6	6.82			
Total	221.27	11				
Decision:	Fail to Reject Ho					
Decision:	Reject Ho					

Table 84 Two-way ANOVA on ARS-1400 flow-through-rate at 10 percent slope

	Rainfall Intensity		
Rainfall Events (#)	1 in./hr.	3 in./hr.	5 in./hr.
1	15	64	100
2	12	69	88
3	19	47	65
4	13	57	80

Source of Variation	SS	df	MS	F	P-value	F crit
Rows	465.93	3	155.31	1.8646	0.2364	4.7571
Columns	9733.42	2	4866.71	58.4283	0.0001	5.1433
Error	499.76	6	83.29			
Total	10699.11	11				
Decision:	Fail to Reject Ho					
Decision:	Reject Ho					

Table 85 Two-way ANOVA on BSRF flow-through-rate at 25 percent slope

	Rainfall Intensity		
Rainfall Events (#)	1 in./hr.	3 in./hr.	5 in./hr.
1	59	58	54
2	102	35	31
3	59	45	30
4	57	14	23

Source of Variation	SS	df	MS	F	P-value	F crit
Rows	1280.01	3	426.67	1.4885	0.3098	4.7571
Columns	2910.64	2	1455.32	5.0769	0.0512	5.1433
Error	1719.92	6	286.65			
Total	5910.56	11				
Decision:	Fail to Reject Ho					
Decision:	Fail to Reject Ho					

Table 86 Two-way ANOVA on BSRF flow-through-rate at 10 percent slope

	Rainfall Intensity		
Rainfall Events (#)	1 in./hr.	3 in./hr.	5 in./hr.
1	51		149
2	122		121
3	264		145
4	21	52	102

Source of Variation	SS	df	MS	F	P-value	F crit
Rows	21900.34	3	7300.11	1.4940	0.3747	9.2766
Columns	439.22	1	439.22	0.0899	0.7839	10.1280
Error	14659.36	3	4886.45			
Total	36998.916	7				
Decision:	Fail to Reject Ho					
Decision:	Fail to Reject Ho					

APPENDIX M
SHARP MODEL COMPUTER PROGRAM USER INTERFACE

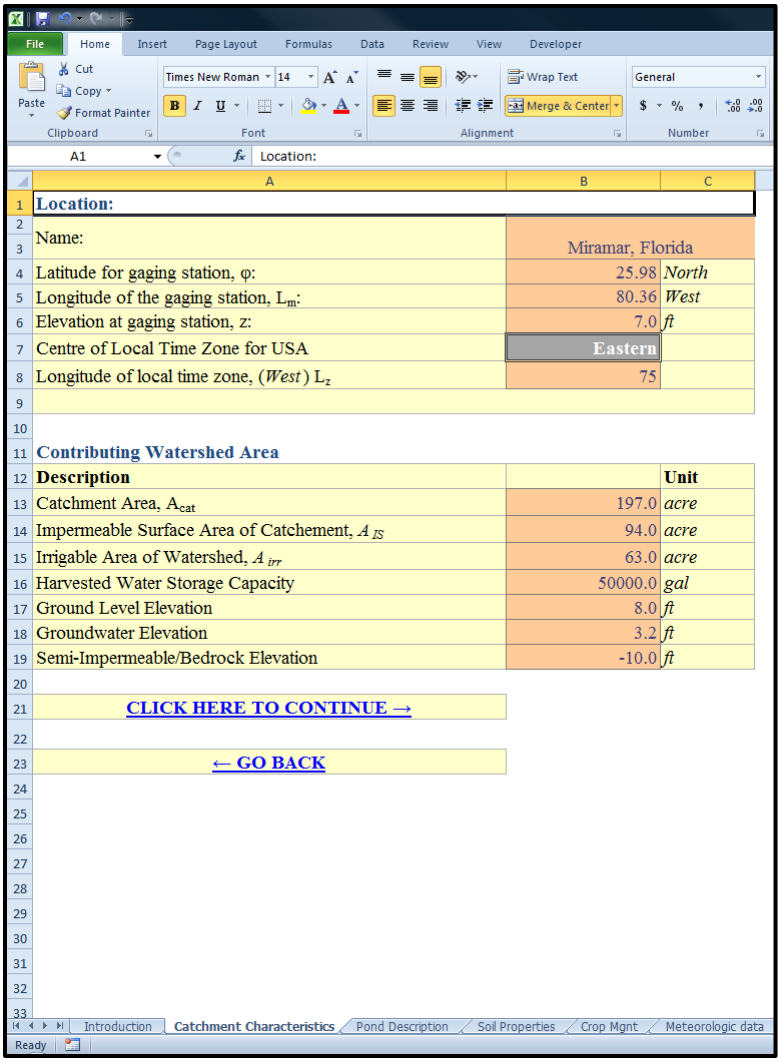

	A	B	C
1	**Location:**		
2			
3	Name:	Miramar, Florida	
4	Latitude for gaging station, φ:	25.98	*North*
5	Longitude of the gaging station, L_m:	80.36	*West*
6	Elevation at gaging station, z:	7.0	*ft*
7	Centre of Local Time Zone for USA	Eastern	
8	Longitude of local time zone, (*West*) L_z	75	
9			
10			
11	**Contributing Watershed Area**		
12	**Description**		**Unit**
13	Catchment Area, A_{cat}	197.0	*acre*
14	Impermeable Surface Area of Catchement, A_{IS}	94.0	*acre*
15	Irrigable Area of Watershed, A_{irr}	63.0	*acre*
16	Harvested Water Storage Capacity	50000.0	*gal*
17	Ground Level Elevation	8.0	*ft*
18	Groundwater Elevation	3.2	*ft*
19	Semi-Impermeable/Bedrock Elevation	-10.0	*ft*
20			
21	CLICK HERE TO CONTINUE →		
22			
23	← GO BACK		

Figure 64 Pond location and catchment area input interface

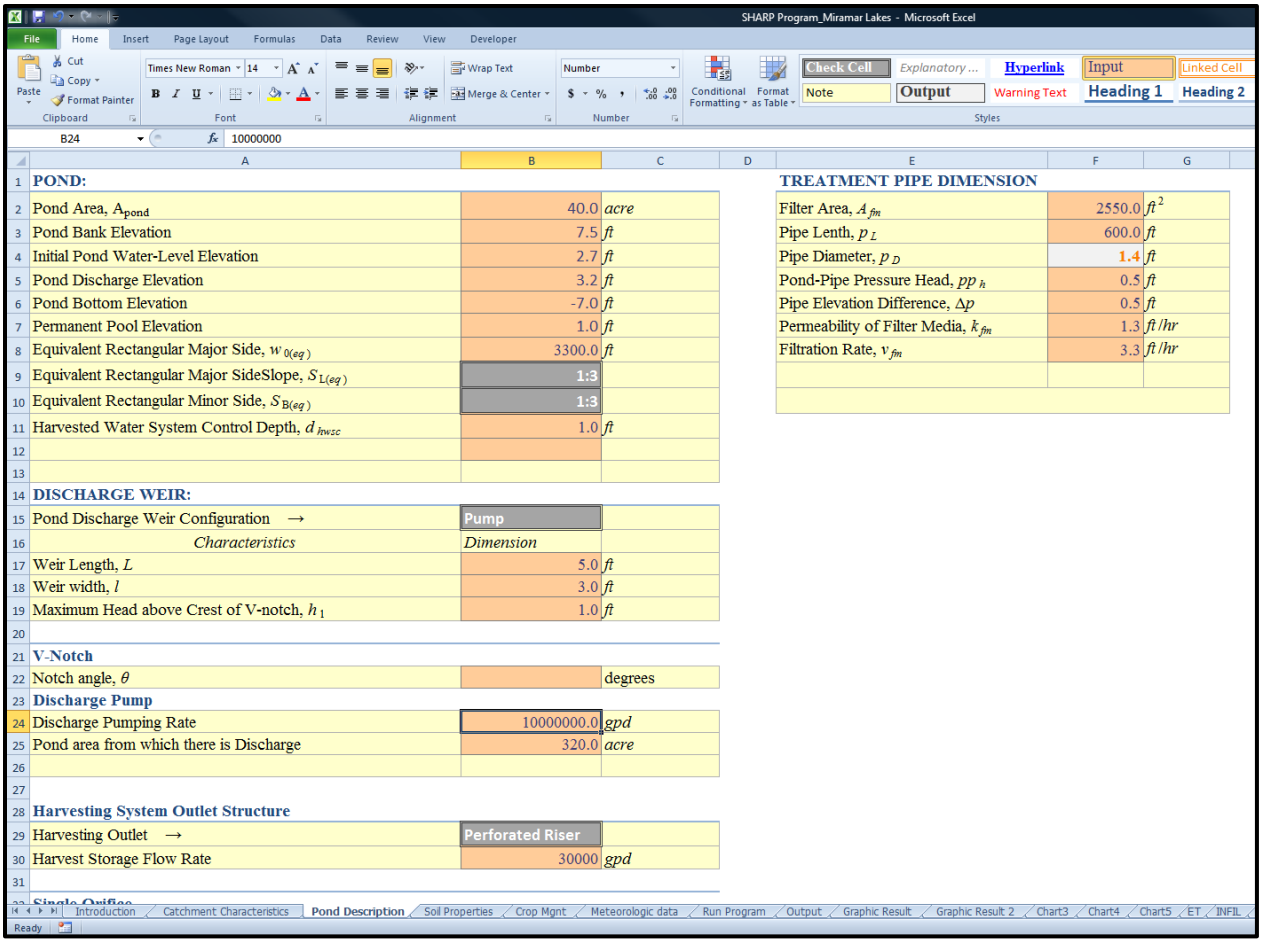

Figure 65 Pond description and treatment piping input interface

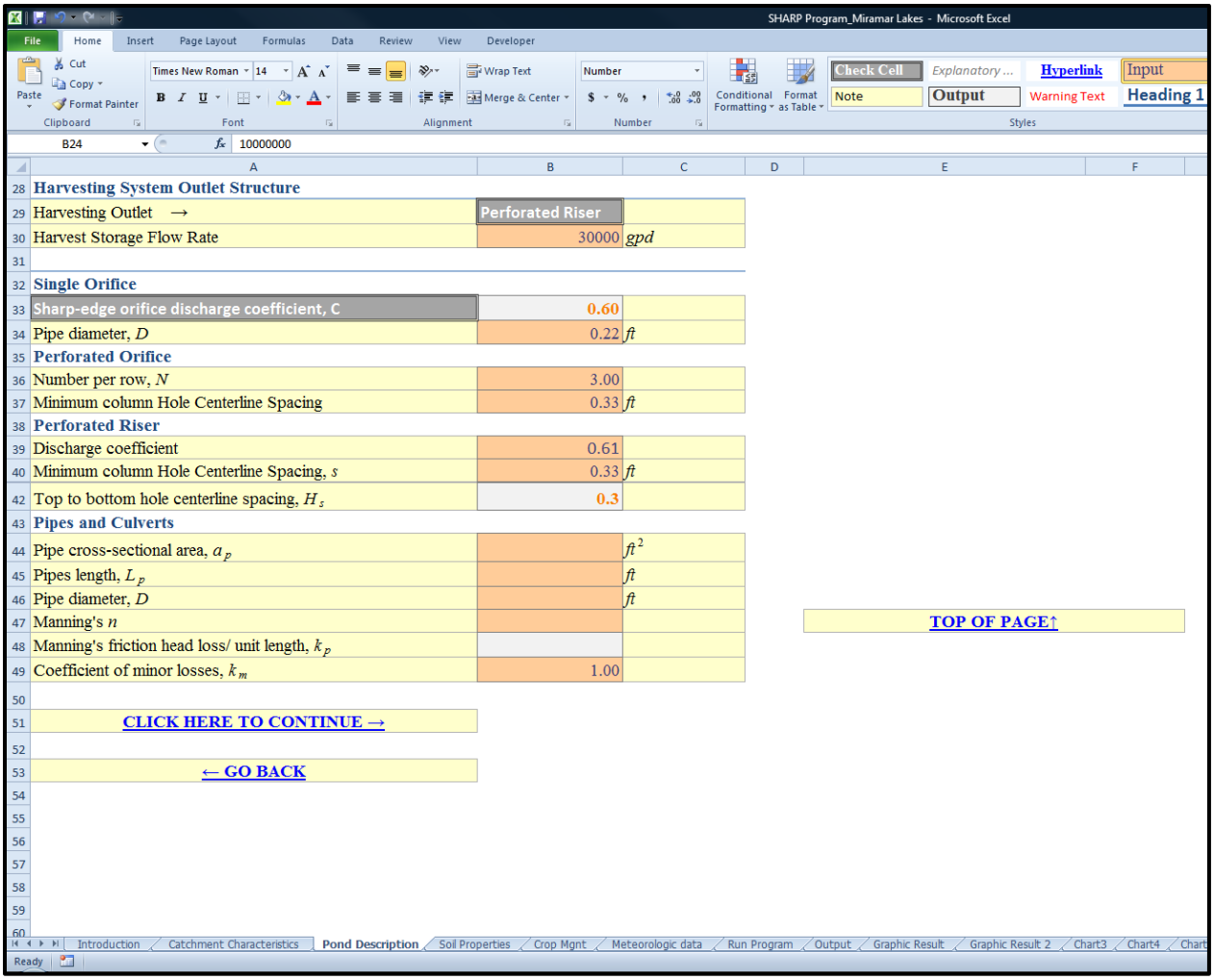

Figure 66 Pond description and outfall characteristics

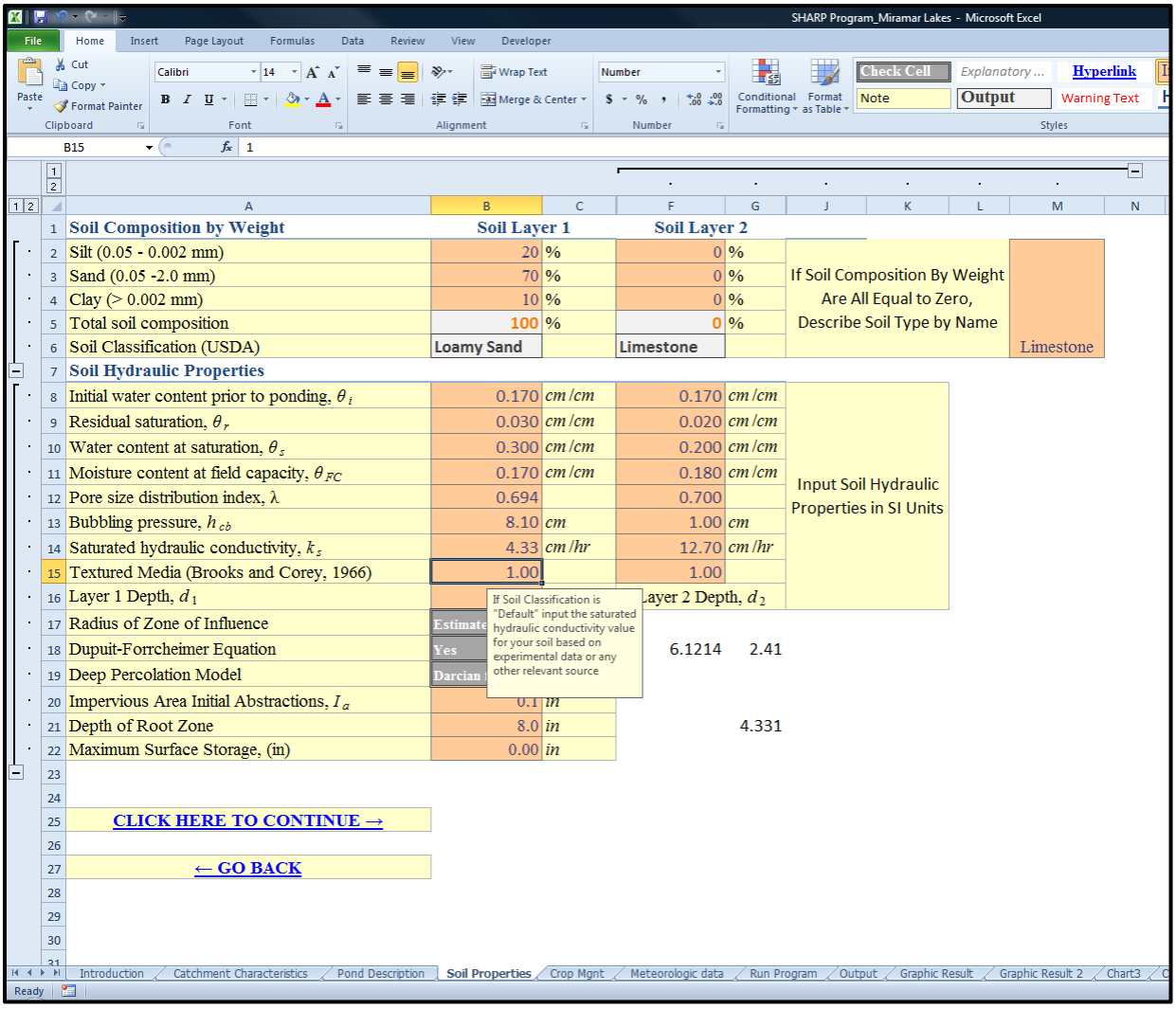

Figure 67 Soil type and hydraulic properties input interface

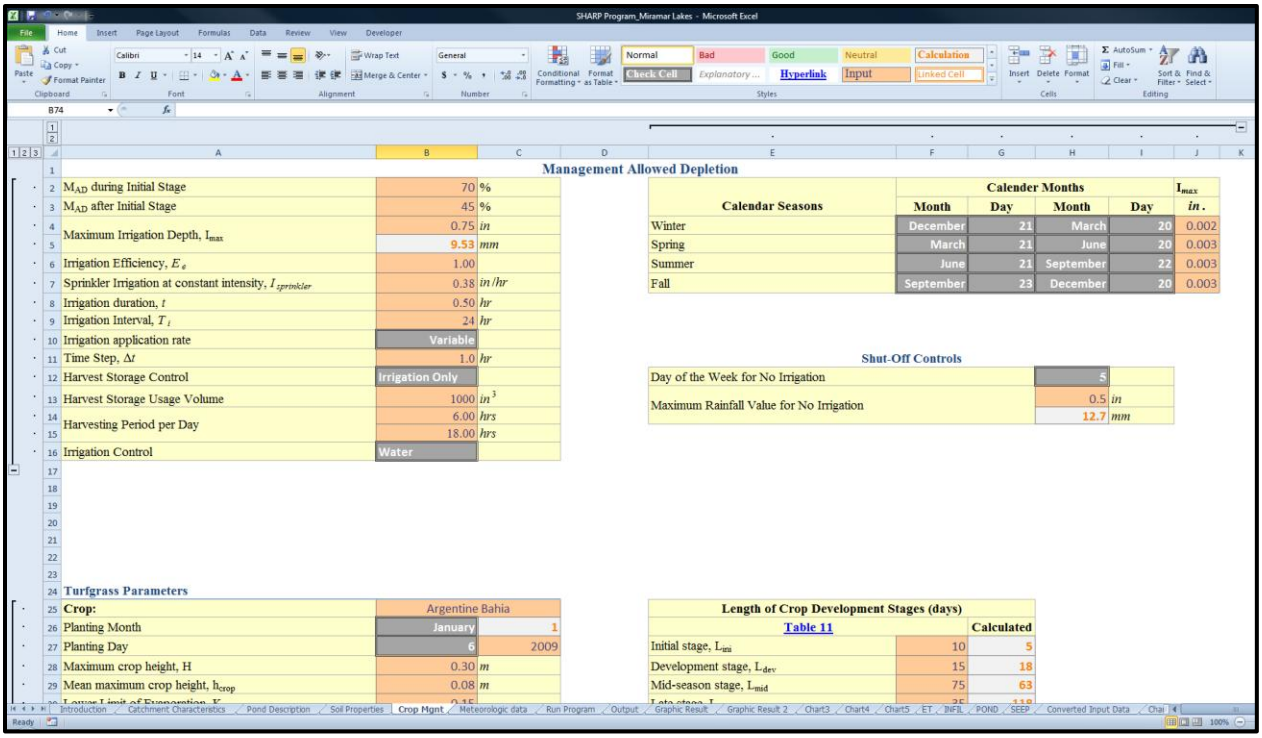

Figure 68 Management allowed depletion input interface

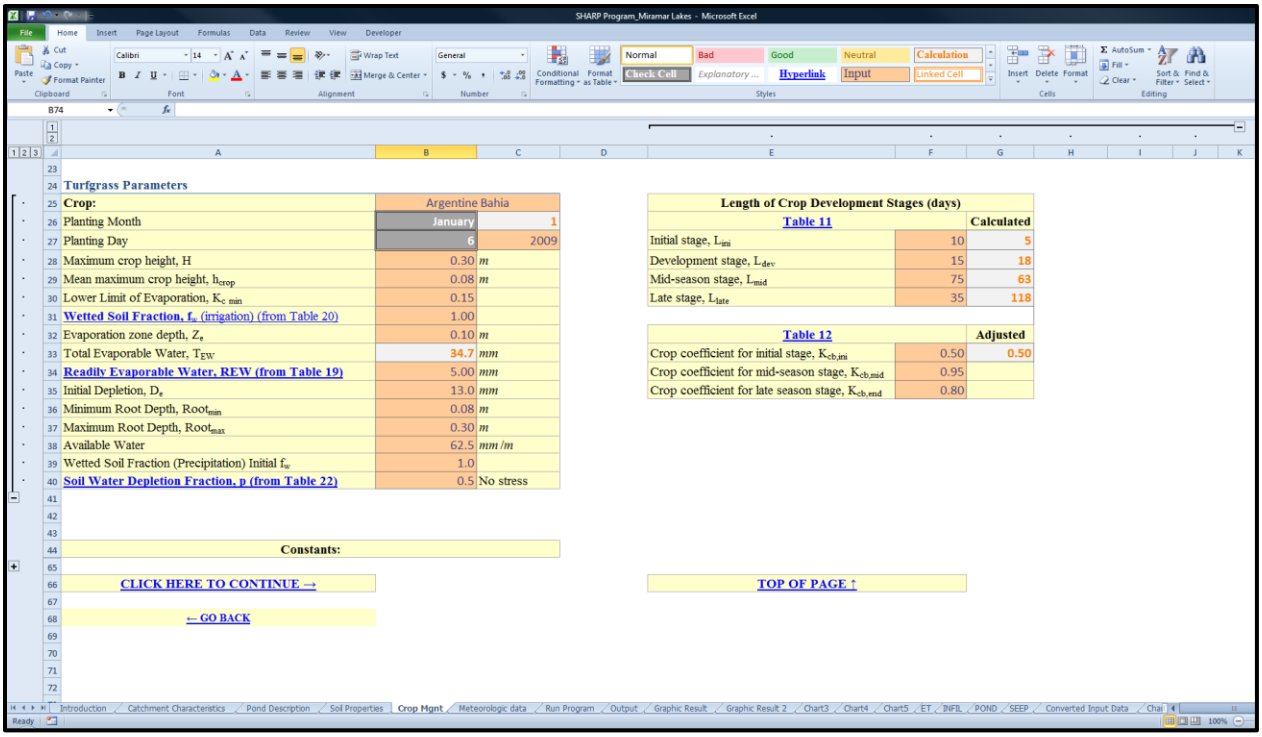

Figure 69 Turfgrass parameter input interface

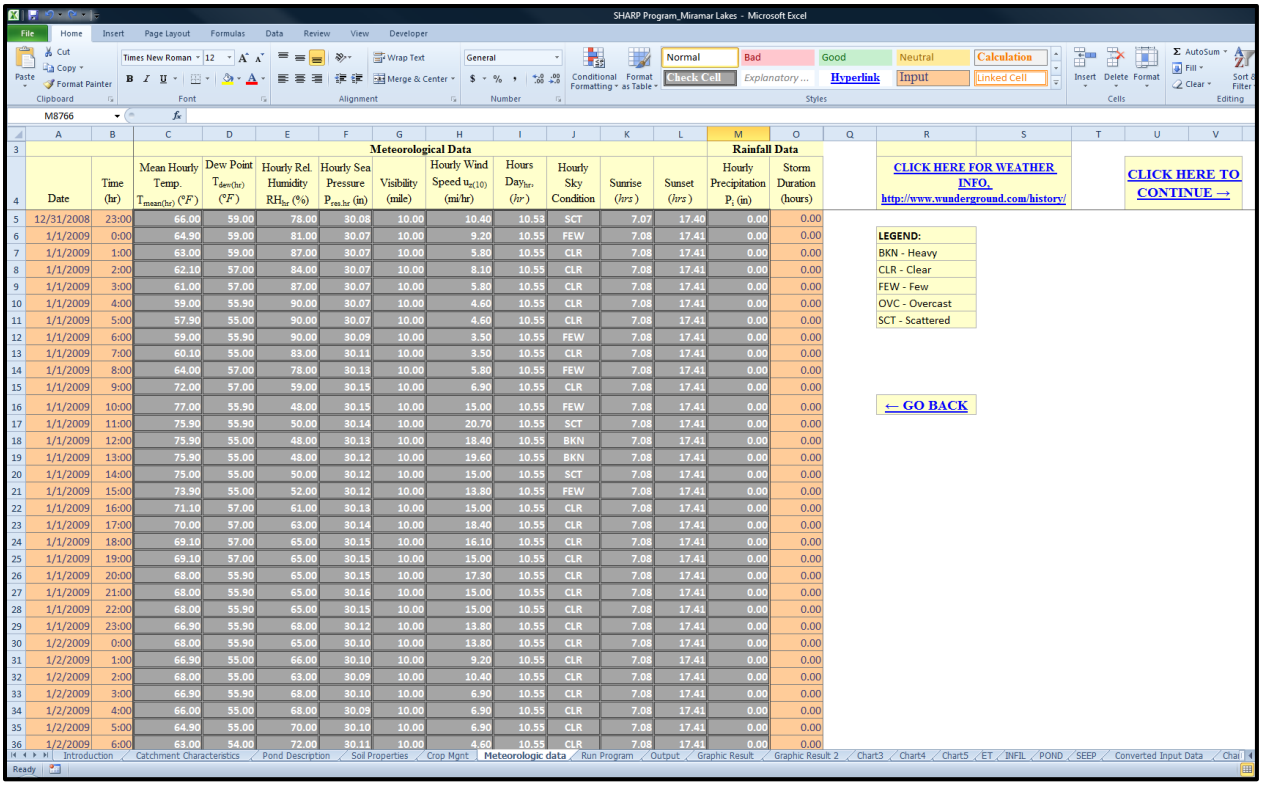

Date	Time (hr)	Mean Hourly Temp. $T_{mean(hr)}$ (°F)	Dew Point $T_{dew(hr)}$ (°F)	Hourly Rel. Humidity RH_{hr} (%)	Hourly Sea Pressure $P_{res,hr}$ (in)	Visibility (mile)	Hourly Wind Speed $u_{z(10)}$ (mi/hr)	Hours Day_{hr}, (hr)	Hourly Sky Condition	Sunrise (hrs)	Sunset (hrs)	Hourly Precipitation P_i (in)	Storm Duration (hours)
12/31/2008	23:00	66.00	59.00	78.00	30.08	10.00	10.40	10.53	SCT	7.07	17.40	0.00	0.00
1/1/2009	0:00	64.90	59.00	81.00	30.07	10.00	9.20	10.55	FEW	7.08	17.41	0.00	0.00
1/1/2009	1:00	63.00	59.00	87.00	30.07	10.00	5.80	10.55	CLR	7.08	17.41	0.00	0.00
1/1/2009	2:00	62.10	57.00	84.00	30.07	10.00	8.10	10.55	CLR	7.08	17.41	0.00	0.00
1/1/2009	3:00	61.00	57.00	87.00	30.07	10.00	5.80	10.55	CLR	7.08	17.41	0.00	0.00
1/1/2009	4:00	59.00	55.90	90.00	30.07	10.00	4.60	10.55	CLR	7.08	17.41	0.00	0.00
1/1/2009	5:00	57.90	55.00	90.00	30.07	10.00	4.60	10.55	CLR	7.08	17.41	0.00	0.00
1/1/2009	6:00	59.00	55.90	90.00	30.09	10.00	3.50	10.55	FEW	7.08	17.41	0.00	0.00
1/1/2009	7:00	60.10	55.00	83.00	30.11	10.00	3.50	10.55	CLR	7.08	17.41	0.00	0.00
1/1/2009	8:00	64.00	57.00	78.00	30.13	10.00	5.80	10.55	FEW	7.08	17.41	0.00	0.00
1/1/2009	9:00	72.00	57.00	59.00	30.15	10.00	6.90	10.55	CLR	7.08	17.41	0.00	0.00
1/1/2009	10:00	77.00	55.90	48.00	30.15	10.00	15.00	10.55	FEW	7.08	17.41	0.00	0.00
1/1/2009	11:00	75.90	55.90	50.00	30.14	10.00	20.70	10.55	SCT	7.08	17.41	0.00	0.00
1/1/2009	12:00	75.90	55.00	48.00	30.13	10.00	18.40	10.55	BKN	7.08	17.41	0.00	0.00
1/1/2009	13:00	75.90	55.00	48.00	30.12	10.00	19.60	10.55	BKN	7.08	17.41	0.00	0.00
1/1/2009	14:00	75.00	55.00	50.00	30.12	10.00	15.00	10.55	SCT	7.08	17.41	0.00	0.00
1/1/2009	15:00	73.90	55.00	52.00	30.12	10.00	13.80	10.55	FEW	7.08	17.41	0.00	0.00
1/1/2009	16:00	71.10	57.00	61.00	30.13	10.00	15.00	10.55	CLR	7.08	17.41	0.00	0.00
1/1/2009	17:00	70.00	57.00	63.00	30.14	10.00	18.40	10.55	CLR	7.08	17.41	0.00	0.00
1/1/2009	18:00	69.10	57.00	65.00	30.15	10.00	16.10	10.55	CLR	7.08	17.41	0.00	0.00
1/1/2009	19:00	69.10	57.00	65.00	30.15	10.00	15.00	10.55	CLR	7.08	17.41	0.00	0.00
1/1/2009	20:00	68.00	55.90	65.00	30.15	10.00	17.30	10.55	CLR	7.08	17.41	0.00	0.00
1/1/2009	21:00	68.00	55.90	65.00	30.16	10.00	15.00	10.55	CLR	7.08	17.41	0.00	0.00
1/1/2009	22:00	68.00	55.90	65.00	30.15	10.00	15.00	10.55	CLR	7.08	17.41	0.00	0.00
1/1/2009	23:00	66.90	55.90	68.00	30.12	10.00	13.80	10.55	CLR	7.08	17.41	0.00	0.00
1/2/2009	0:00	68.00	55.90	65.00	30.10	10.00	13.80	10.55	CLR	7.08	17.41	0.00	0.00
1/2/2009	1:00	66.90	55.00	66.00	30.10	10.00	9.20	10.55	CLR	7.08	17.41	0.00	0.00
1/2/2009	2:00	68.00	55.00	63.00	30.09	10.00	10.40	10.55	CLR	7.08	17.41	0.00	0.00
1/2/2009	3:00	66.90	55.90	68.00	30.10	10.00	6.90	10.55	CLR	7.08	17.41	0.00	0.00
1/2/2009	4:00	66.00	55.00	68.00	30.09	10.00	6.90	10.55	CLR	7.08	17.41	0.00	0.00
1/2/2009	5:00	64.90	55.00	70.00	30.10	10.00	6.90	10.55	CLR	7.08	17.41	0.00	0.00
1/2/2009	6:00	63.00	54.00	72.00	30.11	10.00	4.60	10.55	CLR	7.08	17.41	0.00	0.00

Figure 70 Meteorological data input interface

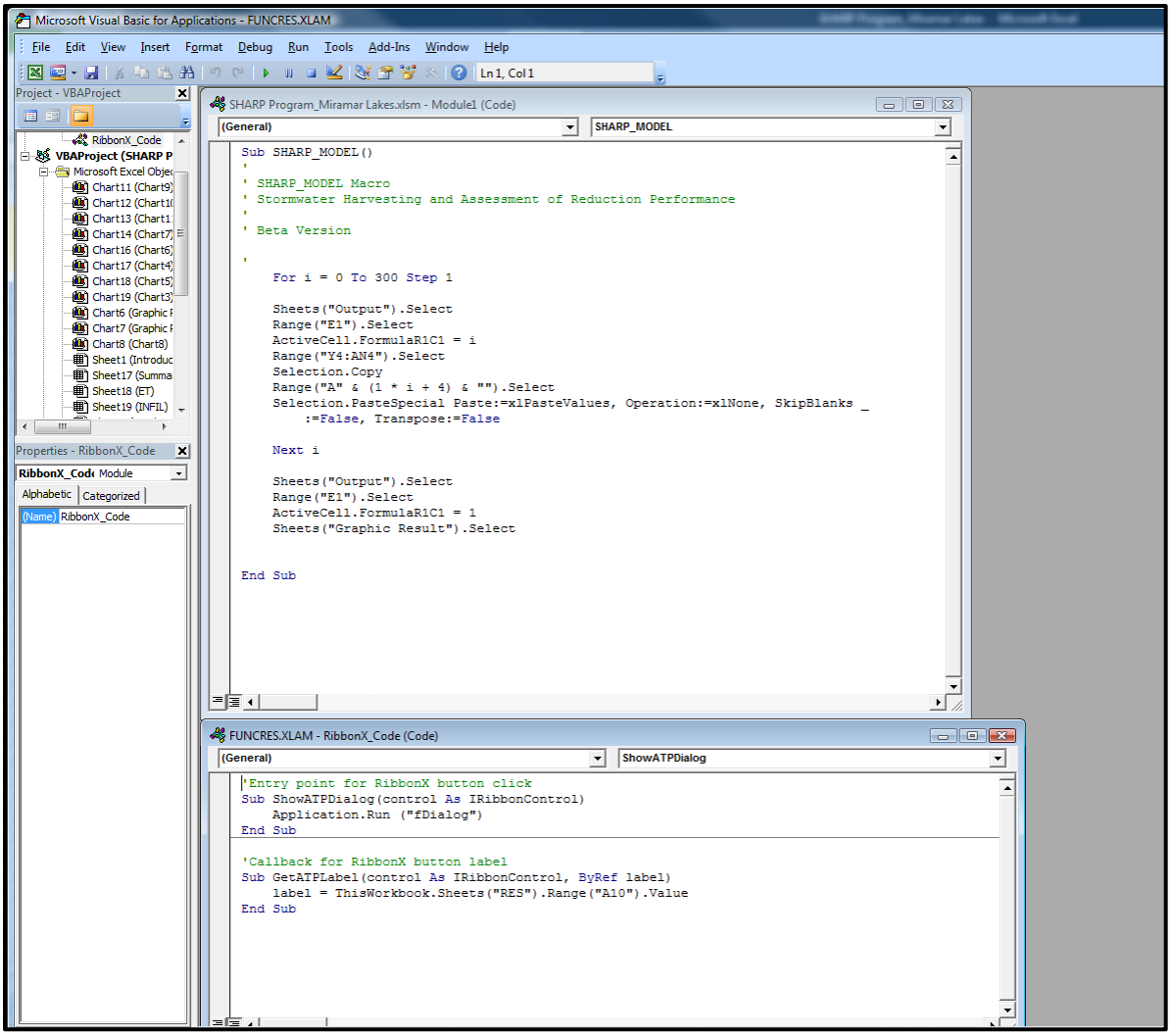

Figure 71 SHARP program execution interface

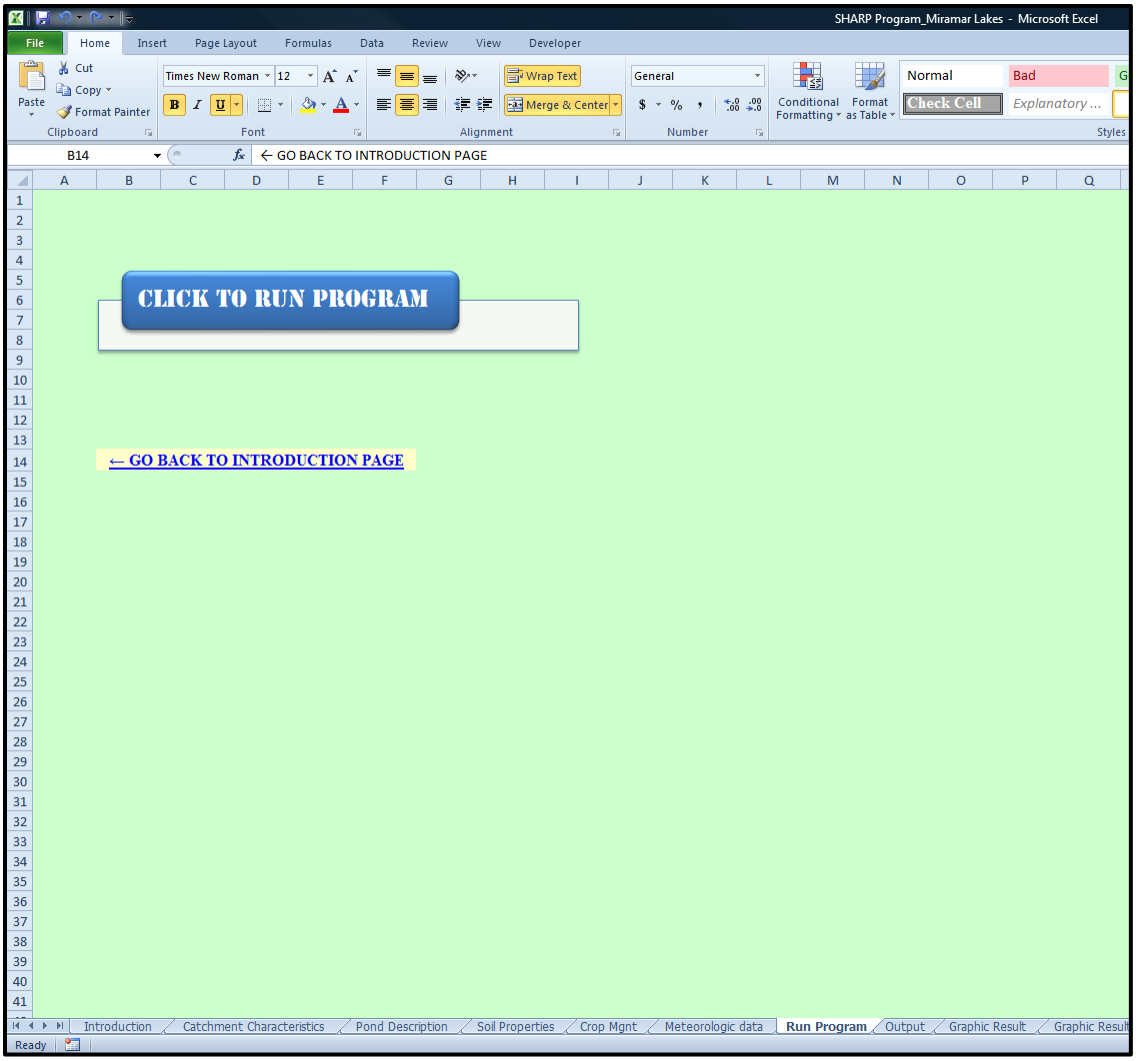

Figure 72 SHARP program initiation interface

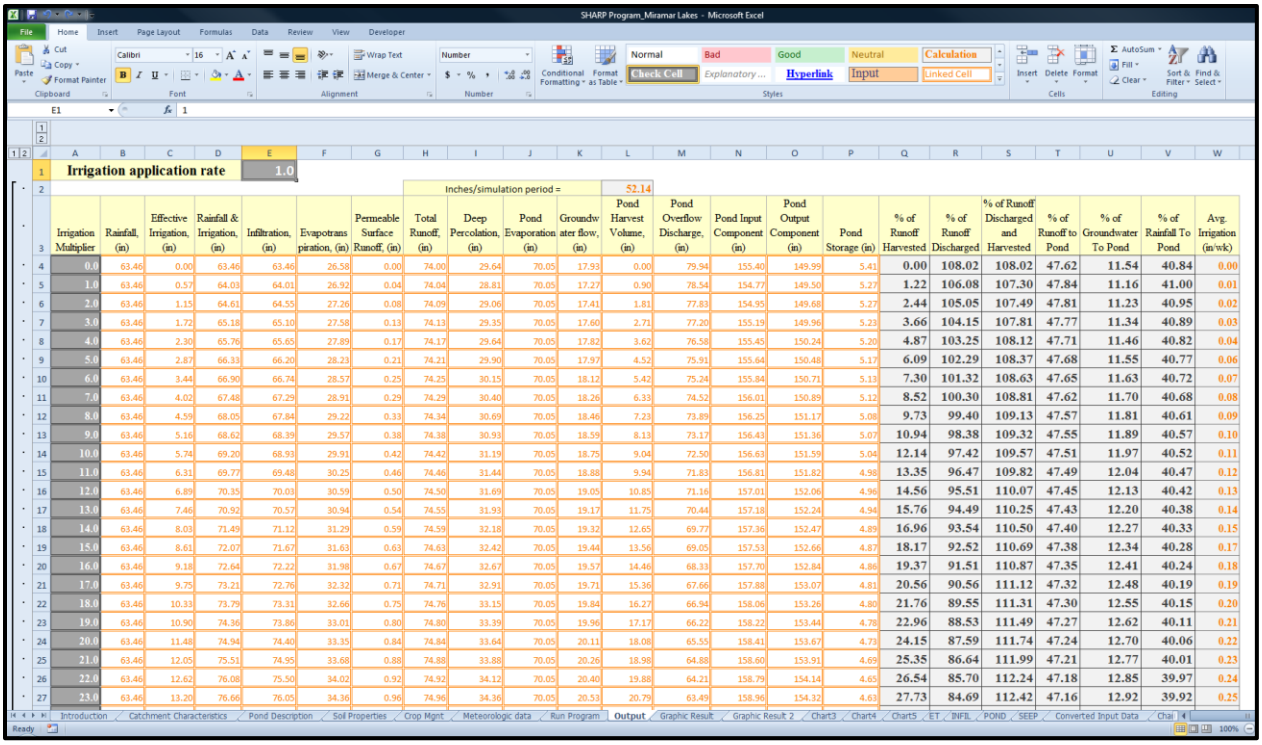

Irrigation Multiplier	Rainfall, (in)	Effective Irrigation, (in)	Rainfall & Irrigation, (in)	Infiltration, (in)	Evapotranspiration, (in)	Permeable Surface Runoff, (in)	Total Runoff, (in)	Deep Percolation, (in)	Pond Evaporation (in)	Groundwater flow, (in)	Pond Harvest Volume, (in)	Pond Overflow Discharge, (in)	Pond Input Component (in)	Pond Output Component (in)	Pond Storage (in)	% of Runoff Harvested	% of Runoff Discharged	% of Runoff Discharged and Harvested	% of Runoff to Pond	% of Groundwater To Pond	% of Rainfall To Pond	Avg. Irrigation (in/wk)
0.0	63.46	0.00	63.46	63.46	26.58	0.00	74.00	29.64	70.05	17.93	0.00	79.94	155.40	149.99	5.41	0.00	108.02	108.02	47.62	11.54	40.84	0.00
1.0	63.46	0.57	64.03	64.01	26.92	0.04	74.04	28.81	70.05	17.27	0.90	78.54	154.77	149.50	5.27	1.22	106.08	107.30	47.84	11.16	41.00	0.01
2.0	63.46	1.15	64.61	64.55	27.26	0.08	74.09	29.06	70.05	17.41	1.81	77.83	154.95	149.68	5.27	2.44	105.05	107.49	47.81	11.23	40.95	0.02
3.0	63.46	1.72	65.18	65.10	27.58	0.13	74.13	29.35	70.05	17.60	2.71	77.20	155.19	149.96	5.23	3.66	104.15	107.81	47.77	11.34	40.89	0.03
4.0	63.46	2.30	65.76	65.65	27.89	0.17	74.17	29.64	70.05	17.82	3.62	76.58	155.45	150.24	5.20	4.87	103.25	108.12	47.71	11.46	40.82	0.04
5.0	63.46	2.87	66.33	66.20	28.23	0.21	74.21	29.90	70.05	17.97	4.52	75.91	155.64	150.48	5.17	6.09	102.29	108.37	47.68	11.55	40.77	0.06
6.0	63.46	3.44	66.90	66.74	28.57	0.25	74.25	30.15	70.05	18.12	5.42	75.24	155.84	150.71	5.13	7.30	101.32	108.63	47.65	11.63	40.72	0.07
7.0	63.46	4.02	67.48	67.29	28.91	0.29	74.29	30.40	70.05	18.26	6.33	74.52	156.01	150.89	5.12	8.52	100.30	108.81	47.62	11.70	40.68	0.08
8.0	63.46	4.59	68.05	67.84	29.22	0.33	74.34	30.69	70.05	18.46	7.23	73.89	156.25	151.17	5.08	9.73	99.40	109.13	47.57	11.81	40.61	0.09
9.0	63.46	5.16	68.62	68.39	29.57	0.38	74.38	30.93	70.05	18.59	8.13	73.17	156.43	151.36	5.07	10.94	98.38	109.32	47.55	11.89	40.57	0.10
10.0	63.46	5.74	69.20	68.93	29.91	0.42	74.42	31.19	70.05	18.75	9.04	72.50	156.63	151.59	5.04	12.14	97.42	109.57	47.51	11.97	40.52	0.11
11.0	63.46	6.31	69.77	69.48	30.25	0.46	74.46	31.44	70.05	18.88	9.94	71.83	156.81	151.82	4.98	13.35	96.47	109.82	47.49	12.04	40.47	0.12
12.0	63.46	6.89	70.35	70.03	30.59	0.50	74.50	31.69	70.05	19.05	10.85	71.16	157.01	152.06	4.96	14.56	95.51	110.07	47.45	12.13	40.42	0.13
13.0	63.46	7.46	70.92	70.57	30.94	0.54	74.55	31.93	70.05	19.17	11.75	70.44	157.18	152.24	4.94	15.76	94.49	110.25	47.43	12.20	40.38	0.14
14.0	63.46	8.03	71.49	71.12	31.29	0.59	74.59	32.18	70.05	19.32	12.65	69.77	157.36	152.47	4.89	16.96	93.54	110.50	47.40	12.27	40.33	0.15
15.0	63.46	8.61	72.07	71.67	31.63	0.63	74.63	32.42	70.05	19.44	13.56	69.05	157.53	152.66	4.87	18.17	92.52	110.69	47.38	12.34	40.28	0.17
16.0	63.46	9.18	72.64	72.22	31.98	0.67	74.67	32.67	70.05	19.57	14.46	68.33	157.70	152.84	4.86	19.37	91.51	110.87	47.35	12.41	40.24	0.18
17.0	63.46	9.75	73.21	72.76	32.32	0.71	74.71	32.91	70.05	19.71	15.36	67.66	157.88	153.07	4.81	20.56	90.56	111.12	47.32	12.48	40.19	0.19
18.0	63.46	10.33	73.79	73.31	32.66	0.75	74.76	33.15	70.05	19.84	16.27	66.94	158.06	153.26	4.80	21.76	89.55	111.31	47.30	12.55	40.15	0.20
19.0	63.46	10.90	74.36	73.86	33.01	0.80	74.80	33.39	70.05	19.96	17.17	66.22	158.22	153.44	4.78	22.96	88.53	111.49	47.27	12.62	40.11	0.21
20.0	63.46	11.48	74.94	74.40	33.35	0.84	74.84	33.64	70.05	20.11	18.08	65.55	158.41	153.67	4.73	24.15	87.59	111.74	47.24	12.70	40.06	0.22
21.0	63.46	12.05	75.51	74.95	33.68	0.88	74.88	33.88	70.05	20.26	18.98	64.88	158.60	153.91	4.69	25.35	86.64	111.99	47.21	12.77	40.01	0.23
22.0	63.46	12.62	76.08	75.50	34.02	0.92	74.92	34.12	70.05	20.40	19.88	64.21	158.79	154.14	4.65	26.54	85.70	112.24	47.18	12.85	39.97	0.24
23.0	63.46	13.20	76.66	76.05	34.36	0.96	74.96	34.36	70.05	20.53	20.79	63.49	158.96	154.32	4.63	27.73	84.69	112.42	47.16	12.92	39.92	0.25

Figure 73 SHARP model tabulated output interface

APPENDIX N
SHARP MODEL SUPPLEMENTARY CHARTS

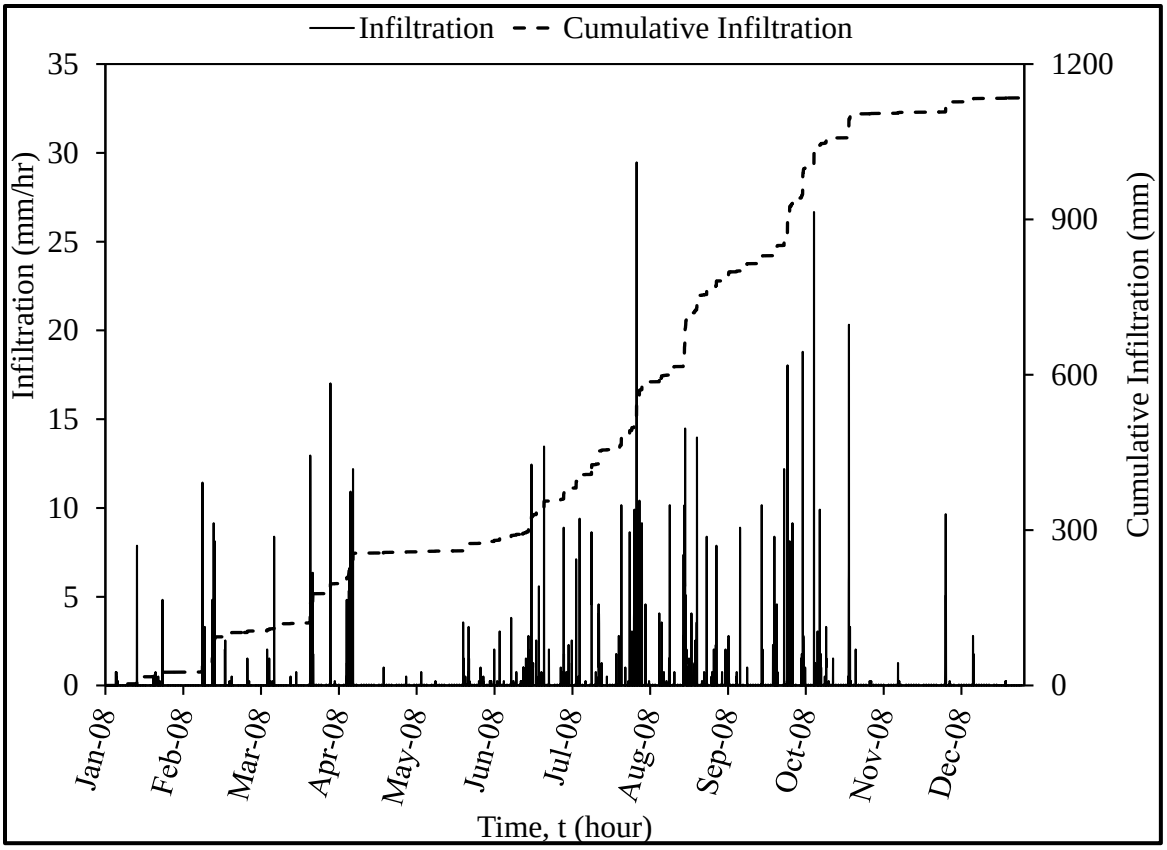

Figure 74 Plot of infiltration volume (F) for validation period

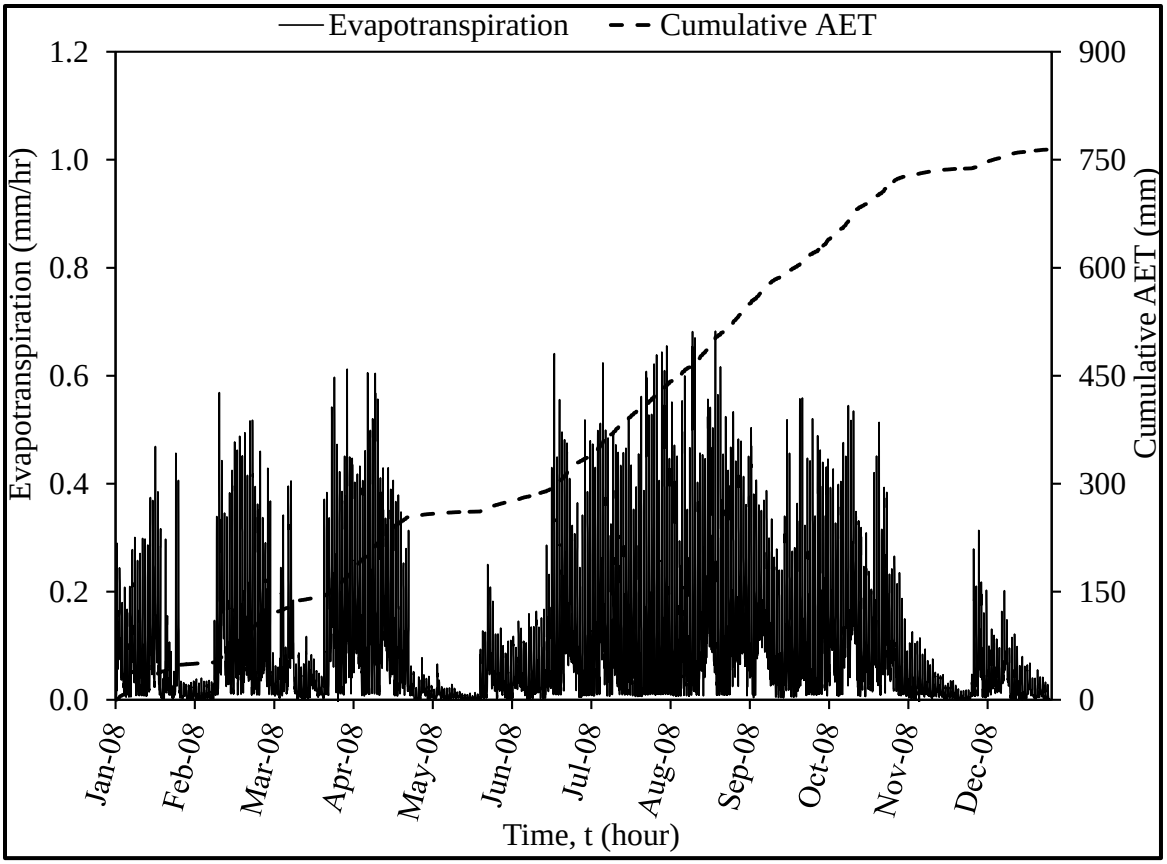

Figure 75 Plot of actual evapotranspiration (AET) for validation period

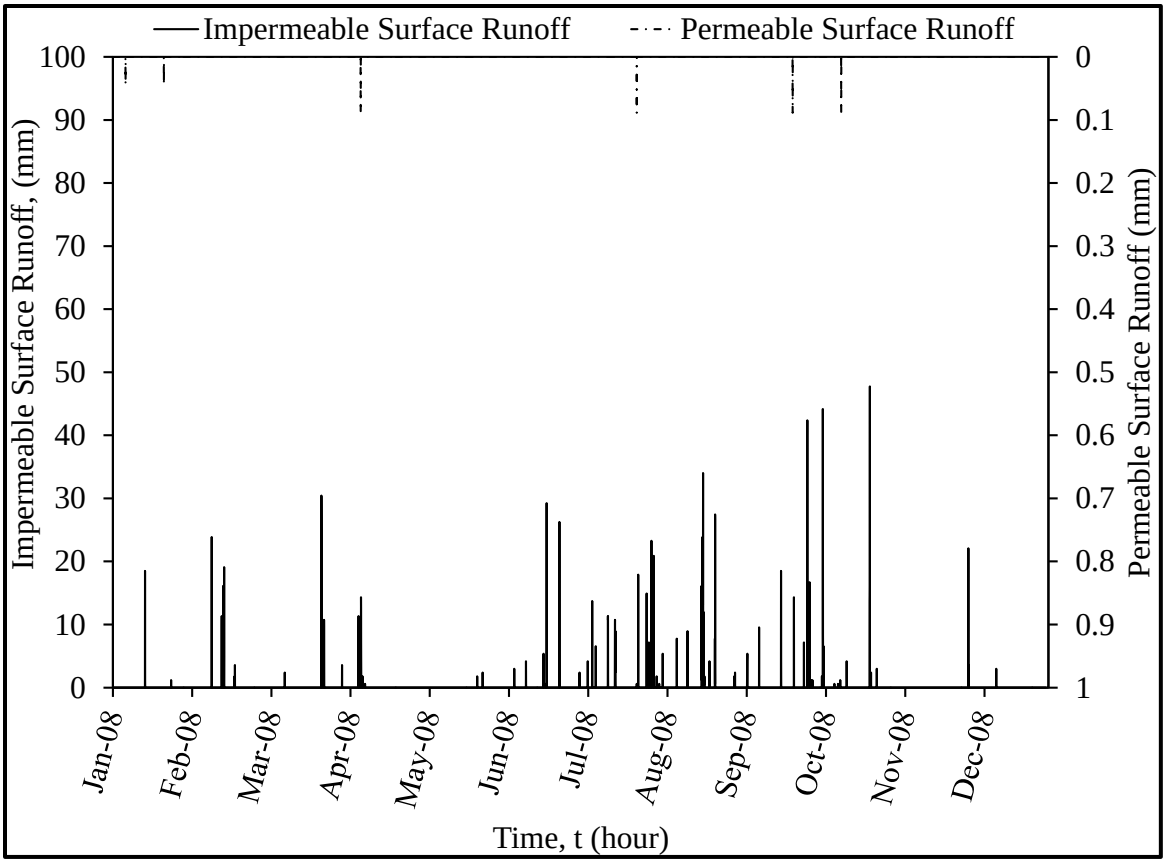

Figure 76 Plot of runoff (RO) volume per pond area for validation period

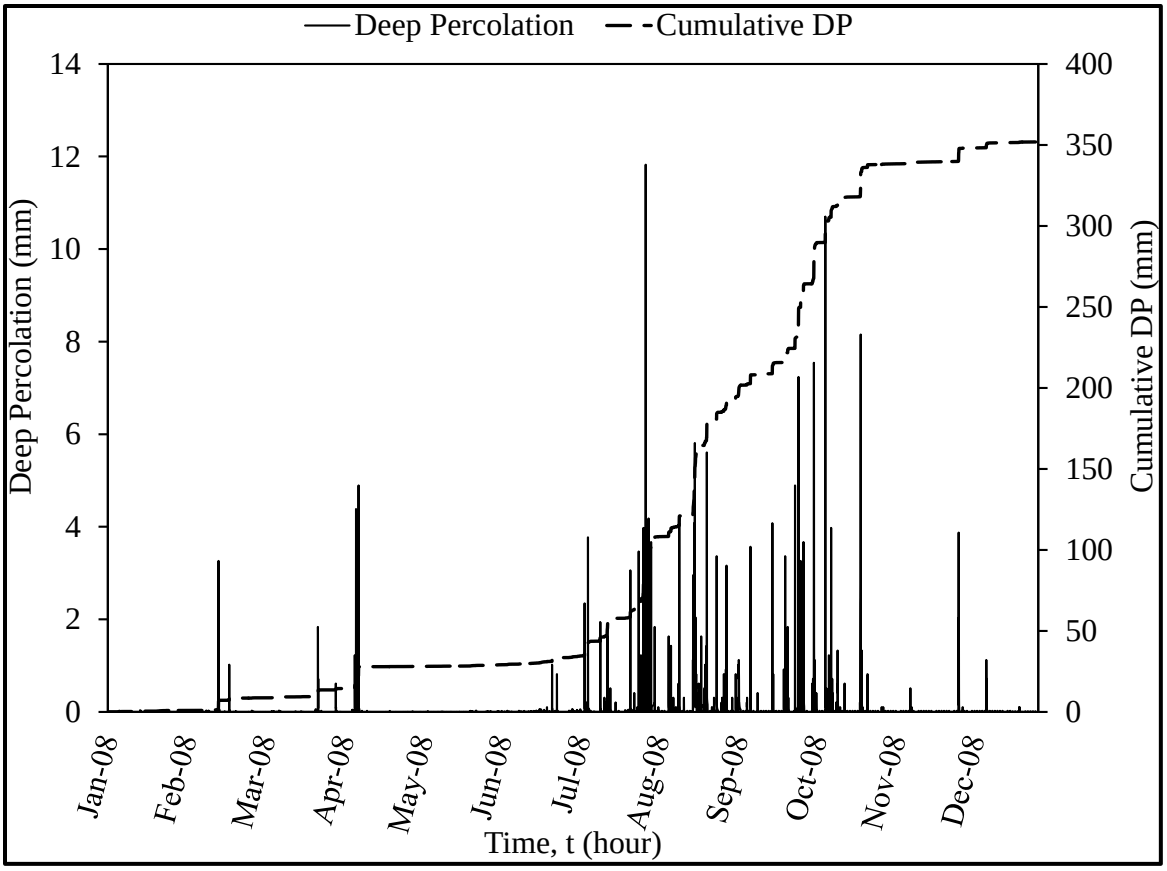

Figure 77 Plot of deep percolation (DP) per effective catchment area for validation period

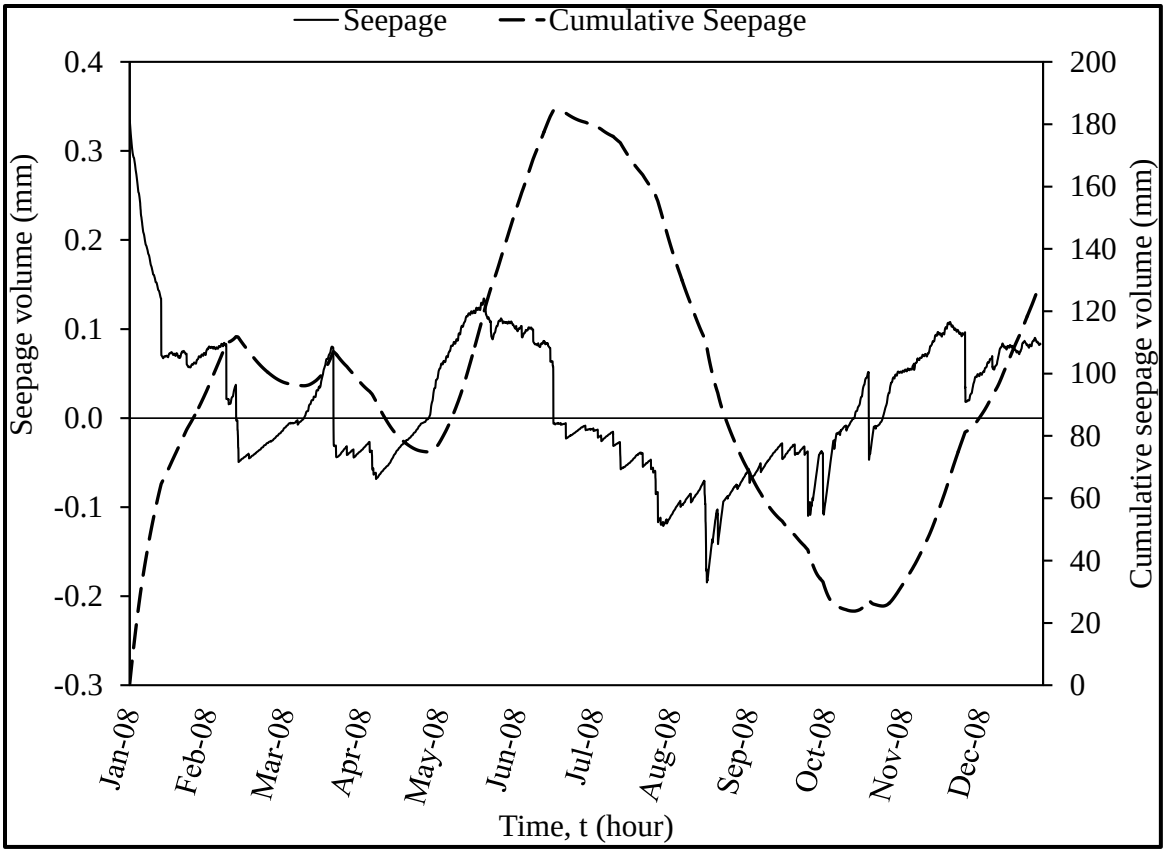

Figure 78 Plot of seepage volume per pond area for validation period

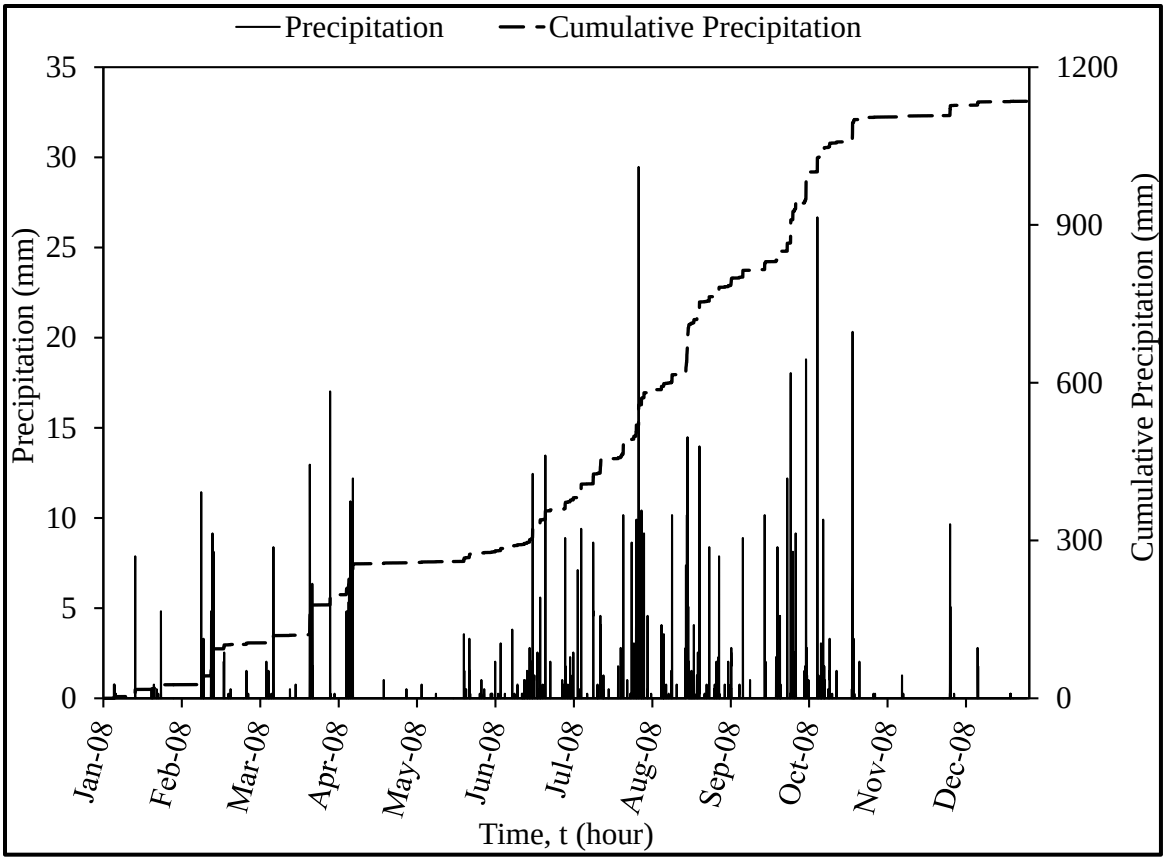

Figure 79 Precipitation volume for year 2008 at North Perry Airport, Hollywood, Florida (HWO)

LIST OF REFERENCES

Ahuja, L. R., K. W. Roas, J. D. Hanson, M. J. Shaffer and L. Ma (2000). "Root Zone Water Quality Model: Modelling Management Effects on Water Quality and Crop Production". Colorado, USA, Water Resources Publications, LLC.

Allen, R. G., L. S. Pereira, D. Raes and M. Smith (1998). "Crop evapotranspiration - Guidelines for computing crop water requirements - FAO irrigation and drainage paper 56". Rome, Food and Agriculture Organization of the United Nations.

APHA, AWWA and WEF (2005). "Standard Methods for the Examination of Water and Wastewater". A. D. Eaton. Washington D.C.

Ardaman & Associates (2007). "Subsurface exploration report, city of Miramar pump station", Miramar: City of Miramar**:** 16.

Arjunan, J., S. Yer, E. Stevens and B. J. Barfield (2005). "Application of polyacrylamide to enhance silt fence performance." *ASCE Conference Proceedings of World Water and Environmental Resources Congress*.

Arjunan, J., S. Yer, E. Stevens, B. J. Barfield and K. A. M. Gasem (2005). "Application of Polyacrylamide to Enhance Silt Fence Performance." *Journal of Environmental and Water Research Institute*.

Assurence Corp. (2006). "Assurence Silt Fence ASR-1400.")

ASTM D4355 (2007). "Standard Test Method for Deterioration of Geotextiles by Exposure to Light, Moisture and Heat in a Xenon Arc Type Apparatus". *ASTM Book of Standards* West Conshohocken, PA, ASTM International. 04.13.

ASTM D4491 (2009). "Test Methods for Water Permeability of geotextiles by Permittivity". West Conshohocken, PA, ASTM International. 04.13.

ASTM D4632 (2008). "Test Method for Grab Breaking Load and Elongation of Geotextiles". *Annual Book of ASTM Standards*. West Conshohocken, PA, ASTM International. 04.13.

ASTM D4751 (2004). "Test Method for Determining Apparent Opening Size of a Geotextile". West Conshohocken, PA, ASTM International. 04.13.

ASTM D4833 (2007). "Test Method for Index Puncture Resistance of Geomembranes and Related Products". *Annual Book of ASTM Standards*. West Conshochocken, PA, ASTM International. 04.13.

ASTM D5141 (2011). "Standard Test Method for Determining Filtering Efficiency and Flow Rate of the Filtration Component of a Sediment Retention Device". *Geotechnical Engineering Standards*. West Conshohocken, PA, ASTM International.

ASTM D6461 (2007). "Standard Specification for Silt Fence Materials". *Annual Book of ASTM Standards*. West Conshohocken, PA, ASTM International**:** 3.

Barrett, M. E., J. F. Malina and R. J. Charbeneau (1998). "An evaluation of geotextiles for temporary sediment control." *Water Environmental Federation* 70(3): 8.

Barvenik, F. W. (1994). "Polyacrylamide Characteristics Related to Soil Applications." *Soil Science* 158: 235-243.

Beier, A. (1992). "Managing Nonpoint Source Pollution, Final Report to Congress on Section 319 of the Clean Water Act (1989)". Washington, D.C., U.S. Environmental Protection Agency**:** 206.

Bethune, M. G., B. Selle and Q. J. Wand (2008). "Understanding and predicting deep percolation under surface irrigation." *Water Resources Research* 44.

Brooks, R. H. and A. T. Corey (1966). "Properties of porous media affecting fluid flow." *Journal of Irrigation and Drainage Division* 92(IR2): 61-88.

Cazzuffi, D. A., A. Mazzucato, N. Moraci and M. Tondello (1999). "A New Test Apparatus for the Study of Geotextiles Behaviour as Filters in Unsteady Flow Conditions: Relevance and Use." *Geotextiles and Geomembranes* 17(5-6): 313-329.

Chew, S. H., H. i. Tian, S. A. Tan and G. P. Karunaratne (2003). "Erosion Stability of Punctured Geotextile Filters Subjected to Cyclic Wave Loadings-A Laboratory Study." *Geotextiles and Geomembranes* 21(4): 221-239.

Chopra, M., M. Wanielista, I. Gogo-Abite and M. Hardin (2010). "Index Testing to Support the Stormwater Management Erosion and Sediment Control Laboratory"**:** 101.

Clark, G. A., C. D. Stanley, F. Z. Zazueta and E. E. Albregts (2002). "Farm ponds in Florida irrigation systems". Gainsville, University of Florida**:** 14.

Crebbin, C. (1988). "Laboratory Evaluation of Geotextile Performance in Silt Fence Applications Using a Subsoil of Glacial Origin". Seattle, University of Washington.

Cronshey, R., R. H. McCuen, W. Rawls, S. Robbins and D. Woodward (1986). "Urban hydrology for small watersheds". Washington DC., United States Department of Agriculture**:** 164.

Dierickx, W. and P. V. D. Berghe (2004). "Natural Weathering of Textiles Used in Agricultural Applications." *Geotextiles and Geomembrane* 22(4): 255-272.

Elliott, A. H. and S. A. Trowsdale (2007). "A review of models for low impact urban stormwater drainage." *Environmental Modelling & Software* 22: 12.

Ersoy, B., I. l. Tosun, A. Gunay and S. Dikmen (2009). "Turbidity Removal from Wastewaters of Natural Stone Processing by Coagulation/Flocculation Methods." *CLEAN - Soil, Air, Water* 37(3): 225-232.

Fannin, J. R., Y. P. Vaid, E. M. Palmeira and Y. C. Shi (1996). "A Modified Gradient-Ratio Test Device." *Recent Developments in Geotextile Filters and Prefabricated Drainage Geocomposites*. S. K. Bhatia and D. L. Suits. West Conshohocken, PA, ASTM International.

Faucette, L. B., J. Governo, R. Tyler, G. Gigley, C. F. Jordan and B. G. Lockaby (2009). "Performance of compost filter socks and conventional sediment control barriers used for perimeter control on construction sites." *Journal of Soil and Water Conservation* 64(1): 8.

Faure, Y. H., A. Baudoin, P. Pierson and O. Ple (2006). "A Contribution for Predicting Geotextile Clogging During Filtration of Suspended Solids." *Geotextiles and Geomembranes* 24(1): 11-20.

FDEP (2007). "State of Florida Erosion and Sediment Control Designer and Reviewer Manual". R. Browne. Tallahassee, Florida, University of Central Florida**:** 299.

FDEP (2008). "Florida Stormwater Erosion and Sedimentation Control Inspector's Manual". Tallahassee, Florida Department of Environmental Protection**:** 378.

FDEP (2010). "Environmental Resource Permit Stormwater Quality Applicant's Handbook". F. D. o. E. P. a. W. M. Districts. Tallahassee, FDEP**:** 376.

FDOT (2006). "Florida Department of Transportation".

Fifield, J. S. (2004). "Designing for Effective Sediment and Erosion Control on Construction Sites". Santa Barbara, California, Forester Communications. 340.

Fisher, L. S. and A. R. Jarrett (1984). "Sediment Retention Efficiency of Synthetic Fabrics." *Transactions of the American Society of Agricultural Engineers* 27(2): 429-436.

Flanagan, D. C., K. Chaudhari and L. D. Norton (2002). "Polyacrylamide Soil Amendment Effects on Runoff and Sediment Yield on Steep Slopes: Part I. Simulated Rainfall Conditions." *Transaction of the ASAE* 46(1): 1327-1337.

Fourie, A. B. and P. C. Addis (1999). "Changes in Filtration Opening Size of Woven Geotextiles Subjected to Tensile Loads." *Geotextile and Geomembranes* 17(5-6): 331-340.

Glover, R. E. (1963). "Ground-Water Movement". Denver, Water Resources Technical Publications.

Hammer, T. R. (1972). "Stream channel enlargement due to urbanization." *Water Resources Research* 8: 11.

Harmel, R. D., P. K. Smith and K. W. Migliaccio (2010). "Modifying goodness-of-fit indicators to incorporate both measurement and model uncertainty in model calibration and validation." *Transaction of the American Society of Agricultural and Biological Engineers* 53(1): 9.

Harper, H. H. and D. M. Baker (2007). "Evaluation of current stormwater design criteria within the state of Florida". Tallahassee, Florida**:** 327.

Hayes, S. A., R. A. McLaughlin and D. L. Osmond (2005). "Polyacrylamide use for erosion and turbidity control on construction sites." *Journal of Soil and Water Conservation* 60(4): 7.

Heitz, L. F., S. Khosrowpanah and J. Nelson (2000). "Sizing of surface water runoff detention ponds for water quality improvement." *Journal of the American Water Resources Association* 36(3): 541-548.

Henry, K. S., M. R. Walsh and S. H. Morin (1999). "Selection of Silt Fence to Retain Suspended Toxic Particles." *Geotextiles and Geomembranes* 17(5-6): 371-387.

Horner, R. R., J. Guedry and M. H. Kortenhof (1990). "Improving the Cost Effectiveness of Highway Construction Site Erosion and Pollution Control". Seattle, Washington State Department of Transportation.

Hwang, A. H. S. and D. Draper (2006). "Public perceptions and attitudes toward stormwater recycling for irrigation." *Canadian Water Resources Journal* 31(3): 185-196.

Iwinski, S. (2010) "Polymer Enhanced Best Management Practices for Erosion and Sedimentation Control, Water Clarification with a Focus on Nutrient Control and Soil Stabilization." 13.

Jaber, F. H. and S. Shukla (2004). "Simulating water dynamics in agricultural stormwater impoundments for irrigation water supply." *Transaction of Ameracian Society of Agricultural Engineers* 47(5): 12.

Jaber, F. H. and S. Shukla (2005). "Hydrodynamic modeling approaches for agricultural storm waterimpoundments." *Journal of Irrigation and Drainage Engineering* 131(4): 10.

Kehoe, M. (1993). "Water Quality Survey of Twenty-Four Stormwater Wet Detention Ponds - Final Report". Brooksville, FL**:** 84.

Kehoe, M., C. Dye and B. Rushton (1994). "A Survey of Water Quality of Wetlands-Treatment Stormwater Ponds". Brooksville, FL**:** 40.

Koerner, R. M. (1997). "Designing with Geosynthetics". Upper Saddle River, New Jersey, Prentice-Hall Inc.

Kouwen, N. (1990). "Silt Fences to Control Sediment Movement on Costruction Sites". Ontario, Ministry of Transportation.

Krause, P., D. P. Boyle and F. Base (2005). "Comparison of different efficiency criteria for hydrologic model assessment." *Advances in Geosciences* 5: 9.

Lentz, R. D., R. E. Sojka and C. W. Ross (2000). "Polymer charge and molecular weight effects on treated irrigation furrow processes." *International Journal of Sediment Research*(1): 14.

McCarthy, J. E. (1995). "Engineering use of geotextiles". D. o. t. A. a. t. A. Force. Washington, DC, Headquaters Department of the Army and the Air Force**:** 58.

McLaughlin, R. A., S. E. King and G. D. Jennings (2009). "Improving Construction Site Runoff Quality with Fiber Check Dams and Polyacrylamide." *Soil and Water Conservation* 64(2): 144-154.

Morton, J. F. (1990). "Trees, Shrubs and Plants for Florida Landscapping - Native and Exotic". Tallahassee, FL, Florida Department of Agriculture and Consumer Services**:** 232.

Narejo, D. B. (2003). "A Simple Tilt Table Device to Measure Index Friction Angle of Geosynthetics." *Geotextiles and Geomembranes* 21(1): 49-57.

Orts, W. J., R. E. Sojka, G. M. Blenn and M. Gregory (2000). "Biopolymer Additives to Reduce Erosion-Induced Soil Losses During Irrigation." *Industrial Crops and Products* 11: 19-29.

Owens, D. W., P. Jopke, D. W. Hall, J. Balousek and A. Roa (2000). "Soil Erosion from Two Small Construction Sites, Dane County, Wisconsin". Middleton, WI, U.S. Department of the Interior**:** 4.

Palmeira, E. M., F. N. Remigio, M. L. G. Ramos and R. S. Bernardes (2008). "A Study on Biological Clogging of Nonwoven Geotextiles Under Leachate Flow." *Geotextiles and Geomembranes* 26(3): 205-219.

Paul, M. J. and J. L. Meyer (2001). "Streams in the urban landscape." *Annual Review of Ecology and Systematics*. 333-365.

Peluso, V. F. and A. Marshall (2002). "Best Management Practices for South Florida Urban Stormwater Management Systems". West Palm Beach, South Florida Water Managemnet District**:** 33.

Penman, H. L. (1948). "Natural Evaporation form Open Water, Bare Soil and Grass." *Royal Society of Agriculture*, London. 120-146.

Rawls, W. J., D. L. Brakensiek and K. E. Saxton (1982). "Estimation of soil water properties." *Transaction of Ameracian Society of Agricultural Engineers* 25(5): 5.

Risse, L. M., S. Thompson and J. Governo (2007). "Belted Strand Retention Fabric: An Alternative to Silt Fence for Erosion and Sediment Control." *Georgia Water Resources Conference*, Athens, University of Georgia

Roa, A., G. D. Bubenzer and E. S. Miyashita (1998). "Determination of PAM Use Potential in Erosion Control." *Proceedings of the First European Conference of Water and Environment Innovation Issues in Irrigation and Drainage*, International Commission on Irrigation and Drainage. 49-57.

Schroeder, P. R., T. S. Dozier, P. A. Zappi, B. M. McEnroe, J. W. Sjostrom, R. L. Peyton and N. M. Aziz (1994). "Hydrologic Evaluation of Landfill Performance (HELP) Model". Vicksburg, MS., USA, Army Engineer Waterways Experiment Station**:** 128.

Schueler, T. (1994). "Review of Pollutant Removal Performance of Stormwater Ponds and Wetlands". *Watershed Protection Techniques*. 1**:** 17-18.

Schueler, T. (1996). "Irreducible Pollutant Concentrations Discharged from Urban BMPs". *Watershed Protection Techniques*. 2**:** 369-371.

Schueler, T. R. (2000). "The Importance of Imperviousness". *The Practice of Watershed Protection*. T. R. Schueler and H. K. Holland. Ellicott City, MD, Center for Watershed Protection**:** 7-17.

Seymour, R. M. (2005). "Capturing rainwater to replace irrigation water for landscapes: rain harvesting and rain gardens." *Proceedings of the 2005 Georgia Water Resources Conference,* University of Georgia, Athens, Georgia

Shuttleworth, J. W. (2007). "Putting the 'vap' into evaporation." *Hydrology and Earth System Science* 11(1): 35.

Skaggs, R. W. and R. Khaleel (1982). "Infiltration." *Infiltration In hydrologic modeling of small watersheds*. St. Joseph, MI, USA, American Society of Agricultural Engineers**:** 121-162.

Smajstral, A. G. (1990). "Field scale irrigation requirements simulation (AFSIRS) model. Version 5.5". Gainsville, University of Florida.

Smoot, J. T., T. D. Moore, J. H. Deatherage and B. A. Tschantz (1992). "Reducing Nonpoint Source Water Pollution by Preventing Soil Erosion and Controlling Sediment on Construction Sites", University of Tennessee.

Soupir, M. L. S., S. Mostaghimi, A. Masters, K. Flahive, D. H. . Vaughan and A. M. P. W. McClellan (2004). "Effectiveness of Polyacrylamide (PAM) in Improving Runoff Water Quality from Construction Sites." *The American Water Resources Association* 40(1): 53-66.

Suits, D. L. and G. Y. Hsuan (2003). "Assessing the Photo-Degradation of Geosynthetics by Outdoor Exposure and Laboratory Weatherometer." *Geotextiles and Geomembranes* 21(2): 111-122.

Tadav, B. K., S. Mathur and M. A. Siebel (2009). "Soil moisture flow modeling with water uptake by plants (wheat) under varying soil and moisture conditions." *Journal of Irrigation and Drainage Engineering* 135(3): 375-381.

TenCate. (2009). "Erosion Control." <http://www.tencate.com/smartsite.dws?id=9026> (Retrieved June 09, 2009)

Tindall, J. A. and J. R. Kunkel (1999). "Unsaturated Zone Hydrology for Scientists and Engineers". Upper Saddle River, New Jersey, USA, Prentice-Hall, Inc.

Trout, T. J., R. E. Sojka and R. D. Lentz (1995). "Polyacrylamide Effect on Furrow Erosion and Infiltration." *Transaction of American Society of Agricultural Engineers* 38(3): 761-766.

USACE. (2011). "Gridded Surface Subsurface Hydrologic Analysis." <http://chl.erdc.usace.army.mil/gssha> (Retrieved, 2012)

USDA. (2008). "TR-55 Urban hydrology for small watersheds." <http://www.nrcs.usda.gov/wps/portal/nrcs/detailfull/national/technical/alphabetical/water/hydrology/?&cid=stelprdb1042925> (Retrieved April 10, 2011)

USEPA. (1996). "Water: outreach and communication." *Nonpoint source pollution: The nation's water largest water quality problem* <http://water.epa.gov/polwaste/nps/outreach/point1.cfm> (Retrieved November 12, 2009)

USEPA (1999). "National Pollution Discharge Elimination System - Storm Water Phase II". Washington D.C. 64**:** 68721-68851.

USEPA. (2007). "BASINS (Better Assessment Science Integrating point & Non-point Sources)." *BASINS 4.0* <http://water.epa.gov/scitech/datait/models/basins/index.cfm> (Retrieved February 27, 2012)

USEPA (2007). "Options for expressing daily loads in TMDLs". U. S. E. P. Agency. Washington, D.C., USEPA**:** 62.

USEPA. (2009). "Stormwater Discharges From Construction Activities." <http://cfpub.epa.gov/npdes/stormwater/const.cfm> (Retrieved February 11, 2011)

USEPA. (2010). "Watershed and Water Quality Modeling Technical Support Center." <http://www.epa.gov/athens/wwqtsc/Tech_Center_Fact_Sheet.pdf> (Retrieved January 10, 2010)

USGS. (2012). "Modeling of watershed systems." <http://wwwbrr.cr.usgs.gov/projects/SW_MoWS/index.shtml> (Retrieved March, 17, 2012)

USHUD (1970). *Proccedings of the National Conference on Sediement Control*, Washington, D.C., U.S. Department of Housing and Urban Development

VNDCR (2006). "Virginia Erosion and Sediment Control Handbook". Richmond, Virgina Department of Conservation and Recreation.

Wang, R. H., C. S. Wu and Y. S. Hong (2008). "The Influence of Uniaxial Tensile Strain on the Pore Size and Filtration Characteristics of Geotextiles." *Geotextiles and Geomembranes* 26(3): 250-262.

Wanielista, M. (1993). "Stormwater reuse: an alternative method of infiltration." *National Conference on Urban Runoff Management: Enhancing Urban Watershed Management at the Local, County, and State Levels*, Chicago, USEPA. 363-371.

Wanielista, M. (2007). "Regional stormwater irrigation facilities". Tallahassee, Florida Department of transportation**:** 111.

Wanielista, M. and M. Chopra (2010). "State of Florida Manuals for Erosion and Sediment Control and the Rainfall Rrunoff Simulator at the Stormwater Management Academy". Tallahasse, Florida, University of Central Florida**:** 54.

Wanielista, M., Y. Yousef and C. Boss (1988). "Alternative for the Treatment of Groundwater Contaminant: A Detention Pond with Groundwater Inflows", Florida Department of Transportation**:** 98.

Wanielista, M. P. and J. N. Bradner (1992). "Restoration and Demonstration Project Smart. Orlando, Florida"**:** 107.

Wanielista, M. P. and A. Y. Yousef (1993). "Design and analysis of an irrigation pond using urban stormwater runoff." *Engineering Hydrology*, San Francisco, California, American Society of Civil Engineering (ASCE). 724-729.

Watson, P. D. J. and N. W. M. John (1999). "Geotextile Filter Design and Simulated Bridge Formation at Soil-Geotextile Interface." *Geotextiles and Geomembranes* 17(5-6): 265-280.

Willmott, C. J. and K. Matsuura (2005). "Advantages of the mean absolute error (MAE) over the root mean square error (RMSE) in assessing average model performance." *Climate Research* 30: 4.

Wishowski, J. M., M. Mamo and G. D. Bubenzer (1998). "Trap Efficiencies of Filter Fabric Fence."

Wu, C. S., Y. S. Hong, Y. W. Yan and B. S. Chang (2006). "Soil-Nonwoven Geotextile Filtration Behavior Under Contact with Drainage Materials." *Geotextiles and Geomembranes* 24(1): 1-10.

Wunderground.com. (2010). "History for Hollywood, Florida." <http://www.wunderground.com/> (Retrieved Apr. 4, 2010)

Wyant, D. C. (1981). "Evaluation of Filter Fabrics for Use in Silt Fence." *Transportation Research Record* 832(6): 6-12.

Yu, J., T. Lei, I. Shainberg, A. I. Mamedov and G. J. Levy (2003). "Infiltration and Erosion in Soils Treated with Dry PAM and Gypsum." *Soil Science Society of America* 67(2): 630-636.